Journal of Paleontology, Volume 98, Memoir 95, 2024, p. 1–79

Published by Cambridge University Press
on behalf of Paleontological Society
0022-3360/24/1937-2337
doi: 10.1017/jpa.2023.92

JOURNAL OF PALEONTOLOGY
A PUBLICATION OF THE Paleontological SOCIETY

Silicified microfossils from the Ediacaran Doushantuo Formation along a shelf margin-slope-basin transect in Hunan Province, South China, with stratigraphical implications

Qing Ouyang,[1,2]* Chuanming Zhou,[1,3] Shuhai Xiao,[4] Chengxi Wu,[1,5] Zhe Chen,[1] Xianguo Lang,[6] Hongyi Shi,[1,5] and Yunpeng Sun[1,5]

[1]State Key Laboratory of Palaeobiology and Stratigraphy, Nanjing Institute of Geology and Palaeontology, Chinese Academy of Sciences, Nanjing 210008, China <qouyang@nigpas.ac.cn>, <cmzhou@nigpas.ac.cn>, <cxwu@nigpas.ac.cn>, <zhechen@nigpas.ac.cn>, <hyshi@nigpas.ac.cn>, <ypsun@nigpas.ac.cn>
[2]State Key Laboratory of Biogeology and Environmental Geology, China University of Geosciences (Wuhan), Wuhan 430074, China
[3]University of Chinese Academy of Sciences, Nanjing, Nanjing 211135, China
[4]Department of Geosciences, Virginia Tech, Blacksburg, VA 24061, USA <xiao@vt.edu>
[5]University of Chinese Academy of Sciences, Beijing 100049, China
[6]State Key Laboratory of Oil and Gas Reservoir Geology and Exploitation, and Institute of Sedimentary Geology, Chengdu University of Technology, Chengdu 610059, China <langxianguo19@cdut.edu.cn>

Non-technical Summary.—The Ediacaran (ca. 635–539 million years ago) Doushantuo Formation in South China yields abundant microfossils preserved in cherts and phosphorites, yet most of the published materials originate from paleogeographically more proximal shelf-lagoon and shelf margin environments. In this paper, we report microfossils preserved in chert nodules from the Doushantuo Formation in a variety of environments, from the shallow-water shelf margin, to the distal, deep-water slope and basinal environments. We also analyze the abundance and occurrence data of Doushantuo acanthomorphs based on the present and previously published studies. The results show that different environments have largely similar fossil composition at the level of major morphological groups. However, acanthomorphic acritarchs, as a biostratigraphically important fossil group in the correlation of lower–middle Ediacaran strata, vary significantly in diversity among different environments. Using quantitative and data-visualization methods (e.g., rarefaction analysis, non-parametric multidimensional scaling, and network analysis), we show that variations in acritarch diversity among environments are largely due to insufficient sampling in slope and basinal areas, as well as differences in preservational modes. Nonetheless, numerous acritarch species occur widely in different environments, highlighting their potential in regional stratigraphic correlation of the Doushantuo Formation.

Abstract.—Silicified microfossils are reported from nine stratigraphic sections of the Ediacaran Doushantuo Formation deposited in shelf margin, slope, and basin environments in Hunan Province of South China. These microfossils include sphaeromorphic and acanthomorphic acritarchs (15 genera and 29 species, including three new acanthomorph species, *Bullatosphaera*? *colliformis* n. sp., *Eotylotopalla inflata* n. sp., and *Verrucosphaera*? *undulata* n. sp.), multicellular algae, tubular microfossils, and other problematic forms, representing major fossil groups similar to those from the Doushantuo Formation in more proximal facies (e.g., inner shelf and shelf lagoon). A database of the abundance and occurrences of Doushantuo acanthomorphs is assembled and analyzed using quantitative and data-visualization methods (e.g., rarefaction analysis, non-parametric multidimensional scaling, and network analysis). The results show that, at the genus and species levels, taxonomic richness of Doushantuo acanthomorphs exhibits considerable variation among facies, but this variation is largely due to sampling and taphonomic biases. The results also show that numerous acanthomorph taxa have broad facies distribution, affirming their biostratigraphic value. The analysis confirms that acanthomorphs in the Weng'an biota of shelf margin facies are composed of a mixture of Member II and Member III assemblages of shelf-lagoon facies in the Yangtze Gorges area. The study shows the biostratigraphic potential of acanthomorphs in the establishment of regional biozones using the first appearance datum of widely distributed taxa, highlighting the importance of continuing exploration of under-sampled Doushantuo sections in slope and basinal facies.

UUID: http://zoobank.org/6fc92858-4054-4117-8043-1f06cfe77155

*Corresponding author

Introduction

Globally distributed organic-walled microfossil assemblages from lower–middle Ediacaran strata indicate that microscopic eukaryotes dominated the diversity of the marine ecosystem shortly after the Cryogenian Marinoan global glaciation (Knoll and Walter, 1992; Xiao, 2004a; Peterson and Butterfield, 2005; Butterfield, 2007; Zhou et al., 2007; Moczydłowska, 2008; Narbonne et al., 2012). Because these microfossil assemblages are preserved in multiple taphonomic windows and in various depositional environments with relatively few age constraints (e.g., Grey, 2005; Xiao et al., 2014; Anderson et al., 2017; Willman et al., 2020), the integration of these assemblages to form a global picture is a challenging task. Acanthomorphic acritarchs are the most diverse eukaryotic microfossils that widely occur in lower–middle Ediacaran strata (Xiao and Narbonne, 2020). Currently available paleontological data indicate that most Ediacaran acanthomorphs are constrained between the basal Ediacaran cap dolostone and the ca. 574–567 Ma Shuram negative carbon isotope excursion (Rooney et al., 2020), although some acanthomorph taxa appear to extend into the late Ediacaran Period (e.g., Anderson et al., 2017; Arvestål and Willman, 2020; Morais et al., 2021), and even younger strata (e.g., Grazhdankin et al., 2020). Thus, Ediacaran acanthomorphic acritarchs are particularly useful for stratigraphic correlation of lower–middle Ediacaran strata (Knoll and Walter, 1992; Knoll et al., 2006b; Xiao et al., 2016; Xiao and Narbonne, 2020).

As the first attempt to establish acritarch-based Ediacaran biostratigraphy, five biozones, including four defined by acanthomorphs, were proposed and successfully applied to the subdivision and correlation of Ediacaran strata in Australia (Grey, 2005; Grey and Calver, 2007; Willman and Moczydłowska, 2008, 2011). Later studies, however, concluded that these acritarch biozones cannot be recognized and applied in Ediacaran biostratigraphic correlation in Siberia and South China (Golubkova et al., 2010; Moczydłowska and Nagovitsin, 2012; Liu et al., 2013). Acritarch biozones were also proposed based on materials from the Ediacaran Doushantuo Formation in South China, where acritarchs are as abundant and diverse as in Australia (McFadden et al., 2009; C. Yin et al., 2011; Liu et al., 2013, 2014a, b; Xiao et al., 2014; Liu and Moczydłowska, 2019). Constrained by litho- and chemostratigraphic records, acritarch biozones recognized in South China were considered promising in the subdivision and correlation of the Ediacaran System (Xiao et al., 2016; Xiao and Narbonne, 2020). However, as has been the case in Australia, efforts to recognize these biozones outside South China achieved only limited success (e.g., Xiao et al., 2022). Thus, a more comprehensive understanding of the distribution of Ediacaran acanthomorphs and their controlling factors is needed before acanthomorph biozones can be applied globally.

Permineralized microfossils from the Ediacaran Doushantuo Formation, including diverse acanthomorphic acritarchs, have been intensively studied for nearly half a century since Yin and Li (1978), with data recovered from various depositional environments and stratigraphic intervals (Liu and Moczydłowska, 2019, and references therein). Most published data came from shelf-lagoon facies in the Yangtze Gorges area of western Hubei Province, where the stratigraphic framework of the Doushantuo Formation based on litho- and chemostratigraphy has been well established (Zhou et al., 2019). Using data from the Yangtze Gorges area, acritarch biozonation schemes were recognized, based on stratigraphic variations in taxonomic composition of acritarchs and the first appearance of specific acritarch taxa (McFadden et al., 2009; C. Yin et al., 2011; Liu et al., 2013, 2014a, b; Xiao et al., 2014; Liu and Moczydłowska, 2019). Whether these variations represent evolutionary changes, environmental shifts, or preservational vagaries, however, has not been thoroughly investigated.

To assess these possibilities, microfossil investigation of the Doushantuo Formation needs to expand beyond the shelf-lagoon facies in order to capture a broader understanding of regional variations in environment and taphonomy. Several recent studies offer promising insights into Doushantuo micropaleontology in inner shelf facies in the Zhangcunping and Shennongjia areas (e.g., Ouyang et al., 2019; Ye et al., 2022) and slope facies in western Hunan Province (e.g., Hawkins et al., 2017; Ouyang et al., 2017). However, the sampling intensity of the slope facies remains low compared with the shelf-lagoon facies in the Yangtze Gorges area. Importantly, there has been no report of Doushantuo acanthomorphs from basinal facies, representing a key knowledge gap to be addressed.

In this study, we present and describe new microfossils from the Doushantuo Formation deposited in shelf margin, slope, and basinal facies in Hunan Province. Based on a compilation of Doushantuo data and updated taxonomy, we are able to present a summary of the paleogeographic and stratigraphic distribution of Ediacaran acritarch species in South China. Building upon the paleogeographic and stratigraphic distribution, we assess the wider applicability of acritarch biozones previously recognized in the Yangtze Gorges area, and tentatively correlate the Doushantuo Formation at a basinal section with the Yangtze Gorges area using these biozones. Results from this study may contribute to a more comprehensive understanding of acritarch biostratigraphy in South China and may have implications for the subdivision and correlation of the Ediacaran System.

Geological setting

The South China block consists of the Yangtze and Cathaysia blocks, which amalgamated during assembly of the Rodinia supercontinent in the early Neoproterozoic (Li et al., 2009; Li and Zhao, 2020). The South China block was positioned in middle–low latitudes in the Ediacaran Period, with a stable passive continental margin facing to the southeast (Macouin et al., 2004; Zhang et al., 2015). Overlying the Cryogenian Nantuo Formation diamictite, the Ediacaran succession in the Yangtze block consists of, in ascending order, the Doushantuo and Dengying formations or their equivalents (Cao et al., 1989).

The passive continental margin on the Yangtze block exhibited a southeastward deepening facies trend when the Doushantuo Formation was deposited, with depositional facies transitioning from shallow-water platform facies (including inner shelf, shelf lagoon, and carbonate shoal complex at the

https://doi.org/10.1017/jpa.2023.92 Published online by Cambridge University Press

platform margin) in the northwest, to deep-water slope and basinal facies in the southeast of the Yangtze block (Fig. 1.1; Cao et al., 1989; Zhu et al., 2003; Jiang et al., 2011). This first-order facies trend provides a framework for understanding the environmental distribution of early–middle Ediacaran microfossils in the Yangtze block (e.g., Xiao et al., 2012; Muscente et al., 2015), although a number of nuances (such as the spatial continuity and temporal extent of the carbonate shoal complex) are still debated (e.g., Zhu et al., 2019).

Despite the facies changes, first-order stratigraphic correlation of the Doushantuo Formation across the Yangtze block is supported by lithostratigraphic marker beds, sedimentary sequences, and carbon-isotope chemostratigraphic features. The Doushantuo Formation is subdivided into four lithostratigraphic members at its type locality in the Yangtze Gorges area (Fig. 2.1; Wang et al., 1998; Jiang et al., 2011). Member I cap dolostone can be traced across the entire Yangtze block (Zhou et al., 2004a; Jiang et al., 2011). Two shallowing-upward sequences developed in members II and III and can be recognized in different facies in the Yangtze block (Jiang et al., 2011). Member IV in the uppermost Doushantuo Formation is a black shale unit at the type section and can be used as a marker bed in the Yangtze Gorges area. In addition to lithostratigraphy, carbon isotopic profiles also serve as a useful correlation tool, especially the negative $\delta^{13}C$ excursions at the basal and in the upper Doushantuo Formation, EN1 and EN3, respectively, which have been recognized globally (Zhou et al., 2019, and references therein). These litho- and chemostratigraphic features allow us to bookend the Doushantuo Formation, even if the precise correlation of the subunits within the Doushantuo Formation can be sometimes ambiguous.

The nine study sections are located in northern Hunan Province and represent shelf margin, slope, and basinal facies in the

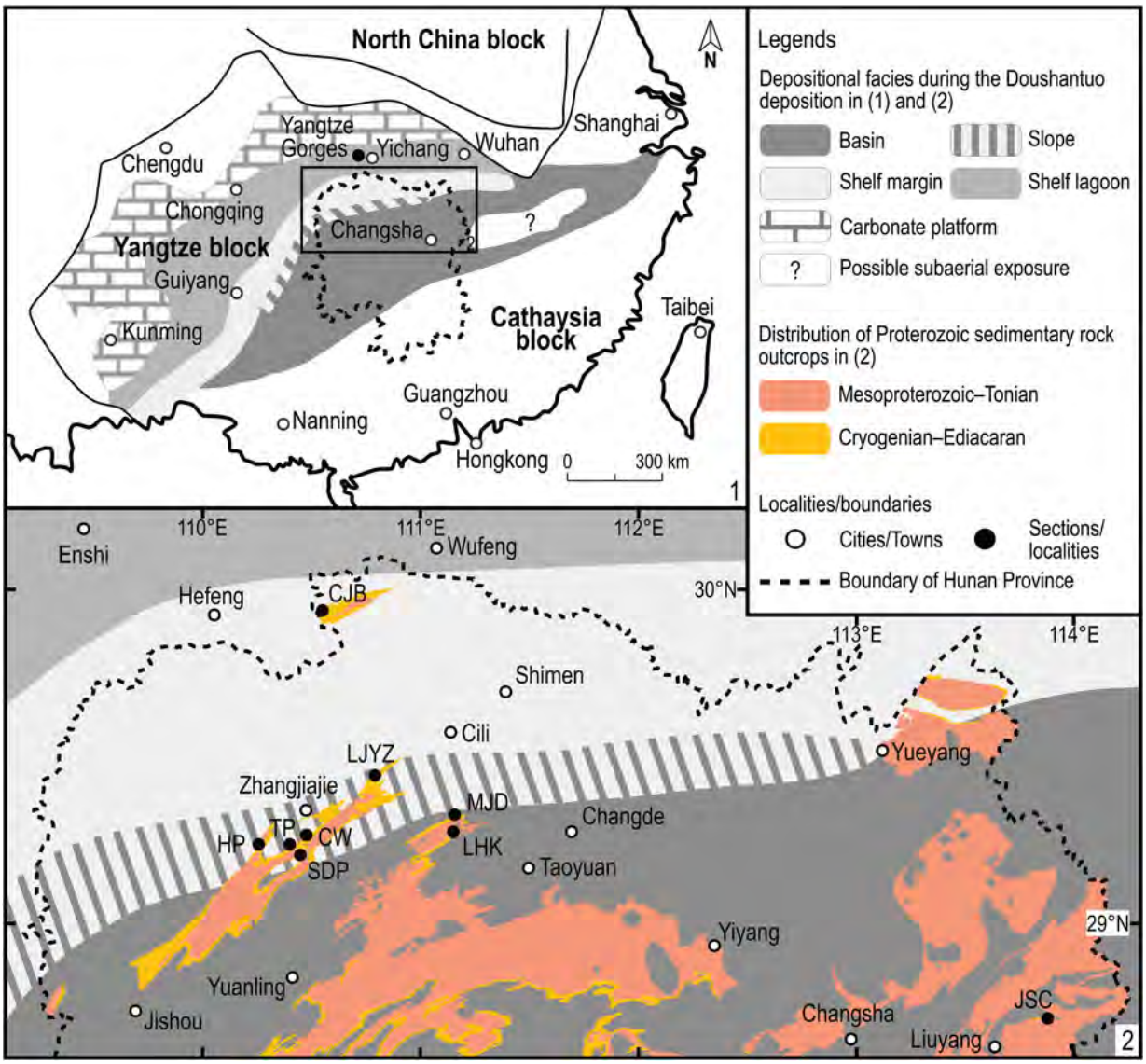

Figure 1. Ediacaran paleogeography and Proterozoic outcrop distribution in Hunan Province of South China. (**1**) Paleogeographic map of the Yangtze block during deposition of the Doushantuo Formation (modified from Jiang et al., 2011). Rectangle frame marks the location of (**2**). (**2**) Simplified geological map (modified from Luo et al., 2002) showing the distribution of Proterozoic strata in northern Hunan Province where the studied sections are located. Section abbreviations: CJB, Caojunba; LJYZ, Lujiayuanzi; HP, Heping; TP, Tianping; CW, Caowan; SDP, Siduping; MJD, Majindong; LHK, Lianghekou; JSC, Jinshichong.

https://doi.org/10.1017/jpa.2023.92 Published online by Cambridge University Press

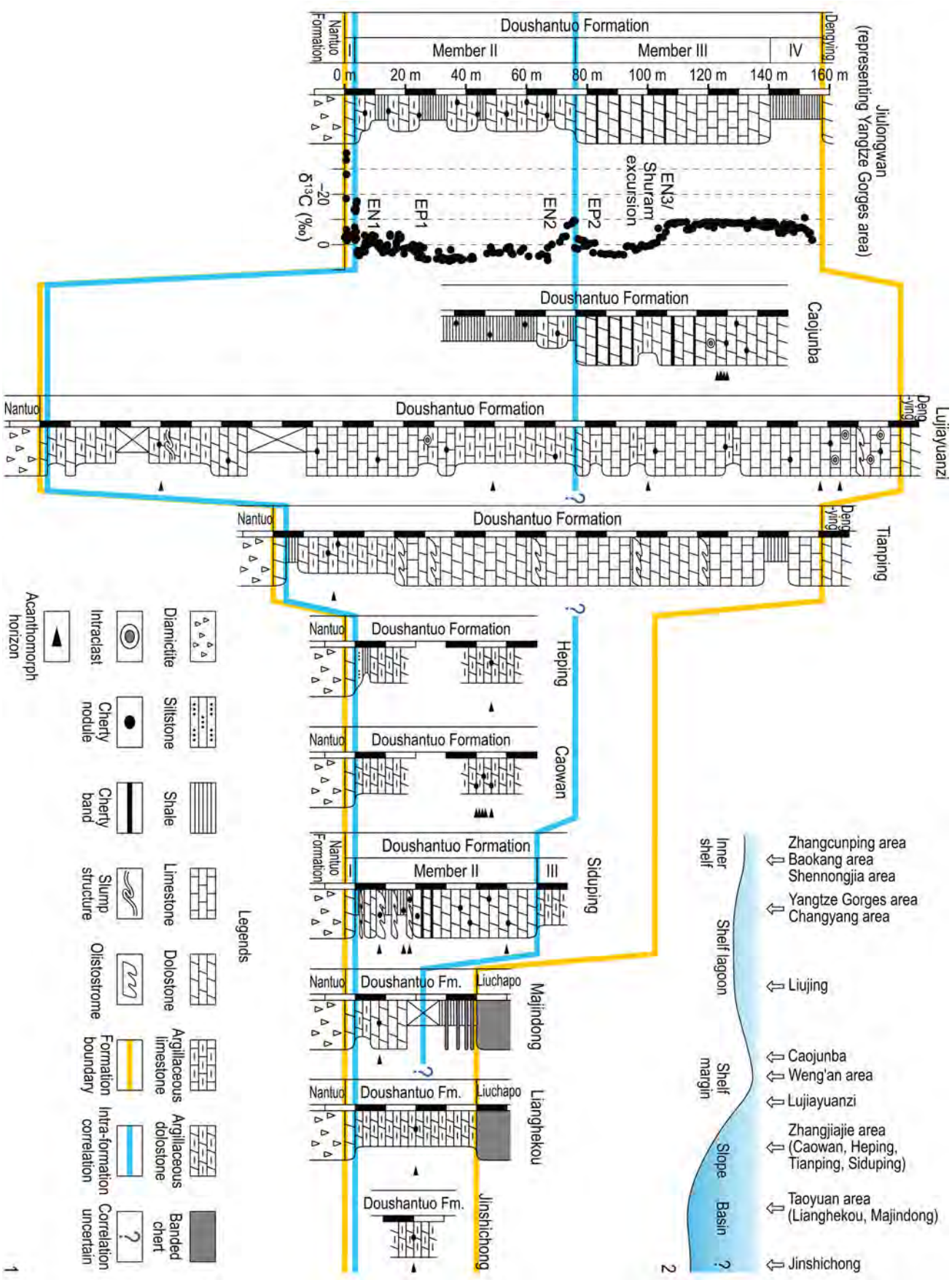

Figure 2. (**1**) Lithostratigraphic sequence of the Doushantuo Formation at studied localities, acanthomorph-bearing sampling horizons, and their correlations with those in the Yangtze Gorges area (represented by the Jiulongwan section). Lithostratigraphic column and C-isotopic profile of the Jiulongwan section modified from McFadden et al. (2008). (**2**) Generalized paleobathymetric profile showing location of Doushantuo Formation sections known to be fossiliferous. Horizontal distances and water depth are not to scale.

https://doi.org/10.1017/jpa.2023.92 Published online by Cambridge University Press

Yangtze block (Fig. 1). At some sections (e.g., the Caowan section), the Doushantuo Formation is not well exposed due to vegetation and weathering, thus field observations were made, and samples were collected from multiple adjacent outcrops, resulting in imprecise measurements of the stratigraphic heights.

The Caojunba section (GPS: 29°53′53″N, 110°32′54″E) crops out on a hill near Caojunba village, Nanbeizhen Town, Shimen County (Fig. 1.2). The Doushantuo Formation at Caojunba is composed of a lower part of grayish calcareous shale intercalated with argillaceous dolostones, and an upper part of carbonate rocks (Fig. 2.1). Detailed lithostratigraphic information on the Doushantuo Formation at Caojunba and its correlation with the adjacent Yangjiaping and Zhongling sections can be found in Shi et al. (2022). Phosphatic and silicified intraclasts occur at multiple horizons in both lower and upper parts of the Doushantuo Formation, and pisoid layers occur in the upper Doushantuo Formation, indicating a high-energy, likely upper subtidal environment. Storm-induced breccias occasionally occur in the lower part of the carbonate interval, possibly indicating a relatively deeper environment below fair-weather wave base. Millimeter-sized chert nodules occur commonly in the shales of the lower Doushantuo Formation, and centimeter-sized chert nodules occur in a 6-m-thick interval of carbonates in the upper Doushantuo Formation.

The Lujiayuanzi section (GPS: 29°13′51″N, 110°47′43″E) crops out along a country road from Lujiayuanzi village to Hu'ao village in Xikou Town, Cili County (Fig. 1.2). The Doushantuo Formation at Lujiayuanzi has a total thickness of about 280 m, beginning with the basal Ediacaran cap dolostone that is succeeded by calcareous shale and argillaceous dolostone, micritic carbonates, organic-rich limestone, and peloidal and dolomitic limestones capped by massive dolostones of the overlying Dengying Formation (Fig. 2.1). Detailed lithostratigraphic data of the Doushantuo Formation at Lujiayuanzi can be found in Ouyang et al. (2017). Abundant intraclasts were found at multiple horizons in the Doushantuo Formation at Lujiayuanzi, and cross-bedding structures occur in the upper Doushantuo Formation, possibly indicating a subtidal environment. Centimeter- and meter-scale slump structures were observed in the lower and upper Doushantuo Formation, respectively, indicating deposition in a slope environment, as is the case for many other sections in western Hunan Province (Vernhet et al., 2006; Vernhet and Reijmer, 2010). Chert nodules were found throughout the Doushantuo Formation at Lujiayuanzi.

The Caowan, Heping, Siduping, and Tianping sections are all located near Zhangjiajie City (Fig. 1.2), and the Doushantuo Formation at these sections shares similar sequences. The Siduping section (GPS: 28°55′1″N, 110°26′56″E), cropping out along a river near Siduping village about 25 km to the south of Zhangjiajie City, is one of the well-studied sections in this area (e.g., Wang et al., 2016; Hawkins et al., 2017; Nie et al., 2017). At Siduping, the Doushantuo Formation is subdivided into four members similar to those in the Yangtze Gorges area. Detailed lithostratigraphic data can be found in Wang et al. (2016). Olistostromes occur at multiple horizons throughout the Doushantuo Formation at Siduping. This study mainly focuses on the second member of the Doushantuo Formation, which is about 60 m in total thickness (Fig. 2.1). The lower 19 m is primarily shales or mudstones with olistostrome beds containing breccia that might have originated from debris flows (Fig. 3.1), and the upper 41 m mainly consist of carbonates of various bed thicknesses. Eight chert-nodule horizons were collected in the second member (Fig. 3.2), with two in olistostrome beds.

The Caowan section (GPS: 28°59′56″N, 110°28′25″E), about 2 km to the southwest of Tianmenshan Town, crops out along the road from Tianmenshan Town to Huangzhuang village. Outcrops of the Doushantuo Formation at Caowan are scattered. One outcrop of the lower Doushantuo Formation containing four chert nodule-bearing layers (Fig. 3.5) is exposed near Caowan village, and is mainly argillaceous dolostone interbedded with shales (Fig. 2.1).

The Heping section (GPS: 28°57′43″N, 110°15′21″E) is located near Heping village close to Yongmao Town, about 28 km to the southwest of Zhangjiajie City. At the Heping section, strata of the uppermost Nantuo Formation to basal Doushantuo Formation (cap dolostone and a few meters of black shale) are relatively well exposed, but overlying strata (mainly black shales with pyrite nodules) are mostly covered. Abundant millimeter- to centimeter-sized chert nodules occur in an ~0.5-m-thick shale interval of the lower–middle Doushantuo Formation and were found as float in an outcrop of the lower Doushantuo Formation.

The Tianping section (GPS: 28°57′44″N, 110°23′54″E) crops out along a creek near Tianping village, which is on the road from Caowan to Siduping. Here the Doushantuo Formation is composed of the basal Ediacaran cap dolostone, followed by a lower unit of argillaceous dolostone and dolomitic mudstone, and then an upper unit of carbonate rocks with olistostrome blocks (Fig. 3.4) and cross-stratification structures. A detailed description of the Doushantuo lithostratigraphic sequence at Tianping can be found in Shang and Liu (2020). Chert nodules occur in both the lower and upper Doushantuo Formation, and the sampled horizon in the present study (Fig. 3.3) likely correlates with the chert nodule interval in the lower Doushantuo Formation reported by Shang and Liu (2020).

The Lianghekou and Majindong sections are both in the western part of Taoyuan County (Fig. 1.2). At the Lianghekou section (GPS: 29°0′46″N, 111°8′56″E) near Dingjiafang village, the Doushantuo Formation is about 40 m thick, and is composed mainly of argillaceous dolostone and dolomitic shale (Fig. 2.1). Chert nodules (Fig. 3.6) were found at one horizon about 20 m above the cap dolostone or about 20 m below the bedded cherts of the overlying Liuchapo Formation. At the Majindong section (GPS: 29°4′57″N, 111°9′21″E) near Majindong village, which is about 6 km to the west of Ligonggang Town, the lower Doushantuo Formation crops out along a river and consists of, in ascending order, ~3 m of cap dolostone (Fig. 3.7), ~5 m of chert-nodule-bearing argillaceous dolostone and dolomitic mudstone, and ~10 m of thick-bedded dolostone (Fig. 2.1). The middle–upper Doushantuo Formation at Majindong is largely covered, and the overlying Liuchapo Formation consists of bedded cherts intercalated with black shales that yield fragments of carbonaceous compressions. At both Lianghekou and Majindong sections, the highly condensed Doushantuo Formation (total thickness less than 50 m) is characterized by the occurrence of horizontal laminations, whereas slump structures or olistostrome blocks, which are common in slope facies, have not been observed.

https://doi.org/10.1017/jpa.2023.92 Published online by Cambridge University Press

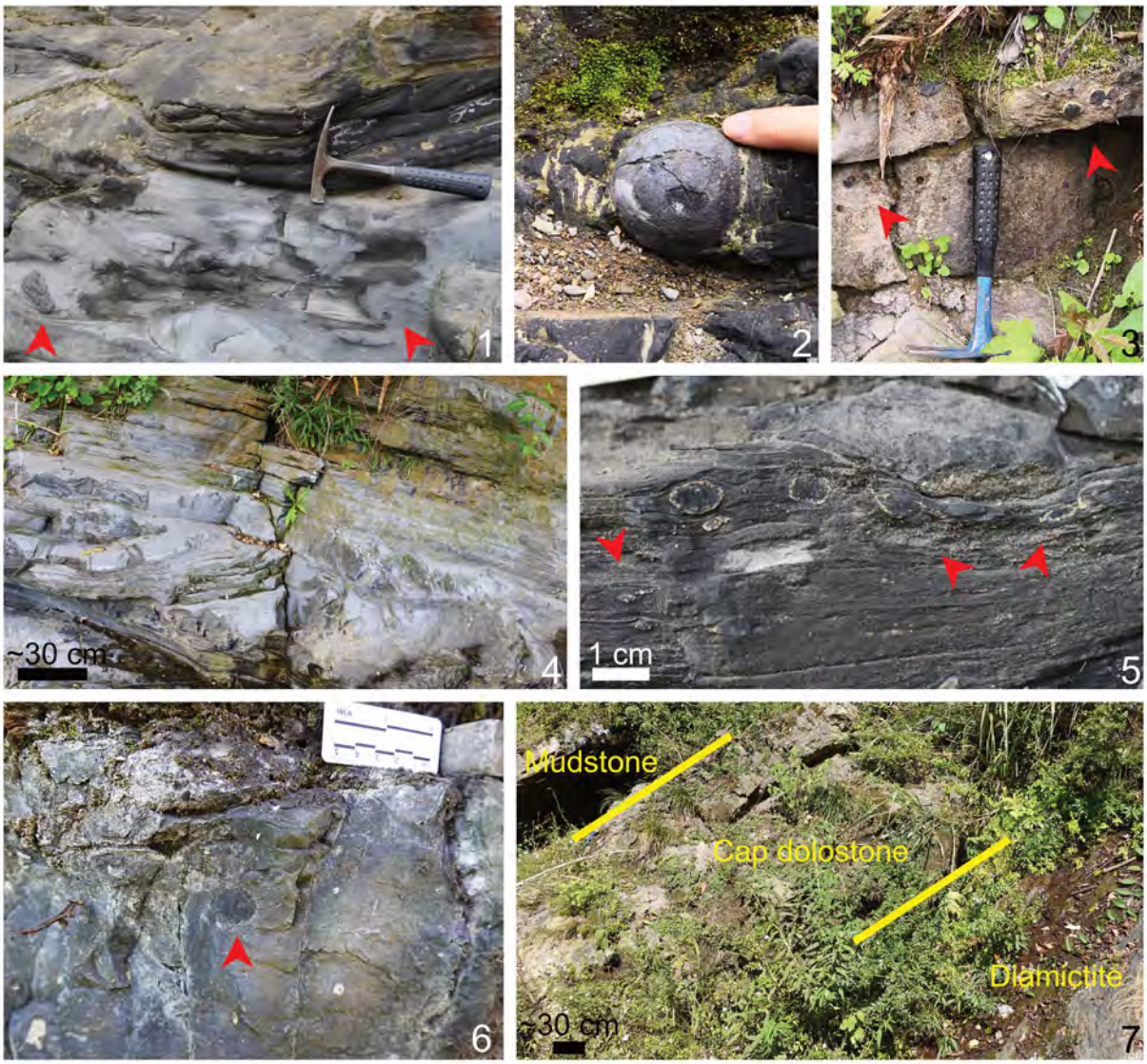

Figure 3. Outcrop photos of the Doushantuo Formation at the studied sections. (**1**) Olistostrome containing breccia (arrowheads) in shales of the lower Member II at Siduping section. (**2**) Chert nodules from the lower Member II at Siduping section (sample 19SDP-2). (**3**) Chert nodules (arrowheads) from the lower Doushantuo Formation at Tianping section (sample 19TP-1). (**4**) Olistostrome from the lower Doushantuo Formation at Tianping section. (**5**) Chert nodules (arrowheads) from shales of the lower Doushantuo Formation at Caowan section (sample 19CW-8). (**6**) A chert nodule (arrowheads) from the middle Doushantuo Formation at Lianghekou section (sample 21LHK-1). (**7**) Stratigraphic sequence of Nantuo Formation diamictite, basal Doushantuo Formation cap dolostone, and lower Doushantuo Formation calcareous shale and mudstone at Majindong section.

The Jinshichong section (GPS: 28°16′22″N, 113°52′22″E) is located at a phosphorite mine near Jinshichong village, about 3 km to the southeast of Yonghe Town, Liuyang City (Fig. 1.2). Here only several meters of black shales with millimeter- to centimeter-sized chert nodules were observed (Fig. 2.1), which belong to the lower Doushantuo Formation according to a report of the local geological survey (Geological Bureau of the Hunan Provincial Revolutionary Committee, 1976).

Lithostratigraphic sequences of the Doushantuo Formation, supplemented with carbon isotope profiles, have been applied to the correlation among different areas in South China (e.g., Wang et al., 2016, 2020; Ouyang et al., 2017, 2019; Ye et al., 2022). In most areas of South China, the Doushantuo Formation above the cap dolostone can be generally divided into two parts: the lower part dominated by siliciclastic rocks or argillaceous carbonate rocks (corresponding to Member II in the Yangtze Gorges area), and the upper part dominated by carbonates (corresponding to Member III in the Yangtze Gorges area) (Fig. 2.1). These two parts are widely interpreted by various authors as representing two shallowing-upward sequences, although recognition of a particular physical surface that separate these two sequences is still open to debate (e.g., Jiang et al., 2007, 2011; Zhou et al., 2007; Zhu et al., 2007; McFadden et al., 2008). The lower and the upper parts of the Doushantuo Formation each exhibits chemo- and biostratigraphic features that are regionally consistent (e.g., Zhou et al., 2007; Xiao et al., 2012; Liu and Moczydłowska, 2019), indicating that they likely represent chronostratigraphic units. Under this bipartite framework, samples of the studied Doushantuo successions can be correlated with either the lower part (all sampled horizons at sections in

https://doi.org/10.1017/jpa.2023.92 Published online by Cambridge University Press

the Zhangjiajie area, at the Majindong section, and at the Jinshichong section; the lower five sampled horizons at the Caojunba section; and the lower four sampled horizons at the Lujiayuanzi section), or the upper part (the upper six sampled horizons at the Caojunba section; and the upper 15 sampled horizons at the Lujiayuanzi section) of the Doushantuo Formation (Table 1, Fig. 2.1). The Doushantuo Formation at the Lianghekou section is not well exposed and for most part is dominated by argillaceous carbonates, making it difficult to correlate the single sample horizon at the Lianghekou section. However, since the lower part of the Doushantuo Formation is generally stratigraphically thicker than the upper part in sections where they are easily recognizable, the sampled horizon in the middle of the Doushantuo Formation at the Lianghekou section more likely correlates to the lower part of the Doushantuo Formation elsewhere.

Combined with sedimentary structures and lithofacies analyses, lithostratigraphic sequence data of the Doushantuo Formation are also used to determine the paleogeographic locations of the studied sections during the early Ediacaran Period. The Caojunba section, with plenty of intraclast-rich carbonate deposits (such as reworked breccia and pisoidal layers) in its upper part, is inferred to be located on the proximal side of the shelf margin carbonate shoal complex, with the Doushantuo Formation being deposited in a shallow subtidal environment (Shi et al., 2022). The Doushantuo Formation at the Lujiayuanzi section has the greatest stratigraphic thickness, is dominated by carbonate lithologies, and contains intraclasts, cross-beds, and slump structures at different scales. These structures indicate that the Lujiayuanzi section was likely deposited in a shallow subtidal environment of the upper slope facies (Ouyang et al., 2017). Sections in the Zhangjiajie area were likely located in the lower slope facies, considering the occurrence of olistostromes and debris flows (e.g., Vernhet et al., 2006; Wang et al., 2016; Hawkins et al., 2017). The Doushantuo Formation at Lianghekou and Majindong is highly condensed and rich in fine-grained siliciclastic sediments, potentially indicating deposition in an offshore low-energy basinal environment, which is consistent with the absence of olistostromes and with previously published paleogeographic reconstructions (e.g., Vernhet et al., 2006; Jiang et al., 2011; Zhu et al., 2019). Eastern Hunan Province is generally considered to have been in the basin during deposition of the Doushantuo Formation (Cao et al., 1989; Zhu et al., 2003; Jiang et al., 2011; Zhu et al., 2019). However, the local occurrence of intraclastic phosphorite at the Jinshichong section indicates deposition in relatively shallow-water environments (Muscente et al., 2015). In this study, we provisionally accept the traditional view that the Jinshichong section was deposited in a basinal environment, but this interpretation may be revised pending further detailed sedimentological investigations in this area.

Variation in the abundance of chert nodule layers in the studied successions also supports the inferred paleogeographic location of the studied sections (see Fig. 2.2). At the shallow-water Caojunba and Lujiayuanzi sections, chert nodule horizons are found throughout the Doushantuo Formation (i.e., >10 horizons at each section). At the sections in the Zhangjiajie area, chert nodules are also abundant, but occur at fewer horizons (maximum eight horizons in each section). At the Majindong and the Lianghekou sections, chert nodules are only found at one horizon in the entire Doushantuo Formation. The decrease in the number of chert nodule horizons from the shallow-water shelf margin (Caojunba and Lujiayuanzi sections) to the deep-water basinal environment (Majindong and Lianghekou sections) is consistent with the view that chert nodules are more likely to form in shallow-water settings with enriched SiO_4^{2-} and sufficient supply of organic matter (Knoll, 1985; Muscente et al., 2015; Gao et al., 2020).

Materials and methods

Sample collection, microfossil examination, and systematic descriptions.—Forty-nine rock samples were collected from chert-nodule and -band horizons in the Doushantuo Formation at Caojunba, Lujiayuanzi, Tianping, Caowan, Heping, Siduping, Majindong, Lianghekou, and Jinshichong sections (Fig. 2.1, Table 1), from which 508 thin sections (mostly cut parallel to bedding surfaces) were made for micropaleontological investigations. Details of samples and thin sections are given in Table 1. Thin sections were examined for microfossils under Olympus BX-51 and Zeiss Axioscope A1 transmitted light microscopes, with microfossils photographed using Olympus DP 72 and DP 74 digital cameras attached to the microscopes. All microfossils encountered in thin sections were recorded with stage coordinates, and illustrated specimens were additionally positioned using an England Finder slide. Dimensions of microfossils were measured using Image Pro Express and ImageJ software on digital photographs. Numbers of specimens were counted for each acanthomorphic acritarch species in each chert sample and at each stratigraphic section, and the relative abundance of each species was calculated.

Systematic descriptions are given for acanthomorphic acritarchs that are identifiable at the species level, with descriptive terminology following that of Xiao et al. (2014), and taxonomical nomenclature following the International Code of Nomenclature for Algae, Fungi, and Plants (Turland et al., 2018). Statistics relating to dimension measurements are given in the systematic description of each taxon: "n" represents the number of specimens measured, "mean" the average among the specimens, and "SD" the standard deviation among the specimens. For each specimen, the measurement of each morphological feature was repeated multiple times (depending on preservation state) on different positions to obtain an average value.

Taxonomic revision and data analysis.—Occurrence data of Doushantuo acanthomorphic acritarchs and certain sphaeromorphic taxa considered stratigraphically useful (e.g., *Schizofusa zangwenlongii* Grey, 2005) are compiled from 55 previously published studies, with many taxonomic revisions based on systematic treatments in this study and in recently published systematic works (e.g., Ouyang et al., 2021; Xiao et al., 2022; Ye et al., 2022). Details of taxonomic revisions of published acanthomorph specimens from the Doushantuo Formation are summarized in the Supplemental Materials and described in the Systematic paleontology section. Fossil occurrence data without clear, published, microfossil images or stratigraphic horizons were excluded from our compilation. Also excluded were fossils described in open nomenclature, with the exception of *Weissiella* cf. *W. grandistella*, which has been systematically reviewed by Ouyang et al. (2021), confirming its presence from multiple localities and facies.

https://doi.org/10.1017/jpa.2023.92 Published online by Cambridge University Press

Table 1. Sample number, stratigraphic height, number for thin sections, and microfossil abundance data of the Doushantuo Formation from the nine studied sections in Hunan Province. Refer to Figure 2 for stratigraphic height measurements. Refer to Geological setting section for GPS coordinates of the sections. PN = present, not counted; \ = not observed.

stratigraphic section	sample	stratigraphic height (m)	number of thin sections	acanthomorphic acritarchs	sphaeromorphic acritarchs	multicellular algae	tubular microfossils	*Polybessurus*	filaments and coccoids
Caojunba	21CJB-82	−38	5	\	\	\	\	\	PN
(0 m at the boundary	21CJB-81	−28	1	\	\	\	\	\	\
between the calcareous	21CJB-79	−19	1	\	\	\	\	\	\
shale interval and the	21CJB-74	−0.8	7	\	\	\	\	\	\
carbonate interval); shelf	21CJB-72	0.2	12	\	PN	\	\	\	PN
margin facies	21DC-5	46.7	4	43	PN	\	\	\	PN
	21DC-4	47.7	12	5	PN	\	\	\	PN
	21DC-6	48	15	4	PN	\	\	\	PN
	21DC-3	48.9	5	5	PN	\	\	\	PN
	21DC-2	49.9	40	41	PN	\	3	\	PN
	21DC-1	52.3	2	\	\	\	\	\	\
Lujiayuanzi	14HA-30	40	3	1	\	\	\	\	PN
(0 m at the base of the	14HA-53	91.4	5	\	\	\	\	\	PN
Doushantuo Formation);	14HA-67	114.8	5	\	\	1	\	\	\
slope facies	14HA-85	149.5	5	1	\	\	\	\	\
	14HA-114	199.7	5	\	\	\	\	\	\
	14HA-115	200.7	3	5	\	\	\	\	PN
	14HA-121	212.8	8	\	PN	\	\	\	PN
	14HA-122	213.3	5	\	\	\	\	\	\
	14HA-123	213.4	5	\	PN	\	\	\	\
	14HA-124	213.5	5	\	\	\	\	\	\
	15HA-30	227.4	3	\	\	\	\	\	\
	15HA-31	228.4	5	\	PN	\	\	\	\
	15HA-4	257.5	5	1	\	\	\	\	\
	15HA-6	258.5	5	\	\	\	\	\	\
	14HA-140	264	5	20	\	\	\	\	\
	15HA-10	264.2	2	\	\	\	\	\	\
	15HA-12	269.5	1	\	\	\	\	\	\
	15HA-13	270	4	\	\	\	\	\	PN
	15HA-14	279	4	\	\	\	\	\	\
Caowan	19CW-5	0	34	8	PN	\	\	\	PN
(0 m at an arbitrary horizon	19CW-6	1	21	18	PN	1	2	\	PN
in middle part of the	19CW-7	2	3	\	\	\	\	\	\
Doushantuo Formation);	19CW-8	3	6	\	\	\	\	\	\
slope facies	19CW-9	5	7	1	\	\	\	\	PN
Heping;	19HP-1	lower–middle Doushantuo Formation	36	2	PN	\	\	\	PN
slope facies	19HP-2	lower Doushantuo Formation (float)	7	\	\	\	\	\	PN
Siduping	19SDP-1	8	30	3	\	4	\	\	PN
(0 m at the top of cap	(olistostrome)								
dolostone);	19SDP-2	16	6	1	\	\	\	\	\
slope facies	19SDP-3	18	22	1	\	\	\	\	PN
	(olistostrome)								
	19SDP-4	20	4	\	\	\	\	\	\
	19SDP-5	21	6	\	\	\	\	\	\
	19SDP-6	24	6	\	\	\	\	\	\
	19SDP-7	50	27	22	PN	\	1	\	PN
	19SDP-8	55	1	\	\	\	\	\	\
Tianping;	19TP-1	lower Doushantuo Formation	41	14	PN	\	\	1	PN
slope facies									

Table 1. Continued.

stratigraphic section	sample	stratigraphic height (m)	number of thin sections	acanthomorphic acritarchs	sphaeromorphic acritarchs	multicellular algae	tubular microfossils	*Polybessurus*	filaments and coccoids
Majindong (0 m at the base of the Doushantuo Formation); basinal facies	21MJD-1	8	13	2	\	\	1	1	PN
Lianghekou (0 m at the top of cap dolostone); basinal facies	21LHK-1	20	20	7	PN	\	\	\	PN
Jinshichong; basinal facies	18JSC-2	lower–middle Doushantuo Formation	31	1	PN	\	\	\	PN

Rarefaction analysis was performed on selected acritarch abundance data from this and previously published studies to assess the influence of sample size on taxonomic richness (Raup, 1975). Rarefaction curves were generated in Rstudio using the rarefy function in the vegan package (R Core Team, 2018; Oksanen et al., 2019).

A non-parametric multidimensional scaling (NMDS) analysis was employed to compare taxonomically revised acanthomorph occurrence data from 82 Doushantuo collections in this and 55 previously published studies (see Supplemental Materials). A collection is defined as an acanthomorphic acritarch assemblage from a stratigraphic unit (differentiated as Member II or Member III and their correlatives) at a specific area reported in an independent study. The NMDS analysis was applied on presence/absence data of taxonomic occurrences in each collection, using the metaMDS function from the vegan package in Rstudio, with distance using the Raup-Crick similarity and maximum iteration = 100. The collections ordinated by two-dimensional NMDS were then shown in a scatterplot defined by NMDS1 and NMDS2, with collections grouped into and color-coded by depositional facies or stratigraphic intervals, which were outlined by convex hulls.

Network analysis was performed to visualize the spatial and stratigraphic distribution of Ediacaran acanthomorphs in South China. The graph_from_incidence_matrix function in the Rstudio igraph package (Csárdi and Nepusz, 2006) with its default parameters was used to analyze the same taxonomic occurrence data of Doushantuo acanthomorphs used in the NMDS analysis in order to generate an unweighted bipartite network graph, in which each species is linked to its hosting collections. As in NMDS plots, collections are grouped into and color-coded by depositional facies or stratigraphic intervals.

Repository and institutional abbreviation.—All samples and thin sections are reposited in the Nanjing Institute of Geology and Palaeontology, Chinese Academy of Sciences (NIGPAS). Illustrated specimens are housed at the Fossil Repository of NIGPAS, with a catalog number prefix of PB.

Systematic paleontology

Group Acritarcha Evitt, 1963

Genus *Appendisphaera* Moczydłowska, Vidal, and Rudavskaya, 1993, emend. Moczydłowska, 2005

Type species.—*Appendisphaera* grandis Moczydłowska, Vidal, and Rudavskaya, 1993, emend. Moczydłowska, 2005.

Other species.—*Appendisphaera anguina* Grey, 2005; *A.*? *brevispina* Liu et al., 2014a; *A. clava* Liu et al., 2014a; *A. clustera* Liu and Moczydłowska, 2019; *A. fragilis* Moczydłowska, Vidal, and Rudavskaya, 1993; *A. heliaca* (Liu and Moczydłowska, 2019) Ouyang et al., 2021; *A.*? *hemisphaerica* Liu et al., 2014a; *A. lemniscata* Liu and Moczydłowska, 2019; *A. longispina* Liu et al., 2014a; *A. longitubularis* (Liu et al., 2014a) Liu and Moczydłowska, 2019; *A. magnifica* (Zhang et al., 1998) Liu et al., 2014a; *A. setosa* Liu et al., 2014a; *A. tabifica* Moczydłowska, Vidal, and Rudavskaya, 1993; *A. tenuis* Moczydłowska, Vidal, and Rudavskaya, 1993.

https://doi.org/10.1017/jpa.2023.92 Published online by Cambridge University Press

Remarks.—The latest emendation diagnoses *Appendisphaera* as a genus of acanthomorphic acritarch with "simple, homomorphic, slim, cylindrical or ciliate" processes, which can be either straight or tapering, and can have a basal expansion and a rounded or blunt termination (Moczydłowska, 2005, p. 293). These features, however, are found in many other genera such as *Cavaspina*, *Knollisphaeridium*, *Tanarium*, and even *Xenosphaera*. Therefore, systematic morphometric work is required to develop a practical workflow to distinguish these taxa, including *Appendisphaera*, that fall into the category of "acanthomorphs with hollow, tapering, conical processes" by Grey (2005, p. 172–175).

Appendisphaera grandis Moczydłowska, Vidal, and Rudavskaya, 1993, emend. Moczydłowska, 2005
Figure 4

1993 *Appendisphaera grandis* Moczydłowska, Vidal, and Rudavskaya, p. 503, text-fig. 5, pl. 1, figs. 1, 2.
2005 *Appendisphaera grandis* Moczydłowska et al.; Moczydłowska, p. 294, figs. 3, 4.
2006a *Appendisphaera grandis*; Knoll et al., fig. 3g.
2008 *Appendisphaera grandis* Moczydłowska et al., emend. Moczydłowska; Willman and Moczydłowska, p. 519, fig. 6C.
2010 *Appendisphaera grandis*; Chen et al., fig. 2.1.
2010 *Appendisphaera grandis* Moczydłowska et al.; Golubkova et al., pl. 1, fig. 1, pl. 3, figs 4, 10.
2014 *Appendisphaera grandis* Moczydłowska et al., emend. Moczydłowska; Xiao et al., p. 9, fig. 3.1–3.3.
non 2014 *Appendisphaera grandis* Moczydłowska et al., emend. Moczydłowska; Shukla and Tiwari, p. 215, fig. 4D, E.
2015 *Appendisphaera grandis* Moczydlowska et al. [sic]; Nagovitsin and Kochnev, fig. 4.I.1, 4.I.2.
2016 *Appendisphaera grandis* Moczydłowska et al., emend. Moczydłowska; Prasad and Asher, p. 42, pl. II, figs. 3, 4.
2017 *Appendisphaera grandis*; Anderson et al., fig. 2B.
2017 *Appendisphaera crebra*; Hawkins et al., fig. 9E, F.
2017 *Appendisphaera fragilis*; Ouyang et al., fig. 8D–F.
2019 *Appendisphaera grandis* Moczydłowska et al., emend. Moczydłowska; Anderson et al., p. 507, fig. 6A–D.
2019 *Appendisphaera grandis* Moczydłowska et al., emend. Moczydłowska; Liu and Moczydłowska, p. 48, figs. 21–23.
2019 *Appendisphaera grandis*; Ouyang et al., fig. 8I–K.
2019 *Appendisphaera grandis* Moczydłowska et al., emend. Moczydłowska; Shang et al., p. 7, fig. 3.
2019 *Appendisphaera clava*; Ouyang et al., fig. 8E, F.
2020 *Appendisphaera grandis* Moczydłowska et al., emend. Moczydłowska; Shang and Liu, p. 156, fig. 4.
2021 *Appendisphaera grandis* Moczydłowska et al., emend. Moczydłowska; Ouyang et al., fig. 10M–P.
non 2021 *Appendisphaera grandis*; Liu et al., fig. 5.4.
2022 *Appendisphaera grandis* Moczydłowska et al., emend. Moczydłowska; Shi et al., fig. 7A, B.
2022 *Appendisphaera grandis* Moczydłowska et al., emend. Moczydłowska; Xiao et al., fig. 7.
2022 *Appendisphaera grandis* Moczydłowska et al., emend. Moczydłowska; Ye et al., fig. 10A–D.
non 2022 *Appendisphaera grandis* Moczydłowska et al., emend. Moczydłowska; Ye et al., fig. 10E, F.
2023 *Appendisphaera grandis* (Moczydłowska et al.) emend. Moczydłowska; Golubkova, pl. 7, fig. 1.

Holotype.—PMU-Sib.1-R/63/2, reposited at Uppsala University, from the Ediacaran Khamaka Formation, Nepa–Botuoba region, Yakutia, Siberia (Moczydłowska, Vidal, and Rudavskaya, 1993, p. 503, text-fig. 5A–D).

Description and measurements.—Vesicle mostly compressed but originally spheroidal, medium to large in size, bearing numerous, evenly and densely distributed processes. Processes hollow, long and slim, cylindrical for most part, lack significant basal expansion. Three least-deformed specimens yield vesicle diameters of ~152–373 µm. Approximately 12–28 processes per 100 µm of vesicle periphery. Full length of processes difficult to measure due to deformation but estimated to exceed 20 µm and making up >10% of vesicle diameter (18.5–39.5 µm, 9.0–12.2% of vesicle diameter). Process width 0.1–1.3 µm (N = 8, mean = 0.6 µm, SD = 0.4 µm).

Material.—Five illustrated specimens (Fig. 4) and three additional specimens.

Remarks.—As for the type species of *Appendisphaera*, *A. grandis* was initially distinguished by its proportionally long and hair-like processes (Moczydłowska et al., 1993), but the processes were later found to be hollow and cylindrical (Moczydłowska, 2005). Measurements on photos of the eight *A. grandis* specimens from its type locality published by Moczydłowska et al. (1993) and Moczydłowska (2005) reveal relatively small morphological variations: small to medium-sized vesicle (diameter 77–130 µm, mean = 107 µm, SD = 16 µm), relatively long and thin processes (process length 12.0–25.3 µm, mean = 18.4 µm, SD = 5.4 µm; process length to vesicle diameter ratio 10.8–23.0%, mean = 17.2%, SD = 4.7%; process basal width 0.4–1.8 µm, mean = 1.2 µm, SD = 0.4 µm), and large process density (46–65 processes per 100 µm of vesicle periphery, but this may be an overestimation since these eight specimens are all preserved as carbonaceous compressions). In summary, the processes of *A. grandis* from the type locality make up almost 20% of vesicle diameter and are so thin (basal width ~1 µm) that their shape is better described as cylindrical than conical, even though gradual terminal tapering can be observed on both holotype and paratype of this species.

With additional specimens assigned to this species in recent years (especially permineralized specimens), the morphospace of *A. grandis* has grown rapidly. *Appendisphaera grandis* currently contains specimens with a large vesicle (diameter up to several hundred microns) and process lengths about 10% of

https://doi.org/10.1017/jpa.2023.92 Published online by Cambridge University Press

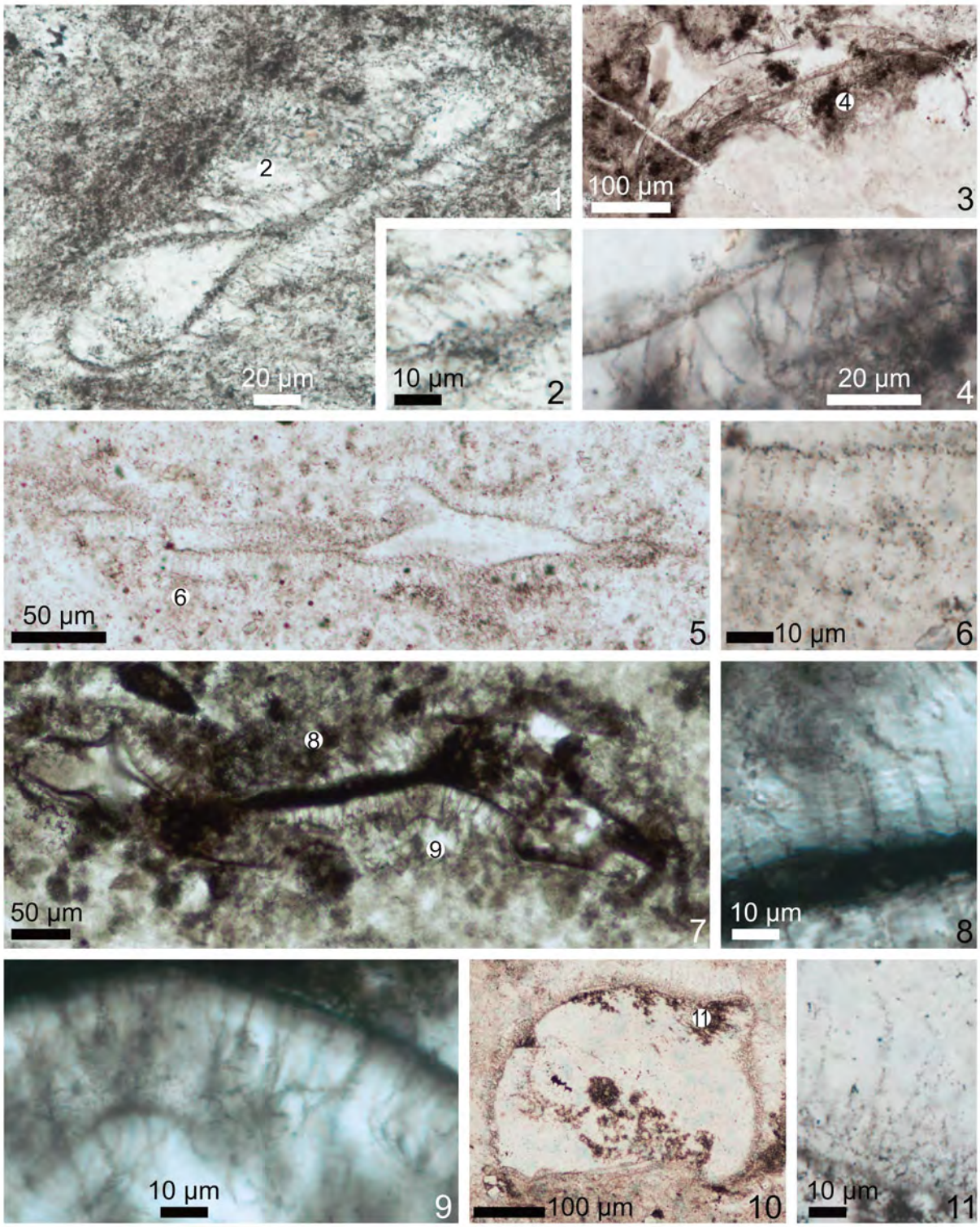

Figure 4. *Appendisphaera grandis* Moczydłowska, Vidal, and Rudavskaya, 1993, emend. Moczydłowska, 2005. (**1, 2**) PB201998, thin section 18JSC-2-5, U40/4; circled 2 in (**1**) marks area magnified in (**2**). (**3, 4**) PB201999, thin section 19HP-1-33, N41/1; circled 4 in (**3**) marks area magnified in (**4**). (**5, 6**) PB202000, thin section 19TP-1-19, D49/4; circled 6 in (**5**) marks area magnified in (**6**). (**7–9**) PB202001, thin section 19SDP-2-d1, Y24/1; circled 8 and 9 in (**7**) mark areas magnified in (**8**) and (**9**), respectively. (**10, 11**) PB202002, thin section 21DC-5-4, V34/1; circled 11 in (**10**) marks area magnified in (**11**).

vesicle diameter. Despite this, *A. grandis* is still characterized by its relatively long, thin, and almost cylindrical processes, which differentiates it from other *Appendisphaera* species with relatively short processes (e.g., *A. clava* and *A. tenuis*) and those species with basally expanded processes (e.g., *A. longitubularis*, *A. longispina*, and *A. magnifica*; see also remarks under *A. magnifica*). In this study, only specimens with process basal width around 1 μm and no more than 2 μm, and process

https://doi.org/10.1017/jpa.2023.92 Published online by Cambridge University Press

proportional length greater than 10% of vesicle diameter are accepted as *A. grandis*. Based on these criteria, the specimen illustrated by Liu et al. (2021, fig. 5.4) is removed from *A. grandis*. Its long, thick, terminally cylindrical processes resemble those of *A. longitubularis* and *Tanarium gracilentum* (Yin in Yin and Liu, 1988) Ouyang et al., 2021, which also have distally tapered and densely arranged processes. Similarly, the specimen illustrated as *A. grandis* by Ye et al. (2022, fig. 10E, F), bearing apparently conical processes with a basal width exceeding 5 μm, is more appropriately placed in *A. longispina*.

Appendisphaera magnifica (Zhang et al., 1998) Liu et al., 2014a
Figure 5

1998 *Meghystrichosphaeridium magnificum* Zhang et al., p. 36, fig. 10.5, 10.6.
?2007 *Meghystrichosphaeridium magnificum*; Zhou et al., fig. 4E.
2011 *Meghystrichosphaeridium magnificum*; C. Yin et al., fig. 5d.
2013 *Meghystrichosphaeridium magnificum* Zhang et al.; Liu et al., fig. 11I, J.
2014a *Appendisphaera magnifica* (Zhang et al.), Liu et al., p. 21, figs. 5.8, 19.1–19.6, 20.1–20.6.
2015 *Appendisphaera magnifica* (Zhang et al.) Liu et al.; Ouyang et al., p. 215, pl. I, figs. 1, 2, 4.
2017 *Appendisphaera magnifica*; Hawkins et al., fig. 9A, B.
2021 *Appendisphaera magnifica* (Zhang et al.) Liu et al.; Ouyang et al., fig. 11I, J.

Holotype.—WCHB-789b-24, reposited at Peking University Paleontological Collection, from the Ediacaran Doushantuo Formation, Weng'an area, Guizhou Province, South China (Zhang et al., 1998, p. 36, fig. 10.5, 10.6).

Description and measurements.—Vesicle medium-sized, originally spheroidal but some deformed to varying degrees. Processes uniformly conical, long, and thin, tapering gradually toward the terminal end, evenly and densely arranged on the vesicle, basally separate. Vesicle diameter 98–167 μm (N = 16, mean = 132 μm, SD = 19 μm); process length 12.2–26.3 μm (N = 17, mean = 18.6 μm, SD = 3.8 μm), 9.5–21.3% of vesicle diameter (N = 16, mean = 14.2%, SD = 3.0%), process basal width 2.0–4.9 μm (N = 17, mean = 3.0 μm, SD = 0.8 μm); 16–30 processes (N = 16, mean = 22, SD = 4) per 100 μm of vesicle periphery.

Material.—Six illustrated specimens (Fig. 5) and 11 additional specimens.

Remarks.—The 17 specimens described here are similar to the holotype of *Appendisphaera magnifica* in the closely arranged, basally separate, and acutely tapering processes. But they are significantly smaller than the holotype, whose vesicle diameter is about 350 μm. However, they are similar to the *A. magnifica* specimens in Liu et al. (2014a) in dimensions, with the latter yielding a vesicle diameter of 100–160 μm, process length of 19–36 μm (14–30% of vesicle diameter), process basal width of 2.1–3.4 μm, and 20–24 processes per 100 μm of vesicle periphery.

Liu et al. (2014a) transferred "*Meghystrichosphaeridium*" *magnificum* to *Appendisphaera*, on the basis of its very thin and densely distributed processes. However, Liu and Moczydłowska (2019) synonymized *Appendisphaera magnifica* with *A. grandis* without justification. *Appendisphaera* is one of the richly speciose genera of Ediacaran acanthomorphs (Xiao et al., 2022), and the differentiation of species within this genus has become a problem. Morphological analysis of the Cambrian acanthomorphic genus *Skiagia* indicates that morphological variation of this richly speciose genus may reflect phenotypic plasticity (Wallet et al., 2022). The same can be said of *Appendisphaera*, and it is possible that *A. magnifica* and *A. grandis* are synonymous. Although *A. magnifica* and *A. grandis* do share morphological similarities (e.g., process density, proportional length), the processes of *A. magnifica* have a relatively wider base, making its processes more conical in shape and different from the more cylindrical processes of *A. grandis* (Moczydłowska, 2005). Post-mortem degradation or deformation may cause process shrinkage and account for the thinner processes of *A. grandis*, but there are many delicately preserved specimens of *A. grandis*, both permineralized (e.g., Liu and Moczydłowska, 2019, figs. 21, 22) and preserved as carbonaceous compressions (e.g., type specimens from Siberia, Moczydłowska et al. 1993) that are unlikely to be deformed variants of *A. magnifica*. Thus, we retain *A. magnifica* as a distinct form species.

Appendisphaera tenuis Moczydłowska, Vidal, and Rudavskaya, 1993, emend. Moczydłowska, 2005
Figure 6

1993 *Appendisphaera tenuis* Moczydłowska, Vidal, and Rudavskaya, p. 506, text-fig. 7.
2004 *Appendisphaera minima* Nagovitsin and Faizullin in Nagovitsin et al., p. 12, pl. I, figs. 1–3.
2005 *Appendisphaera tenuis* Moczydłowska et al.; Grey, p. 224, figs. 88F, 113A–D.
2005 *Appendisphaera tenuis* Moczydłowska et al., emend. Moczydłowska, p. 296, fig. 5.
2005 *Ericiasphaera polystacha* Grey, p. 264, figs. 169, 170.
non 2007 *Appendisphaera tenuis*; Yin et al., fig. 1b.
?2008 *Appendisphaera tenuis* Moczydłowska; Vorob'eva et al., fig. 2k, l.
2008 *Appendisphaera tenuis* Moczydłowska et al., emend. Moczydłowska; Willman and Moczydłowska, p. 520, figs. 7B, C, 8A, B.
2010 *Appendisphaera tenuis* Moczydłowska et al.; Golubkova et al., pl. I, fig. 2, pl. III, figs. 5, 6.
?2010 *Ericiasphaera* aff. *E. addspersa* Grey; Golubkova et al., pl. IV, fig. 6a, b.
2011 *Appendisphaera tenuis* Moczydłowska et al., emend. Moczydłowska; Sergeev et al., p. 1002, fig. 5.4–5.6.
?2011 *Cavaspina amplitudinis* Willman in Willman and Moczydłowska, p. 25, pl. I, figs. 1–6.
2014a *Appendisphaera tenuis* Moczydłowska et al., emend. Moczydłowska; Liu et al., p. 31, fig. 23.

https://doi.org/10.1017/jpa.2023.92 Published online by Cambridge University Press

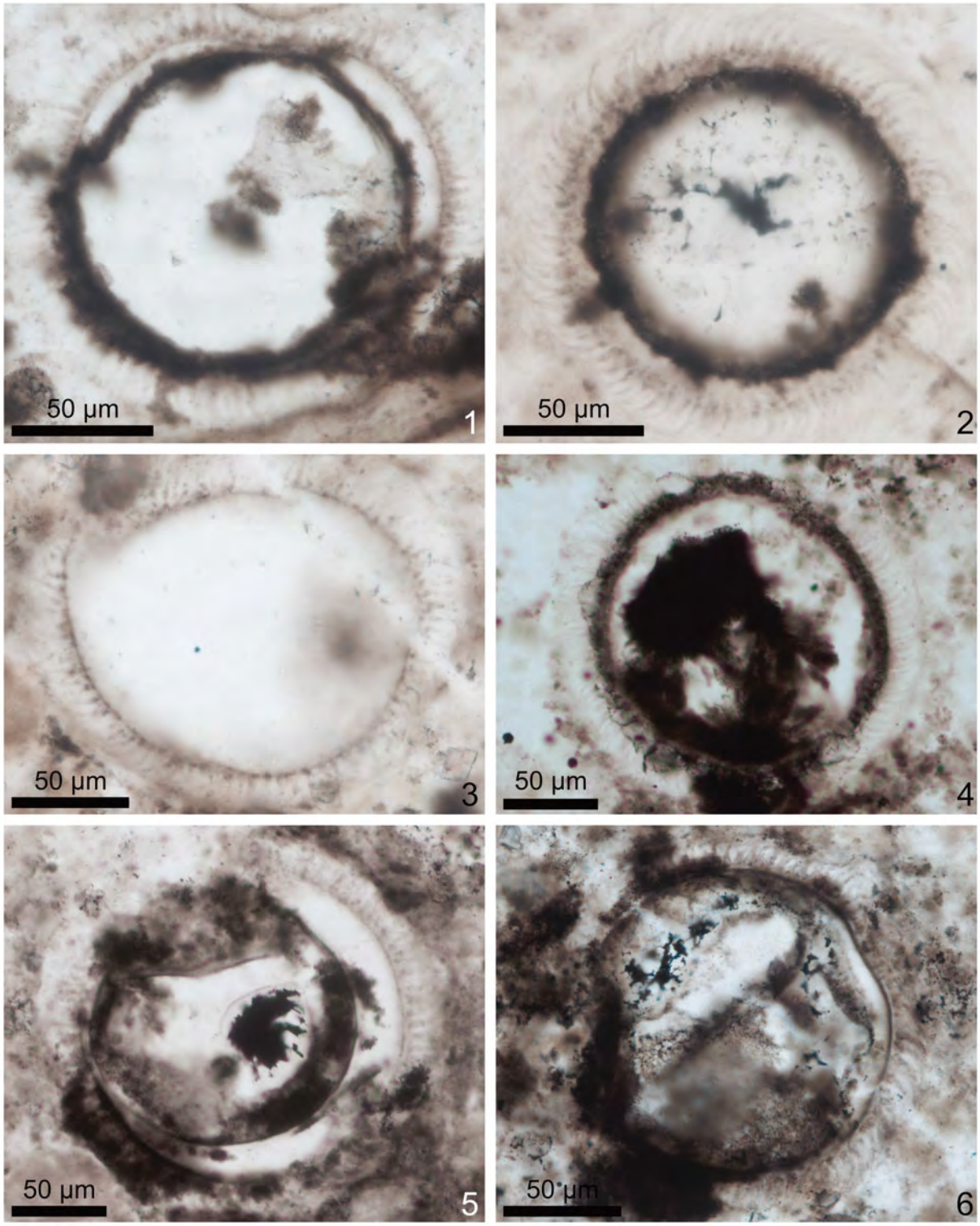

Figure 5. *Appendisphaera magnifica* (Zhang et al., 1998) Liu et al., 2014a. (**1**) PB202003, thin section 19SDP-7-1, N38/3. (**2**) PB202004, thin section 19SDP-7-3, E39/2. (**3**) PB202005, thin section 19SDP-7-3, E30/2. (**4**) PB202006, thin section 19SDP-7-3, K30/2. (**5**) PB202007, thin section 19SDP-7-24, H37. (**6**) PB202008, thin section 19SDP-7-24, H34.

2014 *Appendisphaera tenuis* Moczydłowska et al., emend. Moczydłowska; Xiao et al., p. 9, fig. 3.4.

2014 *Appendisphaera grandis*; Shukla and Tiwari, p. 215, fig. 4D, E.

2015 *Appendisphaera tenuis* Moczydłowska et al.; Golubkova et al., fig. 2a.

2015 *Appendisphaera tenuis* Moczydlowska [sic]; Nagovitsin and Kochnev, fig. 4.I.3.

https://doi.org/10.1017/jpa.2023.92 Published online by Cambridge University Press

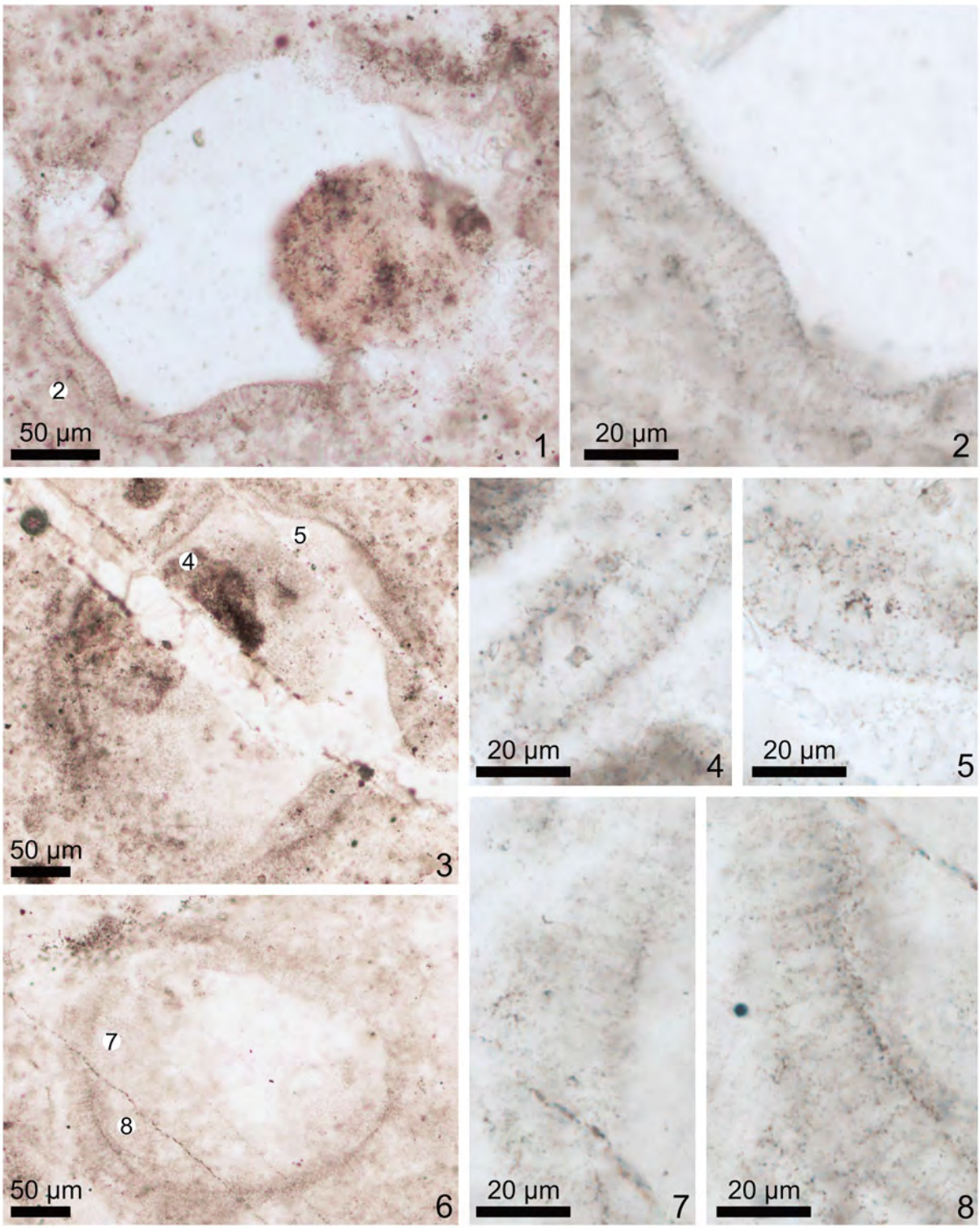

Figure 6. *Appendisphaera tenuis* Moczydłowska, Vidal, and Rudavskaya, 1993, emend. Moczydłowska, 2005. (**1, 2**) PB202009, thin section 19TP-1-14, J27; circled 2 in (**1**) marks area magnified in (**2**). (**3–5**) PB202010, thin section 19TP-1-39, J47/1; circled 4 and 5 in (**3**) mark areas magnified in (**4**) and (**5**), respectively. (**6–8**) PB202011, thin section 19TP-1-40, F37; circled 7 and 8 in (**6**) mark areas magnified in (**7**) and (**8**), respectively.

?2015 *Appendisphaera* sp.; Ye et al., p. 48, pl. I, figs. 9–14.

2016 *Appendisphaera tenuis* Moczydłowska et al., emend. Moczydłowska; Prasad and Asher, p. 44, pl. III, figs. 3–6.

2016 *Gyalosphaeridium multispinulosum* Grey; Prasad and Asher, p. 52, pl. VI, figs. 3, 4.

2016 *Gyalosphaeridium pulchrum* Zang in Zang and Walter; Prasad and Asher, p. 52, pl. VI, figs. 5, 6.

https://doi.org/10.1017/jpa.2023.92 Published online by Cambridge University Press

2019 *Appendisphaera tenuis* Moczydłowska et al., emend. Moczydłowska; Liu and Moczydłowska, p. 61, figs. 29, 30.
2019 *Appendisphaera tenuis* Moczydłowska et al., emend. Moczydłowska; Anderson et al., p. 509, fig. 6H, I.
2019 *Appendisphaera tenuis* Moczydłowska et al., emend. Moczydłowska; Shang et al., p. 10, fig. 5.
2020 *Appendisphaera tenuis* Moczydłowska et al., emend. Moczydłowska; Shang and Liu, p. 157, fig. 5A, B.
2020 *Appendisphaera tenuis* Moczydłowska et al., emend. Moczydłowska; Vorob'eva and Petrov, p. 370, pl. I, figs. 3, 4.
2021 *Appendisphaera tenuis* Moczydłowska et al., emend. Moczydłowska; Ouyang et al., fig. 11Q, R.
2022 *Appendisphaera tenuis* Moczydłowska et al., emend. Moczydłowska; Xiao et al., fig. 17.
2022 *Appendisphaera tenuis* Moczydłowska et al., emend. Moczydłowska; Ye et al., fig. 12E, F.
2023 *Appendisphaera tenuis* (Moczydłowska et al.) emend. Moczydłowska; Golubkova, pl. 7, fig. 2.

Holotype.—PMU-Sib.1-M/33, reposited at Uppsala University, from the Ediacaran Khamaka Formation, Nepa–Botuoba region, Yakutia, Siberia (Moczydłowska et al., 1993, p. 506, text-fig. 7).

Description and measurements.—Vesicle large, with relatively short, slim processes evenly distributed on the vesicle. Processes thin, cylindrical or acutely conical, some with a minute basal expansion (Fig. 6.5), closely arranged but basally separated. Vesicle diameter 224–276 μm (N = 4, mean = 248 μm, SD = 22 μm); process length 11.6–18.4 μm (N = 4, mean = 14.1 μm, SD = 3.0 μm), 4.6–7.7% of vesicle diameter (N = 4, mean = 5.7%, SD = 1.4%), process basal width 1.3–3.1 μm (N = 3, mean = 2.1 μm, SD = 0.9 μm); 16–21 processes (N = 4, mean = 20, SD = 2) per 100 μm of vesicle periphery.

Material.—Three illustrated specimens (Fig. 6) and one additional specimen.

Remarks.—*Appendisphaera tenuis* was originally diagnosed as an *Appendisphaera* species that has relatively short processes with a possible minute basal expansion—features used to differentiate this species from *A. grandis* (Moczydłowska, Vidal, and Rudavskaya, 1993). The hollow nature of the processes was later recognized and added to the emended diagnosis of *A. tenuis* (Moczydłowska, 2005), with other diagnostic features unchanged. Specimens assigned to *A. tenuis* in subsequent studies mostly resemble the holotype and other specimens from the type locality in Siberia in their relatively short, densely arranged, conical or cylindrical processes, with or without a small basal expansion, except that some of them (including those reported here) have larger vesicles than the Siberian specimens.

Appendisphaera tenuis shares some morphological similarities with *A. clava*. Both species have relatively short and densely distributed processes, which were described as cylindrical despite the slightly expanded bases (Moczydłowska, 2005; Liu et al., 2014a). The holotype of *A. clava* has a vesicle diameter of 420 μm, process length of 12 μm, which is 2.9% of vesicle diameter, process basal width of ~1 μm, and about 40 processes per 100 μm of vesicle periphery. Other *A. clava* specimens published together with the holotype have vesicle diameters of 250–510 μm, process length of 6–13 μm (1.7–4% of vesicle diameter), and process width and density similar to the type specimen, although basal width can be up to 3.6 μm (measured on Liu et al., 2014a, fig. 8.5). These dimensions show that *A. clava* has overall larger vesicles (>200 μm and up to 500 μm), proportionally shorter processes (<5% of vesicle diameter), and possibly larger process density than *A. tenuis*, which has a medium-sized vesicle with process length about 10% of vesicle diameter based on measurements of specimens from the type locality in Siberia. However, several specimens listed as synonyms of *A. tenuis* by Liu and Moczydłowska (2019) are similar to *A. clava* in measurements: one *A. tenuis* specimen (vesicle diameter 280 μm, process length 7.1–8.9 μm, which is 2.5–3.2% of vesicle diameter, process basal width 0.4–2.2 μm, Vorob'eva et al., 2008), specimens originally published as *Cavaspina amplitudinis* (vesicle diameter 500–900 μm, process length 20–30 μm, which is 3.3–5.5% of vesicle diameter, process basal width 2–5 μm, Willman and Moczydłowska, 2011), and two specimens originally identified as *Appendisphaera* sp. (vesicle diameter 550 μm, process length 10–20 μm, process basal width 2–5 μm, Ye et al., 2015). The assignment of these specimens to *A. tenuis* may obscure the morphological boundary between *A. clava* and *A. tenuis*, and thus remains questionable. The same argument goes for the specimen originally identified as *Ericiasphaera* aff. *E. addspersa* by Golubkova et al. (2010, pl. IV, fig. 6a, b) that was later synonymized with *A. tenuis* by Sergeev et al. (2011).

In some cases, *Appendisphaera tenuis* can also be akin to *Cavaspina basiconica*, which is differentiated from *A. tenuis* by its less densely arranged processes with a more prominent basal expansion. In practice, however, some specimens with a moderate density of processes can fit the diagnosis of either *A. tenuis* or *C. basiconica* (e.g., Liu and Moczydłowska, 2019, fig. 39A–D), and more quantitative criteria are needed to distinguish these two species.

Genus *Asterocapsoides* Yin and Li, 1978, emend. Xiao et al., 2014

Type species.—*Asterocapsoides sinensis* Yin and Li, 1978, emend. Xiao et al., 2014.

Other species.—*Asterocapsoides fluctuensis* Liu and Moczydłowska, 2019; *A. robustus* Xiao et al., 2014; *A. wenganensis* (Chen and Liu, 1986) Xiao et al., 2014.

Asterocapsoides wenganensis (Chen and Liu, 1986) Xiao et al., 2014
Figure 7

1986 *Meghystrichosphaeridium wenganensis* Chen and Liu, p. 51, pl. II, figs. 1, 3.

https://doi.org/10.1017/jpa.2023.92 Published online by Cambridge University Press

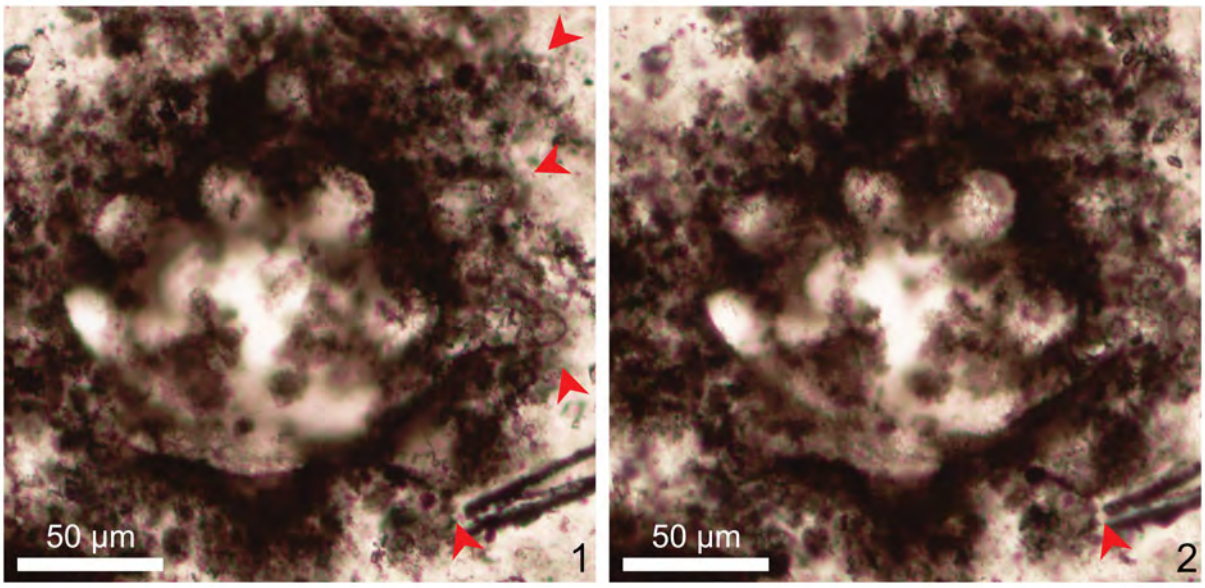

Figure 7. *Asterocapsoides wenganensis* (Chen and Liu, 1986) Xiao et al., 2014. (**1, 2**) PB202012, thin section 21LHK-1-10, R34/4. (**1**) and (**2**) show the same area at different focal levels; red arrowheads denote large conical processes.

non 1998 *Meghystrichosphaeridium wenganensis* Chen and Liu; Yuan and Hofmann, p. 203, fig. 10C, D.
2001 *Meghystrichosphaeridium chadianensis*; Zhou et al., p. 1166, pl. 2, figs. 1–4.
non 2001 *Meghystrichosphaeridium chadianensis*; Zhou et al., p. 1166, pl. 1, figs. 1–8; pl. 2, figs. 5–8.
2002 *Meghystrichosphaeridium chadianensis*; Yuan et al., p. 75, fig. 103.
2004b *Meghystrichosphaeridium chadianensis*; Zhou et al., pl. V, fig. 4.
non 2004b *Meghystrichosphaeridium* sp., Zhou et al., p. 354, pl. V, figs. 5, 6.
2014 *Asterocapsoides wenganensis* (Chen and Liu) Xiao et al., p. 14, fig. 5.4–5.12.
2019 *Asterocapsoides wenganensis* (Chen and Liu) Xiao et al.; Shang et al., p. 11, fig. 6.
?2019 *Asterocapsoides* sp.; Ouyang et al., fig. 9C–E.
2020 *Asterocapsoides wenganensis*; Willman et al., fig. 4c, d.

Neotype.—The specimen illustrated by Xiao et al. (2014, fig. 5.7) is here designated as a neotype (NIGPAS-94038-3193), reposited at NIGPAS, from Doushantuo Formation in Weng'an area, Guizhou Province, South China.

Description and measurements.—Only a tangentially cut specimen was observed in thin section. The vesicle is estimated to be medium to large in size, originally spheroidal, with homomorphic, large conical processes that are likely basally in contact. Vesicle diameter of the tangential cross section is about 127 µm. The full length and basal width of processes are not captured in the thin section, but the process length is at least 42.7 µm and basal width is at least 24.2 µm based on measurements of processes partially captured in the thin section.

Material.—One illustrated specimen (Fig. 7).

Remarks.—Although the true vesicle diameter of the illustrated specimen cannot be determined for this specimen, which seems to be cut tangentially at the periphery of its vesicle, the specimen is probably around 200 µm in vesicle diameter. Accepting the estimated vesicle and process sizes, this specimen is most appropriately identified as *Asterocapsoides wenganensis*, which differs from *A. robustus* mainly in its fewer and proportionally larger conical processes.

One specimen identified as *Asterocapsoides* sp. (Ouyang et al., 2019, fig. 9C–E) is similar to *A. wenganensis* based on its large spheroidal vesicle (~389 µm in diameter) with uniform, conical processes that are about 63.9 µm in length (16.4% of vesicle diameter), about 41.8 µm in basal width, and basally connected. Despite these similarities, however, its processes have slim and slender tips that are bent and twisted, apparently supporting an outer membrane. The process tips may be too fragile to be preserved in the phosphatized *A. wenganensis* specimens reported in Chen and Liu (1986) and Xiao et al. (2014). It is also possible that the process tips may have been lost due to mechanical breakage during reworking or acid extraction of the phosphatized specimens. These possibilities need to be confirmed or rejected with thin-section observation of the phosphatized specimens. Thus, this specimen, illustrated as *Asterocapsoides* sp. in Ouyang et al. (2019), is here tentatively accepted as *A. wenganensis*.

A neotype is designated here for *Asterocapsoides wenganensis* because the repository of the original holotype (specimen illustrated in Chen and Liu, 1986, pl. II, figs. 1, 3) from the Doushantuo Formation in Baiyan, Weng'an area, Guizhou Province, South China, cannot be located.

Genus *Bullatosphaera* Vorob'eva, Sergeev, and Knoll, 2009

Type species.—*Bullatosphaera velata* Vorob'eva, Sergeev, and Knoll, 2009.

https://doi.org/10.1017/jpa.2023.92 Published online by Cambridge University Press

Other species.—*Bullatosphaera*? *colliformis* n. sp.

Bullatosphaera? *colliformis* new species
Figures 8, 9

Holotype.—PB202013, thin section 19CW-6-2, ZEISS Scope A1 coordinates 11×106, England Finder coordinates K30/3 (Fig. 8.1–8.6), reposited at NIGPAS, from Doushantuo Formation at the Caowan section in Zhangjiajie area, Hunan Province, South China.

Diagnosis.—Vesicle spheroidal, small to medium-sized, covered by closely packed, small, spherical or hemispherical structures that are analogous to processes. The spherical or hemispherical structures are uniform in size, hollow, and attached to the vesicle surface by a thin, short, cylindrical, neck-like basal stem, but they do not communicate with the vesicle interior.

Description and measurements.—Vesicle diameter 94 µm in holotype, 81 and 88 µm in the two other specimens. Spherical or hemispherical structures 8.1 µm wide and 5.5 µm high in holotype, whereas those structures in the two other specimens are 7.7 and 9.9 µm wide and 6.5 and 8.1 µm high, respectively, with a density of 11–14 such structures (13 in holotype) per 100 µm of vesicle periphery.

Etymology.—From Latin *collum*, neck, with reference to the neck-like stem that connects the spherical processes to the vesicle wall.

Material.—Three illustrated specimens (Fig. 8).

Remarks.—The three illustrated specimens are characterized by the uniform spherical or hemispherical structures surrounding their vesicles, which are distinctive structures of *Bullatosphaera*. The lack of a second vesicle wall that surrounds the ornamentations, which is a diagnostic feature of *Bullatosphaera*, could be a result of degradation and diagenesis, as is possibly the case for *Bullatosphaera* sp. that was illustrated by Xiao et al. (2014, p. 16, fig. 6.7, 6.8). The basally constricted stem differentiates *B.*? *colliformis* n. sp. from *B. velata* Vorob'eva, Sergeev, and Knoll, 2009, and *Bullatosphaera* sp. (Xiao et al., 2014). However, this feature is not included in the diagnosis for the genus *Bullatosphaera*, therefore the placement of this new species in the genus *Bullatosphaera* remains provisional.

Genus *Cavaspina* Moczydłowska, Vidal, and Rudavskaya, 1993

Type species.—*Cavaspina acuminata* (Kolosova, 1991) Moczydłowska, Vidal, and Rudavskaya, 1993.

Other species.—*Cavaspina basiconica* Moczydłowska, Vidal, and Rudavskaya, 1993; *C. conica* Liu and Moczydłowska, 2019; *C. tiwariae* Xiao in Xiao et al., 2022; *C. uria* (Nagovitsin and Faizullin in Nagovitsin et al., 2004) Nagovitsin and Moczydłowska in Moczydłowska and Nagovitsin, 2012.

Cavaspina acuminata (Kolosova, 1991) Moczydłowska, Vidal, and Rudavskaya, 1993
Figure 10.1

1990 3-D preserved spinose microsphere; Yin et al., pl. II.A–B.
1993 *Cavaspina acuminata* (Kolosova) Moczydłowska, Vidal, and Rudavskaya, p. 509, text-fig. 10A–B.
1998 *Goniosphaeridium acuminatun* (Kolosova); Zhang et al., p. 28, fig. 8.3.
2002 *Goniosphaeridium acuminatun* (Kolosova) Zhang et al.; Yuan et al., p. 74, fig. 99.
2004 *Cavaspina acuminata* (Kolosova) Moczydłowska et al.; Nagovitsin et al., p. 12, pl. II, figs. 7, 8.
2005 *Cavaspina acuminata* (Kolosova) Moczydłowska et al.; Moczydłowska, p. 298, fig. 6A, B.
2006 *Cavaspina acuminata* (Kolosova) Moczydłowska et al.; Veis et al., pl. I, figs. 5, 6, pl. II, fig. 1.
2008 *Cavaspina acuminata* (Kolosova) Moczydłowska et al.; Willman and Moczydłowska, p. 522, fig. 9C.
2009 *Cavaspina acuminata* (Kolosova) Moczydłowska et al.; Vorob'eva et al., p. 177, fig. 7.11.
2011 *Cavaspina acuminata* (Kolosova) Moczydłowska et al.; Willman and Moczydłowska, p. 24, pl. II, fig. 3.
2012 *Cavaspina acuminata* (Kolosova) Moczydłowska et al.; Moczydłowska and Nagovitsin, p. 13, fig. 4C, E, F.
2013 *Tanarium* sp.; Zeng et al., fig. 3.5.
2014 *Cavaspina acuminata* (Kolosova) Moczydłowska et al.; Xiao et al., p. 16, fig. 7.
2014a *Cavaspina acuminata* (Kolosova) Moczydłowska et al.; Liu et al., p. 44, fig. 27.1, 27.2.
2014 *Cavaspina acuminata* (Kolosova) Moczydłowska et al.; Shukla and Tiwari, p. 216, fig. 5C, D.
2016 *Cavaspina acuminata* (Kolosova) Moczydłowska et al.; Prasad and Asher, p. 46, pl. IV, figs. 5, 6.
2017 *Cavaspina acuminata* (Kolosova) Moczydłowska et al.; Nie et al., p. 374, fig. 5.1–5.4.
2019 *Cavaspina acuminata* (Kolosova, 1991) Moczydłowska et al. 1993; Liu and Moczydłowska, p. 76, fig. 38.
2019 *Cavaspina acuminata* (Kolosova) Moczydłowska et al.; Shang et al., p. 19, fig. 8A–D.
2020 *Cavaspina acuminata* (Kolosova) Moczydłowska et al.; Shang and Liu, p. 157, fig. 5D–H.
2020 *Cavaspina acuminata*; Grazhdankin et al., fig. 4H.
2020 *Cavaspina acuminata*; Willman et al., fig. 4a, b.
2021 *Cavaspina acuminata* (Kolosova) Moczydłowska et al.; Ouyang et al., fig. 13A.
2022 *Cavaspina acuminata* (Kolosova) Moczydłowska et al.; Shi et al., fig. 7C–E (illustrated in Fig. 11.1, one of the two specimens described here).
?2022 *Cavaspina acuminata* (Kolosova) Moczydłowska et al.; Ye et al., fig. 13A, B.
2023 *Cavaspina acuminata* (Kolosova) emend. Moczydłowska; Golubkova, pl. 7, fig. 5.

Holotype.—YIGS Nr 87-123, reposited at the Geological Museum of Yakutian Institute of Geologic Sciences (present Diamond and Precious Metal Geology Institute, Siberian Branch, Russian Academy of Sciences), from the Ediacaran Torgo Formation, Berezovo area, eastern Siberia (Kolosova, 1991, p. 57, fig. 4.1).

https://doi.org/10.1017/jpa.2023.92 Published online by Cambridge University Press

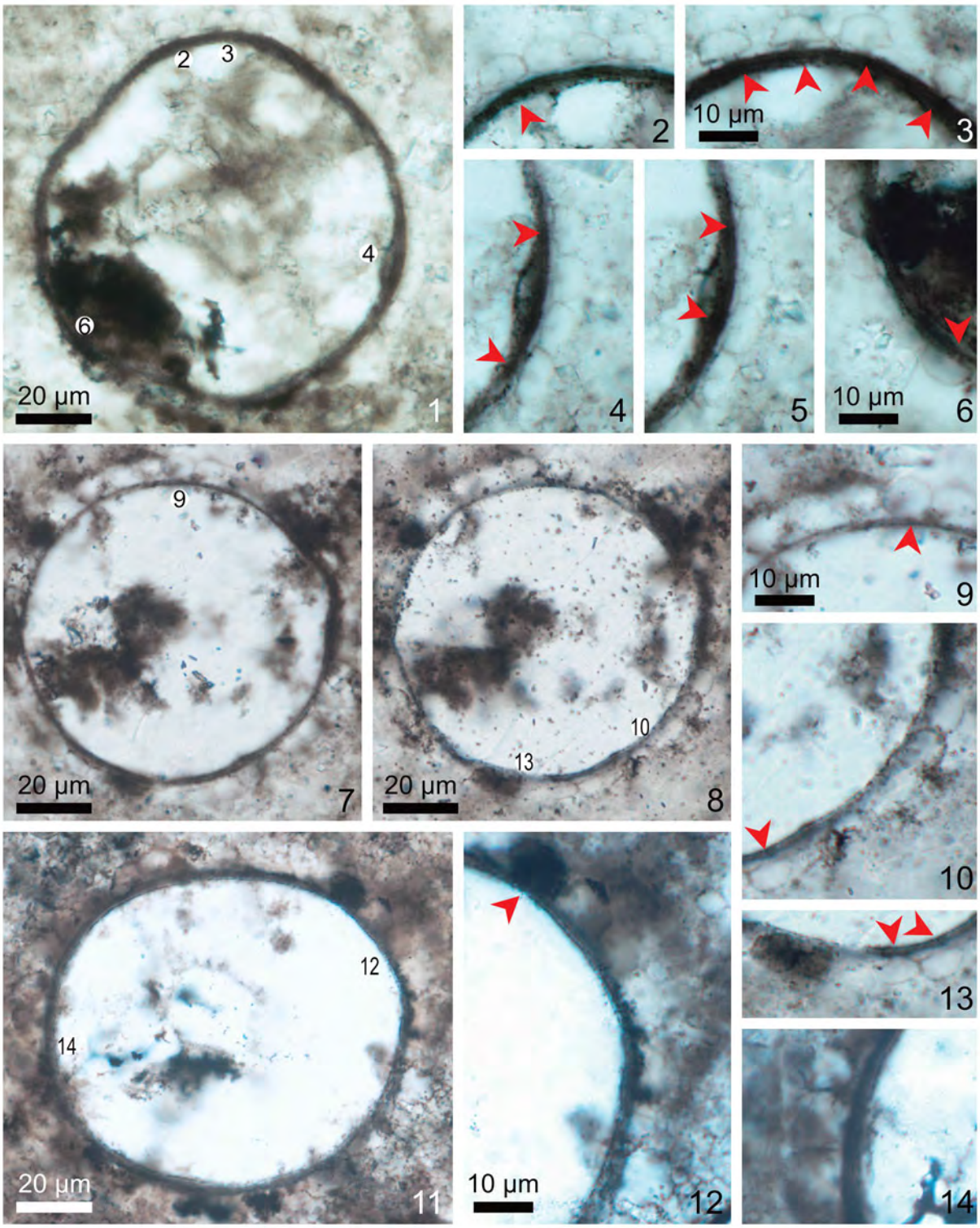

Figure 8. *Bullatosphaera*? *colliformis* new species. Red arrowheads denote basally constricted spherical or hemispherical ornamentations. (**1–6**) Holotype, PB202013, thin section 19CW-6-2, K30/3; circled 2, 3, and 6 in (**1**) mark areas magnified in (**2, 3, 6**), respectively; circled 4 in (**1**) marks areas in (**4, 5**), which show the same area at different focal levels. (**7–10, 13**) PB202014, thin section 19CW-6-12, L31/4. (**7, 8**) Show the same area at different focal levels; circled 9 in (**7**) marks area magnified in (**9**); circled 10 and 13 in (**8**) mark areas magnified in (**10**) and (**13**), respectively. (**11, 12, 14**) PB202015, thin section 19CW-9-7, O35/4; circled 12 and 14 in (**11**) mark areas magnified in (**12**) and (**14**), respectively. Scale bars in (**3**) and (**6**) also apply to (**2, 4, 5**); scale bars in (**9**) and (**12**) also apply to (**10, 13, 14**).

Description and measurements.—Vesicle small, spheroidal, bearing sparsely and evenly distributed, acutely conical processes. The illustrated specimen has a vesicle diameter of about 84 µm, process length about 6.3 µm (7.5% of vesicle diameter), and process basal width about 1.5 µm (process length to basal width ratio ~4.2), with about 23 processes per 100 µm of vesicle periphery. The other specimen has a vesicle diameter of about 41 µm, process length about 5.7 µm (13.8%

https://doi.org/10.1017/jpa.2023.92 Published online by Cambridge University Press

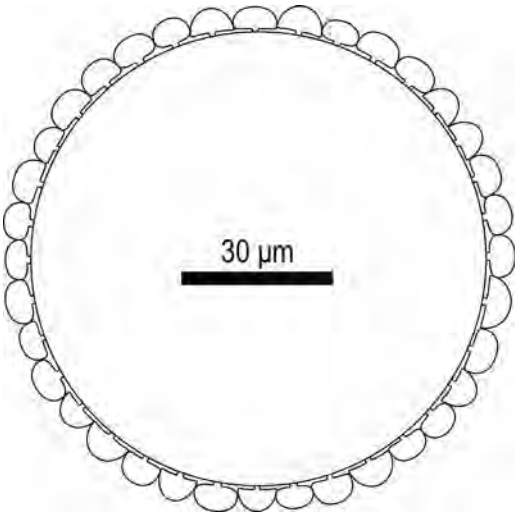

Figure 9. Sketch of *Bullatosphaera*? *colliformis* new species.

of vesicle diameter), and process basal width about 1.8 μm (process length to basal width ratio ~3.2), with 12 processes per 100 μm of vesicle periphery.

Material.—One illustrated specimen (Fig. 10.1) and one additional specimen.

Remarks.—Being one of the most widely distributed Ediacaran acanthomorphic species, *Cavaspina acuminata* is characterized by its relatively sparsely distributed, short, and acutely conical processes. Both specimens described here, although not well preserved and together covering a large variation in size and process density, meet the diagnosis of *C. acuminata*, best demonstrated by the process basal width (<2 μm) and process length to basal width ratio (>3).

One *Cavaspina acuminata* specimen reported by Ye et al. (2022, fig. 13A, B) appears to have terminally branching processes and, if confirmed, would be better identified as *Variomargosphaeridium gracile* Xiao et al., 2014 (see Ouyang et al., 2021, fig. 22A). Therefore, the identification of the specimen illustrated in Ye et al. (2022) as *C. acuminata* is questioned here, pending re-examination of the specimen to confirm or reject the terminal branching structures.

Cavaspina basiconica Moczydłowska, Vidal, and Rudavskaya, 1993
Figure 10.2

1993 *Cavaspina basiconica* Moczydłowska, Vidal, and Rudavskaya, p. 510, text-fig. 11.
1998 *Meghystrichosphaeridium perfectum* (Kolosova, 1991) Zhang et al., p. 36, fig. 10.7, 10.8.
2001 *Meghystrichosphaeridium chadianensis* Chen and Liu, 1986, emend. Zhang et al.; Zhou et al., p. 1166, pl. II, figs. 5, 6.
2005 *Cavaspina basiconica* Moczydłowska et al.; Moczydłowska, p. 300, fig. 6C.
2005 *Gyalosphaeridium basiconicum* (Moczydłowska et al.) Grey, p. 277.
2005 *Gyalosphaeridium multispinulosum* Grey, p. 273, figs. 11I, 44I, 179A–D, 180A–E.
2006 *Cavaspina basiconica* Moczydłowska et al.; Willman et al., p. 26, pl. I, figs. 3, 4.
2008 *Cavaspina basiconica* Moczydłowska et al.; Willman and Moczydłowska, p. 522, fig. 9D–E.
2009 *Meghystrichosphaeridium perfectum* (Kolosova) Zhang et al.; McFadden et al., fig. 5D.
2011 *Cavaspina basiconica* Moczydłowska et al.; Willman and Moczydłowska, p. 25, pl. II, figs. 1, 2.
2014 *Cavaspina basiconica* Moczydłowska et al.; Xiao et al., p. 16, fig. 8.
2014a *Cavaspina basiconica* Moczydłowska et al.; Liu et al., p. 44, fig. 27.3–27.6.
2014 *Cavaspina basiconica* Moczydłowska et al.; Shukla and Tiwari, p. 216, fig. 5E, F.
2016 *Cavaspina basiconica* Moczydłowska et al.; Prasad and Asher, p. 46, pl. IV, figs. 7, 8.
2017 *Cavaspina basiconica* Moczydłowska et al.; Nie et al., p. 374, fig. 5.5, 5.6.
2017 ?*Cavaspina basiconica*; Ouyang et al., fig. 8A–C.
2019 *Cavaspina basiconica* Moczydłowska et al.; Liu and Moczydłowska, p. 78, fig. 39.
2019 *Cavaspina basiconica* Moczydłowska et al.; Anderson et al., p. 509, fig. 7A–F.
2019 *Cavaspina basiconica* Moczydłowska et al.; Shang et al., p. 21, fig. 8E–G.
2020 *Cavaspina basiconica* Moczydłowska et al.; Vorob'eva and Petrov, p. 374, pl. II, figs. 16–18.
2022 *Cavaspina basiconica* Moczydłowska et al.; Ye et al., p. 27, figs. 13C, D, 14E–J.
2022 *Cavaspina* cf. *C. basiconica*; Shi et al., fig. 7F–H (illustrated in Fig. 10.2 of this paper, one of the two specimens described here).

Holotype.—PMU-Sib.1-Y/55/2, reposited at Uppsala University, from the Ediacaran Khamaka Formation, Nepa–Botuoba region, Yakutia, Siberia (Moczydłowska et al., 1993, p. 510, text-fig. 11A, B, D).

Description and measurements.—Vesicle small to medium-sized, spheroidal, bearing a small to moderate number of evenly distributed processes. Processes conical, with a small but clearly defined basal expansion that is deflated. The illustrated specimen has a vesicle diameter of about 138 μm, process length about 12.3 μm (8.9% of vesicle diameter), and process basal width about 10.2 μm (process length to basal width ratio ~1.2), with about one process per 100 μm of vesicle periphery. The other specimen has a vesicle diameter of about 94 μm, process length about 12.5 μm (13.2% of vesicle diameter), and process basal width about 3.8 μm (process length to basal width ratio ~3.3), with 17 processes per 100 μm of vesicle periphery.

Material.—One illustrated specimen (Fig. 10.2) and one additional specimen illustrated in Ouyang et al. (2017, fig. 8A–C).

Remarks.—Both specimens described here are poorly preserved, thus the seemingly ciliate apical part of the

https://doi.org/10.1017/jpa.2023.92 Published online by Cambridge University Press

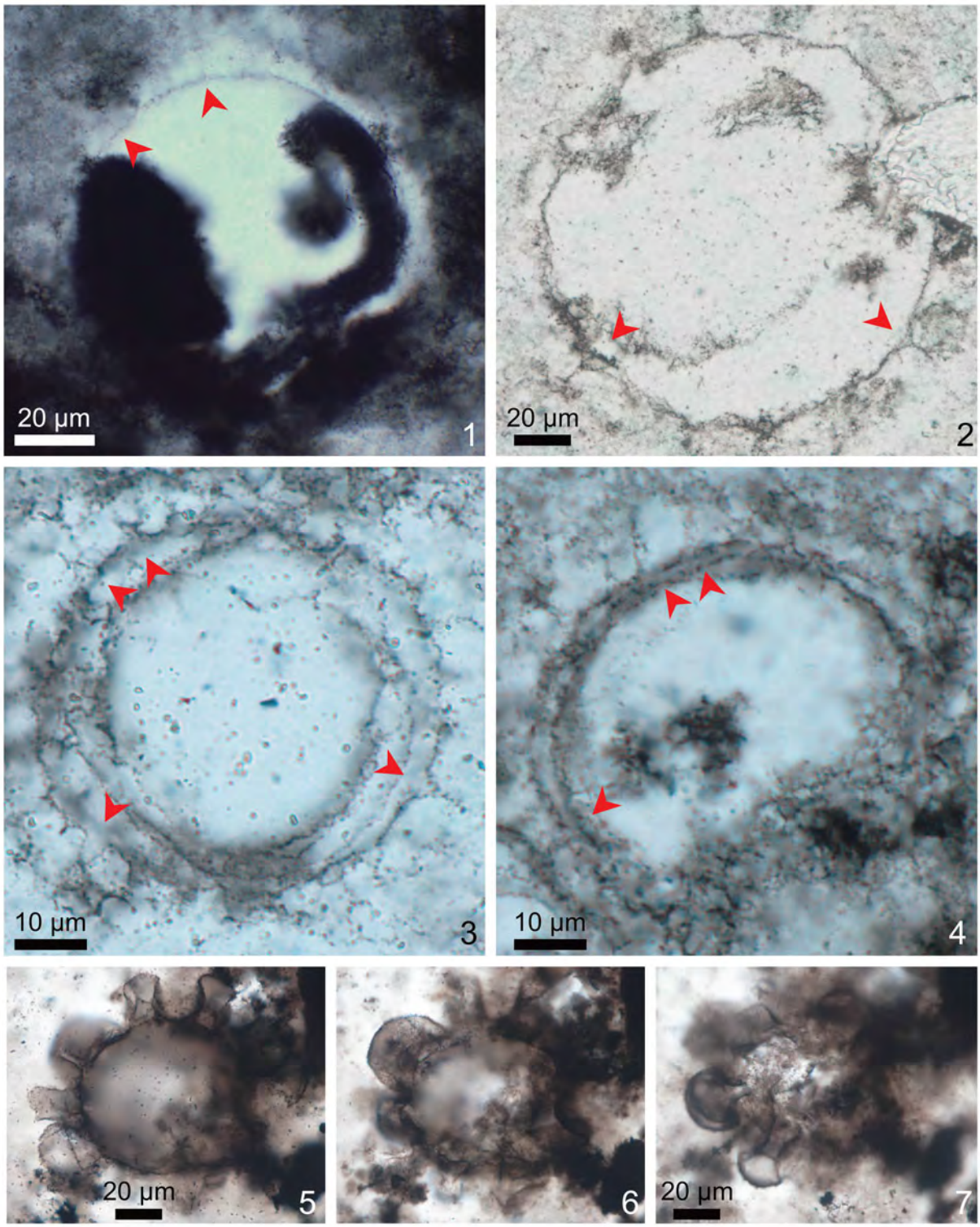

Figure 10. (**1**) *Cavaspina acuminata* (Kolosova, 1991) Moczydłowska, Vidal, and Rudavskaya, 1993, PB202016, thin section 21DC-3-1, Q30/4. (**2**) *Cavaspina basiconica* Moczydłowska, Vidal, and Rudavskaya, 1993, PB202017, thin section 21DC-5-4, M40/1. (**3**, **4**) *Cavaspina uria* (Nagovitsin and Faizullin in Nagovitsin et al., 2004) Nagovitsin and Moczydłowska in Moczydłowska and Nagovitsin, 2012, thin section 21DC-5-4; red arrowheads in (**1–4**) denote conical processes; (**3**) PB202018, G41/1; (**4**) PB202019, E45/4. (**5–7**) *Eotylotopalla* sp. PB202025, thin section 19CW-6-15, O41/1, showing the same area at different focal levels. Scale bars in (**5**) and (**7**) also apply to (**6**).

processes are likely a result of diagenetic contraction of originally acutely tapering processes. Although resembling *Cavaspina acuminata* in morphometrics of process shape, the two *C. basiconica* specimens described here can be readily recognized by their processes with a deflated basal expansion. This feature also distinguishes them from *C. uria*, whose processes have a broad base that is not deflated.

https://doi.org/10.1017/jpa.2023.92 Published online by Cambridge University Press

Cavaspina uria (Nagovitsin and Faizullin in Nagovitsin et al., 2004) Nagovitsin and Moczydłowska in Moczydłowska and Nagovitsin, 2012
Figure 10.3, 10.4

2004 *Goniosphaeridium urium* Nagovitsin and Faizullin in Nagovitsin et al., p. 13, pl. II, fig. 1.
2006 *Cavaspina* sp.; Veis et al., pl. I, fig. 7, pl. II, figs. 3–5.
2011 *Goniosphaeridium minutum* Nagovitsin and Faizullin; Sergeev et al., p. 1003, fig. 7.7.
2012 *Cavaspina uria* (Nagovitsin and Faizullin) Nagovitsin and Moczydłowska in Moczydłowska and Nagovitsin, p. 14, fig. 4G–I.
2019 *Asterocapsoides robustus*; Ouyang et al., fig. 9A, B.
2022 *Cavaspina uria* (Nagovitsin and Faizullin in Nagovitsin et al.) Nagovitsin and Moczydłowska in Moczydłowska and Nagovitsin; Shi et al., fig. 7I–M (specimens illustrated in Fig. 10.3, 10.4, and described here).

Holotype.—Copy 7 of preparation PN 8/17(2)-1, No. 673 CSGM, reposited at Central Siberian Geological Museum of the United Institute of Geology, Geophysics and Mineralogy (present Trofimuk Institute of Petroleum–Gas Geology and Geophysics), Siberian Branch, Russian Academy of Sciences, from the Ediacaran Ura Formation, Patom Uplift, eastern Siberia (Nagovitsin et al., 2004, pl. II, fig. 1).

Description and measurements.—Vesicle spheroidal, small, bearing evenly distributed conical processes. Process uniform, with a triangular outline in thin-sectional view. Vesicle diameter 41–99 μm (N = 6, mean = 60 μm, SD = 20 μm). Based on measurements of four better preserved specimens among the six available ones, process length is 5.2–7.2 μm (N = 4, mean = 6.0 μm, SD = 1.0 μm), representing 8.8–13.4% of vesicle diameter (N = 4, mean = 10.8%, SD = 2.0%), process basal width 3.3–4.6 μm (N = 4, mean = 3.8 μm, SD = 0.6 μm), process length to basal width ratio 1.5–1.8 (N = 4, mean = 1.6, SD = 0.1), and 11–17 processes (N = 4, mean = 15, SD = 3) per 100 μm of vesicle periphery.

Material.—Two illustrated specimens (Fig. 10.3, 10.4), two specimens illustrated in Shi et al. (2022, fig. 7J, M), and two additional specimens.

Remarks.—With conical processes whose length accounts for about 10% of vesicle diameter, *Cavaspina uria* is somewhat similar to *Asterocapsoides robustus* in process shape. However, most published specimens of *A. robustus* are much larger in vesicle size. The specimen identified as *A. robustus* from the Doushantuo Formation in Zhangcunping area, South China (Ouyang et al., 2019, fig. 9A, B) has evenly distributed conical processes, with vesicle diameter of about 70 μm, process length of 7.0 μm, and process basal width of 4.0 μm, which are comparable to those of *C. uria*, especially the holotype (vesicle diameter 80 μm, process length 7–8 μm, process basal width 4–5 μm), but differ significantly from typical *A. robustus* specimens. Thus, we reassign this specimen to *C. uria*.

Genus *Eotylotopalla* Yin, 1987

Type species.—*Eotylotopalla delicata* Yin, 1987.

Other species.—*Eotylotopalla apophysa* (Vorob'eva, Sergeev, and Knoll, 2009) Ye et al., 2022; *E. dactylos* Zhang et al., 1998; *E. quadrata* Liu and Moczydłowska, 2019; *E. strobilata* (Faizullin, 1998) Sergeev et al., 2011 (*E. minorosphaera* Vorob'eva, Sergeev, and Knoll, 2009); *E. inflata* n. sp.

Remarks.—*Eotylotopalla* now accommodates most of the Ediacaran acanthomorphs with inflated processes that are terminally rounded or truncated (i.e., lacking a pointed process tip). Processes of *Eotylotopalla* can be cylindrical (*E. dactylos*), hemispherical (*E. apophysa*, *E. delicata*, *E. strobilata*, differentiated mainly by their proportional process size relative to vesicle diameter), cuboidal (*E. quadrata*), or distally inflated (*E. inflata* n. sp.). With the addition of *E. inflata* n. sp., *Eotylotopalla* can also have biform processes (although different from the basally inflated biform processes of *Mengeosphaera*). Despite these morphological variations, *Eotylotopalla* remains a very distinctive genus characterized by its distally expanded, rounded, flat or truncated processes.

Eotylotopalla dactylos Zhang et al., 1998
Figure 11.1–11.4, 11.7, 11.8

1998 *Eotylotopalla dactylos* Zhang et al., p. 26, fig. 7.8, 7.9.
2007 *Eotylotopalla dactylos*; Zhou et al., fig. 4F.
2011 *Eotylotopalla dactylos*; L. Yin et al., fig. 3G.
2014 *Eotylotopalla dactylos* Zhang et al.; Xiao et al., p. 20, fig. 11.
2014a *Eotylotopalla dactylos* Zhang et al.; Liu et al., p. 50, fig. 31.1–31.9.
2014b *Eotylotopalla dactylos*; Liu et al., fig. 7B.
2014 *Eotylotopalla dactylos* Zhang et al.; Shukla and Tiwari, p. 217, fig. 6A, B.
2014a *Eotylotopalla* sp.; Liu et al., p. 61, fig. 31.10–31.13.
2015 *Eotylotopalla dactylos* Zhang et al.; Ouyang et al., p. 217, pl. I, fig. 11.
2019 *Eotylotopalla dactylos* Zhang et al.; Liu and Moczydłowska, p. 95, fig. 48.
2021 *Eotylotopalla dactylos* Zhang et al.; Ouyang et al., fig. 14K, L.
?2021 *Eotylotopalla dactylos* Zhang et al.; Ouyang et al., fig. 14J.
2021 *Eotylotopalla dactylos* Zhang et al.; Liu et al., fig. 5.6, 5.7.
2022 *Eotylotopalla dactylos* Zhang et al.; Shi et al., fig. 8A (illustrated in Fig. 11.7, 11.8, one of the specimens described here).
2022 *Eotylotopalla dactylos* Zhang et al.; Ye et al., p. 37, fig. 23A–F.
2022 *Eotylotopalla* sp.; Ye et al., p. 37, fig. 23H–J.

Holotype.—Specimen illustrated in Zhang et al. (1998, fig. 7.8), thin section #XDV-29m-6, Leitz coordinates 48×123, reposited at NIGPAS, from the Ediacaran Doushantuo Formation at Xiaofenghe in the Yangtze Gorges area, Hubei Province, South China.

Description and measurements.—Vesicle small and spheroidal, with uniform, near evenly distributed processes that can be

https://doi.org/10.1017/jpa.2023.92 Published online by Cambridge University Press

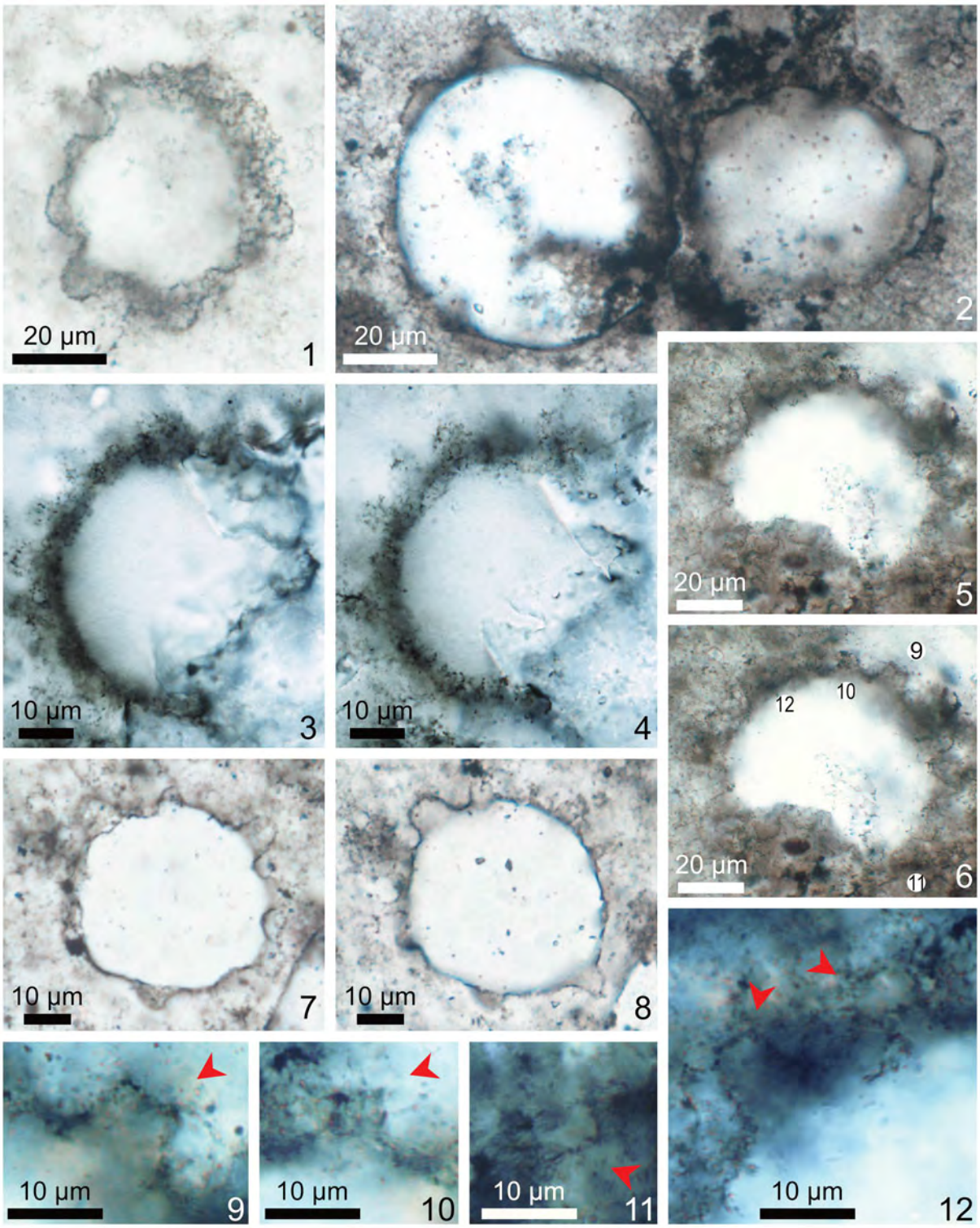

Figure 11. (**1–4**, **7, 8**) *Eotylotopalla dactylos* Zhang et al., 1998. (**1**) PB202020, thin section 19TP-1-13; (**2**) PB202021 (left) and PB202022 (right), thin section 21DC-2-38, Q48; (**3, 4**) PB202023, thin section 14HA-115-1, D47/3, showing the same area at different focal levels; (**7, 8**) PB202024, thin section 21DC-5-3, Q30/3, showing the same area at different focal levels. (**5, 6, 9–12**) *Eotylotopalla* cf. *E. dactylos* Zhang et al., 1998, PB202026, thin section 21DC-2-12, O21/4. (**5, 6**) The same area at different focal levels; (**9–12**) magnified views of the processes denoted by circled 9–12 in (**6**) under cross-polarized light; red arrowheads denote the angular transition from the side wall of the processes to the distal end.

https://doi.org/10.1017/jpa.2023.92 Published online by Cambridge University Press

either basally connected or separated. Processes are cylindrical or taper slightly toward the distal end, with a rounded or blunt terminal end. Vesicle diameter 39–60 µm (N = 5, mean = 49 µm, SD = 7 µm), with 5–11 processes per 100 µm of vesicle periphery (N = 3, mean = 7 µm, SD = 4); process lengths 6.4–10.2 µm (N = 5, mean = 7.7 µm, SD = 0.7 µm) or 13.2–26.0% of vesicle diameter (N = 5, mean = 16.4%, SD = 5.4%), and process basal width 7.1–13.2 µm (N = 5, mean = 9.9 µm, SD = 3.0 µm) or 14.9–24.4% of vesicle diameter (N = 5, mean = 20.3%, SD = 4.0%).

Material.—Five illustrated specimens (Fig. 11.1–11.4, 11.7, 11.8), including one (Fig. 11.7, 11.8) previously illustrated in Shi et al. (2022, fig. 8A) and another (Fig. 11.3, 11.4) previously assigned to "indeterminate acanthomorphs" by Ouyang et al. (2017, table 1).

Remarks.—Compared with other *Eotylotopalla* species with very limited intraspecific morphological variation (*E. delicata*, *E. inflata* n. sp., *E. quadrata*, *E. strobilata*), processes of *E. dactylos* are relatively more variable in morphology, which can be cylindrical (digitate) or conical, basally separate, connected, or joined, with moderate basal or terminal expansions. Measurements of previously published *E. dactylos* illustrations (as listed in synonym list, Fig. 12) show that most published specimens have vesicle diameters of 30–105 µm, 5–31 µm in process length (10–30% of vesicle diameter), 6–26 µm in process basal width (11–28% of vesicle diameter), with 3–12 processes per 100 µm of vesicle periphery. Specimens described here fit the diagnostic features of *E. dactylos* both qualitatively and quantitatively.

Three poorly preserved specimens previously published by Liu et al. (2014a, fig. 31.10–31.13) and Ye et al. (2022, fig. 23H–J) have been identified as *Eotylotopalla* sp. despite their similarities to *E. dactylos* acknowledged by the original authors. These specimens were considered different from *E. dactylos* in their more sparsely distributed processes (Liu et al., 2014a; Ye et al., 2022). However, if we quantitively assess previously published specimens of *E. dactylos*, there is a wide range of process density (Fig. 12). Several *E. dactylos* specimens accepted by various authors also have sparsely distributed processes (e.g., Zhou et al., 2007, fig. 4F), with 2–3 processes per 100 µm of vesicle periphery, which is not much different from the three specimens of *Eotylotopalla* sp. cited above (Fig. 12). Thus, considering the intraspecific variation in process density, we reassign these *Eotylotopalla* sp. specimens to *E. dactylos*.

Ye et al. (2022) transferred *Timanisphaera apophysa* Vorob'eva, Sergeev, and Knoll, 2009, to *Eotylotopalla* and synonymized it with *E. grandis* Tang et al., 2013, thus forming a new combination *E. apophysa* (Vorob'eva, Sergeev, and Knoll, 2009) Ye et al., 2022, characterized by its large vesicles with sparse but proportionally large, hemispherical processes. One specimen assigned to *T. apophysa* (Ye et al., 2022, fig. 23G) is about 170 µm in vesicle diameter and notably smaller than the holotype measurements mentioned in the original diagnosis (vesicle size 265–450 µm in diameter, process 70–-110 µm in length and 50–90 µm in width). However, considering that Ye et al.'s (2022) specimen is silicified and was

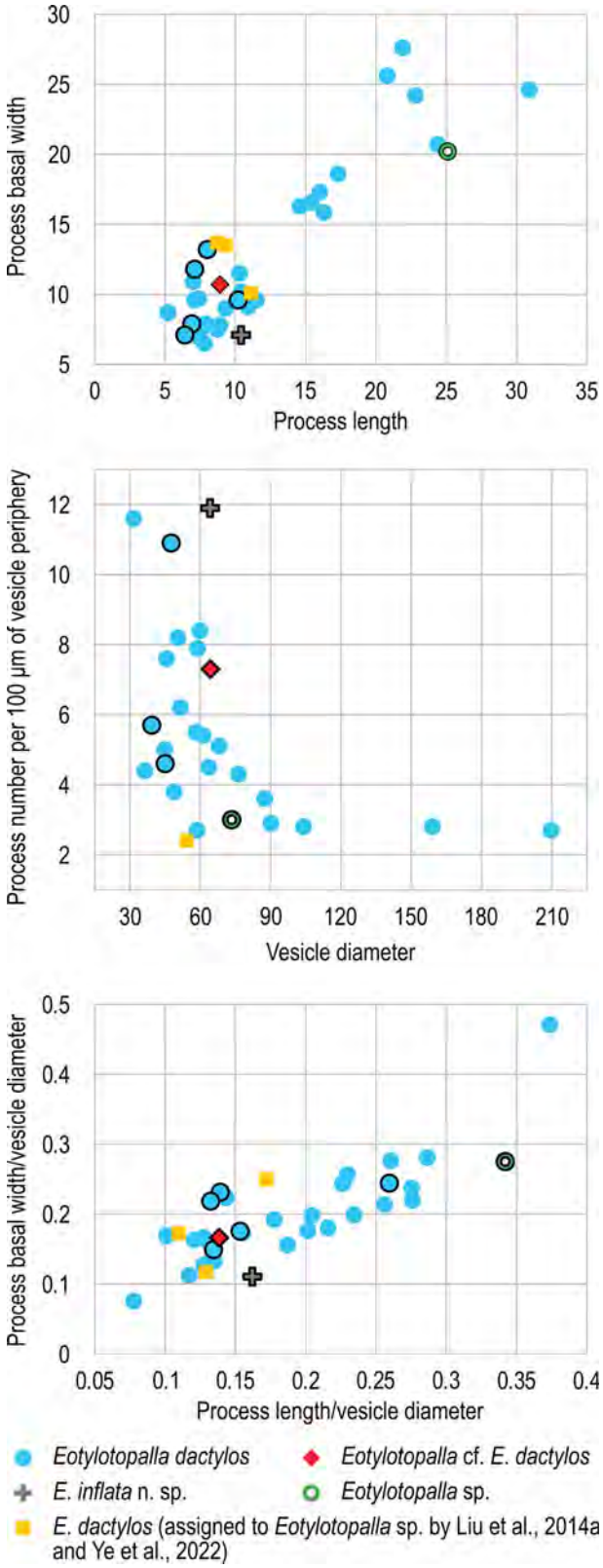

Figure 12. Morphological comparisons between *Eotylotopalla* specimens described here, published *Eotylotopalla dactylos*, and specimens identified as *Eotylotopalla* sp. by Liu et al. (2014a) and by Ye et al. (2022) but reassigned to *Eotylotopalla dactylos* in this study. Symbols with black outline represent specimens described in this study. Note that two of the three specimens published as *Eotylotopalla* sp. (Liu et al., 2014a, fig. 31.10, 31.11, and Ye et al., 2022, fig. 23H–J) are very poorly preserved thus their process density (number of processes per 100 µm of vesicle periphery) is unmeasurable.

https://doi.org/10.1017/jpa.2023.92 Published online by Cambridge University Press

examined in a petrographic thin section, its vesicle diameter measurement is likely a minimum estimate because the specimen may be tangentially cut. Similarly, a specimen of *E. dactylos* illustrated by Ouyang et al. (2021, fig. 14J), characterized by an even smaller vesicle (~59 µm in diameter) and a small number of large processes (~22 µm in length or 37% of vesicle diameter) also may be assigned to *E. apophysa*. Thus, the specimen of *E. dactylos* published in Ouyang et al. (2021) is questionably included in the synonym list.

Eotylotopalla cf. *E. dactylos* Zhang et al., 1998
Figure 11.5, 11.6, 11.9–11.12

cf. 1998 *Eotylotopalla dactylos* Zhang et al., p. 26, fig. 7.8, 7.9.
2022 *Eotylotopalla* cf. *E. dactylos*; Shi et al., fig. 8B (the specimen described here and illustrated in Fig. 11.5, 11.6, 11.9–11.12).

Description and measurements.—Vesicle small and spheroidal, with basally separated processes densely distributed on the vesicle. Processes are uniform and truncated conical in shape. The side walls of processes are straight. Vesicle diameter about 64 µm, with about 7 processes per 100 µm of vesicle periphery; processes length 6.9–10.9 µm (with an average of 8.9 µm measured on four processes) or 10.7–17.0% of vesicle diameter (with an average of 13.8%), process basal width 7.6–12.5 µm (with an average of 10.7 µm measured on four processes), process terminal width 3.7–6.4 µm (with an average of 5.0 µm measured on four processes).

Material.—One illustrated specimen (Fig. 11.5, 11.6, 11.9–11.12).

Remarks.—The illustrated specimen is distinct in its sharply terminated processes but is otherwise comparable to *Eotylotopalla*. Examination under polarized light (Fig. 11.9–11.12) shows that the process terminal truncation is not a taphonomic artifact (e.g., recrystallization). Truncated terminations are common in previously reported *E. dactylos* specimens, but the transition from the side wall to distal end of the processes in these specimens is smooth and gradual, as opposed to the angular transition observed in the illustrated specimen (red arrowheads in Fig. 11.9–11.12). We cannot rule out the possibility that the angular transition is due to mechanical breakage of the processes, however the uniform length of the processes is remarkable for broken processes. Abrasion by tumbling at a constant rate may result in similar process lengths but is unlikely to form flat terminations as observed. Thus, this specimen is currently placed in an open nomenclature related to *E. dactylos*.

Eotylotopalla inflata new species
Figure 13

Holotype.—PB202027, thin section 19TP-1-38, ZEISS Scope A1 coordinates 14×105, England Finder coordinates N30/3 (Fig. 13), reposited at NIGPAS, from Doushantuo Formation at the Tianping section in Zhangjiajie area, Hunan Province, South China.

Diagnosis.—A species of *Eotylotopalla* with terminally inflated processes that have a slightly expanded base, a neck, and a bulbous distal end, with an overall shape resembling a button mushroom.

Description and measurements.—Vesicle small, spheroidal or ovoidal, with evenly distributed, basally connected or separated processes. Processes hollow and open to vesicle cavity, homomorphic, with a widened base, and an inflated bulbous termination, and a neck- or waist-like structure in between. Vesicle diameter about 64 µm, about 12 processes per 100 µm of vesicle periphery; processes length 8.7–11.5 µm with an average of 10.4 µm measured on eight processes or 13.6–18.0% of vesicle diameter with an average of 16.1%, process basal width 5.7–8.5 µm with an average value of 7.1 µm measured on eight processes, maximal width of inflated process termination 4.4–6.4 µm with an average value of 5.5 µm measured on eight processes, minimal width of process waist 2.5–3.2 µm with an average value of 2.8 µm measured on seven processes.

Etymology.—From Latin *inflatus*, inflated, with reference to the inflated terminal end of the processes.

Material.—A single well-preserved specimen (the holotype, Fig. 13).

Remarks.—The illustrated specimen is distinctive in its basally widened and terminally swollen processes that resemble a button mushroom. This distinctive morphology is observed in more than 20 processes in the specimen, supporting the repeatability and arguing against a taphonomic origin of this diagnostic feature. Somewhat similar process morphology has been described in *Stellarossica ampla* Vorob'eva and Sergeev, 2018, from the Ura Formation in Siberia and two species of *Keltmia* (*K. cornifera* Vorob'eva, Sergeev, and Knoll, 2009, and *K. irregularia* Vorob'eva, Sergeev, and Knoll, 2009) from the Vychegda Formation in East European Platform. However, these latter species can be distinguished from *Eotylotopalla inflata* n. sp. by their much larger vesicle, notably fewer processes, much larger proportional lengths of processes, and most importantly, the terminal end of their processes is not as strongly inflated as in the new species where the maximum width of process termination is almost double the minimum width of process waist. There are other acanthomorphs with significantly expanded process bases and terminations, including all *Urasphaera* species and *Weissiella brevis* Xiao et al., 2014. However, *Urasphaera* species and *Weissiella brevis* are characterized by processes with flat or truncated terminations, thus different from the bulbous terminations reported here.

Papillomembrana Spjeldnaes, 1963, emend. Vidal, 1990, is another genus characterized by processes with a bulbous terminal end, but it is diagnosed as an acanthomorph with medium to large vesicle size (Xiao et al., 2014), and the processes of both *P. boletiformis* Xiao et al., 2014, and *P. compta* Spjeldnaes, 1963, emend. Vidal, 1990, lack a well-defined basal expansion and have a basal width smaller than the terminal width. The illustrated specimen is small in vesicle size, and its processes are basally widened, thus different from known *Papillomembrana* species. To assign the illustrated specimen to *Papillomembrana*

https://doi.org/10.1017/jpa.2023.92 Published online by Cambridge University Press

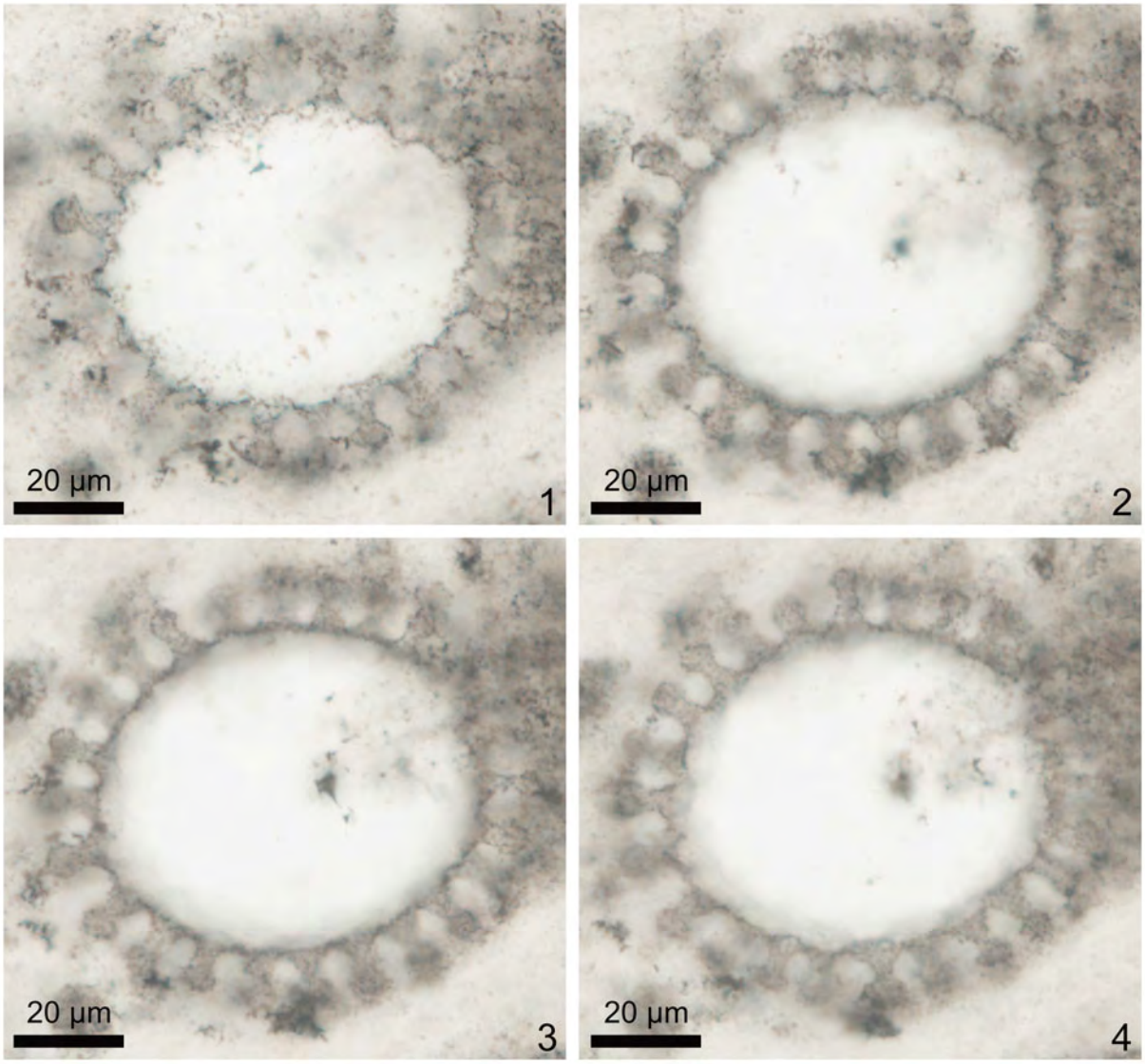

Figure 13. *Eotylotopalla inflata* new species. (**1–4**) Holotype, PB202027, thin section 19TP-1-38, N30/3, showing the same area at different focal levels.

would require an emendation to this genus and would significantly increase the morphological perimeter of this genus. Considering that the small vesicle with densely distributed, distally rounded processes of the specimen described here (Fig. 13) fits the genus diagnosis of *Eotylotopalla*, and that it is different from other existing species of *Eotylotopalla* species in its basally and distally expanded processes, we establish a new species of *Eotylotopalla* even though there is only one available specimen.

Eotylotopalla sp.
Figure 10.5–10.7

Description and measurements.—Small spheroidal vesicle with large, hollow, heteromorphic processes that can be either cylindrical or bulbous. Cylindrical-shaped processes have rounded or blunt terminal ends. Some processes show a notable constriction in the basal or middle part, resulting in mushroom- or dumbbell-like morphology. The processes vary in basal width and the presence of a constriction but are more consistent in length and the rounded terminal end. Vesicle diameter about 73 μm; process length 21.4–30.5 μm (measured on seven processes, with an average of 25.1 μm and a standard deviation of 3.0 μm), process basal width 12.6–30.5 μm (on seven processes, with an average of 20.2 μm and a standard deviation of 6.0 μm), process terminal width 14.7–27.4 μm (on five processes, with an average of 19.3 μm and a standard deviation of 4.6 μm), process constriction width 6.2–19.1 μm (on four processes, with an average of 10.1 μm and a standard deviation of 5.2 μm). About seven processes are present around half of the vesicle periphery, equivalent to three processes per 100 μm of vesicle periphery.

Material.—One specimen illustrated in Figure 10.5–10.7.

Remarks.—The specimen described here is similar to *Eotylotopalla dactylos* in vesicle size (Fig. 12) and the presence of cylindrical processes with rounded or blunt terminal ends. It is also similar to *E. apophysa* and *E. delicata*

https://doi.org/10.1017/jpa.2023.92 Published online by Cambridge University Press

in the presence of bulbous-shaped processes, and to *E. inflata* n. sp. in the presence of mushroom-like processes. However, it is distinct in its remarkably heteromorphic processes, which can be 12.6–30.5 µm in basal width and can be cylindrical or mushroom-like due to the presence of a constriction (Fig. 10.7). Variation in process size and shape has been reported for *E. dactylos* (e.g., Zhou et al., 2007, fig. 4F; Liu et al., 2014a, fig. 31.4), but the amount of morphological variation observed in the single specimen illustrated here is remarkable. On the other hand, the irregular morphology of the only available specimen dissuades us from establishing a new species. Therefore, although this specimen probably represents a new form, it is temporarily placed in open nomenclature.

Genus *Hocosphaeridium* Zang in Zang and Walter, 1992, emend. Xiao et al., 2014.

Type species.—*Hocosphaeridium scaberfacium* Zang in Zang and Walter, 1992, emend. Liu et al., 2014a.

Other species.—*Hocosphaeridium anozos* (Willman in Willman and Moczydłowska, 2008) Xiao et al., 2014; *H. dilatatum* Liu et al., 2014a.

Hocosphaeridium anozos (Willman in Willman and Moczydłowska, 2008), Xiao et al., 2014
Figure 14

1992 *Hocosphaeridium scaberfacium* Zang in Zang and Walter, fig. 45 G (not 45A–F).
2005 *Tanarium irregulare*? Moczydłowska, Vidal, and Rudavskaya; Grey, p. 309, fig. 225.
2008 *Tanarium anozos* Willman in Willman and Moczydłowska, p. 526, fig. 13A–F.
2011 *Tanarium anozos* Willman; C. Yin et al., fig. 6d.
2012 *Tanarium anozos* Willman and Moczydłowska; Liu et al., fig. 3A–C.
2013 *Tanarium anozos*; Liu et al., fig. 11B.
2014 *Hocosphaeridium anozos* (Willman in Willman and Moczydłowska) Xiao et al., p. 28, fig. 16.
2014a *Hocosphaeridium anozos* (Willman in Willman and Moczydłowska) Xiao et al.; Liu et al., p. 75, figs. 37, 38, 39.1.
2014b *Hocosphaeridium anozos*; Liu et al., fig. 8A, B.
non 2016 *Tanarium anozos* Willman in Willman and Moczydłowska; Prasad and Asher, p. 54, pl. VII, figs. 6, 7.
2017 *Hocosphaeridium anozos*; Hawkins et al., fig. 7E, F.
2019 *Hocosphaeridium anozos* (Willman in Willman and Moczydłowska) Xiao et al.; Liu and Moczydłowska, p. 113, fig. 60.
2022 *Hocosphaeridium anozos* (Willman in Willman and Moczydłowska) Xiao et al.; Shi et al., fig. 8G–K (two of the 20 specimens described here).

Holotype.—CPC 39635, reposited at Commonwealth Palaeontological Collection (CPC) at Geoscience Australia, Canberra, from the Ediacaran Tanana Formation of the Giles 1 drillhole in Officer Basin, South Australia.

Description and measurements.—Most vesicles are deformed to various degrees, but were originally spheroidal in shape, and measurements can be taken on relatively well-preserved specimens. Processes evenly distributed on the vesicle surface, cylindrical or slightly tapering toward a distal end that is hooked or recurved. Vesicle diameter 88–227 µm (N = 13, mean = 143 µm, SD = 39 µm); process length 20.8–54.8 µm (N = 19, mean = 33.4 µm, SD = 7.4 µm), 14.0–34.9% of vesicle diameter (N = 13, mean = 24.6%, SD = 7.3%); process width (diameter) 1.0–2.4 µm (N = 20, mean = 1.9 µm, SD = 0.3 µm); process density unmeasurable due to the small number of processes with a well-preserved base.

Material.—Four illustrated specimens (Fig. 14) and 16 additional specimens (including the one illustrated by Shi et al., 2022, fig. 8J, K).

Remarks.—These specimens are poorly preserved in general, but all bear a characteristically hooked tip in the terminal end of their thin, cylindrical processes. They can be differentiated from *Hocosphaeridium scaberfacium* by their cylindrical processes, and from *H. dilatatum* by their low process density and the lack of a process basal expansion in most specimens. In some processes, an obtusely conical or even slightly inflated base is observed (e.g., process on the right in Fig. 14.13). However, such structures only appear in deformed specimens, and thus are likely to be taphonomic in origin. Only specimens with well-defined process terminal ends are accepted as *Hocosphaeridium*. There are far more acanthomorphic specimens that resemble *H. anozos* in overall size and morphology but are taxonomically unidentifiable because the terminal ends of their processes are not captured in thin sections. Therefore, the reported abundance of *H. anozos* in this study is likely an underestimate.

Hocosphaeridium scaberfacium Zang in Zang and Walter, 1992, emend. Liu et al., 2014a
Figure 15

1992 *Hocosphaeridium scaberfacium* Zang in Zang and Walter, p. 61, fig. 45A–F (not 45G).
1998 *Hocosphaeridium scaberfacium* Zang and Walter; Yuan and Hofmann, p. 203, fig. 10A, B.
1998 *Goniosphaeridium conoideum* (Kolosova) Zhang et al., p. 32, fig. 9.1–9.4.
2002 *Goniosphaeridium conoideum* (Kolosova) Zhang et al.; Yuan et al., p. 74, fig. 100.
2005 *Tanarium conoideum* Kolosova; emend. Moczydłowska et al.; Grey, p. 299, figs. 212, 213.
2006 *Tanarium conoideum* Kolosova, emend. Moczydłowska et al.; Willman et al., p. 32, pl. VI, figs. 1, 2.
2008 *Tanarium conoideum* Kolosova, emend. Moczydłowska et al.; Willman and Moczydłowska, p. 526, fig. 12C.
2010 *Tanarium conoideum* (Kolosova) emend. Moczydłowska et al.; Golubkova et al., pl. III, fig. 7, pl. IV, fig. 2.
2012 *Tanarium anozos* Willman in Willman and Moczydłowska; Moczydłowska and Nagovitsin, p. 18, fig. 8A–C.
2012 *Tanarium anozos* Kolosova; Liu et al., fig. 3D–F.

https://doi.org/10.1017/jpa.2023.92 Published online by Cambridge University Press

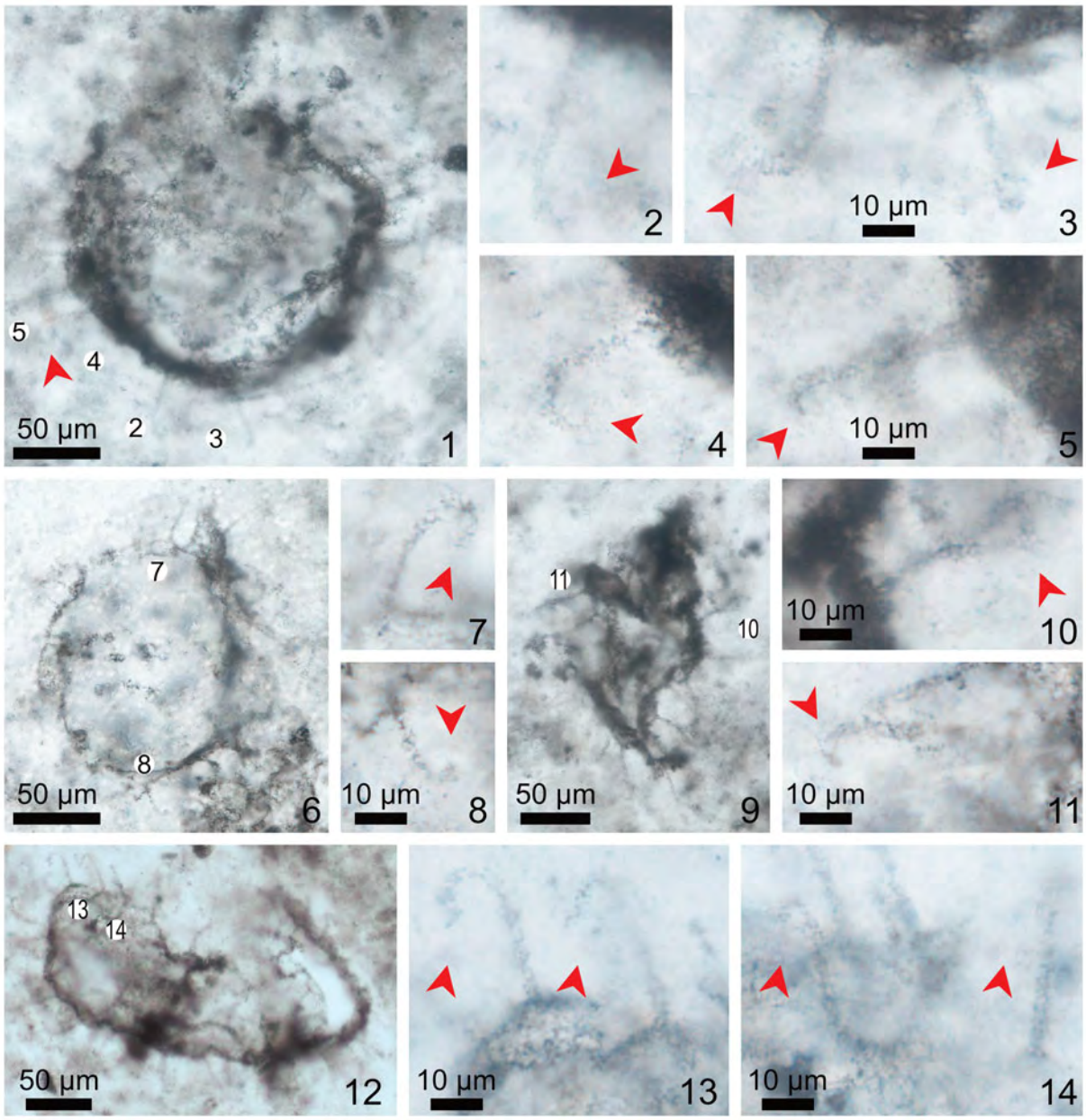

Figure 14. *Hocosphaeridium anozos* (Willman in Willman and Moczydłowska, 2008) Xiao et al., 2014; red arrowheads denote hooked process terminations. (**1–5**) PB202028, thin section 21DC-2-20, R20/2; circled 2–5 in (**1**) mark areas magnified in (**2–5**), respectively; scale bars in (**3**) and (**5**) also apply to (**2**) and (**4**). (**6–8**) PB202029, thin section 21DC-2-20, P18/2; circled 7 and 8 in (**6**) mark areas magnified in (**7**) and (**8**), respectively; scale bar in (**8**) also applies to (**7**). (**9–11**) PB202030, thin section 21DC-2-20, R21; circled 10 and 11 in (**9**) mark areas magnified in (**10**) and (**11**), respectively. (**12–14**) PB202031, thin section 21DC-2-20, O18/3; circled 13 and 14 in (**12**) mark areas magnified in (**13**) and (**14**), respectively.

2013 *Tanarium conoideum*; Liu et al., fig. 11A.
2014 *Hocosphaeridium scaberfacium* Zang in Zang and Walter; Xiao et al., p. 27.
2014a *Hocosphaeridium scaberfacium* Zang in Zang and Walter, emend. Liu et al., p. 78, figs. 39.3, 41, 42.
2014b *Hocosphaeridium scaberfacium*; Liu et al., fig. 8C.
2021 *Hocosphaeridium scaberfacium*; Liu et al., fig. 6.3, 6.4.
2022 *Hocosphaeridium scaberfacium* Zang in Zang and Walter; Shi et al., fig. 8L, M (one of the specimens described here).
2022 *Hocosphaeridium scaberfacium* Zang in Zang and Walter, 1992, emend. Liu et al.; Ye et al., p. 41, fig. 26H–J.

Holotype.—CPC 27765, thin section 87ZW01-8, reposited at Commonwealth Palaeontological Collection (CPC) at Geoscience Australia, Canberra, from the Ediacaran Pertatataka Formation of the Rodinga 4 drill core in Amadeus Basin, Northern Territory, Australia.

Description and measurements.—Vesicles mostly medium-sized, compressed to different degrees but were originally spheroidal based on several less severely compressed specimens (Fig. 15.1–15.3, 15.4–15.7). Vesicles bear a varying number of conical and distally tapering processes with a relatively wide base and a hooked or recurved tip. Vesicle diameter 114–212 μm

https://doi.org/10.1017/jpa.2023.92 Published online by Cambridge University Press

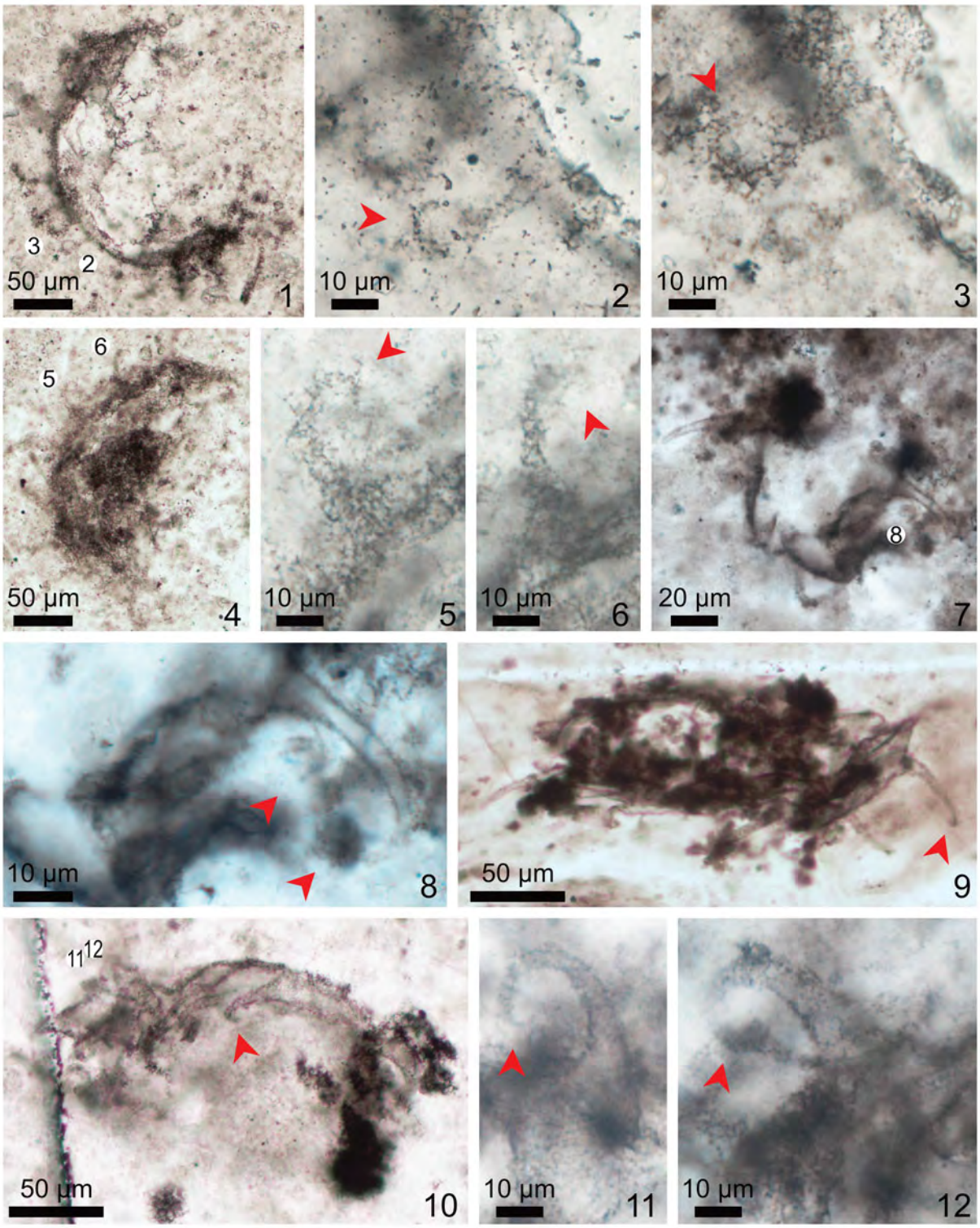

Figure 15. *Hocosphaeridium scaberfacium* Zang in Zang and Walter, 1992, emend. Liu et al., 2014a; red arrowheads denote hooked process terminations. (**1–3**) PB202032, thin section 19HP-1-28, Q33; circled 2 and 3 in (**1**) mark the same area magnified in (**2**) and (**3**), respectively, at different focal levels to show different processes. (**4–6**) PB202033, thin section 19TP-1-40, K44; circled 5 and 6 in (**4**) mark areas magnified in (**5**) and (**6**), respectively. (**7, 8**) PB202034, thin section 19CW-6-15, N40/4; circled 8 in (**7**) marks the area magnified in (**8**). (**9**) PB202035, thin section 19SDP-7-3, G41/1. (**10–12**) PB202036, thin section 21DC-2-20, P18; circled 11 and 12 in (**10**) mark areas magnified in (**11**) and (**12**), respectively.

(N = 6, mean = 170 µm, SD = 38 µm); process length 36.3–58.3 µm (N = 9, mean = 45.2 µm, SD = 7.9 µm), 18.6–39.5% of vesicle diameter (N = 6, mean = 26.5%, SD = 8.4%); process basal width 6.8–22.8 µm (N = 9, mean = 12.9 µm, SD = 4.8 µm). As measured on one specimen (Fig. 15.1–15.3), there are about two processes per 100 µm of vesicle periphery.

https://doi.org/10.1017/jpa.2023.92 Published online by Cambridge University Press

Material.—Five illustrated specimens (Fig. 15) and four additional specimens (including the one illustrated by Shi et al., 2022, fig. 8L, M).

Remarks.—Despite the modest preservation quality, the conical processes with a hooked termination and the lack of a basal expansion structure are clearly discernable in our specimens. These features allow the taxonomical identification to *Hocosphaeridium scaberfacium*. Although the distal part of processes is recurved for at least 180° and up to 270° (e.g., Fig. 15.2, 15.3), the basal part of the processes remains straight, indicating that the hooked structures are biological in origin. As in the case of *H. anozos*, there are some specimens in our collection that could be *H. scaberfacium* but are currently placed in the category of unidentified acanthomorphs because the distal part of the processes is not captured in the thin sections.

Genus *Knollisphaeridium* Willman and Moczydłowska, 2008, emend. Liu and Moczydłowska, 2019

Type species.—*Knollisphaeridium maximum* (Yin, 1987) Willman and Moczydłowska, 2008, emend. Liu and Moczydłowska, 2019.

Other species.—*Knollisphaeridium*? *bifurcatum* Xiao et al., 2014; *K. coniformum* Liu and Moczydłowska, 2019; *K. denticulatum* Liu et al., 2014a; *K. gravestockii* (Grey, 2005) Willman and Moczydłowska, 2008; *K. longilatum* Liu et al., 2014a; *K. obtusum* Liu et al., 2014a; *K. parvum* Liu et al., 2014a; *K. triangulum* (Zang in Zang and Walter, 1992) Willman and Moczydłowska, 2008, emend. Xiao et al., 2014.

Knollisphaeridium maximum (Yin, 1987), Willman and Moczydłowska, 2008, emend. Liu and Moczydłowska, 2019
Figure 16

1987 *Baltisphaeridium maximum* Yin, p. 439, pl. 14, figs. 14, 15.
1992 *Echinosphaeridium maximum* (Yin) Knoll, p. 765, pl. 5, figs. 5, 6.
1994 *Echinosphaeridium maximum* (Yin) Knoll; Tiwari and Knoll, p. 196, pl. I, fig. 3.
1998 *Echinosphaeridium maximum* (Yin) Knoll; Zhang et al., p. 26, figs. 6.9, 6.10, 7.1, 7.2.
non 1998 *Echinosphaeridium maximum* (Yin) Knoll; Zhang et al., p. 26, fig. 6.7, 6.8.
non 1998 *Echinosphaeridium maximum* (Yin) Knoll; Yuan and Hofmann, p. 202, fig. 8A–D.
non 1999 *Echinosphaeridium maximum* (Yin) Knoll; Yin, pl. 4, figs., 4, 5.
non 1999 *Echinosphaeridium maximum*; Xiao and Knoll, fig. 11A–C.
non 2001 *Echinosphaeridium maximum*; Zhou et al., pl. 3, figs. 1, 2.
2004b *Echinosphaeridium maximum* (Yin) Knoll; Zhou et al., p. 353, pl. IV, figs. 1–4.
2008 *Knollisphaeridium maximum* (Yin) Knoll; Willman and Moczydłowska, p. 523, fig. 5E, F.
2009 *Echinosphaeridium maximum*; Liu et al., fig. 2m, n.
2009a *Echinosphaeridium maximum* (Yin) Knoll; Yin et al., pl. 1, fig. 5.
2010 *Echinosphaeridium maximum*; Chen et al., fig. 2.2, 2.3.
2011 *Knollisphaeridium maximum* (Yin) Willman and Moczydłowska; Sergeev et al., p. 1004, fig. 7.5.
2011 *Knollisphaeridium maximum* (Yin, 1987; Knoll, 1992) Willman, 2007 [sic]; C. Yin et al., figs. 5f, 6e.
2013 *Knollisphaeridium maximum*; Liu et al., fig. 11N, O.
2013 *Knollisphaeridium* sp.; Zeng et al., fig. 4.3, 4.4.
2014a *Knollisphaeridium maximum* (Yin) Willman and Moczydłowska; Liu et al., p. 83, figs. 44.4, 46, 47.
2014b *Knollisphaeridium maximum*; Liu et al., fig. 8D, E.
2014b *Knollisphaeridium* sp.; Liu et al., fig. 8H.
non 2014 *Knollisphaeridium maximum* (Yin) Willman and Moczydłowska; Xiao et al., p. 30, fig. 19.
2017 *Knollisphaeridium maximum*; Ouyang et al., fig. 9A–H.
2019 *Knollisphaeridium maximum* (Yin) Willman and Moczydłowska, emend. Liu and Moczydłowska, p. 118, fig. 64.
non 2019 *Knollisphaeridium maximum* (Yin) Willman and Moczydłowska, emend. Liu and Moczydłowska, fig. 65.
2019 *Knollisphaeridium maximum*; Ouyang et al., fig. 13A–D.
2020 *Knollisphaeridium maximum* (Yin) emend. Willman and Moczydłowska; Vorob'eva and Petrov, p. 374, pl. II, figs. 19, 20.
non 2020 *Knollisphaeridium maximum*; Grazhdankin et al., fig. 3D.
2021 *Knollisphaeridium maximum* (Yin) Willman and Moczydłowska; Ouyang et al., fig. 15K–N.
2022 *Knollisphaeridium maximum* (Yin) Willman and Moczydłowska; Shi et al., fig. 9A–C (illustrated in Fig. 16.5, 16.7, 16.8, one of the specimens described here).
2022 *Knollisphaeridium maximum* (Yin) Willman and Moczydłowska, emend. Liu and Moczydłowska; Ye et al., p. 42, fig. 28D–G.
2023 *Knollisphaeridium maximum* (Yin) emend. Willman; Golubkova, pl. 7, fig. 7.

Holotype.—Specimen illustrated in Yin (1987, pl. 14, figs. 14, 15), thin section #Hm80-8-6, reposited at NIGPAS, from the Ediacaran Doushantuo Formation at Shipai in the Yangtze Gorges area, Hubei Province, South China (also illustrated in Liu and Moczydłowska, 2019, fig. 64A–C).

Description and measurements.—Vesicle large, spheroidal (some deformed to various degrees), covered by evenly and closely distributed, basally separated processes. Processes homomorphic, conical, most taper gradually toward a pointed tip. In some specimens, processes with (blue arrowhead in Fig. 16.7) and without (red arrowhead in Fig. 16.7) a basal

https://doi.org/10.1017/jpa.2023.92 Published online by Cambridge University Press

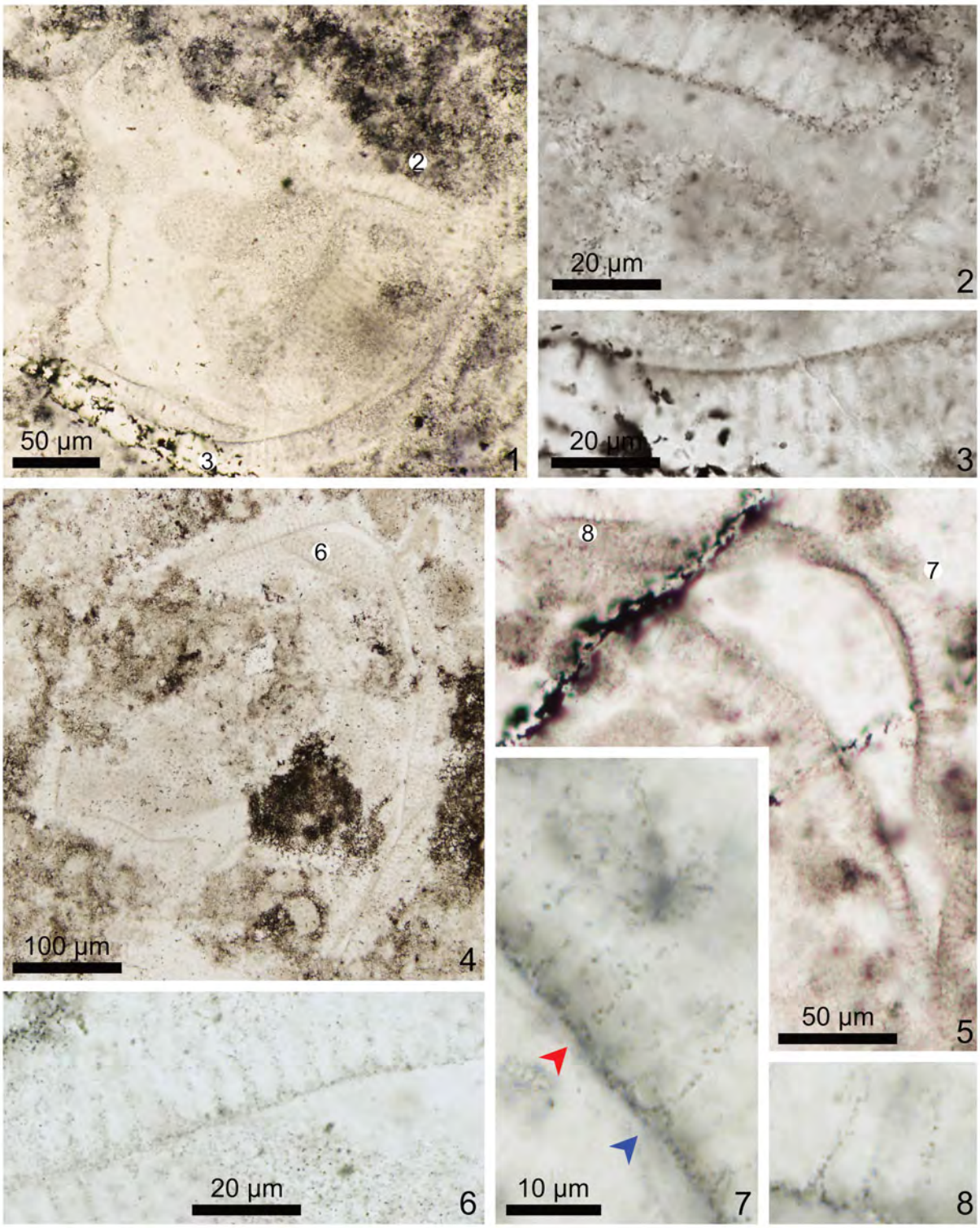

Figure 16. *Knollisphaeridium maximum* (Yin, 1987) Willman and Moczydłowska, 2008, emend. Liu and Moczydłowska, 2019. (**1–3**) PB202037, thin section 14HA-140-1, S53/4; circled 2 and 3 in (**1**) mark areas magnified in (**2**) and (**3**), respectively. (**4, 6**) PB202038, thin section 14HA-140-3, E28/4; circled 6 in (**4**) marks the area magnified in (**6**). (**5, 7, 8**) PB202039, thin section 21DC-6-9, H34; circled 7 and 8 in (**5**) mark areas magnified in (**7**) and (**8**), respectively; scale bar in (**7**) also applies to (**8**); red and blue arrowheads in (**7**) denote undeformed and slightly deformed processes, respectively.

expansion can be found on the same vesicle. No outer membrane is observed. Vesicle diameter 193–448 µm (N = 9, mean = 332 µm, SD = 114 µm); process length 9.5–19.0 µm (N = 11, mean = 14.9 µm, SD = 2.9 µm), 2.9–8.5% of vesicle diameter (N = 8, mean = 5.0%, SD = 2.0%); process basal width 2.4–5.6 µm (N = 12, mean = 3.7 µm, SD = 1.1 µm); 15–27 processes per 100 µm of vesicle periphery (N = 11, mean = 20, SD = 4 µm).

https://doi.org/10.1017/jpa.2023.92 Published online by Cambridge University Press

Material.—Three illustrated specimens (Fig. 16) and nine additional specimens (including the two illustrated in Ouyang et al., 2017, fig. 9A–C, 9F–H).

Remarks.—*Knollisphaeridium maximum* is one of the most widely distributed Ediacaran acanthomorphic taxa and is distinctive in its large vesicle size and proportionally small, densely distributed, echinate conical processes. As most previously reported specimens of this species, the current specimens lack a multilayered membrane, which is considered diagnostic of *K. maximum* as emended by Liu and Moczydłowska (2019), but they possess all other diagnostic features of this species. Some specimens described here have processes with a slightly broadened basal expansion (blue arrowhead in Fig. 16.7), resembling processes of *K. coniformum* or *K. triangulum*. However, most processes do not have a basal expansion (red arrowhead in Fig. 16.7), indicating the apparent basal expansions may be taphonomic artifacts (e.g., subtle deformation at the process base during degradation and compression in early diagenesis).

Sixty-one specimens identified as small-sized *Knollisphaeridium maximum* by Liu and Moczydłowska (2019, fig. 65, vesicle diameter 40–86 µm and process length 4.2–10.5% of vesicle diameter) are here excluded from this species, and likely belong to *Appendisphaera heliaca*. These specimens have small vesicles and proportionally long processes, features that contradict the diagnosis of *Knollisphaeridium*. According to the emended diagnosis of Liu and Moczydłowska, 2019, this genus is characterized by its medium-sized to large vesicle. Instead, these specimens are similar to *A. heliaca* in almost all morphological features, including vesicle size (55 µm for holotype, 43–72 µm for other published specimens; Liu and Moczydłowska, 2019; Ouyang et al., 2021), relative process length (14.5% of vesicle diameter for holotype, 5.7–21.1% for other published specimens; Liu and Moczydłowska, 2019; Ouyang et al., 2021), and process density and distribution.

Genus *Megasphaera* Chen and Liu, 1986, emend. Xiao et al., 2014.

Type species.—*Megasphaera inornata* Chen and Liu, 1986, emend. Xiao et al., 2014.

Other species.—*Megasphaera cymbala* Xiao et al., 2014; *M. ornata* Xiao and Knoll, 2000, emend. Xiao et al., 2014; *M. patella* Xiao et al., 2014; *M. puncticulosa* Xiao et al., 2014; *M. minuscula* Anderson et al., 2019 (although the validity of this species is questionable).

Remarks.—Generally described together with acanthomorphs, *Megasphaera* is a special genus that contains both ornamented and unornamented species. To date, two unornamented species have been erected under the genus *Megasphaera*, including *M. inornata* and *M. minuscula*, with the former as the type species. Vesicle ornamentations are the key feature that distinguish acanthomorphs from sphaeromorphs (e.g., leiospheres). Therefore, the validity of *M. inornata* (thus also *Megasphaera*) is related with how it differs from leiospheres. Morphological and structural differences between *M. inornata* and leiospheres are threefold. Firstly, although leiospheres also contain large species, they are mostly small to medium-sized (Butterfield et al., 1994). On the contrary, *Megasphaera* was erected emphasizing its large size (Chen and Liu, 1986), and a large vesicle is still the major diagnostic feature of this genus (Xiao et al., 2014, in which a large vesicle is defined as vesicle diameter > 200 µm). Secondly, *M. inornata* exhibits a cell division sequence as recorded by various numbers (one to more than 100) of uniformly shaped and tightly packed daughter cells within the vesicle, which were separately named *Megaspheara*, *Parapandorina*, and *Megaclonophycus* (Xiao et al., 2014). Leiospheres may also contain cells within the vesicle, but these cells are irregular in shape and size (Liu et al., 2014a), do not form a closely compacted spheroidal body, and do not form a cell division sequence as generally seen in *Megasphaera* specimens. Third and importantly, the smooth-walled *M. inornata* may represent a taphonomic or developmental variation of *M. ornata*, which does have a sculptured vesicle surrounding a smooth vesicle, therefore these two species may be biologically conspecific (Xiao et al., 2014). However, the above-mentioned features that distinguish *M. inornata* from leiospheres do not apply to *M. minuscula*, which has a relatively small vesicle (inconsistent with current diagnosis of *Megasphaera*) that contains internal bodies of various size and has no ornamented counterpart. Thus, it is uncertain whether *M. minuscula* should be accepted as a species of *Megasphaera*.

Megasphaera inornata Chen and Liu, 1986, emend. Xiao et al., 2014
Figure 17.1

1986 *Megasphaera inornata* Chen and Liu, p. 51, pl. 1, fig. 4.
1995 *Parapandorina raphospissa* Xue et al., p. 692, pl. I, figs. 1–3.
1995 *Parapandorina beidoushanensis* Xue et al., p. 692, pl. II, figs. 1, 3–5.
1995 *Parapandorina beidoushanensis* var. *cylindrica* Xue et al., p. 693, pl. II, fig. 2.
1995 *Megacolonophycus onustus* Xue et al., p. 695, pl. III, figs. 3, 4, pl. IV, figs. 1–6, pl. V, figs. 2, 6–9.
1995 *Colossotetrahedrion ovimpositum* Xue et al., p. 696, pl. V, figs. 3, 5.
2000 *Megasphaera inornata* Chen and Liu, 1986, emend. Xiao and Knoll, p. 773, fig. 3.1, 3.2, 3.4, 3.5, 3.7, 3.11.
2002 *Megasphaera inornata* Chen and Liu; Zhou et al., p. 182, pl. II, figs. 1, 2.
2004b *Parapandorina raphospissa* Xue et al.; Zhou et al., pl. VI, figs. 5–9.
2004b *Megacolonophycus onustus* Xue et al.; Zhou et al., pl. VI, fig. 10.
2008 *Parapandorina raphospissa* (Xue et al.) Xiao and Knoll; Xie et al., p. 285, pl. II, fig. 4.
2008 *Megacolonophycus onustus* Xue et al.; Xie et al., p. 284, pl. II, figs. 5, 6.
2009b *Megasphaera inornata* Chen and Liu; Yin et al., fig. 3a, b.
2009b *Megacolonophycus onustus* Xue et al.; Yin et al., fig. 4b–d.

https://doi.org/10.1017/jpa.2023.92 Published online by Cambridge University Press

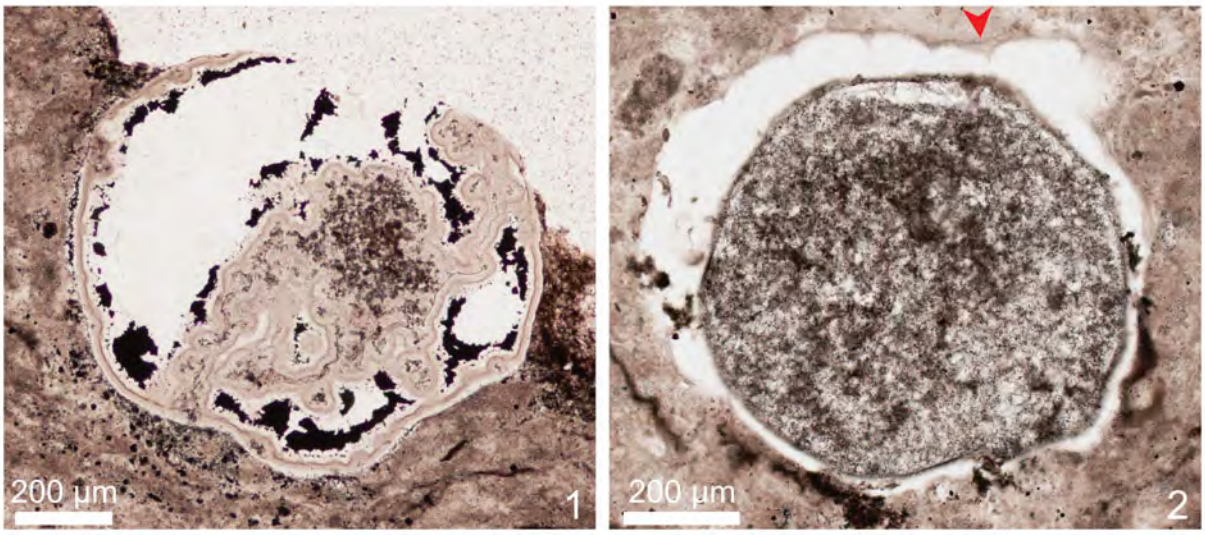

Figure 17. (**1**) *Megasphaera inornata* Chen and Liu, 1986, emend. Xiao et al., 2014; PB202040, thin section 19SDP-1-13, K42/2. (**2**) *Megasphaera ornata* Xiao and Knoll, 2000, emend. Xiao et al., 2014; PB202041, thin section 19SDP-1-22, P39/2; red arrowhead denotes the outer surface of the sculptured vesicle wall.

2014 *Megasphaera inornata* Chen and Liu, emend. Xiao et al., p. 35.
2015 *Megasphaera inornata* Chen and Liu, emend. Xiao et al.; Ye et al., p. 50, pl. II, figs. 1–13.
2017 *Megasphaera inornata* Chen and Liu, emend. Xiao et al.; Nie et al., p. 380, fig. 10.
2019 *Megasphaera inornata*; Ouyang et al., fig. 9L.
2019 *Megasphaera inornata* Chen and Liu, emend. Xiao et al.; Shang et al., p. 24, fig. 14A, B.
2020 *Megasphaera inornata*; Ouyang et al., figs. 3A–J, 4.
2020 *Megasphaera inornata* Chen and Liu, emend. Xiao et al.; Shang and Liu, p. 158, fig. 5C.
2020 *Megasphaera inornata* Chen and Liu, emend. Xiao et al.; Yang et al., p. 9, fig. 3.
2020 Acritarcha gen. et sp. indet.; Shang and Liu, p. 159, fig. 6D, E.
2021 *Megasphaera inornata* Chen and Liu, emend. Xiao et al.; Ouyang et al., fig. 16A–D.
2022 *Megasphaera inornata* Chen and Liu, emend. Xiao et al.; Ye et al., p. 47, fig. 49.

Neotype.—The specimen illustrated by Xiao and Knoll (2000, fig. 3.1) was designated as a neotype (HUHPC-64837, SRA-1, photo 419) by Xiao et al. (2014).

Description and measurements.—A large, oval vesicle with a diameter of about 896 µm. No ornamentation is observed.

Material.—One illustrated specimen (Fig. 17.1).

Remarks.—With a relatively regular shape, the described specimen is likely an acritarch vesicle without ornamentation. Its large size and uniformly thick vesicle wall are comparable to those of *Megasphaera inornata*. No primary internal structures, such as internal bodies, are present, likely due to degradation and secondary mineral precipitation, as evinced by the abundance of botryoidal cements and spherules, which are interpreted as possible bacterial infection in degrading specimens (Xiao and Knoll, 1999).

Megasphaera ornata Xiao and Knoll, 2000, emend. Xiao et al., 2014
Figure 17.2

1993 tubercle-spheroidal type with tortuous tumour; Yin and Xue, pl. I, figs. a, b.
1993 plate-spheroidal type with polygonal plates; Yin and Xue, pl. I, fig. e, pl. II, figs. g–l.
2000 *Megasphaera ornata* Xiao and Knoll, p. 773, figs. 3.12, 3.13, 4.11, 4.12, 5.1–5.4.
2003 *Tianzhushania ornata* (Xiao and Knoll) Yin et al., 2004; Yin et al., pl. II, figs. 1–8.
2003 Unnamed specimens; Yin et al., pl. II, figs. 9–12.
2004 *Tianzhushania ornata* (Xiao and Knoll) Yin et al., figs. 4A, 5C, 6, 7A.
2004 *Tianzhushania* sp.; Yin et al., fig. 4B, C.
2007 *Megasphaera ornata*; Xiao et al., fig. 1A.
2008 *Megasphaera ornata* Xiao and Knoll; Xie et al., p. 284, pl. I, figs. 4, 5.
2011 *Tianzhushania ornata*; C. Yin et al., fig. 4c, e.
2014 *Megasphaera ornata* Xiao and Knoll, emend. Xiao et al., p. 35, fig. 22.
2017 *Megasphaera ornata*; Zhang and Zhang, figs. 3h–l, 4a–d.
2020 *Megasphaera ornata*; Ouyang et al., fig. 3M–R.
2021 *Megasphaera ornata* Xiao and Knoll, emend. Xiao et al.; Ouyang et al., fig. 15R, S.

Holotype.—HUHPC-62990, reposited at the Harvard University Herbaria Paleobotanical Collection, from the Ediacaran Doushantuo Formation in the Weng'an area, Guizhou Province, South China (Xiao and Knoll, 2000, fig. 5.4).

Description and measurements.—A large, spheroidal body with a diameter of about 709 µm, surrounded by an outer layer with sculptures of various size.

https://doi.org/10.1017/jpa.2023.92 Published online by Cambridge University Press

Material.—One illustrated specimen (Fig. 17.2).

Remarks.—This specimen is assigned to *Megasphaera ornata* based on its large vesicle and an outer layer with sculptures that manifest as indentations in thin-section view (red arrowhead in Fig. 17.2). The light-colored zone between the outer sculpture layer and the internal spheroidal body represents secondary cement of micro-quartz. The uneven thickness of the light-colored zone may be caused by taphonomic deformation of the outer vesicle wall and displacement of the internal spheroidal body.

Genus *Mengeosphaera* Xiao et al., 2014

Type species.—*Mengeosphaera chadianensis* (Chen and Liu, 1986) Xiao et al., 2014.

Other species.—*Mengeosphaera angusta* Liu et al., 2014a; *M. bellula* Liu et al., 2014a; *M. constricta* Liu et al., 2014a; *M. eccentrica* Xiao et al., 2014; *M. flammelata* Liu and Moczydłowska, 2019; *M. gracilis* Liu et al., 2014a; *M. grandispina* Liu et al., 2014a; *M. latibasis* Liu et al., 2014a; *M. lunula* Liu and Moczydłowska, 2019; *M. mamma* Ye et al., 2022; *M. matryoshkaformis* Ouyang et al., 2021; *M. membranifera* Shang, Liu, and Moczydłowska, 2019; *M. minima* Liu et al., 2014a; *M. reticulata* (Xiao and Knoll, 1999) Xiao et al., 2014; *M. spinula* Liu et al., 2014a; *M. stegosauriformis* Liu et al., 2014a; *M. uniformis* Liu et al., 2014a.

Mengeosphaera bellula Liu et al., 2014a
Figure 18.1–18.3

2014a *Mengeosphaera bellula* Liu et al., p. 90, figs. 51.2, 52, 53.

Holotype.—IGCAGS-NPIII-266, reposited at Institute of Geology, Chinese Academy of Geological Sciences, from Member III of the Ediacaran Doushantuo Formation at Niuping section in the Yangtze Gorges area, Hubei Province, South China (Liu et al., 2014a, fig. 52.1–52.3).

Description and measurements.—Vesicle small, originally spheroidal, with homomorphic biform processes closely distributed on the vesicle. The process is composed of a basal expansion that tapers rapidly toward a long and thin apical spine. Specimen illustrated (Fig. 18.1–18.3): vesicle diameter about 73 µm, process length about 17.1 µm (23.5% of vesicle diameter) and basal width about 5.6 µm, with about 21 processes per 100 µm of vesicle periphery; length (height) of basal part (from vesicle wall to the point where the process begins to taper significantly) about 2.8 µm (16.4% of process total length), apical spine width (diameter) about 0.9 µm. The other available specimen: vesicle diameter not measured due to compression, process length about 17.7 µm and basal width about 5.4 µm, about 25 processes per 100 µm of vesicle periphery; length of basal part about 4.8 µm (27.1% of process total length), apical spine width about 1.1 µm.

Material.—One illustrated specimen (Fig. 18.1–18.3) and one additional specimen.

Remarks.—The two described specimens have densely arranged biform processes with a basal expansion and a relatively long, thin apical spine. These features, as well as their measurements, are similar to those in *Mengeosphaera bellula* (holotype 75 µm in vesicle diameter, 16 µm in process length or 21% of vesicle diameter, and 5 µm in process basal width). The two available specimens can alternatively be compared to *M. chadianensis*, but *M. chadianensis* commonly has larger vesicles (500–800 µm in diameter for the holotype), and thus the processes of *M. chadianensis* are proportionally shorter and smaller. In addition, the apical spine of *M. chadianensis* typically takes a smaller percentage of the overall process length than in *M. bellula*. Thus, the two specimens described here are more appropriately identified as *M. bellula*.

Two specimens from the Doushantuo Formation in the Shennongjia area that are identified as *Mengeosphaera chadianensis* in Ye et al. (2022, figs. 32A–C, 33A, B) have homomorphic and biform processes resembling those in *M. bellula*, with the lower part of the basal expansion more or less cylindrical, supporting a long and distally tapering apical spine. Process morphology, proportional process length, and relatively long apical spine of the two Shennongjia specimens are more similar to previously reported *M. bellula* than to *M. chadianensis*. However, the two Shennongjia specimens (vesicle diameter about 142 µm for fig. 32A and about 138 µm for fig. 33A in Ye et al., 2022) are both much larger than *M. bellula* specimens from the type locality in the Yangtze Gorges area (50–90 µm in vesicle diameter). Thus, these two specimens are questionably retained as *M. chadianensis*.

Mengeosphaera constricta Liu et al., 2014a
Figure 18.4–18.8

2013 Unnamed F; Liu et al., fig. 12E, F.
2014a *Mengeosphaera constricta* Liu et al., p. 95, figs. 51.4, 56–58.
2014a *Mengeosphaera spicata* Liu et al., p. 101, figs. 51.10, 64.
2017 *Mengeosphaera spicata*?; Ouyang et al., fig. 8O, P (the specimen described here and illustrated in Fig. 18.4–18.8).
2022 *Mengeosphaera constricta* Liu et al.; Ye et al., p. 53, fig. 34A–C.

Holotype.—IGCAGS–WFG–826, reposited at Institute of Geology, Chinese Academy of Geological Sciences, from lower Member III of the Ediacaran Doushantuo Formation at Wangfenggang section in the Yangtze Gorges area, Hubei Province, South China (Liu et al., 2014a, fig. 56.1, 56.2).

Description and measurements.—Vesicle spheroidal, with uniform processes closely arranged on vesicle surface, although only three processes completely preserved. Processes consist of an overall inflated, near-cylindrical basal part and a conical terminal part. The inflated basal expansion is constricted at the contact with the vesicle wall (Fig. 18.5–18.8), and the terminal

https://doi.org/10.1017/jpa.2023.92 Published online by Cambridge University Press

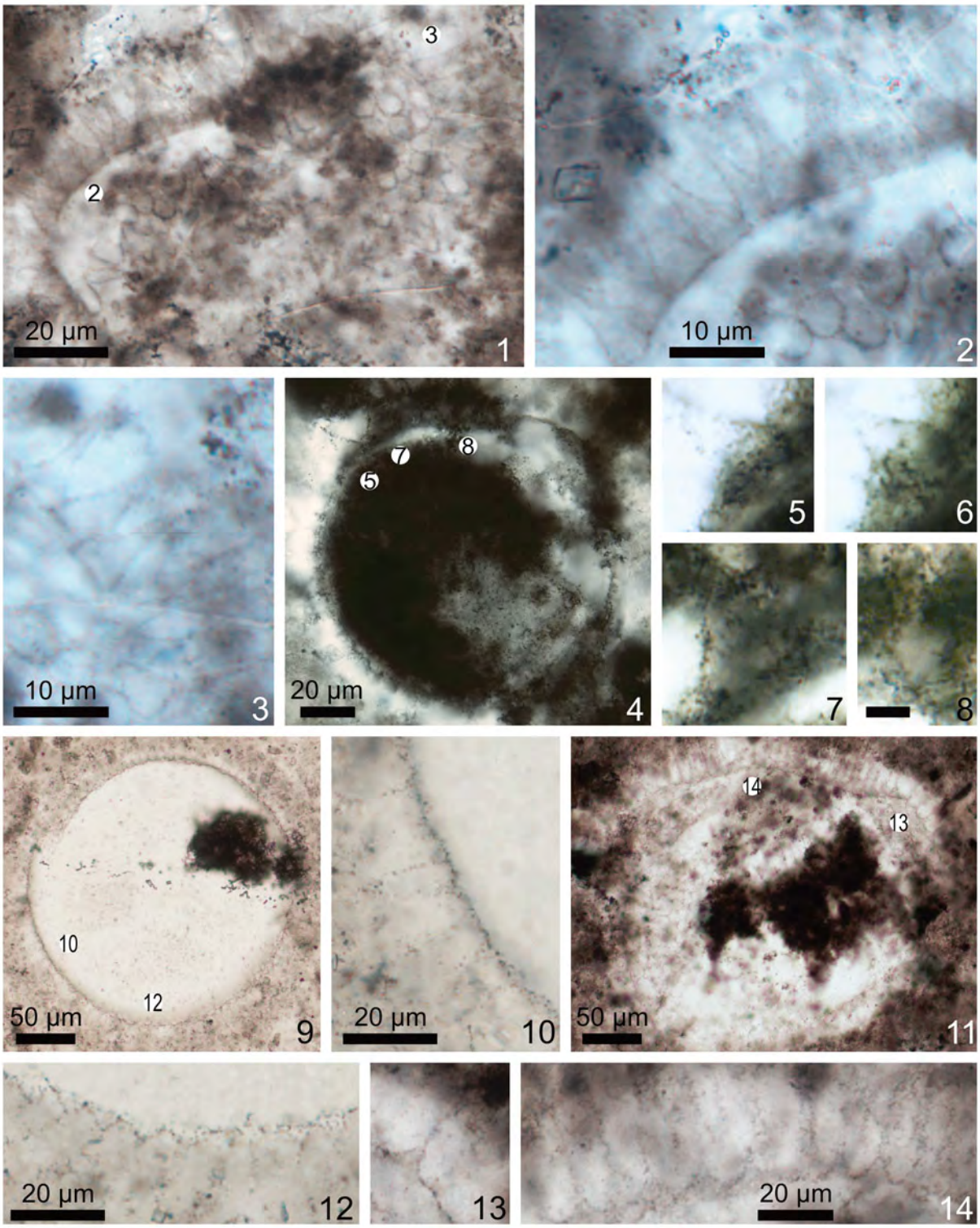

Figure 18. (**1–3**) *Mengeosphaera bellula* Liu et al., 2014a, PB202042, thin section 19CW-6-12, K33; circled 2 and 3 in (**1**) mark areas magnified in (**2**) and (**3**), respectively. (**4–8**) *Mengeosphaera constricta* Liu et al., 2014a, PB202043, thin section 14HA-115-2, W43/2; circled 5 in (**4**) marks the same area magnified in (**5**) and (**6**) at different focal levels; circled 7 and 8 in (**4**) mark areas magnified in (**7**) and (**8**), respectively. (**9–14**) *Mengeosphaera gracilis* Liu et al., 2014a. (**9**, **10**, **12**) PB202044, thin section 19TP-1-12, H43/1; circled 10 and 12 in (**9**) mark areas magnified in (**10**) and (**12**), respectively; (**11**, **13**, **14**) PB202045, thin section 19CW-6-15, G36; circled 13 and 14 in (**11**) mark areas magnified in (**13**) and (**14**), respectively. Scale bar in (**8**) represents 5 µm and applies to (**5–7**); scale bar in (**14**) applies to (**13**).

part tapers gradually to a pointed tip, thus forming an onion-like process. The processes are separated from each other at their base, but are in contact at the inflated basal expansion. Vesicle diameter about 110 µm; process length about 15.6 µm (14.2% of vesicle diameter), maximum width of basal expansion about 9.7 µm, and width of constricted base about 6.9 µm; length of basal

https://doi.org/10.1017/jpa.2023.92 Published online by Cambridge University Press

expansion (from process base to the point where the process begins to taper significantly) about 11.1 µm (71.2% of process total length).

Material.—One illustrated specimen (Fig. 18.4–18.8).

Remarks.—This specimen was previously published in Ouyang et al. (2017) as *Mengeosphaera spicata*. Although Liu and Moczydłowska (2019) synonymized *M. spicata* and *M. constricta*, they did not provide any explanation. We follow Xiao et al. (2022) to tentatively accept this synonymy, and thus reassign this specimen to *M. constricta*. Due to the poor preservation, only three processes (magnified in Fig. 18.5–18.8) are completely preserved with a discernable basal constriction. The consistent morphology of these three processes, however, indicates that the basal constriction is not a taphonomic artifact.

Mengeosphaera gracilis Liu et al., 2014a
Figure 18.9–18.14

2014a *Mengeosphaera*? *gracilis* Liu et al., p. 96, fig. 60.
2019 *Mengeosphaera gracilis* Liu et al.; Liu and Moczydłowska, p. 132, fig. 71.
2019 *Mengeosphaera gracilis* Liu et al.; Shang et al., p. 25, fig. 14F–G.
2020 *Mengeosphaera gracilis* Liu et al.; Shang and Liu, p. 158, fig. 6F–L.
2021 *Mengeosphaera gracilis* Liu et al.; Ouyang et al., fig. 16K–M.
2022 *Mengeosphaera gracilis* Liu et al.; Ye et al., p. 56, fig. 34D–F.

Holotype.—IGCAGS-WFG-727, reposited at Institute of Geology, Chinese Academy of Geological Sciences, from lower Member III of the Ediacaran Doushantuo Formation at Wangfenggang section in the Yangtze Gorges area, Hubei Province, South China (Liu et al., 2014a, fig. 60.1, 60.2).

Description and measurements.—Vesicle large and spheroidal, bearing densely distributed, basally connected biform processes. Processes uniform, with a conical basal expansion and a thin cylindrical apical spine. First specimen (Fig. 18.9, 18.10, 18.12): vesicle diameter about 226 µm; process length about 17.4 µm (7.7% of vesicle diameter), basal width about 6.4 µm, basal expansion length about 4.8 µm (27.6% of process total length); about 14 processes per 100 µm of vesicle periphery. Second specimen (Fig. 18.11, 18.13, 18.14): vesicle diameter about 250 µm; process length about 30.4 µm (12.2% of vesicle diameter), basal width about 8.5 µm, basal expansion length about 6.9 µm (22.7% of process total length); about seven processes per 100 µm of vesicle periphery.

Material.—Two illustrated specimens (Fig. 18.9–18.14).

Remarks.—*Mengeosphaera gracilis* can be differentiated from *Cavaspina basiconica* by its clearly defined biform processes with a more prominent and wider basal expansion. The two available specimens have processes with a conical basal expansion, unlike the deflated base of processes in *C. basiconica*. These two specimens also differ from *Appendisphaera hemisphaerica* in their relatively shorter and thicker process apical spine (process length ~14.3% of vesicle diameter in holotype of *A. hemisphaerica*), and especially the smaller process density (~21 processes per 100 µm of vesicle periphery in the holotype of *A. hemisphaerica*).

Mengeosphaera latibasis Liu et al., 2014a, emend. Liu and Moczydłowska, 2019
Figure 19.1, 19.2

2014a *Mengeosphaera latibasis* Liu et al., p. 97, figs. 51.7, 62.
?2017 *Mengeosphaera latibasis* Liu et al.; Nie et al., p. 376, fig. 6.3–6.7.
2017 *Mengeosphaera latibasis*?; Ouyang et al., fig. 8K–N (the specimen described here and illustrated in Fig. 19.1, 19.2).
2019 *Mengeosphaera latibasis* Liu et al., emend. Liu and Moczydłowska, p. 133, fig. 72.
2021 *Mengeosphaera latibasis* Liu et al., emend. Liu and Moczydłowska; Ouyang et al., fig. 17A, B.

Holotype.—IGCAGS–NPIII–540, reposited at Institute of Geology, Chinese Academy of Geological Sciences, from the upper Member III of the Ediacaran Doushantuo Formation at Niuping section in the Yangtze Gorges area, Hubei Province, South China (Liu et al., 2014a, fig. 62.1, 62.2).

Description and measurements.—Vesicle large, originally spheroidal but slightly deformed. Processes densely arranged on vesicle surface, basally connected or separated. Processes biform, with a broad, obtusely conical, and slightly inflated basal expansion, and a relatively thick but flexible apical spine that is more or less cylindrical in shape. Vesicle diameter about 465 µm; process length about 52.2 µm (11.2% of vesicle diameter), basal width about 31.2 µm, basal expansion length about 16.6 µm (31.8% of process total length), apical spine width about 4.9 µm; about three processes per 100 µm of vesicle periphery.

Material.—One illustrated specimen (Fig. 19.1, 19.2).

Remarks.—*Mengeosphaera latibasis* is distinct in its inflated basal expansion that is wider than long. In many *Mengeosphaera* specimens, processes with a slightly obtuse basal expansion are common (as in the two specimens of *M. gracilis* described above), but basal expansions that are twice as wide as they are long are characteristic of *M. latibasis*.

Mengeosphaera mamma Ye et al., 2022
Figure 19.5–19.11

1996 Unnamed form A; Yin, pl. I, figs. 4–6.
2021 *Mengeosphaera* sp. 2; Ouyang et al., fig. 17H, L.
2022 *Mengeosphaera mamma* Ye et al., p. 57, figs. 35, 36.

Holotype.—The specimen illustrated in Ye et al. (2022, fig. 35A–C), thin section LHGd3 + 30 cm-1–17 (36.3×76.1), reposited at China University of Geosciences (CUG), Wuhan,

https://doi.org/10.1017/jpa.2023.92 Published online by Cambridge University Press

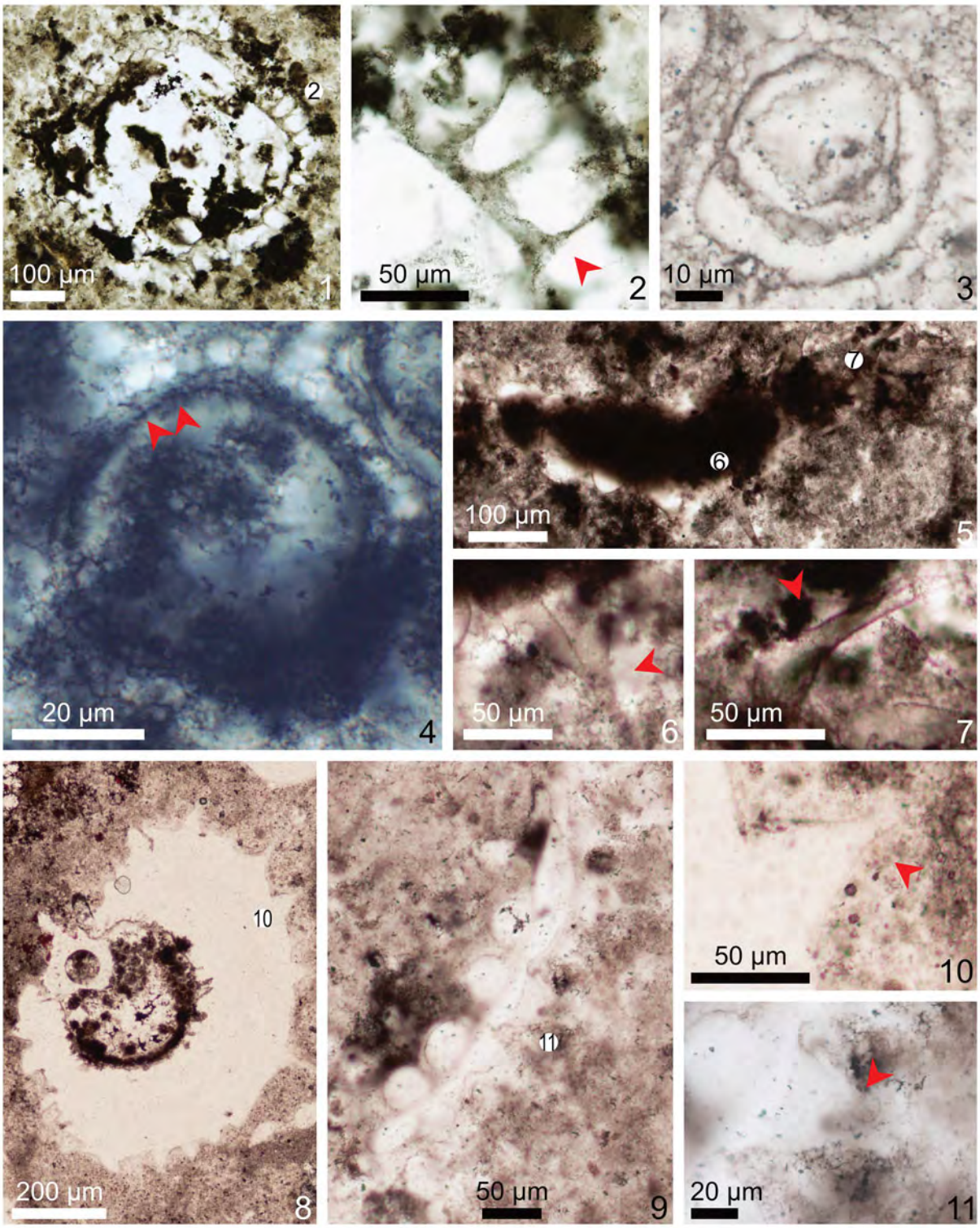

Figure 19. (**1**, **2**) *Mengeosphaera latibasis* Liu et al., 2014a, emend. Liu and Moczydłowska, 2019, PB202046, thin section 14HA-115-1, T49/4; circled 2 in (**1**) marks the area magnified in (**2**). (**3**) *Mengeosphaera minima* Liu et al., 2014a, PB202047, thin section 21DC-5-4, T31/2. (**4**) *Mengeosphaera minima*? PB202048, thin section 21DC-3-1, G23/3. (**5–11**) *Mengeosphaera mamma* Ye et al., 2022. (**5–7**) PB202049, thin section 21LHK-1-10, L38/1; circled 6 and 7 in (**5**) mark areas magnified in (**6**) and (**7**), respectively; (**8**, **10**) PB202050, thin section 21MJD-1-10, L45; circled 10 in (**8**) marks the area magnified in (**10**); (**9**, **11**) PB202051, thin section 21MJD-1-11, L33; circled 11 in (**9**) marks the area magnified in (**11**). Red arrowheads in (**2**), (**5–7**), (**10**), and (**11**) denote reflection points of biform processes; red arrowheads in (**4**) denote the basally joined, strongly inflated processes.

China, from the Ediacaran Doushantuo Formation at Lianhuacun section in Shennongjia area, Hubei Province, South China.

Description and measurements.—Most specimens are not entirely captured in thin section due to their large size. Vesicles range from oval to completely compressed, but were

https://doi.org/10.1017/jpa.2023.92 Published online by Cambridge University Press

originally spheroidal. Processes large, biform, with the apical spine in most specimens poorly preserved and their full length unavailable. Four specimens with adequately preserved vesicles reveal a vesicle diameter of 350–632 μm, with the largest illustrated in Figure 19.8. Process basal width 37.7–77.0 μm (N = 9, mean = 50.5 μm, SD = 11.3 μm), basal expansion length 30.0–69.0 μm (N = 5, mean = 40.0 μm, SD = 16.3 μm), apical spine width 6.8–18.6 μm (N = 2); 1–2 processes per 100 μm of vesicle periphery. In some better-preserved processes (e.g., Fig. 19.10, 19.11), the basal expansion is as long as or longer than it is wide, and it is possible that the measurements of basal expansion length given above may be underestimates when the basal expansions are cut obliquely (in which case the apical spines are often missed in the thin section).

Material.—Three illustrated specimens (Fig. 19.5–19.11) and six additional specimens (including the one illustrated in Shi et al., 2022, fig. 8E, F).

Remarks.—Of all *Mengeosphaera* species, *M. flammelata*, *M. grandispina*, *M. mamma*, and *M. stegosauriformis* have processes tens of micrometers in basal width. Among these four species, processes are flame-shaped in *M. flammelata*, have a conical and somewhat deflated basal expansion in *M. grandispina*, have a strongly inflated basal expansion in *M. stegosauriformis*. The nine specimens described here are most similar to *M. mamma* in both process size and shape.

The specimen published as "unnamed form A" from the Doushantuo Formation at the Diaoyapo section in the Yangtze Gorges area (Yin, 1996) has processes with large, significantly inflated basal expansions (35–55 μm in basal length, ~40 μm in basal width), and cylindrical apical spine. These features fall within the perimeter of *Mengeosphaera mamma,* and this specimen is here reassigned to *M. mamma*.

Mengeosphaera minima Liu et al., 2014a
Figure 19.3

2011 *Meghystrichosphaeridium chadianensis*; L. Yin et al., fig. 5A, H.
2014a *Mengeosphaera minima* Liu et al., p. 101, figs. 51.8, 63.
2017 *Mengeosphaera minima*; Hawkins et al., fig. 7C.
non 2020 *Mengeosphaera minima*; Grazhdankin et al., fig. 4A.
2021 *Mengeosphaera minima* Liu et al.; Ouyang et al., fig. 17M, N.
2022 *Mengeosphaera minima* Liu et al.; Ye et al., p. 57, fig. 34G, H.
2022 *Mengeosphaera minima* Liu et al.; Shi et al., fig. 8C (illustrated in Fig. 19.3, one of the two specimens described here).

Holotype.—IGCAGS–NPIII–090A, reposited at Institute of Geology, Chinese Academy of Geological Sciences, from the upper Member III of the Ediacaran Doushantuo Formation at Niuping section in the Yangtze Gorges area, Hubei Province, South China (Liu et al., 2014a, fig. 63.1).

Description and measurements.—Vesicle small, spheroidal, with uniform processes evenly distributed on the vesicle. Processes closely arranged but basally separated. Processes biform, with a conical basal expansion and a thin, cylindrical or distally tapering apical spine. The specimen illustrated in Figure 19.3 has a vesicle diameter of about 54 μm, process length about 7.0 μm (13.0% of vesicle diameter), basal expansion width about 4.1 μm, basal expansion length about 3.0 μm (42.9% of process total length), with about 14 processes per 100 μm of vesicle periphery. The other specimen has a vesicle diameter of about 92 μm, process length about 20.3 μm (22.0% of vesicle diameter), basal expansion width about 4.2 μm, basal expansion length about 4.6 μm (22.7% of process total length); process density unavailable due to poor preservation.

Material.—One illustrated specimen (Fig. 19.3) and one additional specimen.

Remarks.—Most *Mengeosphaera* species have large or at least medium-sized vesicles. To date, *M. bellula*, *M. minima*, and *M. stegosauriformis* are the only three *Mengeosphaera* species that have small vesicles, with *M. minima* being the smallest of all. The two available specimens are assigned to *M. minima* for their small size with biform processes that consist of a generally conical and proportionally large (at least 20% of process total length) basal expansion.

Mengeosphaera minima?
Figure 19.4

2022 *Mengeosphaera minima*?; Shi et al., fig. 8D (the same specimen described here and illustrated in Fig. 19.4).

Description and measurements.—Vesicle small, spheroidal, bearing basally connected uniform processes. Processes biform, with clearly inflated basal expansions that take up about half of the total length of processes. Vesicle diameter about 48 μm, process length about 5.8 μm (12.1% of vesicle diameter) and basal width about 3.1 μm, length of basal expansion about 3.0 μm (51.7% of process total length), with about 32 processes per 100 μm of vesicle periphery.

Material.—One illustrated specimen (Fig. 19.4).

Remarks.—Resembling *Mengeosphaera minima* in the small vesicle size and the biform processes, this specimen is distinct in its basally connected and strongly inflated processes (red arrowheads in Fig. 19.4). Since these features appear consistently on all processes of this specimen, they are unlikely to be taphonomic artifacts, and probably represent morphological variations of taxonomic importance. Since there is only one such specimen in our collection, it is uncertain whether these variations are intraspecific or interspecific in nature. As such, we tentatively assign this specimen in an open nomenclature but note its similarity to *M. minima*.

https://doi.org/10.1017/jpa.2023.92 Published online by Cambridge University Press

Genus *Tanarium* Kolosova, 1991, emend. Moczydłowska, Vidal, and Rudavskaya, 1993

Type species.—*Tanarium conoideum* Kolosova, 1991, emend. Moczydłowska, Vidal, and Rudavskaya, 1993.

Other species.—*Tanarium acus* Liu et al., 2014a; *T. araithekum* Grey, 2005; *T. capitatum* Liu and Moczydłowska, 2019; *T. columnatum* Ye et al., 2022; *T. cuspidatum* (Liu et al., 2014a) Liu and Moczydłowska, 2019; *T. digitiforme* (Nagovitsin and Faizullin in Nagovitsin et al., 2004) Sergeev, Knoll, and Vorob'eva, 2011; *T. elegans* Liu et al., 2014a; *T. gracilentum* (Yin in Yin and Liu, 1988) Ouyang et al., 2021; *T. irregulare* Moczydłowska, Vidal, and Rudavskaya, 1993; *T. longidigitatum* Golubkova, 2023; *T. mattoides* Grey, 2005; *T. megaconicum* Grey, 2005; *T.*? *minimum* Liu et al., 2014a; *T.*? *muntense* Grey, 2005; *T. obesum* Liu et al., 2014a; *T. paucispinosum* Grey, 2005; *T. pilosiusculum* Vorob'eva, Sergeev, and Knoll, 2009; *T. pluriprotensum* Grey, 2005; *T. pycnacanthum* Grey, 2005; *T. triangulare* (Liu et al., 2014a) Liu and Moczydłowska, 2019; *T. tuberosum* Moczydłowska, Vidal, and Rudavskaya, 1993; *T. uniformum* Liu and Moczydłowska, 2019; *T. varium* Liu et al., 2014a; *T. victor* Xiao et al., 2014.

Remarks.—Like *Appendisphaera*, *Tanarium* encompasses a remarkably large range of morphological variations. The currently accepted species of *Tanarium* contain taxa with homomorphic (e.g., *T.*? *muntense*) or heteromorphic (*T. irregulare*) processes, with slim (e.g., *T. gracilentum*) to obtusely conical (e.g., *T. tuberosum*) processes, with cylindrical (e.g., *T. digitiforme*) to biform (e.g., *T. triangulare*) processes, with terminally pointed (e.g., *T. acus*) to bifurcated (e.g., *T. victor*) processes, with sparsely arranged (e.g., *T. megaconicum*) to densely arranged (e.g., *T. pycnacanthum*) processes, and with relatively short (process length <10% of vesicle diameter, e.g., *T. pilosiusculum*) to remarkably long (process length >50% of vesicle diameter, e.g., *T. mattoides*) processes. These morphological variations make it nearly impossible to define the genus *Tanarium*, and a taxonomical revision, preferably based on morphometric analyses, is urgently needed.

Tanarium cf. *T. capitatum* Liu and Moczydłowska, 2019
Figure 20.1, 20.2

cf. 2019 *Tanarium capitatum* Liu and Moczydłowska, p. 143, fig. 79.
2022 *Tanarium* cf. *T. capitatum*; Shi et al., fig. 8N, O (the specimen described here and illustrated in Fig. 20.1, 20.2).

Description and measurements.—Vesicle large, compressed but originally spheroidal. Processes evenly distributed with moderate density, basally departed. Processes conical, with a wide base and tapering gradually toward a thin terminal end. Vesicle diameter approximately 348 µm. The full length of processes is difficult to obtain due to the relatively large size of the processes (so the terminal part is often not captured in thin sections), with one measurement of about 62.6 µm (18.0% of vesicle diameter) and two partially preserved processes 42.5 µm and 49.6 µm in length. Process basal width about 16.3 µm, process basal spacing about 13.2 µm, and about 3 processes per 100 µm of vesicle periphery.

Material.—One specimen illustrated in Figure 20.1, 20.2.

Remarks.—The described specimen is morphologically similar to *Tanarium capitatum* in vesicle size, process shape and proportional size, and process density and distribution. However, it lacks the key diagnostic feature of *T. capitatum*—the knob-like, bulge process tip. It is possible that the process tips are not preserved due to taphonomic loss, and this specimen is otherwise more similar to *T. capitatum* than to other species. The processes in this specimen are also similar to those of *T. pilosiusculum* in proportional length, but they are thinner and more acutely conical than processes in *T. pilosiusculum* (Vorob'eva et al., 2009). Therefore, we compare this specimen to *T. capitatum* but tentatively place it in an open nomenclature.

Tanarium conoideum Kolosova, 1991, emend. Moczydłowska, Vidal, and Rudavskaya, 1993
Figure 20.3, 20.5

1991 *Tanarium conoideum* Kolosova, p. 57, fig. 5.1–5.3.
1993 *Tanarium conoideum* Kolosova, emend. Moczydłowska, Vidal, and Rudavskaya, p. 514, 516, text-fig. 10C–D.
2005 *Tanarium conoideum* Kolosova, emend. Moczydłowska et al.; Moczydłowska, p. 302, fig. 7A, C, E.
non 2005 *Tanarium conoideum* Kolosova; emend. Moczydłowska et al.; Grey, p. 299, figs. 212, 213.
non 2006 *Tanarium conoideum* Kolosova, emend. Moczydłowska et al.; Willman et al., p. 32, pl. VI, figs. 1, 2.
non 2008 *Tanarium conoideum* Kolosova, emend. Moczydłowska et al.; Willman and Moczydłowska, p. 526, fig. 12C.
non 2008 *Tanarium conoideum* Kolosova; Vorob'eva et al., fig. 2a.
non 2009 *Tanarium conoideum* Kolosova, Moczydłowska et al.; Vorob'eva et al., p. 180, fig. 7.4, 7.7.
non 2009a *Tanarium conoideum* (Kolosova, 1991) Moczydłowska et al. [sic]; Yin et al., pl. I, figs. 3, 4.
non 2010 *Tanarium conoideum* (Kolosova) emend. Moczydłowska et al. [sic]; Golubkova et al., pl. III, fig. 7, pl. IV, fig. 2.
2011 *Tanarium conoideum* Kolosova, emend. Moczydłowska et al.; Sergeev et al., p. 1005, fig. 6.1, 6.2.
non 2011 *Tanarium conoideum* (Kolosova, 1991) Moczydłowska et al. [sic]; C. Yin et al., fig. 6c (the same specimen as pl. I, figs. 3, 4 in Yin et al., 2009a).
non 2013 *Tanarium conoideum*; Liu et al., fig. 11A.
2014 *Tanarium conoideum* Kolosova, emend. Moczydłowska et al.; Xiao et al., p. 51, fig. 33.
2014a *Tanarium conoideum* Kolosova, emend. Moczydłowska et al.; Liu et al., p. 109, figs. 76.2, 77.
2019 *Tanarium conoideum* Kolosova, emend. Moczydłowska et al.; Shang et al., p. 26, fig. 16A–E.

https://doi.org/10.1017/jpa.2023.92 Published online by Cambridge University Press

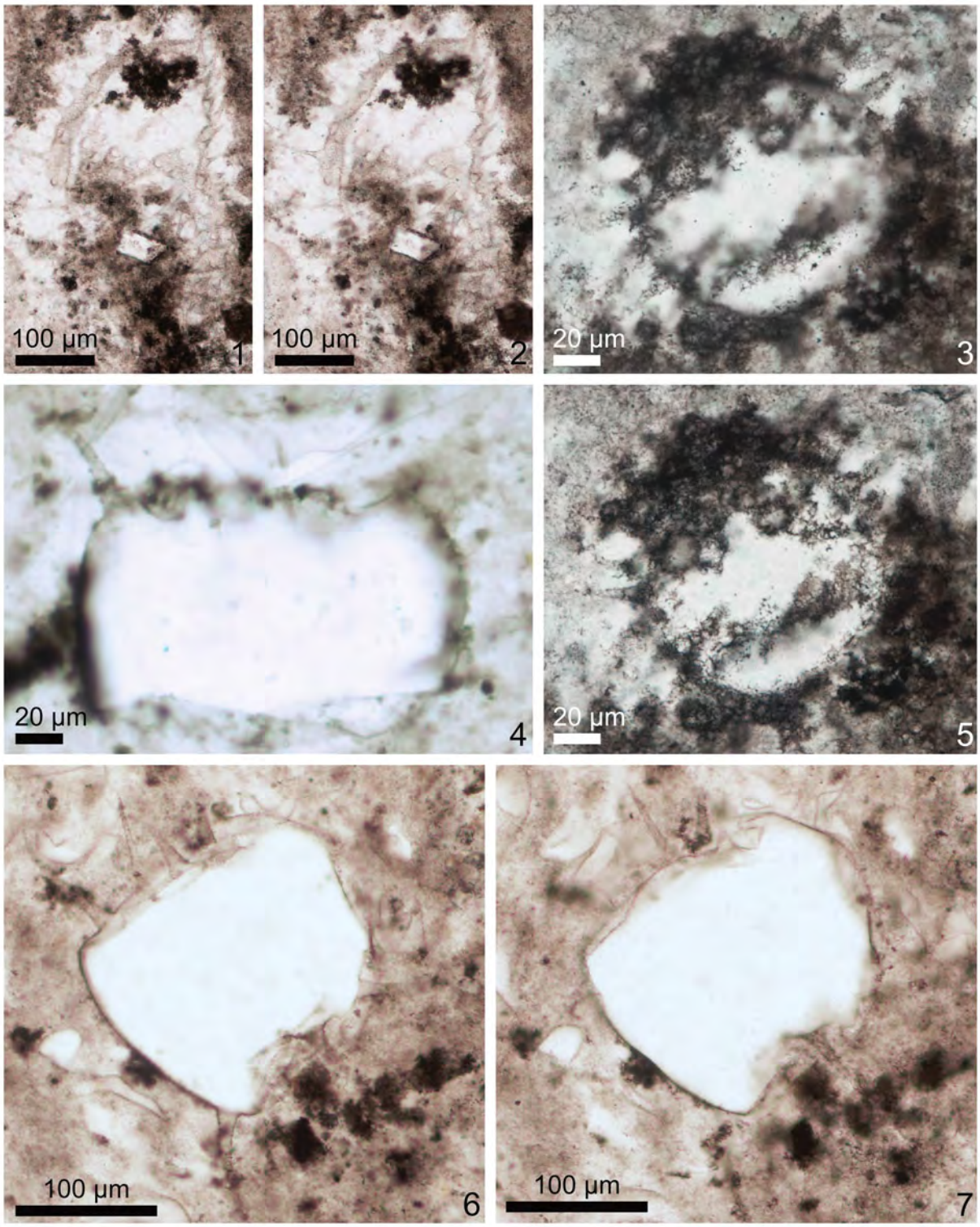

Figure 20. (**1**, **2**) *Tanarium* cf. *T. capitatum* Liu and Moczydłowska, 2019, PB202052, thin section 21DC-2-35, M32/1, showing the same area at different focal levels. (**3**, **5**) *Tanarium conoideum* Kolosova, 1991, emend. Moczydłowska, Vidal, and Rudavskaya, 1993, PB202053, thin section 21DC-5-4, R43/3, showing the same area at different focal levels. (**4**, **6**, **7**) *Tanarium paucispinosum* Grey, 2005: (**4**) PB202054, thin section 19CW-6-9, N35/3; (**6**, **7**) PB202055, thin section 19CW-5-29, H38, showing the same area at different focal levels.

2020 *Tanarium conoideum* Kolosova, emend. Moczydłowska et al.; Vorob'eva and Petrov, p. 374, pl. I, fig. 15.

non 2020 *Tanarium conoideum* Kolosova, emend. Moczydłowska et al.; Yang et al., p. 6, fig. 2K.

2022 *Tanarium conoideum*; Shi et al., fig. 9D, E (the specimen described here and illustrated in Fig. 21.3, 21.5).

2022 *Tanarium conoideum* Kolosova, emend. Moczydłowska et al.; Ye et al., p. 65, figs. 42, 43A–E.

https://doi.org/10.1017/jpa.2023.92 Published online by Cambridge University Press

2023 *Tanarium conoideum* (Kolosova) emend. Moczydłowska [sic]; Golubkova, pl. 7, fig. 6.

Holotype.—YIGS Nr 87-115, reposited at the Geological Museum of Yakutian Institute of Geologic Sciences (present Diamond and Precious Metal Geology Institute, Siberian Branch, Russian Academy of Sciences), from the Ediacaran Kursov Formation, Anabar area, eastern Siberia (Kolosova, 1991, p. 57, fig. 5.1, 5.2).

Description and measurements.—Vesicle spheroidal, medium-sized, bearing evenly distributed processes. Processes uniform, conical, distally tapering toward a pointed tip. Vesicle diameter about 108 µm; process length about 24.9 µm (23.1% of vesicle diameter), basal width about 8.8 µm, about seven processes per 100 µm of vesicle periphery.

Material.—One specimen illustrated in Figure 20.3, 20.5.

Remarks.—Previously published specimens of *Tanarium conoideum* represent a large range of morphological variations. The specimen described here is comparable to the holotype of *T. conoideum* in many morphological aspects, including the vesicle size, proportional size of processes, and process shape (for comparison, the holotype of *T. conoideum* has a vesicle diameter of ~114 µm, process length ~34.3 µm, and process basal width ~16.2 µm, as remeasured on fig. 5.1–5.3 of Kolosova, 1991). The specimen described here differs from the holotype and many other published *T. conoideum* specimens in its greater process density; the holotype of *T. conoideum* has only about 1–2 processes per 100 µm of vesicle periphery, although it should be noted that the holotype has a relatively larger vesicle. However, process density is somewhat variable among previously published specimens of *T. conoideum* (e.g., ~4 processes per 100 µm of vesicle periphery in both Moczydłowska, 2005, fig. 7C and in Golubkova, 2023, pl. 7, fig. 6, and about 7 processes per 100 µm of vesicle periphery in Xiao et al., 2014, fig. 33.3). Thus, we chose to place the specimen illustrated in Figure 20.3 and 20.5 in *T. conoideum*.

Tanarium paucispinosum Grey, 2005
Figure 20.4, 20.6, 20.7

2005 *Tanarium paucispinosum* Grey, p. 318, figs. 45G, 208G, 237, 239.
2010 *Tanarium paucispinosum* Grey; Golubkova et al., pl. II, fig. 1, pl. III, fig. 8.
2019 *Tanarium paucispinosum* Grey; Liu and Moczydłowska, p. 149, 151, fig. 83.
2021 *Tanarium paucispinosum*; Liu et al., fig. 4.7.
2022 *Tanarium paucispinosum* Grey; Ye et al., p. 66, fig. 44E–F.

Holotype.—CPC 36552, reposited at Commonwealth Palaeontological Collection (CPC) at Geoscience Australia, Canberra, from the Ediacaran Wilari Dolomite Member of Observatory Hill I drill core in Officer Basin, South Australia (Grey, 2005, fig. 237D).

Description and measurements.—Vesicle medium-sized to large, originally spheroidal but may be deformed to different degrees. A small number of conical processes unevenly distributed on the vesicle wall. Vesicle diameter 149–201 µm (N = 5, mean = 170 µm, SD = 19 µm); processes length 38.1–83.8 µm (N = 7, mean = 62.2 µm, SD = 15.4 µm) and 23.7–36.2% of vesicle diameter (N = 4, mean = 32.8%, SD = 6.1%); process basal width 9.7–16.2 µm (N = 9, mean = 12.1 µm, SD = 2.0 µm); on average one process per 100 µm of vesicle periphery (measured on one specimen illustrated in Figure 20.6, 20.7).

Material.—Two illustrated specimens (Fig. 20.4, 20.6, 20.7) and seven additional specimens.

Remarks.—The described specimens are placed in *Tanarium paucispinosum* mainly for their sparsity of processes, which is the key diagnosis of *T. paucispinosum*. These two specimens also resemble specimens of *T. paucispinosum* reported from Australia in proportional length of the processes (~20–40% of vesicle diameter, calculated based on dimensions provided in Grey, 2005) and the thin conical shape of the processes, although the vesicle size of the current specimens is greater than the Australian specimens (64–148 µm in vesicle diameter).

Tanarium pilosiusculum Vorob'eva, Sergeev, and Knoll, 2009
Figure 21

2006 *Echinosphaeridium* sp.; Vorob'eva et al., fig. 2l.
2009 *Tanarium pilosiusculum* Vorob'eva, Sergeev, and Knoll, p. 182, fig. 7.1, 7.2.
2013 *Tanarium pilosiusculum*; Liu et al., fig. 13B.
2014a *Tanarium pilosiusculum* Vorob'eva et al.; Liu et al., p. 113, figs. 76.7, 83.
2019 *Tanarium pilosiusculum* Vorob'eva et al.; Liu and Moczydłowska, p. 151, fig. 84.
2019 *Tanarium pilosiusculum* Vorob'eva et al.; Shang et al., p. 27, fig. 17A–C.
2020 *Tanarium pilosiusculum* Vorob'eva et al.; Yang et al., p. 7, fig. 2N, O.
2021 *Tanarium pilosiusculum* Vorob'eva et al.; Ouyang et al., fig. 19K–M.
2022 ?*Tanarium pilosiusculum* Vorob'eva et al.; Shi et al., fig. 9F, G (one of the specimens described here).

Holotype.—Specimen 14700-74 (illustrated in Vorob'eva et al., 2009, fig. 7.1), reposited at the Paleontological Collection of the Geological Institute of the Russian Academy of Sciences, from the upper part of the early Ediacaran Vychegda Formation of the Kel'tminskaya-1 borehole in the East European Platform, Russia.

Description and measurements.—Vesicle spheroidal, bearing a moderate number of relatively short processes randomly distributed on the vesicle. Processes conical and simple in shape, taper gradually toward a pointed tip. The specimen illustrated in Figure 21.1–21.4 has a vesicle diameter of about 201 µm, process length about 26.9 µm (13.4% of vesicle diameter), and basal width about 12.0 µm, with about 2–3 processes per 100 µm of vesicle periphery. The specimen illustrated in Figure 21.5–21.7 has a vesicle diameter of about 257 µm,

https://doi.org/10.1017/jpa.2023.92 Published online by Cambridge University Press

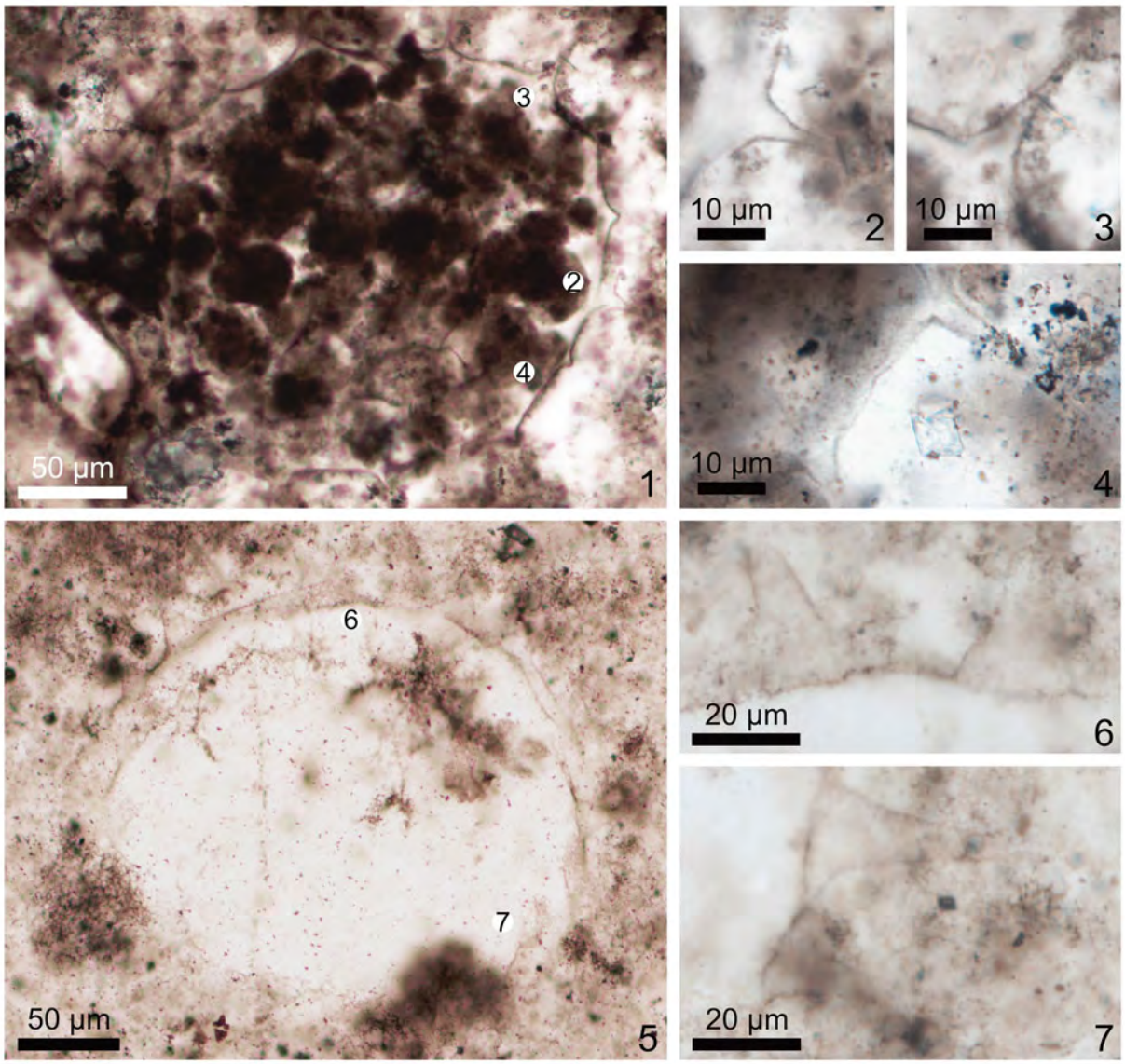

Figure 21. *Tanarium pilosiusculum* Vorob'eva, Sergeev, and Knoll, 2009. (**1–4**) PB202056, thin section 19CW-6-15, O41; circled 2–4 in (**1**) mark areas magnified in (**2–4**), respectively; (**5–7**) PB202057, thin section 21LHK-1-10, M31/2; circled 6 and 7 in (**5**) mark areas magnified in (**6**) and (**7**), respectively.

process length about 49.7 μm (19.4% of vesicle diameter), and basal width about 21.5 μm, with 1–2 processes per 100 μm of vesicle periphery. The third specimen (illustrated in Shi et al., 2022, fig. 9F, G) has a vesicle diameter of about 84 μm, process length about 11.0 μm (12.9% of vesicle diameter), and basal width about 12.3 μm, with about 7 processes per 100 μm of vesicle periphery.

Material.—Two specimens illustrated in Figure 21, and one additional specimen illustrated in Shi et al. (2022, fig. 9F, G).

Remarks.—*Tanarium pilosiusculum* is characterized by processes proportionally shorter (~5–10% of vesicle diameter) than those of other *Tanarium* species (typically >20% of vesicle diameter, as proposed by Grey, 2005). Compared with the holotype of *T. pilosiusculum*, specimens described in this paper have proportionally longer processes that exceed 10% and can be up to 20% of vesicle diameter. However, they are otherwise comparable to *T. pilosiusculum* in process density and distribution; both have numerous conical and basally separated processes that are occasionally wider than long. They also meet the diagnosis of *T. pilosiusculum* in having processes "generally shorter than those of other *Tanarium* species," (Vorob'eva et al., 2009, p. 182) considering that most other *Tanarium* species are characterized by longer processes that are greater than 20% of vesicle diameter. We note that other acanthomorph taxa, including several species of *Appendisphaera*, *Urasphaera fungiformis* Liu et al., 2014a, and *Variomargosphaeridium floridum* Nagovitsin and Moczydłowska in Moczydłowska and Nagovitsin, 2012, also have processes that are 10–20% of vesicle diameter, but their processes can be easily distinguished from the simple conical processes in the specimens described here, which are most appropriately placed in *T. pilosiusculum* on account of their process morphology and density.

https://doi.org/10.1017/jpa.2023.92 Published online by Cambridge University Press

Tanarium triangulare (Liu et al., 2014a) Liu and Moczydłowska, 2019
Figure 22.1–22.3

2014a *Mengeosphaera triangularis* Liu et al., p. 103, figs. 51.13, 68.
2017 *Mengeosphaera*? *cuspidata*; Ouyang et al., fig. 9I–K (specimens described here).
2017 *Mengeosphaera chadianensis*; Ouyang et al., fig. 9L, M (specimen described here).
2019 *Tanarium triangularis* (Liu et al.) Liu and Moczydłowska, p. 151, fig. 85.
2021 *Tanarium triangulare* (Liu et al.) Liu and Moczydłowska; Ouyang et al., fig. 20D.

Holotype.—IGCAGS–NPIII–280, reposited at Institute of Geology, Chinese Academy of Geological Sciences, from the upper Member III of the Ediacaran Doushantuo Formation at Niuping section in the Yangtze Gorges area, Hubei Province, South China (Liu et al., 2014a, fig. 68.1).

Description and measurements.—Vesicle medium-sized to large, oval but originally spheroidal. Processes biform, with a conical or slightly inflated basal expansion supporting a thin and cylindrical apical spine. Processes evenly distributed and basally separated. Vesicle diameter of three specimens 182–194 µm (mean = 187 µm), and a larger specimen about 262 µm in vesicle diameter (Fig. 22.1, 22.2); process length 39.5–75.2 µm (N = 5; mean = 53.4 µm, SD = 2.6 µm) or 21.0–41.4% of vesicle diameter (N = 4; mean = 28.3%; SD = 9.3%), basal width 21.2–31.5 µm (N = 5; mean = 26.8 µm, SD = 3.8 µm); process basal expansion length 16.3–22.9 µm (N = 5; mean = 19.6 µm, SD = 3.0 µm) or 30.1–56.3% of vesicle diameter (N = 5; mean = 38.6%; SD = 10.8%); about 2–3 processes per 100 µm of vesicle periphery.

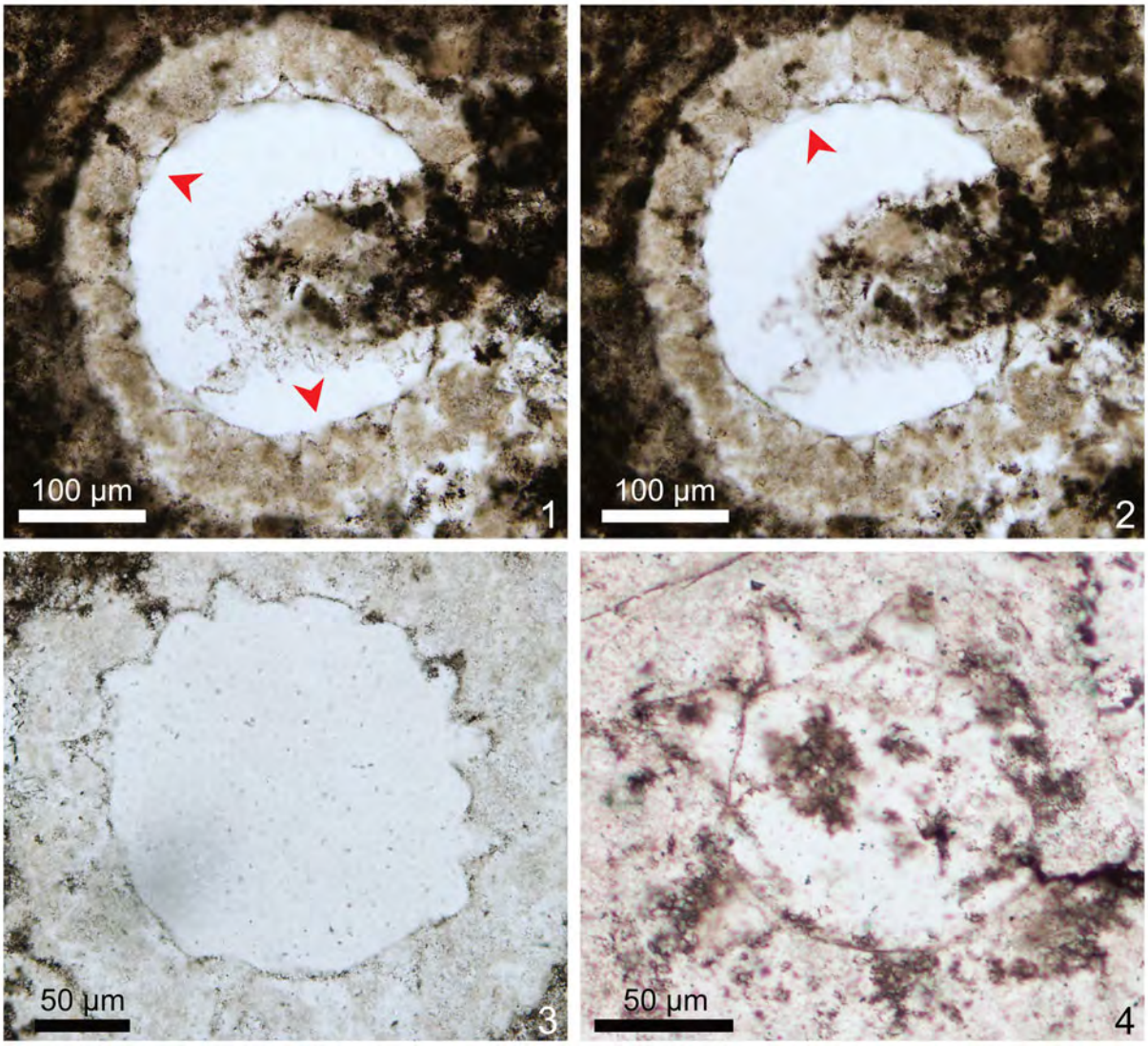

Figure 22. (**1–3**) *Tanarium triangulare* (Liu et al., 2014a) Liu and Moczydłowska, 2019: (**1**, **2**) PB202058, thin section 14HA-140-5, F24/1, same area at different focal levels; (**3**) PB202059, thin section 14HA-140-3, D31/1. (**4**) *Tanarium tuberosum* Moczydłowska, Vidal, and Rudavskaya, 1993, PB202060, thin section 21DC-4-11, U45. Red arrowheads in (**1**) and (**2**) denote typical conical basal part of some processes.

https://doi.org/10.1017/jpa.2023.92 Published online by Cambridge University Press

Material.—Two specimens illustrated in Figure 22.1–22.3 (the specimen in Fig. 22.1, 22.2 also was illustrated in Ouyang et al., 2017, fig. 9J), two specimens illustrated in Ouyang et al. (2017, fig. 9I, L, M), and one additional specimen.

Remarks.—Both *Mengeosphaera*? *cuspidata* Liu et al., 2014a, and *M. triangularis* have been transferred to *Tanarium* (Liu and Moczydłowska, 2019), although both are characterized by biform processes with a clearly defined inflection. Two of the specimens described here were originally illustrated as *M.*? *cuspidata* by Ouyang et al. (2017, fig. 9I–K), and reassigned to *T. triangulare* by Liu and Moczydłowska (2019) without justification, but then again considered to be *T. cuspidatum* (Shang et al., 2019; Ye et al., 2022). These specimens have processes that seem to exhibit a deflated base and thus resemble *T. cuspidatum*, but a re-examination of them has convinced us that most basal expansions are conical or slightly inflated with an inflection point (see red arrowheads in Fig. 22.1, 22.2). Thus, we follow Liu and Moczydłowska (2019) and identify the two specimens illustrated in Ouyang et al. (2017, fig. 9I–K) as *T. triangulare*. One specimen illustrated as *Mengeosphaera chadianensis* in Ouyang et al. (2017, fig. 9L–M) is similar to the two specimens mentioned above in process shape, size, and arrangement, and is also re-assigned to *T. triangulare*.

Tanarium tuberosum Moczydłowska, Vidal, and Rudavskaya, 1993
Figure 22.4

1993 *Tanarium tuberosum* Moczydłowska, Vidal, and Rudavskaya, p. 516, text-fig. 15A–D.
1998 *Tanarium conoideum* Moczydłowska et al.; Faizullin, pl. II, fig. 1, pl. II, figs 2–4, 8.
2004 *Tanarium stellatum* Nagovitsin and Faizullin in Nagovitsin et al., p. 14, pl. II, figs 16–18.
2005 *Tanarium tuberosum* Moczydłowska et al.; Moczydłowska, p. 303, fig. 7B–D.
2006 *Tanarium tuberosum* Moczydłowska et al.; Willman et al., p. 36, pl. VII, figs 3, 4.
2008 *Tanarium tuberosum* Moczydłowska et al.; Willman and Moczydłowska, p. 527, fig. 12F.
2009 *Tanarium tuberosum* Moczydłowska et al.; Vorob'eva et al., p. 182, fig. 7.6, 7.8.
2010 *Tanarium tuberosum* Moczydłowska et al.; Golubkova et al., pl. II, fig. 2, pl. III, fig. 11.
2011 *Tanarium tuberosum* Moczydłowska et al.; Sergeev et al., p. 1006, fig. 6.3.
2012 *Tanarium tuberosum* Moczydłowska et al.; Moczydłowska and Nagovitsin, p. 20, fig. 8G–J.
2016 *Tanarium tuberosum* Moczydłowska et al., emend. Moczydłowska, p. 93, pl. 3, figs 1–6.
2019 *Tanarium tuberosum* Moczydłowska et al., emend. Moczydłowska; Liu and Moczydłowska, p. 153, fig. 86.
2019 *Tanarium tuberosum* Moczydłowska et al., emend. Moczydłowska; Shang et al., p. 27, fig. 18A.
2020 *Tanarium tuberosum* Moczydłowska et al., emend. Moczydłowska; Shang et al., p. 159, fig. 6A–C.
2021 *Tanarium tuberosum* Moczydłowska et al.; Ouyang et al., fig. 19R.
2022 *Tanarium tuberosum* Moczydłowska et al.; Shi et al., fig. 9H (the specimen described here and illustrated in Fig. 22.4).
2023 *Tanarium tuberosum* (Moczydłowska et al.) emend. Moczydłowska [sic]; Golubkova, pl. 7, fig. 8.

Holotype.—PMU-Sib.4-J/30/3, reposited at Uppsala University, from the Ediacaran Khamaka Formation, Nepa-Botuoba region, Yakutia, Siberia (Moczydłowska et al., 1993, p. 517, text-fig. 15A, B, D).

Description and measurements.—Vesicle spheroidal, medium-sized, bearing basally connected, large conical processes. Vesicle diameter about 113 μm, process length about 32.0 μm (28.3% of vesicle diameter), and basal width about 32.4 μm (28.7% of vesicle diameter), with 1–2 processes per 100 μm of vesicle periphery.

Material.—One specimen illustrated in Figure 22.4.

Remarks.—Among all species of *Tanarium*, *T. tuberosum* is unique in its proportionally large conical processes with the broadest base. The specimen described here is larger than but otherwise similar to the holotype of *T. tuberosum* in process morphology and proportional size. For comparison, process length is about 22.8% of vesicle diameter, process basal width is about 20.9% of vesicle diameter, and length to basal width ratio is about 1.1 in the holotype, based on measurements taken from Moczydłowska et al. (1993, text-fig. 15A, B, D). Our specimen differs from the holotype and some other published specimens of *T. tuberosum* in its relatively high process density; however, similar process density is also reported in a few specimens identified as *T. tuberosum* (e.g., Liu and Moczydłowska, 2019, fig. 86A, B). We thus identified our specimen as *T. tuberosum*.

Genus *Tianzhushania* Yin and Li, 1978, emend. Yin et al., 2008

Type species.—*Tianzhushania spinosa* Yin and Li, 1978, emend. Yin in Yin and Liu, 1988.

Other species.—*Tianzhushania polysiphonia* Yin in Yin and Liu, 1988; *T. rara* Xiao et al., 2014.

Tianzhushania spinosa Yin and Li, 1978, emend. Yin in Yin and Liu, 1988
Figure 23

1978 *Tianzhushania spinosa* Yin and Li, p. 95, pl. 8, fig. 13.
1988 *Tianzhushania spinosa* Yin and Li, emend. Yin in Yin and Liu, p. 178, pl. 10, figs. 1–4.
1988 *Tianzhushania tubaeformis* Yin in Yin and Liu, p. 178, pl. 9, figs. 8, 9.
1990 *Tianzhushania spinosa* Yin and Li, emend. Yin in Yin and Liu; Yin, pl. I, figs. 3, 4.

https://doi.org/10.1017/jpa.2023.92 Published online by Cambridge University Press

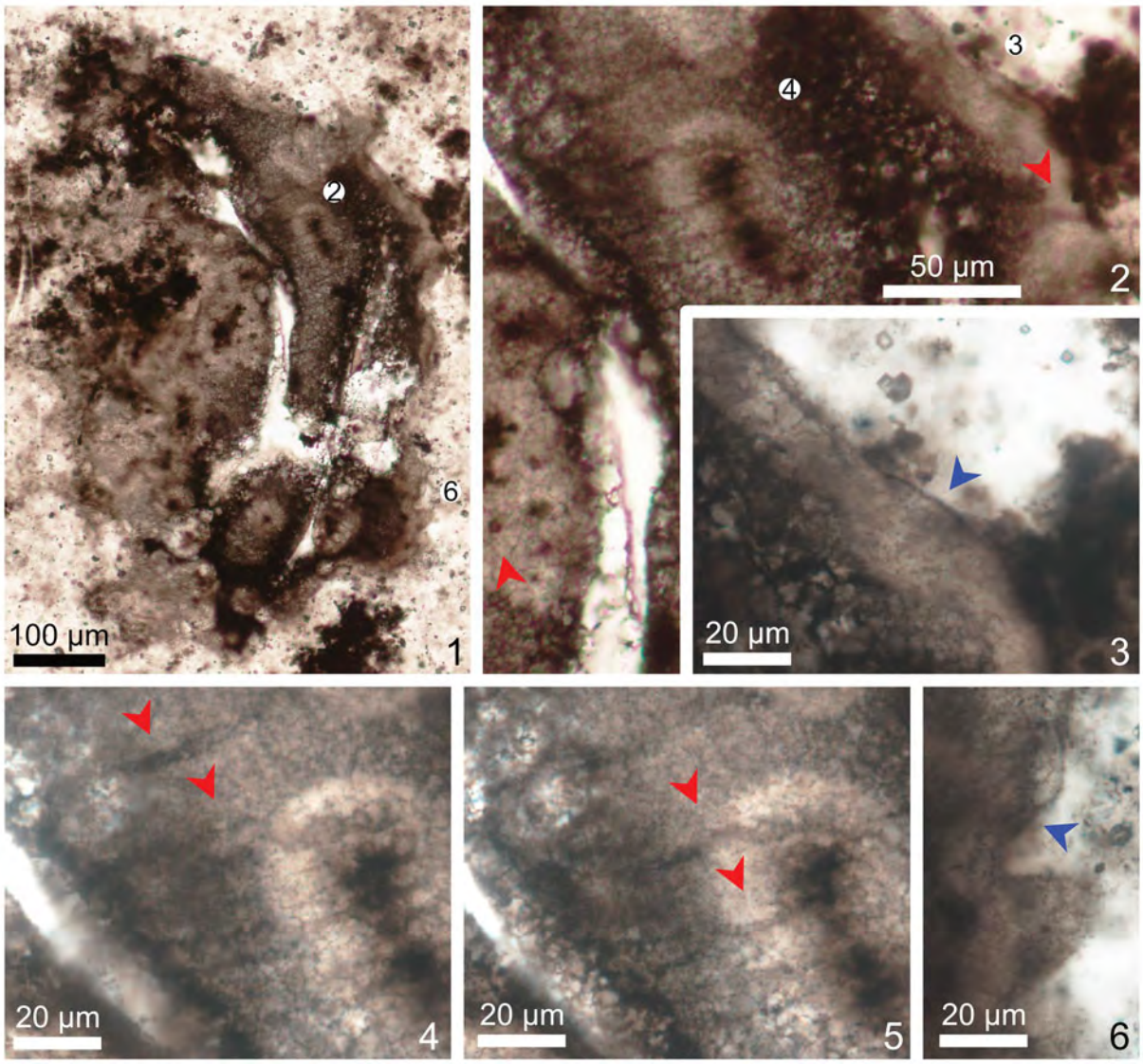

Figure 23. *Tianzhushania spinosa* Yin and Li, 1978, emend. Yin in Yin and Liu, 1988. (**1–6**) PB202061, thin section 21LHK-1-10, O41/4; circled 2 and 6 in (**1**) mark the areas magnified in (**2**) and (**6**), respectively; circled 3 in (**2**) marks the area magnified in (**3**); circled 4 in (**2**) marks the same area magnified in (**4**) and (**5**) at different focal levels. Red arrowheads denote hollow cylindrical processes embedded in multilaminate membrane; blue arrowheads denote poorly preserved multilaminate membrane.

1995 *Tianzhushania spinosa* Yin and Li, emend. Yin in Yin and Liu; Yin and Gao, pl. II, fig. 10.
1996 *Tianzhushania spinosa* Yin and Li, emend. Yin in Yin and Liu; Yin, p. 326, pl. I, fig. 1.
1998 *Tianzhushania spinosa* Yin and Li, emend. Yin in Yin and Liu; Zhang et al., p. 40, fig. 13.1, 13.4.
non 1998 *Tianzhushania spinosa* Yin in Yin and Li; Zhang et al., p. 40, fig. 13.2, 13.3.
1999 *Tianzhushania spinosa* Yin and Li, emend. Yin in Yin and Liu; Yin, p. 12, pl. 4, figs. 1–3.
2001 *Tianzhushania spinosa* Yin and Li, emend. Yin in Yin and Liu; Yin, pl. I, fig. 8.
2001 *Tianzhushania spinosa* Yin and Li, emend. Yin in Yin and Liu; Yin et al., p. 500, pl. I, figs. 1–4, pl. II, figs. 1, 2, 6.
non 2001 *Tianzhushania spinosa* Yin in Yin and Li, emend. Yin in Yin and Liu; Yin, pl. II, figs. 1, 2.
non 2001 *Tianzhushania spinosa* Yin in Yin and Li, emend. Yin in Yin and Liu; Yin et al., pl. II, figs. 3–5.
2003 *Tianzhushania spinosa* Yin and Li, emend. Yin in Yin and Liu; Yin et al., pl, I, figs, 5, 6.
2004 *Tianzhushania spinosa* Yin and Li; Yin et al., figs. 2A, 5D.
2004 *Tianzhushania* sp.; Yin et al., fig. 3A.
non 2004 *Tianzhushania spinosa* Yin in Yin and Li; Yin et al., fig. 3B.
2007 *Tianzhushania spinosa*; Yin et al., fig. 1c–l.
2007 *Tianzhushania spinosa*; Zhou et al., fig. 4A.
2008 *Tianzhushania conferta* Yin et al., p. 138, pl. I, figs. 11–13.
2008 *Tianzhushania fissura* Yin et al., p. 138, pl. I, figs. 2–10.
non 2008 *Tianzhushania spinosa*; Shukla et al., p. 374, pl. III, figs. 1, 2.

https://doi.org/10.1017/jpa.2023.92 Published online by Cambridge University Press

2009 *Tianzhushania spinosa*; Liu et al., fig. 2o–q.
2009a *Tianzhushania spinosa* Yin and Li, emend. Yin in Yin and Liu; Yin et al., pl. I, figs. 1, 8.
2010 *Tianzhushania spinosa*; Chen et al., fig. 2.13, 2.17.
2011 *Tianzhushania spinosa*; C. Yin et al., fig. 4a, b.
2012 *Tianzhushania spinosa*; Xiao et al., fig. 4C–H.
2013 *Tianzhushania spinosa*; Liu et al., fig. 10A.
2013 *Tianzhushania spinosa*; Zeng et al., fig. 3.2.
2013 *Tianzhushania conferta* Yin et al.; Liu et al., fig. 10E.
2013 *Tianzhushania fissura* Yin et al.; Liu et al., fig. 10D.
2013 *Tianzhushania fissura*; Zeng et al., fig. 3.1.
2013 *Tianzhushania* sp.; Zeng et al., fig. 3.3.
2014 *Tianzhushania spinosa* Yin and Li, emend. Yin in Yin and Liu; Xiao et al., p. 56.
2014b *Tianzhushania spinosa*; Liu et al., fig. 7D–F.
2015 *Tianzhushania spinosa* Yin and Li, emend. Yin in Yin and Liu; Ouyang et al., p. 219, pl. III, figs. 1–6.
2016 *Tianzhushania spinosa*; Joshi and Tiwari, p. 332, fig. 4B–E.
2017 *Tianzhushania spinosa*; Hawkins et al., fig. 6A, B.
non 2017 possibly *Tianzhushania spinosa*; Hawkins et al., fig. 7A, B.
2019 *Tianzhushania spinosa*; Ouyang et al., fig. 11A, B.
2020 *Tianzhushania* sp.; Yang et al., p. 9, fig. 2P, Q.
2021 *Tianzhushania spinosa*; Liu et al., fig. 5.1.
2021 *Tianzhushania spinosa* Yin in Yin and Li, emend. Yin in Yin and Liu; Ouyang et al., fig. 21A–L.
non 2021 *Tianzhushania spinosa* Yin and Li; Sharma et al., fig. 9A, D.
2022 *Tianzhushania spinosa*; Joshi et al., fig. 4d (mistakenly presented as 4c in figure caption; fig. 4c is *T. polysiphonia*).

Holotype.—Tian R29 X150, reposited at NIGPAS, from the Ediacaran Doushantuo Formation at Tianzhushan in Changyang area, Hubei Province, South China (Yin and Li, 1978, pl. 8, fig. 13).

Description and measurements.—Vesicle large, strongly deformed, originally spheroidal. Processes hollow and cylindrical (Fig. 23.2, 23.4, 23.5), evenly distributed, penetrating a multilaminate outer membrane (Fig. 23.3, 23.6) that surrounds the vesicle wall. Vesicle diameter unmeasurable due to deformation. Processes about 61.6 μm long and 1.4 μm wide, with about six processes per 100 μm of vesicle periphery. The thickness of the multilaminate outer membrane was not measured because it is likely cut obliquely in the thin section but is estimated to be similar to the length of cylindrical processes.

Material.—One illustrated specimen (Fig. 23).

Remarks.—Although poorly preserved, the specimen does show hollow cylindrical processes penetrating a multilaminate membrane, which are features diagnostic of *Tianzhushania*. The long, evenly and densely arranged processes identify this specimen to *T. spinosa*, which is different from the clustered distribution of processes in *T. polysiphonia* and the short and sparse processes in *T. rara*. Since Ouyang et al. (2021) reassigned the possible *T. spinosa* specimen reported from the Siduping section by Hawkins et al. (2017, fig. 7A, B) to *Crassimembrana multitunica* Ouyang et al., 2021, the specimen reported here represents the only known occurrence of *Tianzhushania* from the Doushantuo Formation in basinal facies or deep-water settings.

Three specimens identified as *Tianzhushania* sp. from the Weng'an, Yangtze Gorges, and Baokang areas (Yin et al., 2004; Zeng et al., 2013; Yang et al., 2020) all bear numerous hollow cylindrical processes that are embedded in a thick multilaminate layer and evenly distributed, and are here reassigned to *T. spinosa*. The specimen identified as *T. spinosa* from the Krol'A Formation in northern India (Sharma et al., 2021, fig. 9A, D) has small conical processes and thus should be excluded from *Tianzhushania*. Considering its small and densely distributed processes, that specimen may belong to *Knollisphaeridium*, possibly *K. coniformum*, as noted in Xiao et al. (2022).

Genus *Trachyhystrichosphaera* Timofeev and Hermann in Timofeev et al., 1976, emend. Tang et al., 2013

Type species.—*Trachyhystrichosphaera aimika* Hermann in Timofeev et al., 1976.

Other species.—*Trachyhystrichosphaera botula* Tang et al., 2013; *T. polaris* Butterfield in Butterfield et al., 1994.

Trachyhystrichosphaera? sp.
Figure 24

non 1988 *Trachyhystrichosphaera* sp.; Yin and Liu, p. 177, p. 180, pl. 11, figs. 3, 4.
non 1992 ?*Trachyhystrichosphaera* sp.; Knoll, p. 770, pl. 4, fig. 1, pl. 5, figs. 1, 2.
non 1999 ?*Trachyhystrichosphaera* sp.; Yin, p. 14, pl. 3, fig. 3.
?2004 *Trachyhystrichosphaera* aff. *aimica* Hermann, 1976 [sic]; Nagovitsin et al., p. 14, pl. I, fig. 10.

Description and measurements.—Vesicle small, spheroidal or ovoidal, with sparsely and irregularly distributed hollow processes. Processes bimorphic, with larger conical and smaller cylindrical ones. Vesicle diameter about 248 μm; conical processes 6.2–14.8 μm in length with an average of 10.7 μm, or 2.5–6.0% of vesicle diameter with an average of 4.3%, and 4.4–11.1 μm in basal width with an average of 7.6 μm; cylindrical processes 5.3–8.1 μm in length with an average of 6.9 μm, or 2.1–3.3% of vesicle diameter with an average of 2.8%, and 0.9–1.6 μm (with an average of 1.3 μm in width). An outer membrane can be found on top of some conical (Fig. 24.2–24.4) and cylindrical (Fig. 24.5–24.8) processes.

Material.—A single fairly well-preserved specimen (Fig. 24).

Remarks.—The illustrated specimen is tentatively assigned to *Trachyhystrichosphaera* based on its bimorphic processes and outer membrane. Some other genera are also characterized

https://doi.org/10.1017/jpa.2023.92 Published online by Cambridge University Press

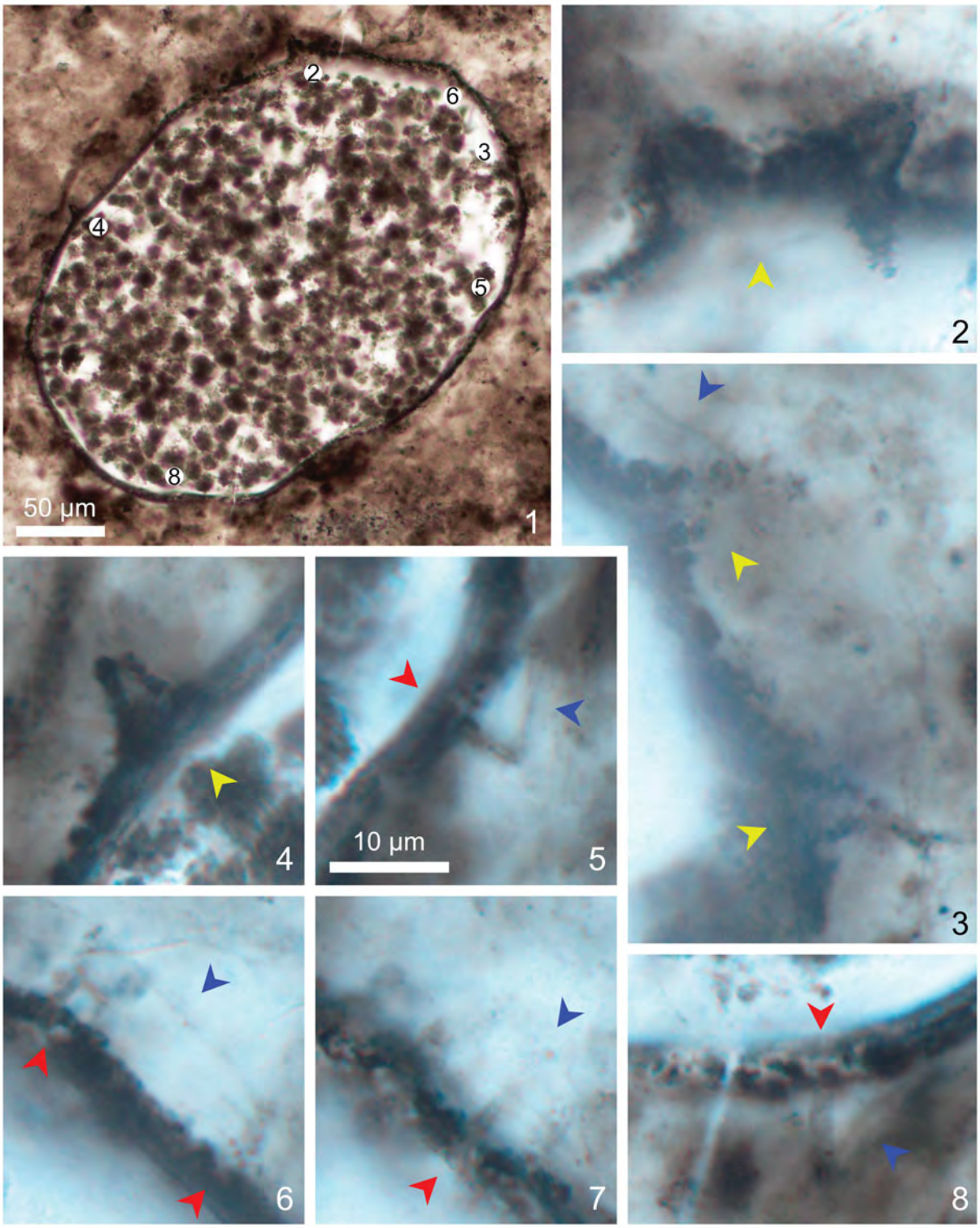

Figure 24. *Trachyhystrichosphaera*? sp. (**1–8**) PB202062, thin section 19CW-6-16, M40/3; circled 2–5 and 8 in (**1**) mark areas magnified in (**2–5**) and (**8**), respectively; circled 6 in (**1**) marks the same area magnified in (**6**) and (**7**) at different focal levels to show different processes. Scale bar in (**5**) also applies to (**2–4, 6–8**). Red arrowheads denote cylindrical processes, yellow arrowheads denote conical processes, blue arrowheads denote outer membrane.

by bimorphic or heteromorphic processes, including *Alicesphaeridium*, *Asseserium*, *Bispinosphaera*, *Distosphaera*, *Duospinosphaera*, *Sinosphaera*, and *Verrucosphaera*. Among them, *Alicesphaeridium*, *Bispinosphaera*, *Distosphaera*, *Duospinosphaera*, *Sinosphaera*, and *Verrucosphaera* are all characterized by their abundant, densely, and somewhat evenly distributed processes that cover the entire vesicle surface. *Asseserium diversum* Nagovitsin and Moczydłowska

https://doi.org/10.1017/jpa.2023.92 Published online by Cambridge University Press

in Moczydłowska and Nagovitsin, 2012, bears heteromorphic and irregularly distributed hollow processes (Moczydłowska and Nagovitsin, 2012), and its process density is similar to the illustrated specimen. However, compared with *Asseserium*, which has a small to medium-sized vesicle bearing processes whose length is 10–40% of the vesicle diameter, the illustrated specimen has a vesicle several times larger and thus proportionally shorter processes. In addition, none of the above-mentioned bimorphic or heteromorphic taxa have an outer membrane, which is observed in the illustrated specimen (blue arrowheads in Fig. 24.3, 24.5–24.8), and diagnostic of *Trachyhystrichosphaera* (Tang et al., 2013).

Trachyhystrichosphaera is a typical Tonian genus (Pang et al., 2020), and has been only infrequently reported, mostly as open nomenclature, from Ediacaran strata (Knoll, 1992; Faizullin, 1998; Nagovitsin et al., 2004). Several previously published specimens of *Trachyhystrichosphaera* lack the diagnostic features of and thus should be excluded from this genus, including *Trachyhystrichosphaera* sp. in Yin and Liu (1988, p. 177, pl. 11, figs. 3, 4), ?*Trachyhystrichosphaera* sp. in Knoll (1992, p. 770, pl. 4, fig. 1, pl. 5, figs. 1, 2), ?*Trachyhystrichosphaera* sp. in Yin (1999, p. 14, pl. 3, fig. 3), *Trachyhystrichosphaera* aff. *aimica* [sic] in Nagovitsin et al. (2004, pl. I, figs. 7 and 11 only), and *T. aimika* in Shukla et al. (2008, p. 374, pl. 2, fig. 1). The specimen identified as *Trachyhystrichosphaera* sp. in Faizullin (1998, pl. I, fig. 16) was poorly illustrated and a re-examination of the specimen is required to assess its taxonomic identification. One of the three specimens identified as *Trachyhystrichosphaera* aff. *aimica* [sic] extracted from shales of the Ediacaran Ura Formation in Siberia (Nagovitsin et al., 2004, pl. I, fig. 10) contains an outer layer enveloping short, hollow, and sparsely distributed processes, resembling the specimen illustrated here, and fits the diagnosis of *Trachyhystrichosphaera*. However, these two possible occurrences of Ediacaran *Trachyhystrichosphaera* are each represented by a single specimen, and may represent morphological variations of other acanthomorphs such as *Tianzhushania rara*. Therefore, we place the illustrated specimen in an open nomenclature.

Genus *Urasphaera* Nagovitsin and Moczydłowska in Moczydłowska and Nagovitsin, 2012

Type species.—*Urasphaera capitalis* Nagovitsin and Moczydłowska in Moczydłowska and Nagovitsin, 2012.

Other species.—*Urasphaera fungiformis* Liu et al., 2014a; *U. nupta* Liu et al., 2014a.

Urasphaera fungiformis Liu et al., 2014a
Figure 25

2013 *Gyalosphaeridium pulchrum* Zang in Zang and Walter, 1992; Liu et al., fig. 13G.
2014a *Urasphaera fungiformis* Liu et al., p. 119, figs. 87, 88, 89.1.
2017 *Urasphaera fungiformis* Liu et al.; Nie et al., p. 380, fig. 9.
2017 *Urasphaera fungiformis*; Ouyang et al., fig. 8G–J (the specimen described here and illustrated in Fig. 26).
2022 *Urasphaera fungiformis* Liu et al.; Ye et al., fig. 48A–C.

Holotype.—IGCAGS-NPIII-482, thin section NPIII13-3-5, Nikon 80i coordinates 23.8×111, England Finder coordinates E23/4, reposited at the Institute of Geology, Chinese Academy of Geological Science, from the Ediacaran Doushantuo Formation at the Niuping section in Yichang area, Hubei Province, South China (Liu et al., 2014a, fig. 87.1–87.4).

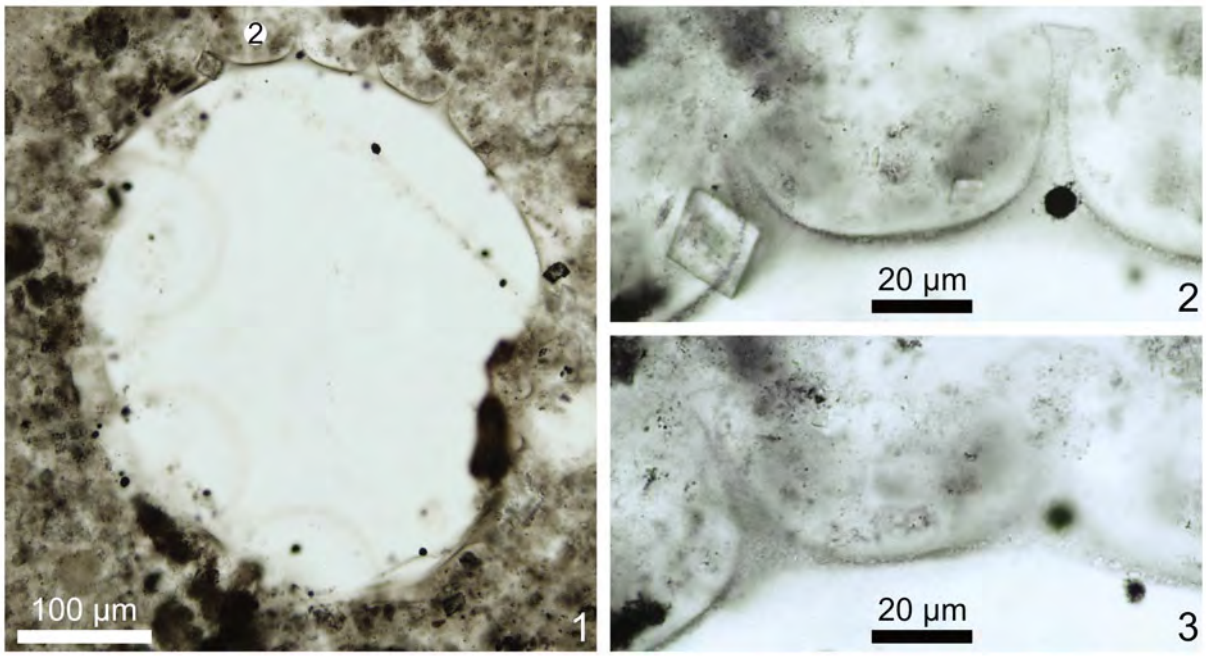

Figure 25. *Urasphaera fungiformis* Liu et al., 2014a. (**1**–**3**) PB202063, thin section 14HA-115-1, N50; circled 2 in (**1**) marks the same area magnified in (**2**) and (**3**) at different focal levels to show different processes.

https://doi.org/10.1017/jpa.2023.92 Published online by Cambridge University Press

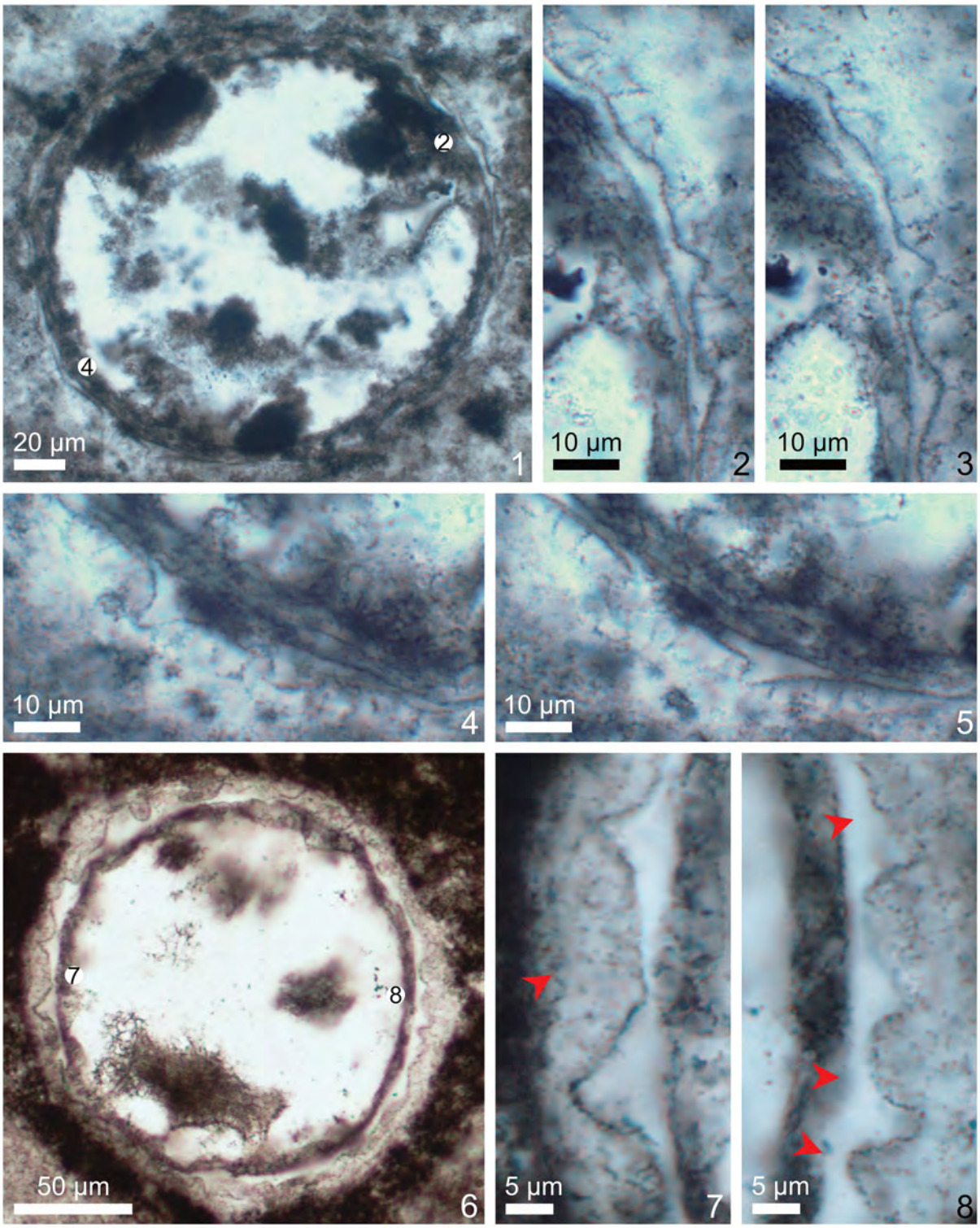

Figure 26. *Verrucosphaera*? *undulata* new species. (**1–5**) Holotype, PB202064, thin section 21DC-6-1, H44; circled 2 in (**1**) marks the same area magnified in (**2**) and (**3**) at different focal levels to show different processes; circled 4 in (**1**) marks the same area magnified in (**4**) and (**5**) at different focal levels to show different processes; (**6–8**) PB202065, thin section 21DC-5-4, S47; circled 7 and 8 in (**6**) mark areas magnified in (**7**) and (**8**), respectively. Red arrowheads denote thin cylindrical processes on top of thick conical processes.

Description and measurements.—Vesicle large, spheroidal, bearing evenly distributed processes. Processes begin with a wide and deflated base that tapers to form a waist and then expands distally to form a truncated terminal end. Vesicle diameter about 400 µm, with 1–2 processes per 100 µm of vesicle periphery. Process length about 39.3 µm and 9.8% of vesicle diameter, basal width about 27.2 µm, terminal width about 9.3 µm, minimum width of process (waist width) about 3.2 µm.

https://doi.org/10.1017/jpa.2023.92 Published online by Cambridge University Press

Material.—One well-preserved specimen (Fig. 25).

Remarks.—The specimen at hand is larger than specimens of *Urasphaera fungiformis* from the type locality at the Niuping section in the Yangtze Gorges area of Hubei Province (Liu et al., 2014a), but comparable to those from the Shennongjia area reported by Ye et al. (2022, fig. 48A–C). Nonetheless, this specimen resembles those from the Yangtze Gorges area in the moderate number of proportionally short processes with a broadened base, features that distinguish *U. fungiformis* from *U. capitalis* and *U. nupta*. The small distal expansion may not be captured in all processes of *Urasphaera* if the processes are cut obliquely in the thin section, thus some processes may appear conical in shape.

Genus *Verrucosphaera* Liu and Moczydłowska, 2019

Type species.—*Verrucosphaera minima* Liu and Moczydłowska, 2019.

Other species.—*Verrucosphaera*? *undulata* n. sp.

Verrucosphaera? *undulata* new species
Figures 26–28

2022 ?*Verrucosphaera* sp.; Shi et al., fig. 10A–F (including the type specimen in fig. 10A, B, D).

Holotype.—PB202064, thin section 21DC-6-1, ZEISS Scope A1 coordinates 8×92, England Finder coordinates H44, illustrated in Figure 26.1–26.5, reposited at NIGPAS, from Doushantuo Formation at the Caojunba section in Shimen area, Hunan Province, South China.

Diagnosis.—Vesicle medium-sized, spheroidal or ovoidal, bearing two sets of bimorphic processes: a set of large conical processes supporting a set of thin filamentous processes. The large processes are hollow, obtusely conical, basally connected or separated, terminally rounded or truncated, irregularly distributed, and variable in both length and basal width. The thin filamentous processes are cylindrical, more or less uniform in length and thickness, densely arranged but basally separated, and evenly distributed on both the vesicle wall and the large processes. The large conical and thin filamentous processes are comparable in length, accounting for about 5% of vesicle diameter.

Description and measurements.—Holotype: vesicle diameter 172 μm; large processes 4.8 μm in length (2.8% of vesicle diameter) and 7.9 μm in basal width; thin processes 4.9 μm in length (2.8% of vesicle diameter) and 0.2 μm in diameter, 27 processes per 100 μm of vesicle periphery. Other specimens: vesicle diameter 126–192 μm (N = 30, mean = 162 μm, SD = 16 μm); large process length 3.8–18.7 μm (N = 25, mean = 8.2 μm, SD = 3.4 μm) or 2.3–10.0% of vesicle diameter (N = 25, mean = 5.1%, SD = 1.9%), process basal width 6.7–44.8 μm (N = 23, mean = 18.5 μm, SD = 9.4 μm); thin process length 2.8–8.7 μm (N = 24, mean = 5.6 μm, SD = 1.3 μm) or 1.7–5.6% of vesicle diameter (N = 24, mean = 3.5%, SD = 0.9%), process width 0.2–0.6 μm (N = 22, mean = 0.3 μm, SD = 0.1 μm), 23–47 processes per 100 μm of vesicle periphery.

Etymology.—From Latin *undulatus*, wavy, with reference to the wavy profile of the vesicle wall as viewed in thin sections due to the irregular arrangement of large processes which are obtusely conical in shape.

Material.—Five illustrated specimens (Figs. 26, 27) and 26 additional specimens.

Remarks.—There are several other taxa that are characterized by bimorphic processes, with a set of large hollow processes and another set of thin cylindrical processes. These taxa, including *Bispinosphaera*, *Distosphaera*, and *Duospinosphaera*, differ from *Verrucosphaera* in the spatial relationship between the two set of processes: the thin processes in *Bispinosphaera*, *Distosphaera*, and *Duospinosphaera* are initiated from either the inner or outer surface of the vesicle wall and they are not found on top of the large processes. *Verrucosphaera*? *undulata* n. sp. is different from *V. minima* in that the thin processes are only found on top of the large processes in the latter species, but they can be on top of both the large processes and the vesicle wall in the former species. Additionally, the large processes are more or less conical in *V.*? *undulata* n. sp. but hemispherical in *V. minima*. Considering these similarities and differences, *V.*? *undulata* n. sp. is tentatively placed in the genus *Verrucosphaera*, pending an emendation of the genus diagnosis.

Genus *Weissiella* Vorob'eva, Sergeev, and Knoll, 2009

Type species.—*Weissiella grandistella* Vorob'eva, Sergeev, and Knoll, 2009.

Other species.—*Weissiella brevis* Xiao et al., 2014, emend. Ouyang et al., 2021; *Weissiella concentrica* Ye et al., 2022.

Remarks.—The genus *Weissiella* is characterized by hollow and internally septate processes. Several other Ediacaran acanthomorph taxa are also known for their hollow and internally decorated processes. These internal decorations include either transverse septa (as in *Bispinosphaera peregrina* Liu et al., 2014a, *Weissiella*, and *Yushengia ramispina* Liu et al., 2014a) or domal structures (as in *Mengeosphaera matryoshkaformis*). Among these taxa, *Weissiella* has the widest paleogeographic distribution and the greatest morphological variation. Thus far, three species of *Weissiella* have been recognized (*W. grandistella*, *W. brevis*, *W. concentrica*), differentiated from each other by their process morphologies and the presence of an outer wall. In addition to these three species, Ouyang et al. (2021) proposed the assignment of all silicified *Weissiella* specimens from the Doushantuo Formation with large conical processes to *Weissiella* cf. *W. grandistella*, emphasizing both their morphological similarities to and difference from *W. grandistella* specimens from the type locality. Two unnamed species of *Weissiella* (Ye et al., 2015, pl. I, figs. 15–19, and Ouyang et al., 2019, fig. 10E–G) were reassigned to *W. brevis*

https://doi.org/10.1017/jpa.2023.92 Published online by Cambridge University Press

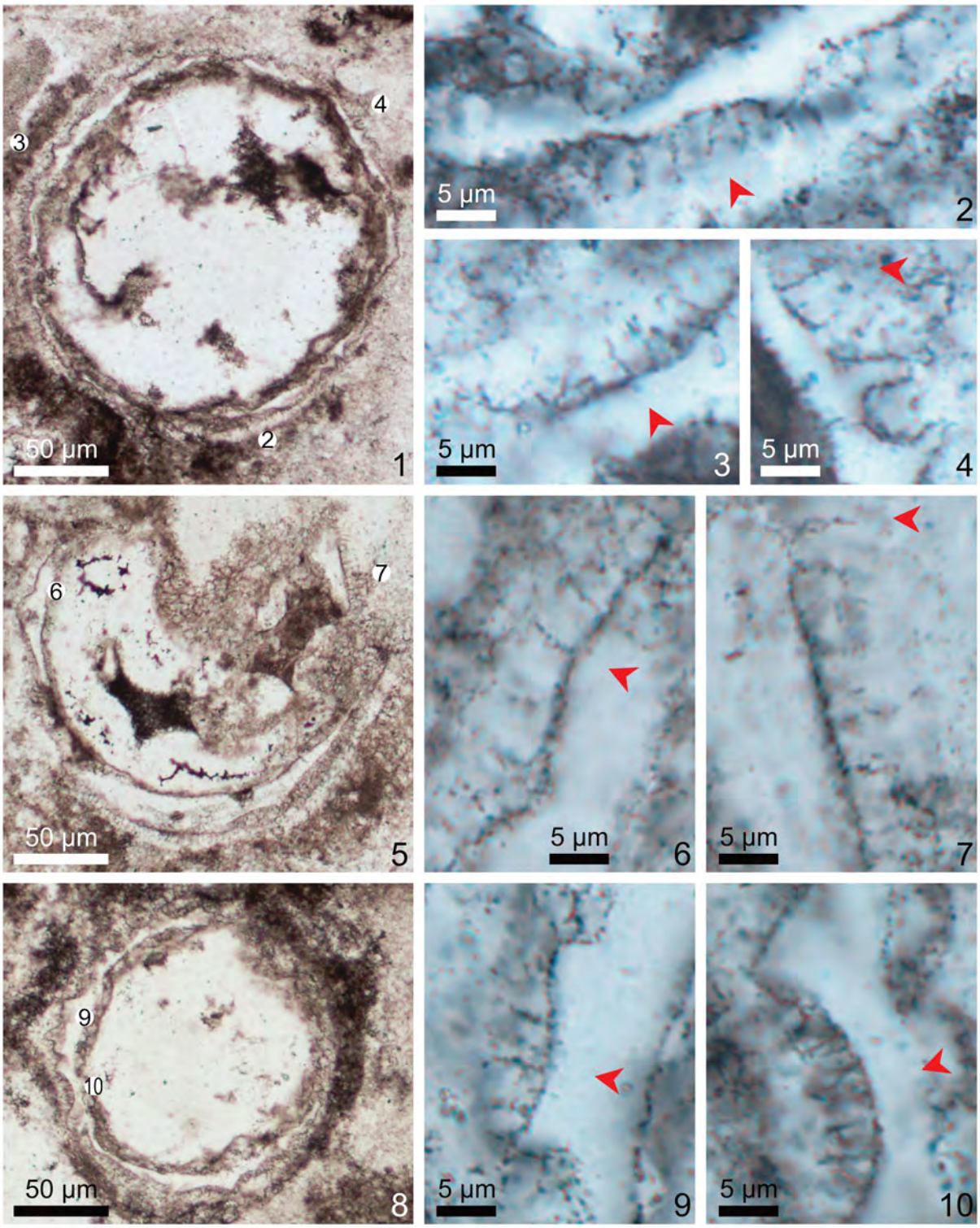

Figure 27. *Verrucosphaera*? *undulata* new species. (**1–4**) PB202066, thin section 21DC-5-4, P41/2; circled 2–4 in (**1**) mark areas magnified in (**2–4**), respectively; (**5–7**) PB202067, thin section 21DC-5-4, T32/4; circled 6 and 7 in (**5**) mark areas magnified in (**6**) and (**7**), respectively; (**8–10**) PB202068, thin section 21DC-5-4, L43/3; circled 9 and 10 in (**8**) mark areas magnified in (**9**) and (**10**), respectively. Red arrowheads denote thin cylindrical processes on top of thick conical processes.

(Xiao et al., 2022); the processes in the former (Ye et al., 2015) are irregularly shaped with occasional branches, whereas those in the latter (Ouyang et al., 2019) are likely biform, both of which are different from *W. brevis* from the type locality but considered as representing intraspecific variations of *W. brevis*. The existence of transverse septa or cross-walls in the processes of *Weissiella* and other taxa raises the interesting question about their functions, a topic worthy of further investigation in the future.

https://doi.org/10.1017/jpa.2023.92 Published online by Cambridge University Press

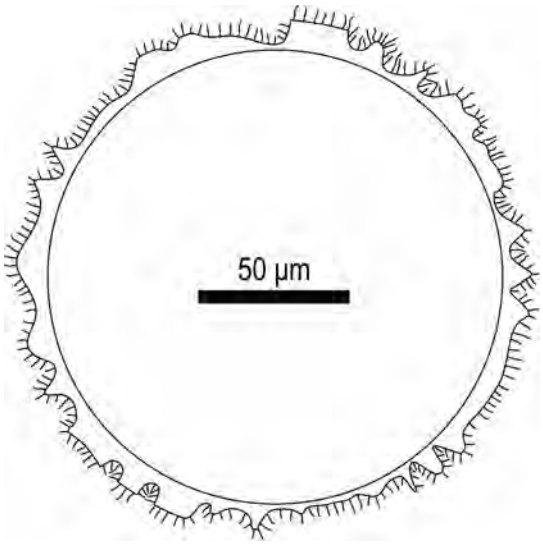

Figure 28. Sketch of *Verrucosphaera*? *undulata* new species.

Weissiella cf. *W. grandistella* Vorob'eva, Sergeev, and Knoll, 2009
Figure 29

2013 *Weissiella grandistella*; Liu et al., fig. 13E.
2014a *Weissiella grandistella* Vorob'eva et al.; Liu et al., p. 128, figs. 94, 95.
2014b *Weissiella grandistella*; Liu et al., fig. 9E.
non 2014 *Weissiella* cf. *W. grandistella*; Shukla and Tiwari, p. 219, fig. 8A–E.
2019 *Weissiella grandistella* Vorob'eva et al.; Liu and Moczydłowska, p. 163, figs. 91F, G, 92.
2021 *Weissiella* cf. *W. grandistella*; Ouyang et al., fig. 24A–H.
2022 *Weissiella* cf. *W. grandistella*; Shi et al., fig. 10G–I (the specimen described here and illustrated in Fig. 29).
2022 *Weissiella* cf. *grandistella* Vorob'eva et al.; Ye et al., fig. 49D–F.

Description and measurements.—Vesicle medium-sized, spheroidal, bearing a modest number of large conical processes evenly distributed on the vesicle surface. Processes hollow but each contains about two thin cross-walls or transverse septa that divide the process into several compartments (red arrowheads in Fig. 29.2–29.4). Cross-walls occur near the base of each process. Vesicle diameter about 114 μm, maximum measurable length of processes 45.0 μm (or 39.6% of vesicle diameter), process basal width 23.4 μm, about 3 processes per 100 μm of vesicle periphery.

Material.—One well-preserved specimen (Fig. 29).

Remarks.—As for specimens identified as *Weissiella* cf. *W. grandistella* from the Doushantuo Formation in Yangtze Gorges area, the specimen described here from the Caojunba section is also much smaller than *W. grandistella* from its type locality and is placed in an open nomenclature (see Ouyang et al., 2021, for a detailed comparison among *W. grandistella*, *W. brevis*, and permineralized Doushantuo acritarchs identified as *Weissiella* cf. *W. grandistella*). One distinctive feature of this specimen is that the cross-walls occur near the base of the processes. Examination under polarized light microscopy (e.g., Fig. 29.5–29.7) indicates that the lack of cross-walls in the distal portion of processes is not a taphonomic artifact related to recrystallization and may thus reflect intraspecific variation.

All specimens of *Weissiella* cf. *W. grandistella* from the Doushantuo Formation in South China are morphologically similar and may constitute a new species of *Weissiella*. However, except for their smaller size, they are otherwise similar to *W. grandistella*, which led Liu and Moczydłowska (2019) to assign them to *W. grandistella*. Current morphological data are not sufficient to conclusively resolve this issue, and these specimens are here treated as an open nomenclature.

Results

Morphological groups of Doushantuo microfossils from the studied sections.—Microfossils from the Doushantuo Formation at the studied localities include acanthomorphic and sphaeromorphic acritarchs, multicellular algae, tubular microfossils, filaments and coccoids, and other problematic fossils (Tables 1, 2). Although chert nodules in these localities are composed mainly of micro-quartz and thus petrographically similar to fossiliferous chert nodules previously obtained from the Doushantuo Formation elsewhere, many microfossils found in this study underwent more severe degradation and destruction due to recrystallization of micro-quartz (up to several micrometers in size; e.g., yellow arrowheads in Figs. 29.5, 29.7, 30), leading to poor preservation of delicate structures. To facilitate discussion, the Doushantuo microfossils recovered in this study are briefly described below in several morphological groups.

Acanthomorphic acritarchs (Table 2, Figs. 4–29, 31).—Acanthomorphic acritarchs appear in the Doushantuo Formation at all studied sections and are a major component of eukaryotic microfossils in most fossiliferous samples. The 206 acanthomorphic acritarch specimens that were recognized from the nine studied stratigraphic sections are classified into 15 genera, 29 species (including three new species: *Bullatosphaera*? *colliformis* n. sp., *Eotylotopalla inflata* n. sp., and *Verrucosphaera*? *undulata* n. sp.), and six unnamed forms (*Eotylotopalla* sp., *Mengeosphaera minima*?, *Tanarium* cf. *T. capitatum*, *Trachyhystrichosphaera*? sp., and *Weissiella* cf. *W. grandistella*), which may represent new taxa. Most of these taxa are represented by only one or a few specimens, and the very few taxa that are relatively abundant (i.e., accounting for ~10% of all acanthomorphic specimens), such as *Appendisphaera magnifica*, *Hocosphaeridium anozos*, and *Verrucosphaera*? *undulata* n. sp., are each found at only one stratigraphic section. Consequently, diversity and relative abundance of different acanthomorphic taxa vary significantly among localities. For example, four of the five species recovered from the basinal facies are from the Lianghekou section. Only two species occur at more

https://doi.org/10.1017/jpa.2023.92 Published online by Cambridge University Press

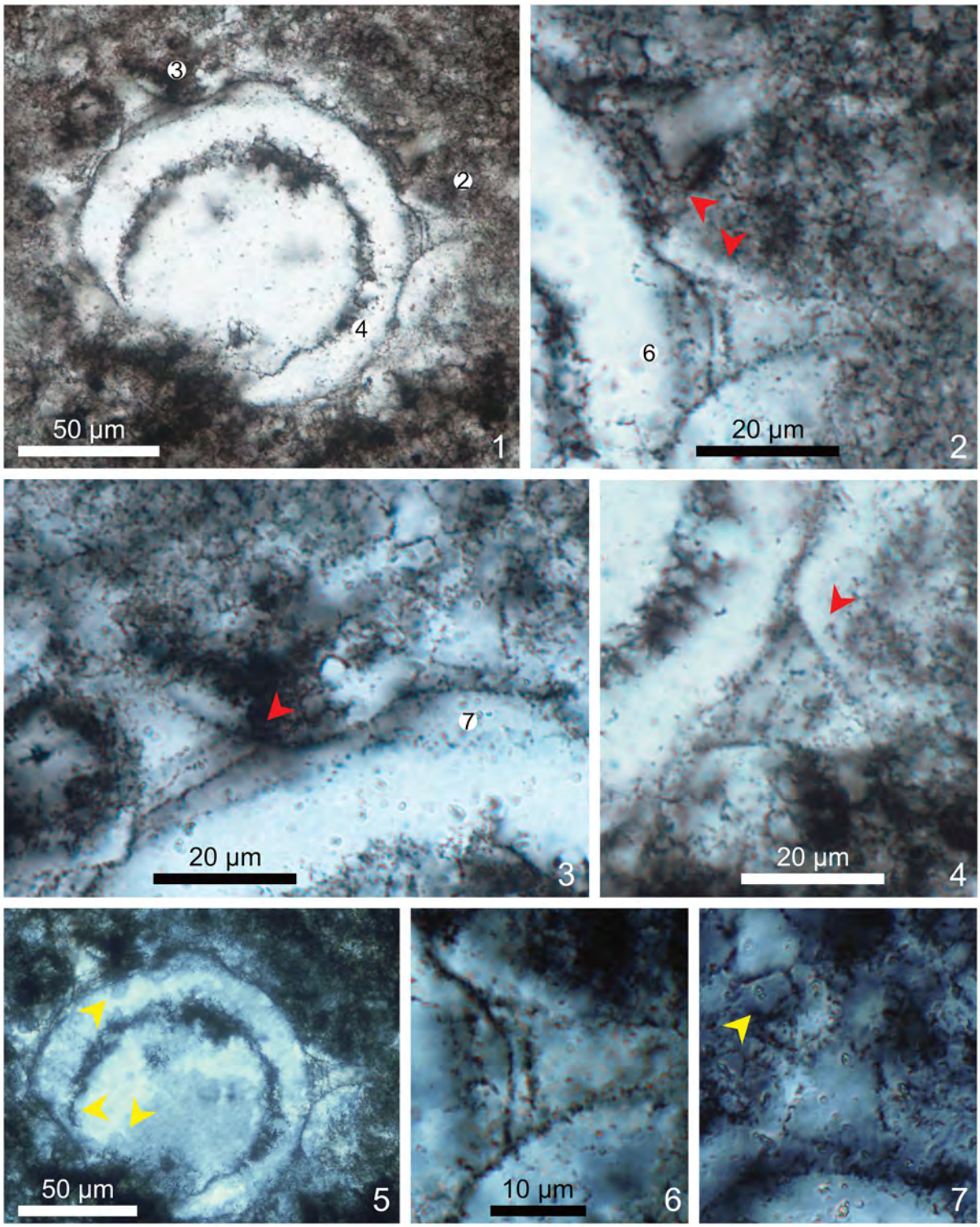

Figure 29. *Weissiella* cf. *W. grandistella*. (**1–7**) PB202069, thin section 21DC-2-30, T35; circled 2–4 in (**1**) mark areas magnified in (**2–4**), respectively; red arrowheads denote cross-walls in the processes; (**5–7**) cross-polarized light microscopic photographs of (**1**); circled 6 in (**2**) and circled 7 in (**3**) showing areas in (**6**) and (**7**), respectively; recrystallized micro-quartz indicated by yellow arrowheads; scale bar in (**6**) also applies to (**7**).

than half of the studied sections: *Appendisphaera grandis* at six sections, and *Hocosphaeridium scaberfacium* at five sections. The two species of *Megasphaera* were recovered only from one olistostrome sample (19SDP-1) at Siduping, and thus may not be representative of the local assemblage.

Sphaeromorphic acritarchs (Fig. 32).—Appearing at eight out of the nine studied sections (Table 1), sphaeromorphic acritarchs are represented by leiospheres of various sizes. The abundance and preservational state of sphaeromorphs vary significantly among localities. In the upper part of the

https://doi.org/10.1017/jpa.2023.92 Published online by Cambridge University Press

Table 2. Summary of acanthomorph occurrence and abundance data at the nine studied sections. Each occurrence is denoted by fossiliferous sample name and number of specimens. For example, "21DC-4, 1" means one acanthomorph specimen recovered from the sample 21DC-4. Notes for superscripts: (1) Identified as *Cavaspina* cf. *C. basiconica* by Shi et al. (2022). (2) Identified as ?*Verrucosphaera* sp. by Shi et al. (2022). (3) Identified as *Appendisphaera fragilis* by Ouyang et al. (2017). (4) Identified as ?*Cavaspina basiconica* by Ouyang et al. (2017). (5) Identified as indeterminate acanthomorph by Ouyang et al. (2017). (6) Identified as *Mengeosphaera spicata* by Ouyang et al. (2017). (7) Identified as *Mengeosphaera latibasis*? by Ouyang et al. (2017). (8) Identified as *Mengeosphaera chadianensis*, *Mengeosphaera* sp. indet., and *M.*? *cuspidata* by Ouyang et al. (2017).

	Caojunba	Lujiayuanzi	Caowan	Heping	Tianping	Siduping	Majindong	Lianghekou	Jinshichong	Sum
Appendisphaera grandis	21DC-4, 1 21DC-5, 2	14HA-85, 1[3]		19HP-1, 1	19TP-1, 1	19SDP-2, 1			18JSC-2, 1	8
A. magnifica						19SDP-7, 17				17
A. tenuis					19TP-1, 4					4
Asterocapsoides wenganensis								21LHK-1, 1		1
Bullatosphaera? *Colliformis* n. sp.			19CW-6, 2 19CW-9, 1							3
Cavaspina acuminata	21DC-3, 1 21DC-5, 1									2
C. basiconica	21DC-5, 1[1]	14HA-30, 1[4]								2
C. uria	21DC-2, 1 21DC-5, 4 21DC-6, 1									6
Eotylotopalla dactylos	21DC-2, 2 21DC-5, 1	14HA-115, 1[5]			19TP-1, 1					5
Eotylotopalla cf. *E. dactylos*	21DC-2, 1									1
E. inflata n. sp.					19TP-1, 1					1
Eotylotopalla sp.			19CW-6, 1							1
Hocosphaeridium anozos	21DC-2, 20									20
H. scaberfacium	21DC-2, 2		19CW-5, 1 19CW-6, 2	19HP-1, 1	19TP-1, 2	19SDP-7, 1				9
Knollisphaeridium maximum	21DC-3, 2 21DC-6, 2	14HA-140, 8								12
Knollisphaeridium sp. indet.		14HA-140, 5								5
Megasphaera inornata						19SDP-1, 1				1
M. ornata						19SDP-1, 1				1
Mengeosphaera bellula			19CW-6, 2							2
M. constricta		14HA-115, 1[6]								1
M. gracilis			19CW-6, 1		19TP-1, 1					2
M. latibasis		14HA-115, 1[7]								1
M. mamma	21DC-2, 5						21MJD-1, 2	21LHK-1, 2		9
M. minima	21DC-4, 1 21DC-5, 1									2
M. minima?	21DC-3, 1									1
Tanarium cf. *T. capitatum*	21DC-2, 1									1
T. conoideum	21DC-5, 1									1
T. paucispinosum			19CW-5, 3 19CW-6, 6							9
T. pilosiusculum	21DC-5, 1		19CW-6, 1					21LHK-1, 1		3
T. triangulare		14HA-140, 5[8]								5
T. tuberosum	21DC-4, 1									1
Tanarium sp. indet.	21DC-2, 1 21DC-4, 1		19CW-6, 1							3
Tianzhushania spinosa								21LHK-1, 1		1
Trachyhystrichosphaera? sp.			19CW-6, 1							1
Urasphaera fungiformis		14HA-115, 1								1
Verrucosphaera? *undulata* n. sp.	21DC-4, 1[2] 21DC-5, 29[2] 21DC-6, 1[2]									31
Weissiella cf. *W. grandistella*	21DC-2, 1									1
Indeterminate	10	4	5		4	6		2		31
Sum	98	28	27	2	14	27	2	7	1	206

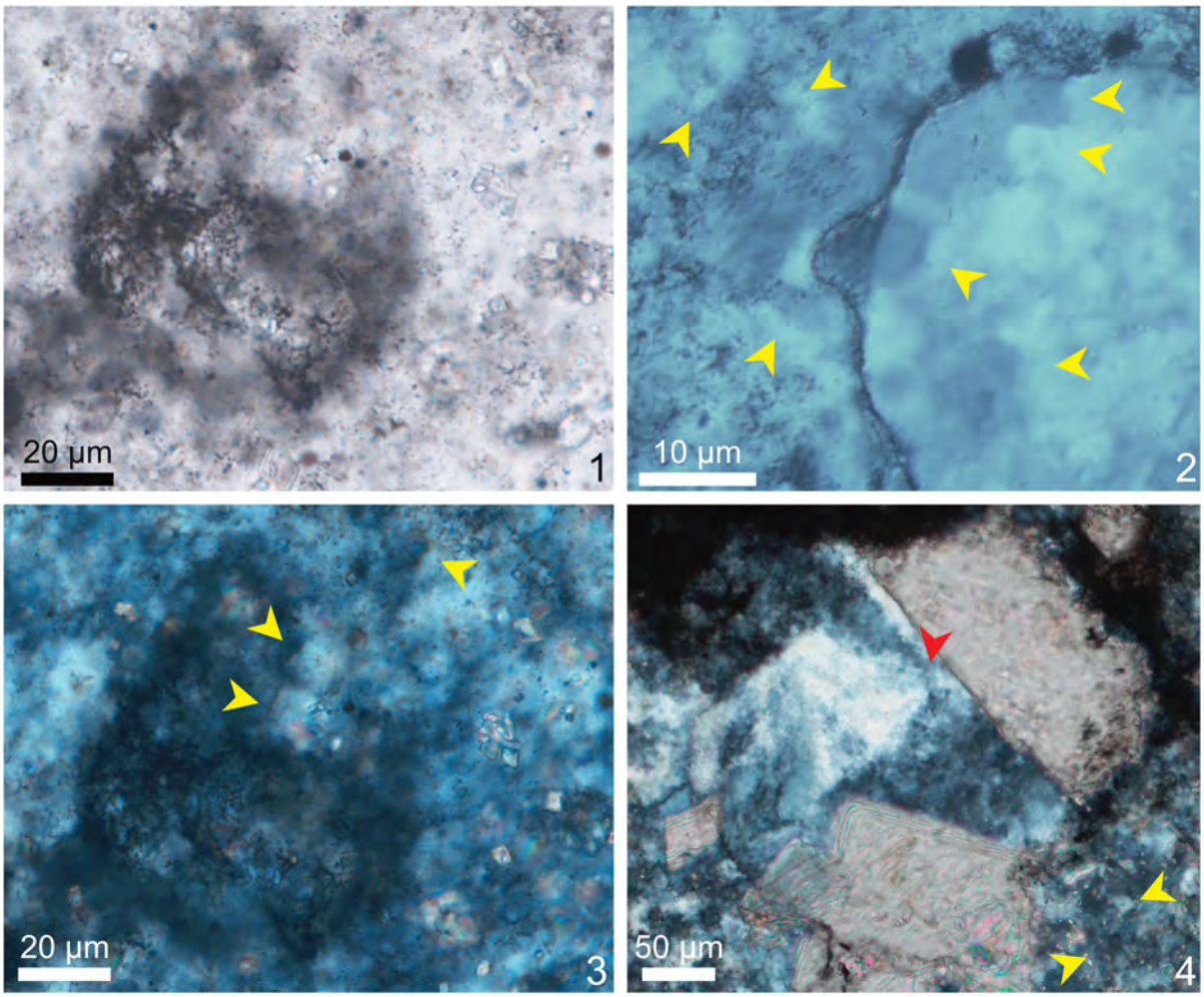

Figure 30. Recrystallized micro-quartz in chert nodules. (**1, 3**) A poorly preserved microfossil under plane- (**1**) and cross- (**3**) polarized light, showing recrystallized micro-quartz up to 7 µm in size (yellow arrowheads); thin section 19TP-1-39. (**2**) A well-preserved microfossil under cross-polarized light, showing recrystallized micro-quartz in various sizes (yellow arrowheads); thin section 21DC-5-3. (**4**) A poorly preserved microfossil under cross-polarized light, with the vesicle interior filled with sightly recrystallized chalcedony (red arrowhead), vesicle wall destroyed by three large calcite crystals, and extra-vesicle matrix filled with micro-quartz in various sizes (yellow arrowheads); thin section 19TP-1-25.

Doushantuo Formation at Caojunba, almost all fossiliferous samples contain clustered or even tightly compacted leiospheres, with many clusters consisting of tens of specimens of similar size (generally about 100–200 µm in diameter; Shi et al., 2022, fig. 6C–G). For samples from other sections or the lower part of the Doushantuo Formation at Caojunba, however, most leiospheres are solitary (Fig. 32.1, 32.2), and only occasionally form small or loosely arranged aggregates (Fig. 32.3, 32.4).

Multicellular algae (Fig. 33).—Multicellular algae recovered in this study are represented by one specimen (*Wengania minuta* Xiao, 2004b; Ouyang et al., 2017, fig. 7A) from the Lujiayuanzi section, one specimen (unnamed thallus, Fig. 33.6) at the Caowan section, and four specimens (one identified as *W. minuta* and three unnamed, all from the olistostrome sample 19SDP-1) at the Siduping section. The three unnamed specimens from the Siduping section (Fig. 33.3–33.5, 33.7) are similar to "Unnamed multicellular form with relatively large cells" (Ouyang et al., 2021, fig. 9I) and "Unnamed species B" (Shang and Liu, 2022, fig. 13) in their exceptionally large (commonly exceeding 20 µm), cuboidal or polyhedral cells with apparently rigid cell walls.

Tubular microfossils (Fig. 34).—Seven tubular microfossil specimens are found from the Doushantuo Formation at Caojunba, Caowan, Siduping, and Majindong sections (Table 1). One specimen (Fig. 34.1) with square cross-sectional view fits the diagnosis of *Quadratitubus orbigoniatus* Xue, Tang, and Yu, 1992, emend. Liu et al., 2008, and three additional specimens (Fig. 34.2) preserved together may represent oblique sectional views of *Q. orbigoniatus*. The remaining three specimens (Fig. 34.3, 34.4) are identified as *Sinocyclocyclicus guizhouensis* Xue, Tang, and Yu, 1992, emend. Liu et al., 2008.

Filamentous and coccoidal microfossils (Figs. 35–37).—Filamentous and coccoidal microfossils, likely of prokaryotic affinities (Butterfield et al., 1994), occur at all studied sections, and are abundant in many fossiliferous samples (Table 1). Among them, the filamentous taxa *Siphonophycus* Schopf, 1968, emend. Knoll et al., 1991 (Fig. 35) and *Salome* Knoll, 1982 (Figs. 35.3, 36.2–36.4) with varying filament diameters, are the two most abundant forms, preserved either as solitary

https://doi.org/10.1017/jpa.2023.92 Published online by Cambridge University Press

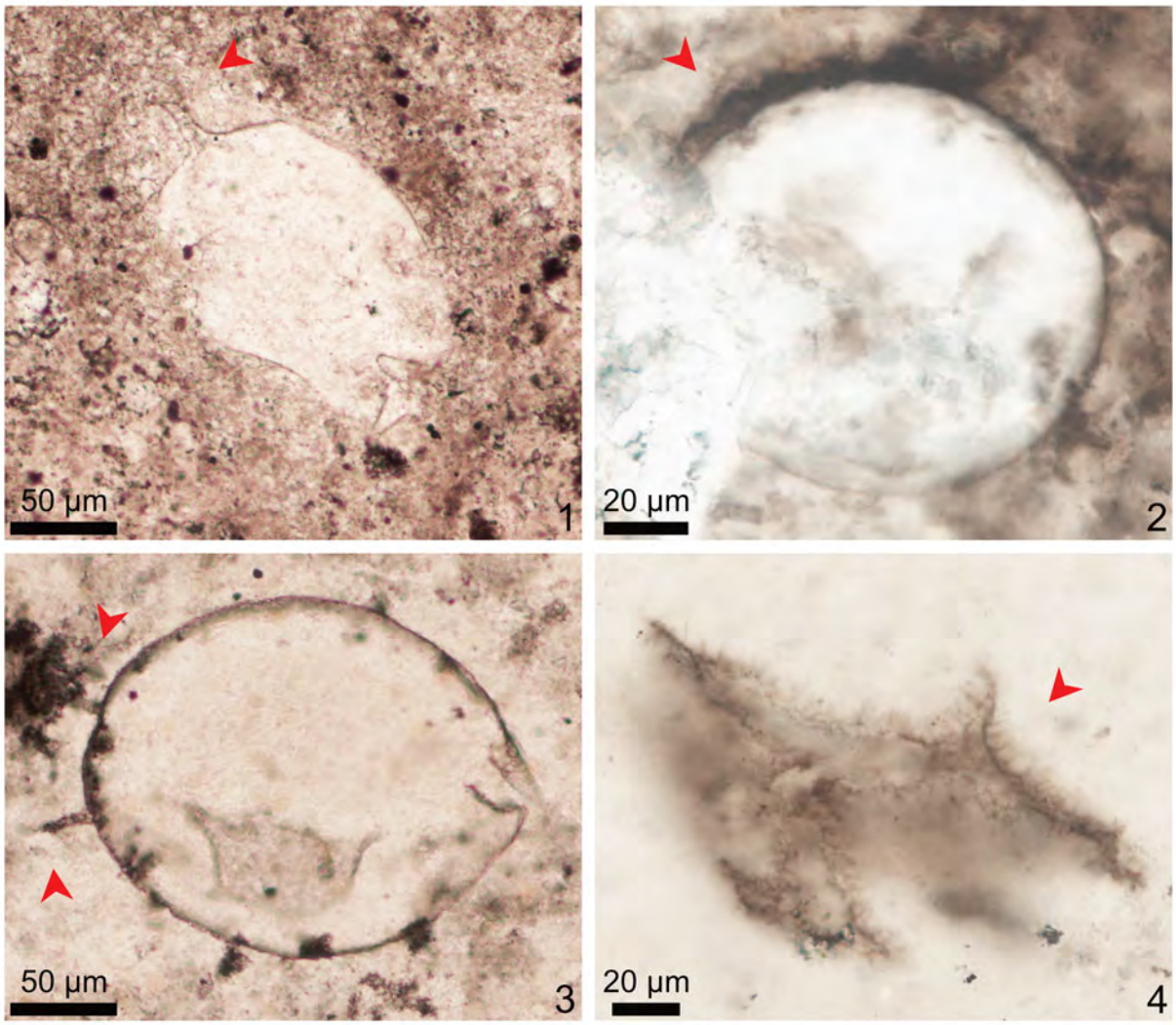

Figure 31. Indeterminate acanthomorphs. (**1**) PB202070, thin section 19SDP-1-5, O23/4. (**2**) PB202071, thin section 19SDP-7-3, J28. (**3**) PB202072, thin section 19CW-5-21, K39. (**4**) PB202073, thin section 21LHK-1-2, P35. Red arrowheads denote processes.

specimens or in microbial mats. Other filamentous microfossils include one specimen of *Obruchevella* Reitlinger, 1948, emend. Yakshin and Luchinina, 1981 (Fig. 36.1), one bundle of thin filaments resembling *Polytrichoides* Hermann, 1974, emend. Hermann in Timofeev et al., 1976 (Fig. 36.5), and one short fragment of a septate filament with an exceptionally large cell width-to-length ratio (on average 257 μm wide and 11 μm long, Fig. 36.6), which to some extent resembles a specimen described as "Large fragment with longitudinal structures" (Arvestål and Willman, 2020, fig. 12S). Other septate filamentous microfossils, such as *Cyanonema* Schopf, 1968, emend. Butterfield et al., 1994, and *Oscillatoriopsis* Schopf, 1968, emend. Butterfield et al., 1994, which are common Ediacaran taxa, are not confirmed in our materials, possibly due to the loss of trichomes or cellular details of the filaments during degradation and/or diagenesis. Coccoidal microfossils are rare compared with filaments, with only two aggregated coccoid specimens discovered from the Lianghekou section (Fig. 36.7, 36.8), and some possible coccoidal microfossils scattered in silicified matrices at other localities. Microbial mats (Fig. 37), which appear to have been built by various species of *Siphonophycus*, are common. Some thin sections are composed entirely of silicified microbial mats. Many observed microbial mats are fragmented, and some mat fragments from the Siduping and Lianghekou sections show evidence of reworking (e.g., rounded outline, Fig. 37.1–37.3; or sharp contact with surrounding matrix, Fig. 37.4).

Problematic microfossils (Fig. 38).—There are some problematic microfossils not readily assigned to any of the groups described above. One is a branching filamentous microfossil that appears to branch unidirectionally and dichotomously (Fig. 38.1–38.4). Its filament diameter is around 1.2 μm (0.8–2.1 μm, SD = 0.4 μm). At least two orders of branching can be observed, but segment lengths between the nodes are hard to measure because the specimen is preserved three-dimensionally, and nodes are captured at different focal levels. The relatively uniform and extremely thin filament diameter indicates a uniseriate rather than multiseriate construction, even though no cellular details are preserved in the available specimen.

https://doi.org/10.1017/jpa.2023.92 Published online by Cambridge University Press

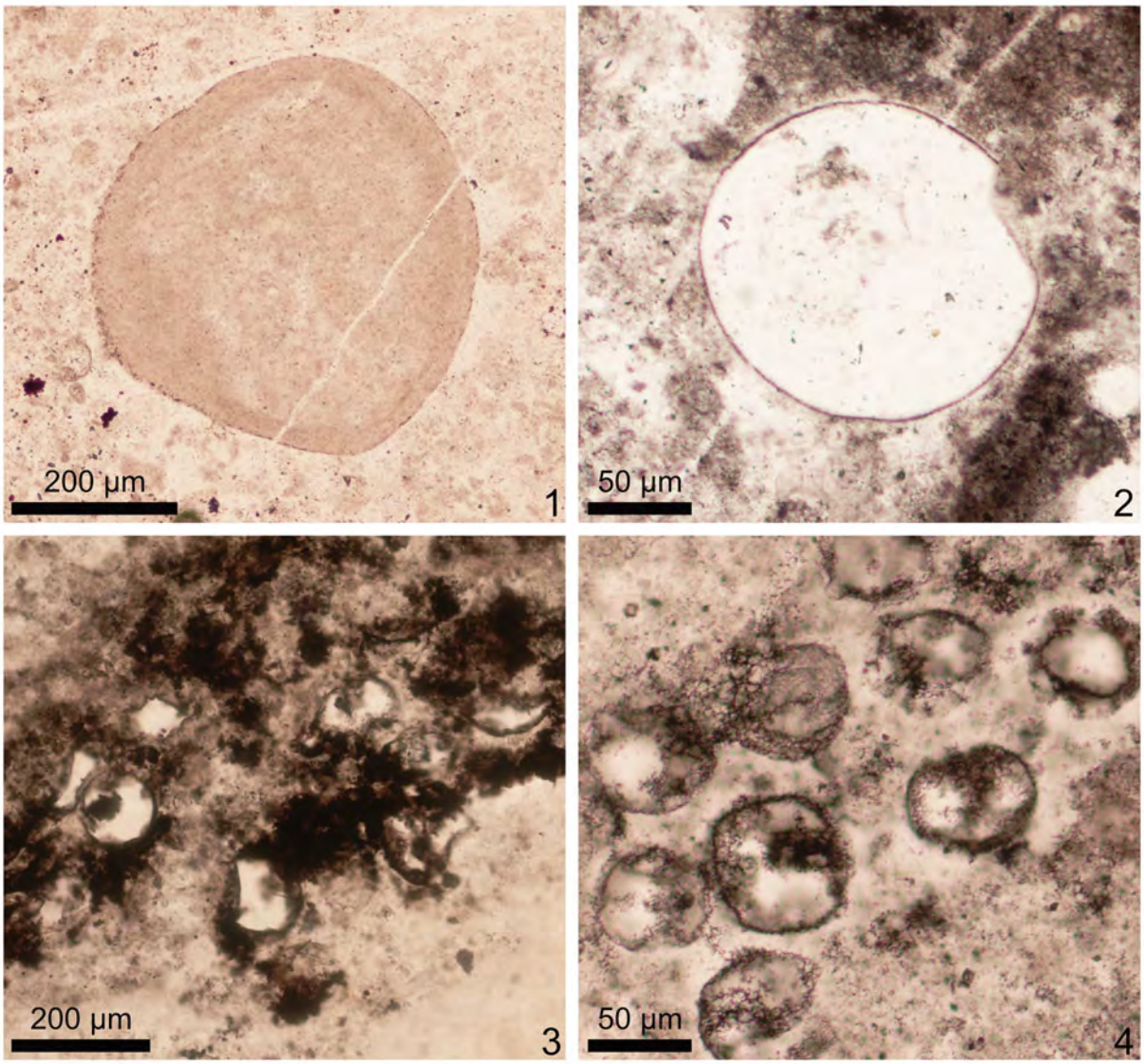

Figure 32. Sphaeromorphic acritarchs. (**1**) PB202074, thin section 21LHK-1-6, E42. (**2**) PB202075, thin section 19HP-1-20, O33/3. (**3**) PB202076, thin section 19CW-5-30, Q36/3. (**4**) PB202077, thin section 19TP-1-26, B40.

Two specimens of *Polybessurus* sp. (Fig. 38.5, 38.6) were recovered from the Majindong section in basinal facies (the large one, Fig. 38.5) and the Tianping section in slope facies (the small one, Fig. 38.6). The larger specimen captured in thin section is about 0.7 mm wide and about 1.9 mm long, and the smaller one is about 30 µm wide and about 120 µm long. The smaller specimen from the Tianping section is similar to *Polybessurus bipartitus* Fairchild, 1975, ex Green et al., 1987, but here we follow Ouyang et al. (2022) and place all *Polybessurus* specimens from the Doushantuo Formation in an open nomenclature. As discussed by Ouyang et al. (2022), *Polybessurus* likely represent a biogenic structure formed by various microorganisms that share a similar movement or migration mechanism, and thus is here considered as a problematic microfossil.

Occurrence of Doushantuo acanthomorphs based on taxonomically revised records.—Together with fossil data presented in this study, the taxonomically revised dataset contains 49 genera and 160 species reported from the Doushantuo Formation (Table 3). Taxonomic diversity is greatest in the shelf-lagoon environment: about 89% of the genera and 84% of the species (44 genera and 135 species) have been reported from shelf-lagoon settings. Only about 10% of the genera and 3% of the species (5 genera and 5 species) are documented in the basinal environment (Fig. 39). Because the presence of *Appendisphaera grandis* in the basinal facies is solely based on its occurrence at the Jinshichong section, the taxonomic richness of acanthomorphs in basinal facies would be even lower if the Jinshichong section were actually classified as the platform environment (see "Geological setting" for the uncertainty about the depositional environment of the Jinshichong section). Regardless, all taxa from slope and basinal facies (except new species) also occur in inner shelf, shelf-lagoon, or shelf margin facies. Among the five species that are present in the basinal facies, *A. grandis* and *Tianzhushania spinosa* are among the most widely distributed and the longest-ranging taxa across all facies in South China. *Tanarium pilosiusculum*,

https://doi.org/10.1017/jpa.2023.92 Published online by Cambridge University Press

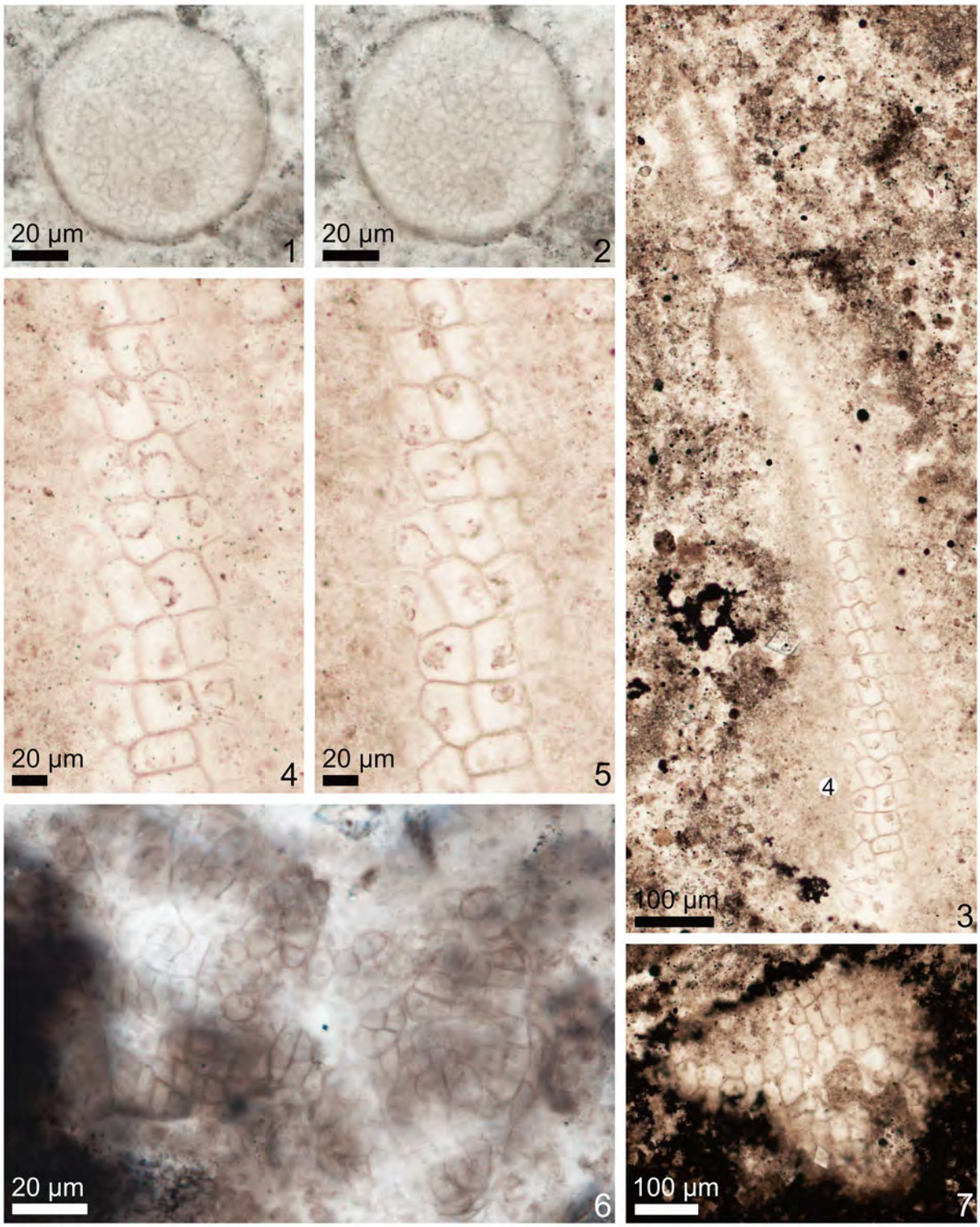

Figure 33. Multicellular algae. (**1**, **2**) *Wengania minuta* Xiao, 2004b, PB202078, thin section 19SDP-1-19, N41/4, showing the same area at different focal levels. (**3–5**, **7**) Unnamed thalli with large cells; (**3–5**) PB202079, thin section 19SDP-1-19, M35; (**7**) PB202081, thin section 19SDP-1-25, K42/3. (**6**) Unnamed multicellular thallus, PB202080, thin section 19CW-6-15, M41.

Asterocapsoides wenganensis, and *Mengeosphaera mamma* also occur in other facies.

Sampling bias and rarefaction analysis.—As shown in Table 2, there are notable variations in the number of fossiliferous samples and the number of acanthomorph specimens recovered from Doushantuo sections. A rarefaction analysis was carried out to correct such sampling bias. Raw abundance data of acanthomorphs from the Caojunba, Caowan, Lujiayuanzi, and Siduping sections (this study), together with

https://doi.org/10.1017/jpa.2023.92 Published online by Cambridge University Press

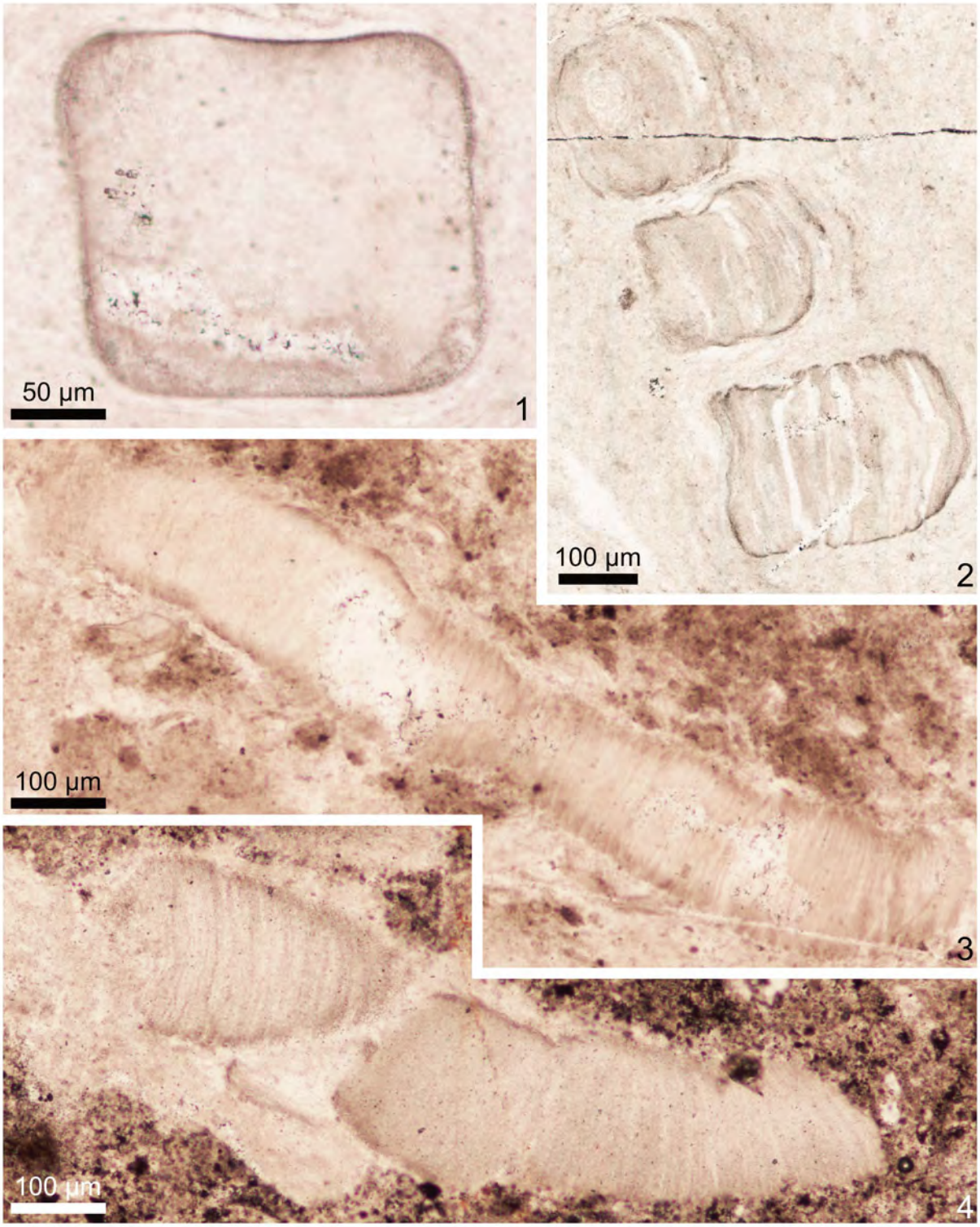

Figure 34. Tubular microfossils. (**1**) *Quadratitubus orbigoniatus* Xue, Tang, and Yu, 1992, emend. Liu et al., 2008, PB202082, thin section 19CW-6-13, M44/3. (**2**) Possible *Quadratitubus orbigoniatus*, PB202083, thin section 21DC-2-36, L40/2. (**3, 4**) *Sinocyclocyclicus guizhouensis* Xue, Tang, and Yu, 1992, emend. Liu et al., 2008; (**3**) PB202084, thin section 19SDP-7-3, J37/2; (**4**) PB202085, thin section 21MJD-1-10, K36/3.

previously published abundance data from six localities in inner shelf (the Bailu section, Ouyang et al., 2019; the Lianhua section, Ye et al., 2022) and shelf-lagoon facies (the Liujing section, Shang et al., 2019; the Jiulongwan, Jinguadun, and Wuzhishan sections, Ouyang et al., 2021) were selected for the rarefaction analysis. The rarefaction curves are shown in Figure 40. With the exception of the Lianhua section in the Shennongjia area representing the inner shelf facies, none of

https://doi.org/10.1017/jpa.2023.92 Published online by Cambridge University Press

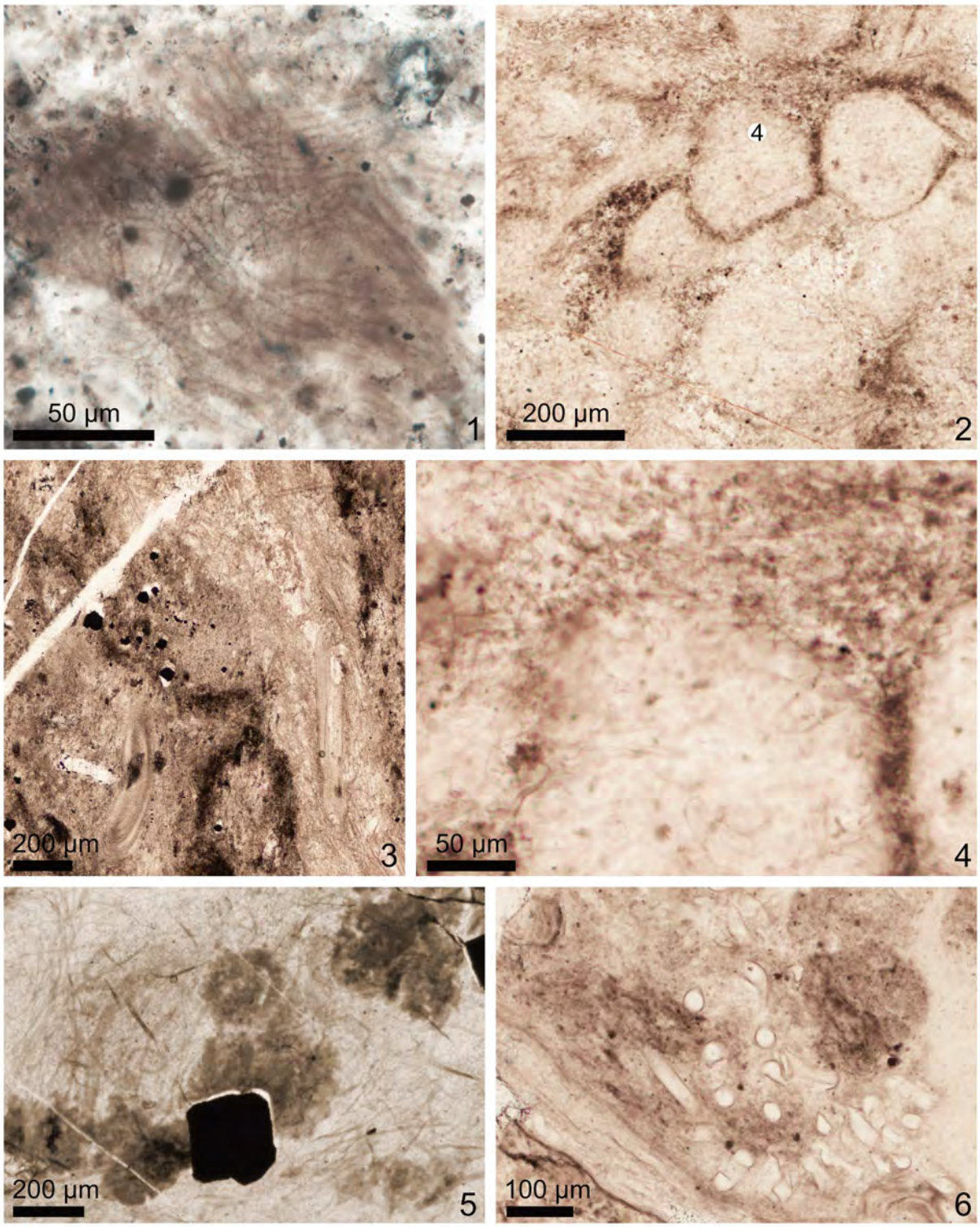

Figure 35. Microbial mats consist of filamentous microfossils. (**1**) A small fragment of *Siphonophycus* mat, PB202086, thin section 21MJD-1-3, K32/2. (**2**, **4**) Mat with thin filaments interwoven into spherical structures, PB202087, thin section 19CW-6-9, L38; circled 4 in (**2**) marks the area magnified in (**4**). (**3**) Microbial mat consists of various filamentous microfossils including *Siphonophycus* Schopf, 1968, emend. Knoll et al., 1991, and *Salome* Knoll, 1982, PB202088, thin section 18JSC-2-3, H34/4. (**5**, **6**) Microbial mat consisting of filamentous microfossils of various sizes; (**5**) PB202089, thin section 19CW-6-6; (**6**) PB202090, thin section 19SDP-7-19, Q36.

the rarefaction curves reaches a clear asymptote, indicating that current sampling intensity is inadequate and greater taxonomic richness would be expected with additional sampling in the future.

NMDS analysis.—To visualize the similarity and difference in taxonomic composition of different acanthomorph collections from different facies, stratigraphic intervals, and localities, an NMDS analysis was conducted on the acanthomorph

https://doi.org/10.1017/jpa.2023.92 Published online by Cambridge University Press

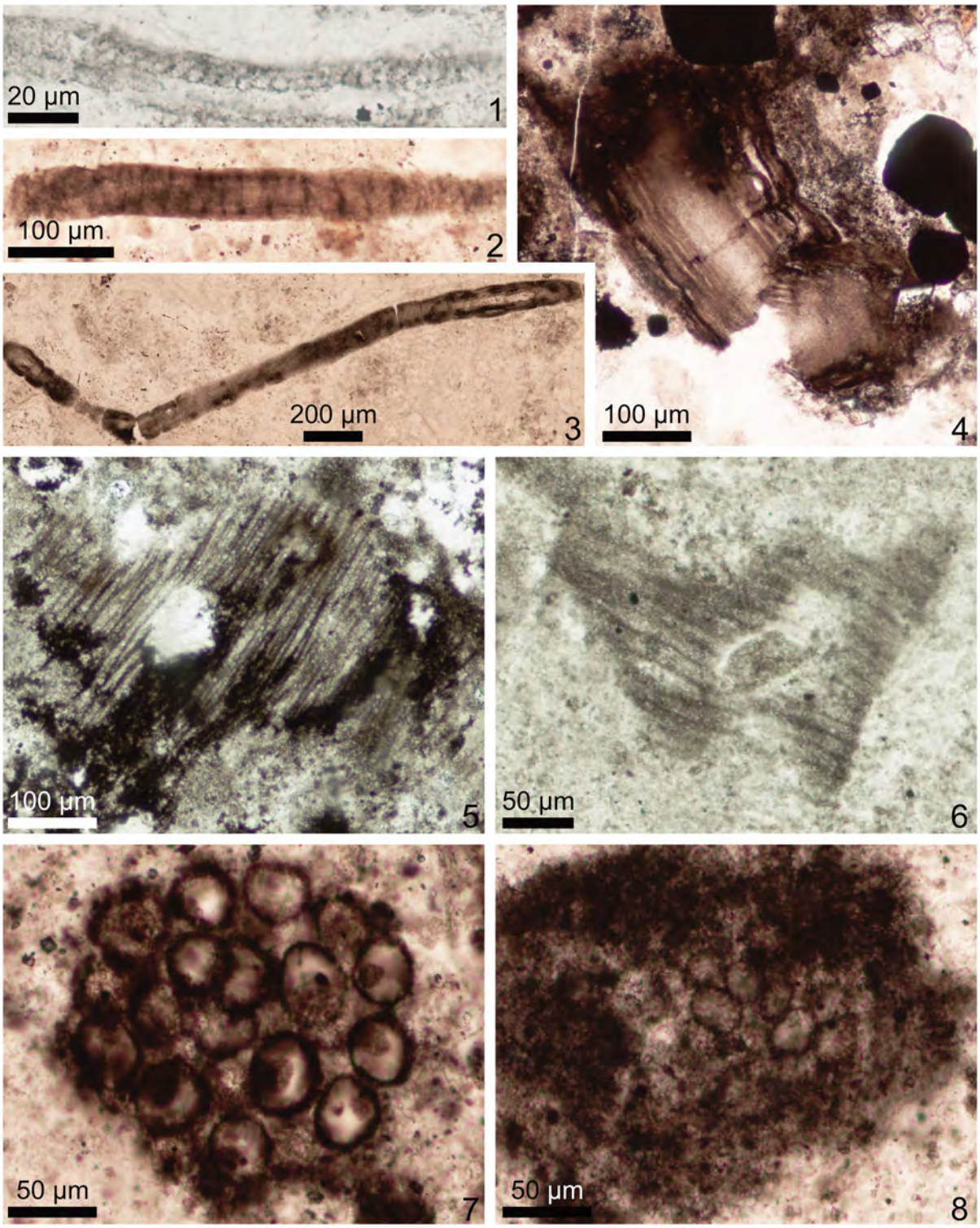

Figure 36. Filamentous and coccoidal microfossils. (**1**) *Obruchevella minor* Zhang, 1984a, PB202091, thin section 18JSC-2-4, T22/2. (**2**) *Salome svalbardense* Knoll, 1982, PB202092, thin section 21LHK-1-6, J38. (**3**, **4**) *Salome hubeiensis* Zhang, 1986: (**3**) PB202093, thin section 19TP-1-40, J33/3, (**4**) PB202094, thin section 19CW-6-14, J36/2. (**5**) Bundled filaments resembling *Polytrichoides* Hermann, 1974, emend. Hermann in Timofeev et al., 1976, PB202095, thin section 19HP-2-6, M40. (**6**) Septate trichome with cells much wider than length resembling *Oscillatoriopsis* Schopf, 1968, emend. Butterfield et al., 1994, PB202096, thin section 19HP-2-3, Q38/3. (**7**, **8**) Aggregated coccoids resembling *Myxococcoides* Schopf, 1968: (**7**) PB202097, thin section 21LHK-1-10, Q43/2; (**8**) PB202098, thin section 21LHK-1-10, N48/3.

occurrence data from 82 collections (see Methods for how a collection is defined and see Supplemental Materials for data). The NMDS results are shown in Figure 41 (grouped by depositional facies in Fig. 41.1 and by both depositional facies and stratigraphic intervals in Fig. 41.2). The stress value of the NMDS analysis is 0.13, indicating acceptable

https://doi.org/10.1017/jpa.2023.92 Published online by Cambridge University Press

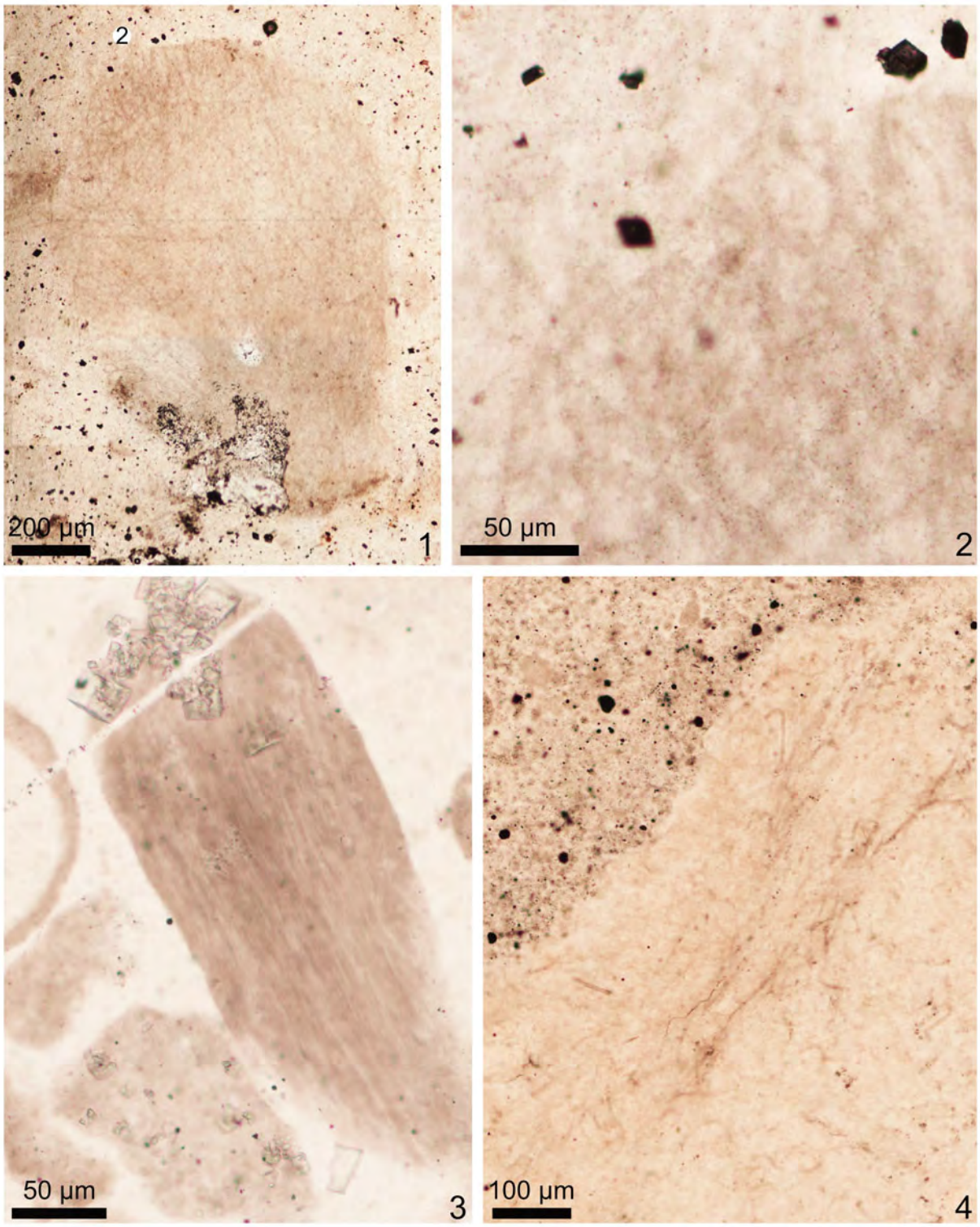

Figure 37. Microbial mat preserved as reworked clasts. (**1**, **2**) PB202099, thin section 21LHK-1-15, N42/2; circled 2 in (**1**) mark the area magnified in (**2**); (**3**) PB202100, thin section 19SDP-7-22, F38/2; (**4**) PB202101, thin section 21LHK-1-3, O44.

representation of ranked distances by the NMDS results (Clarke, 1993).

The NMDS plots visualize the taxonomic similarity among different facies or different stratigraphic intervals. In Figure 41.1, for example, the convex hulls for the slope and basinal facies are completely nested within those of the shelf margin and shelf-lagoon facies, consistent with the observation that acanthomorph taxa from the former are also found in the latter. Among the inner shelf, shelf-lagoon, and shelf margin facies, the convex hulls show a notable degree of overlap, indicating a number of shared taxa. On the other hand, as shown in Figure 41.2, the convex hulls for Member II and Member III

https://doi.org/10.1017/jpa.2023.92 Published online by Cambridge University Press

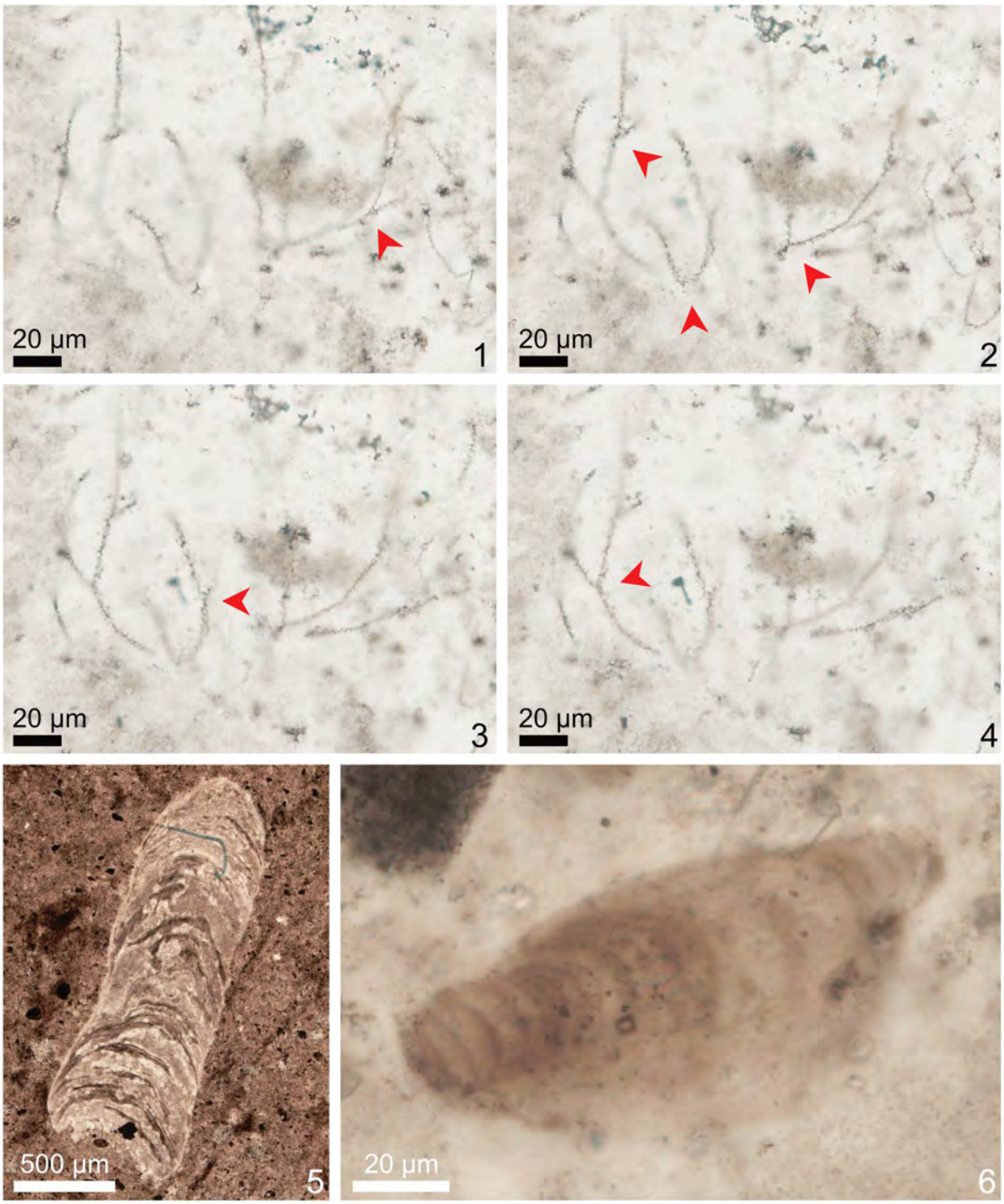

Figure 38. Problematic microfossils. (**1–4**) Microfossil with branching filaments, PB202102, thin section 19SDP-3-14, H34/3, same area at different focal levels to show different branches and bifurcations; red arrowheads denote bifurcations. (**5**, **6**) *Polybessurus* sp. (**5**) PB202103, thin section 21MJD-1-13, P37/2; (**6**) PB202104, thin section 19TP-1-25, M39/4.

in the shelf-lagoon facies are completely separated, indicating that these two stratigraphic intervals contain taxonomically distinct acanthomorphs.

Network analysis.—To further visualize the shared taxonomic occurrences among different acanthomorph collections, we carried out a network analysis of the same dataset used in the NMDS analysis (see Supplemental Materials for data). The bipartite network (Fig. 42) shows that collections from the inner shelf facies (yellow and light blue symbols) and shelf margin facies (orange symbols) are linked to taxa such as *Megasphaera inornata* and *M. ornata*, collections from Member II in shelf-lagoon facies (red symbols) are linked to taxa such as *Tianzhushania* and *Yinitianzhushania tuberifera*

https://doi.org/10.1017/jpa.2023.92 Published online by Cambridge University Press

Table 3. Paleoenvironmental distribution of reported acanthomorphic acritarchs from the Doushantuo Formation in South China. Numbers in each cell refer to data sources, as detailed below. Hashtag sign (#) indicates that the reported specimen was mistakenly assigned to *Briareus vasformis* Liu and Moczydłowska, 2019, by Ouyang et al. (2021), and should be *B. robustus* Liu and Moczydłowska, 2019. Data sources shown in the table: (1) This study. (2) Yin and Li, 1978. (3) Awramik et al., 1985. (4) Chen and Liu, 1986. (5) Yin, 1987. (6) Yin and Liu, 1988. (7) Yin, 1990. (8) Yin et al., 1990. (9) Yin and Xue, 1993. (10) Yuan et al., 1993. (11) Xue et al., 1995. (12) Yin, 1996. (13) Yuan and Hofmann, 1998. (14) Zhang et al., 1998. (15) Xiao and Knoll, 1999. (16) Yin, 1999. (17) Xiao and Knoll, 2000. (18) Yin, 2001. (19) Yin et al., 2001. (20) Zhou et al., 2001. (21) Zhou et al., 2002. (22) Yin et al., 2003. (23) Xiao, 2004b. (24) Yin et al., 2004. (25) Zhou et al., 2004b. (26) Liu and Yin, 2005. (27) Xiao et al., 2007. (28) Yin et al., 2007. (29) Zhou et al., 2007. (30) Xie et al., 2008. (31) Liu et al., 2009. (32) McFadden et al., 2009. (33) Yin et al., 2009a. (34) Yin et al., 2009b. (35) Chen et al., 2010. (36) C. Yin et al., 2011. (37) L. Yin et al., 2011. (38) Liu et al., 2012. (39) Wang et al., 2012. (40) Liu et al., 2013. (41) Zeng et al., 2013. (42) Liu et al., 2014a. (43) Liu et al., 2014b. (44) Xiao et al., 2014. (45) Ouyang et al., 2015. (46) Ye et al., 2015. (47) Hawkins et al., 2017. (48) Nie et al., 2017. (49) Liu and Moczydłowska, 2019. (50) Ouyang et al., 2019. (51) Shang et al., 2019. (52) Shang and Liu, 2020. (53) Yang et al., 2020. (54) Liu et al., 2021. (55) Ouyang et al., 2021. (56) Ye et al., 2022.

Facies	Inner shelf					Shelf lagoon			Shelf margin		Slope		Basin
Locality	Chadian section	Zhangcunping area	Baokang area	Shennongjia area	Chaoyang section	Yangtze Gorges area	Changyang area	Liujing section	Caojunba section	Weng'an area	Lujiayuanzi section	Zhangjiajie area	Majindong, Lianghekou, Jinshichong sections
Acanthomorph richness	23 genera, 66 species					44 genera, 135 species			24 genera, 54 species		13 genera, 30 species		5 genera, 5 species
Alicesphaeridium medusoidum Zang in Zang and Walter						49, 55							
Ancorosphaeridium magnum Sergeev, Knoll, and Vorob'eva, 2011						49							
Annularidens inconditus Ouyang et al., 2021				56		55							
Apodastoides basileus Zhang et al., 1998						14							
Appendisphaera anguina		50		56		42							
Appendisphaera clava		50		56		40, 42, 55							
Appendisphaera clustera						49		51					
Appendisphaera fragilis				56				51		37			
Appendisphaera grandis		35, 50		56		49, 55		51	1	44	1	1, 47, 52	1
Appendisphaera heliaca						45, 49, 55							
Appendisphaera lemniscata						49							
Appendisphaera longispina				56		40, 42, 49, 55		51					
Appendisphaera longitubularis						42, 49							
Appendisphaera magnifica						29, 36, 40, 42, 45, 55				14		1, 47	
Appendisphaera setosa				56		40, 42, 49, 55		51					
Appendisphaera tabifica		50		56		42, 49							
Appendisphaera tenuis		46		56		42, 49, 55		51		44		1, 52	
Appendisphaera? *brevispina*						42							
Appendisphaera? *hemisphaerica*						40, 42		51				47	
Asseserium diversum						49							
Asseserium fusulentum Nagovitsin and Moczydłowska in Moczydłowska and Nagovitsin, 2012						49							
Asterocapsoides fluctuensis						49							
Asterocapsoides robustus										44			
Asterocapsoides sinensis		31			21	14, 42	2			44		47	
Asterocapsoides wenganensis		50	25					51		4, 20, 44			1
Bacatisphaera baokangensis Zhou et al., 2001, emend. Xiao et al., 2014			20, 25			42, 55		51		26, 44			
Bacatisphaera sparga Liu and Moczydłowska, 2019						49							

Table 3. Continued.

Facies	Inner shelf					Shelf lagoon			Shelf margin		Slope		Basin
Locality	Chadian section	Zhangcunping area	Baokang area	Shennongjia area	Chaoyang section	Yangtze Gorges area	Changyang area	Liujing section	Caojunba section	Weng'an area	Lujiayuanzi section	Zhangjiajie area	Majindong, Lianghekou, Jinshichong sections
Bispinosphaera peregrina						42							
Bispinosphaera vacua Ouyang et al., 2021						55							
Bullatosphaera? *colliformis* n. sp.												1	
Briareus borealis Knoll, 1992						43, 49, 55	16, 18			37			
Briareus robustus Liu and Moczydłowska, 2019						49, 55#							
Briareus vasformis						49							
Calyxia xandaros Willman in Willman and Moczydłowska, 2008						49							
Cavaspina acuminata				56		14, 41, 42, 49, 55		51	1	8, 44		48, 52	
Cavaspina basiconica				56		14, 32, 42, 49		20, 51	1	44	1	48	
Cavaspina conica						49		51					
Cavaspina uria		50							1				
Caveasphaera costata										15, 17, 44			
Ceratosphaeridium glaberosum						36, 38, 40, 42							
Crassimembrana crispans Ouyang et al., 2021						55							
Crassimembrana multitunica						49, 55						47	
Crinita paucispinosa Liu et al., 2014a						42							
Cymatiosphaeroides forabilatus Liu and Moczydłowska, 2019, emend. Shang et al., 2019				56		49		51					
Cymatiosphaeroides kullingii Knoll, 1984, emend. Shang et al., 2019		46				49, 55		51					
Cymatiosphaeroides yinii Yuan and Hofmann, 1998						42, 55				13			
Dicrospinasphaera improcera Liu and Moczydłowska, 2019		50				30, 49, 55							
Dicrospinasphaera virgata Grey, 2005										44			
Dicrospinasphaera zhangii Yuan and Hofmann, 1998, emend. Liu and Moczydłowska, 2019						23, 45, 49, 55		51		13, 37, 44			
Distosphaera jinguadunensis Ouyang et al., 2021						55							
Distosphaera speciosa Zhang et al., 1998, emend. Liu and Moczydłowska, 2019		50				37, 43, 49, 55	54			10, 14			
Distosphaera? *corniculate* Liu and Moczydłowska, 2019						49				13, 44			
Duospinosphaera biformis Ye et al., 2022				56									

Table 3. Continued.

Facies	Inner shelf					Shelf lagoon			Shelf margin		Slope		Basin
Locality	Chadian section	Zhangcunping area	Baokang area	Shennongjia area	Chaoyang section	Yangtze Gorges area	Changyang area	Liujing section	Caojunba section	Weng'an area	Lujiayuanzi section	Zhangjiajie area	Majindong, Lianghekou, Jinshichong sections
Duospinosphaera shennongjiaensis Ye et al., 2022				56									
Eotylotopalla apophysa				56									
Eotylotopalla dactylos				56		14, 29, 37, 42, 43, 45, 49, 55	54		1	44	1	1	
Eotylotopalla delicata						5, 14, 33, 36, 40, 42, 49, 55	6, 7, 16			37			
Eotylotopalla inflata n. sp.												1	
Eotylotopalla quadrata						49		51					
Eotylotopalla strobilata						43, 49, 55							
Ericiasphaera crispa Xiao et al., 2014										44			
Ericiasphaera densispina Liu et al., 2014a						14, 42							
Ericiasphaera fibrilla Liu and Moczydłowska, 2019				56		49, 55		51					
Ericiasphaera magna (Zhang, 1984b) Zhang et al., 1998		46		56		28, 36, 42, 49	54			13, 14, 44		47	
Ericiasphaera rigida Zhang et al., 1998		32		56		49				10, 14, 44			
Ericiasphaera sparsa Zhang et al., 1998						14							
Ericiasphaera spjeldnaesii Vidal, 1990		31, 35				30							
Estrella greyae Liu and Moczydłowska, 2019						40, 49							
Estrella recta Liu and Moczydłowska, 2019						49							
Gyalosphaeridium pulchrum						49		51					
Helicoforamina wenganica Wang et al., 2012										17, 27, 39, 44			
Hocosphaeridium anozos						36, 38, 40, 42, 43, 49			1	44		47	
Hocosphaeridium dilatatum		50		56		42							
Hocosphaeridium scaberfacium				56		14, 38, 40, 42, 43	54		1	13, 14		1	
Knollisphaeridium bifurcatum						49		51		44			
Knollisphaeridium conifurmum				56		49, 55				44			
Knollisphaeridium denticulatum				56		42, 55		51					
Knollisphaeridium longilatum						42, 55							
Knollisphaeridium maximum		31, 35, 50	25	56		5, 14, 33, 36, 40, 41, 42, 43, 49, 55			1		1		
Knollisphaeridium obtusum						42							
Knollisphaeridium parvum						42		51					
Knollisphaeridium triangulum		50				40, 43				13, 14, 15, 44			

Table 3. Continued.

Facies	Inner shelf					Shelf lagoon			Shelf margin		Slope		Basin
Locality	Chadian section	Zhangcunping area	Baokang area	Shennongjia area	Chaoyang section	Yangtze Gorges area	Changyang area	Liujing section	Caojunba section	Weng'an area	Lujiayuanzi section	Zhangjiajie area	Majindong, Lianghekou, Jinshichong sections
Laminasphaera capillata Liu and Moczydłowska, 2019						49							
Matosphaera changyangensis Yin, 1999						36	16						
Megasphaera cymbala										44			
Megasphaera inornata		46, 50	25, 34, 53	56	21	30, 55		51		4, 11, 17		1, 48, 52	
Megasphaera ornata						30, 55				9, 17, 22, 24, 27, 36, 44		1	
Megasphaera patella										44			
Megasphaera puncticulosa										44			
Membranosphaera formosa Liu and Moczydłowska, 2019						49, 55							
Mengeosphaera angusta				56		42							
Mengeosphaera bellula						42						1	
Mengeosphaera chadianensis	4, 14		53	56	21	23, 30, 36, 45, 49, 55	6	51		9, 10, 13, 14, 20, 44			
Mengeosphaera constricta				56		40, 42					1		
Mengeosphaera eccentrica										13, 44			
Mengeosphaera flammelata						49							
Mengeosphaera gracilis				56		42, 49, 55		51				1, 52	
Mengeosphaera grandispina						42, 55							
Mengeosphaera latibasis						42, 49, 55					1	48	
Mengeosphaera lunula						49, 55	54						
Mengeosphaera mamma				56		12, 55			1				1
Mengeosphaera matryoshkaformis						55				44			
Mengeosphaera membranifera								51					
Mengeosphaera minima				56		42, 55			1	37		47	
Mengeosphaera reticulata										15, 20, 44			
Mengeosphaera spinula		50				42							
Mengeosphaera stegosauriformis				56		42							
Mengeosphaera uniformis						42							
Multifronsphaeridium pelorium Zang in Zang and Walter, 1992, emend. Grey, 2005						49							
Multifronsphaeridium ramosum Nagovitsin and Moczydłowska in Moczydłowska and Nagovitsin, 2012						49							
Papillomembrana boletiformis										44			
Papillomembrana compta			34			14, 18, 36, 55				18			
Polygonium cratum Zang in Zang and Walter, 1992, emend. Grey, 2005						14							
Schizofusa zangwenlongii						40, 43		51					
Sinosphaera asteriformis Liu et al., 2014a				56		42, 55							
Sinosphaera exilis Ye et al., 2022				56									

Table 3. Continued.

Facies	Inner shelf					Shelf lagoon			Shelf margin		Slope		Basin
Locality	Chadian section	Zhangcunping area	Baokang area	Shennongjia area	Chaoyang section	Yangtze Gorges area	Changyang area	Liujing section	Caojunba section	Weng'an area	Lujiayuanzi section	Zhangjiajie area	Majindong, Lianghekou, Jinshichong sections
Sinosphaera rupina Zhang et al., 1998, emend. Liu et al., 2014a				56		14, 40, 42							
Sinosphaera speciosa (Zhou et al., 2001) Xiao et al., 2014						49, 55				20			
Sinosphaera variabilis Xiao et al., 2014										44			
Spiralicellula bulbifera Xue et al., 1995, emend. Xiao et al., 2014										11, 17, 44			
Taedigerasphaera lappacea Grey, 2005						45				37			
Tanarium acus						42							
Tanarium capitatum						49, 55							
Tanarium columnatum				56									
Tanarium conoideum				56		42		51	1	44			
Tanarium cuspidatum				56		42, 49		51					
Tanarium digitiforme			53			55				44			
Tanarium elegans						42							
Tanarium gracilentum		50		56		3, 6, 7, 14, 37, 55	6, 54						
Tanarium irregulare						37				37			
Tanarium minimum						42, 49							
Tanarium muntense				56		49		51					
Tanarium obesum						40, 42, 55							
Tanarium paucispinosum				56		49	54					1	
Tanarium pilosiusculum			53			40, 42, 49, 55		51	1			1	1
Tanarium pluriprotensum		50		56		55		51					
Tanarium pycnacanthum						40, 42							
Tanarium triangulare						42, 49, 55					1		
Tanarium tuberosum						49, 55		51	1			52	
Tanarium uniformum						49		51					
Tanarium varium				56		42, 55						48	
Tanarium victor										44			
Tianzhushania polysiphonia		35, 50				3, 6, 7, 14, 18, 19, 24, 28, 32, 33, 40, 55				44			
Tianzhushania rara		50				55				14, 44			
Tianzhushania spinosa		31, 35, 50	53			6, 12, 14, 19, 28, 29, 33, 36, 40, 41, 43, 45, 55	2, 6, 7, 16, 19, 47, 54			18, 19, 22, 24			1
Urasphaera capitalis				56									
Urasphaera fungiformis				56		40, 42					1	48	
Urasphaera nupta						42						47	
Variomargosphaeridium floridum				56		40, 42							
Variomargosphaeridium gracile						55				44			

Table 3. Continued.

Facies	Inner shelf					Shelf lagoon			Shelf margin		Slope		Basin
Locality	Chadian section	Zhangcunping area	Baokang area	Shennongjia area	Chaoyang section	Yangtze Gorges area	Changyang area	Liujing section	Caojunba section	Weng'an area	Lujiayuanzi section	Zhangjiajie area	Majindong, Lianghekou, Jinshichong sections
Variomargosphaeridium litoschum Zang in Zang and Walter, 1992						43, 45, 49, 55				26, 44			
Variomargosphaeridium varietatum Liu and Moczydłowska, 2019						43, 49, 55							
Verrucosphaera minima						49			1				
Verrucosphaera? undulata n. sp.													
Weissiella brevis		46, 50		56		45, 49, 55	54	51		44			
Weissiella cf. *W. grandistella*				56		40, 42, 43, 49, 55			1				
Weissiella concentrica				56									
Xenosphaera liantuoensis						5, 37, 40, 42							
Yinitianzhushania tuberifera		31, 33, 35, 50				33, 36, 40, 43, 55	54			19, 22, 24, 44			
Yushengia ramispina						42		51					

(Yin, Gao, and Xing, 2001) Xiao et al., 2014, and collections from Member III in shelf-lagoon facies (green symbols) are linked to numerous taxa, including various species of *Hocosphaeridium* and *Tanarium*.

The position of a species in the network generally reflects its occurrence frequency recorded in the Doushantuo Formation. The closer to the center of the network, the more likely a species occurs in a greater number of areas, stratigraphic intervals, or studies. For example, *Appendisphaera grandis* is located near the center of the network, consistent with its wide paleogeographic distribution and long stratigraphic ranges. Similarly, many species of *Cavaspina*, *Eotylotopalla*, *Hocosphaeridium*, and *Tanarium* are also placed near the center of the network, indicating their wide paleogeographic and stratigraphic occurrences. Species in the periphery of the network are those with limited occurrences, and these include numerous taxa (e.g., *Ceratosphaeridium glaberosum* Grey, 2005; *Schizofusa zangwenlongii* Grey, 2005; *Xenosphaera liantuoensis* Yin, 1987, emend. Liu et al., 2014a) that were only found in the shelf-lagoon facies in the Yangtze Gorges area by Liu and Moczydłowska (2019).

Discussion

Taxonomic richness of the Doushantuo microfossils.—At the level of major morphological groups, Doushantuo microfossils from different facies do not show substantial differences. Acanthomorphs, sphaeromorphs, and filamentous microfossils occur in all facies from the shallow-water inner shelf to the deep-water basin. Tubular microfossils and *Polybessurus* that are relatively rare in shallow-water facies also occur at the basinal Majindong section, despite the limited sampling intensity at this section. However, multicellular algae and coccoid microfossils, which are present in shallow-water and slope facies, are absent in basinal facies. This difference could be related to the low sampling intensity in basinal facies or ecological restriction (i.e., these microfossils may represent benthic photosynthetic organisms and thus may have been ecologically restricted to the photic zone). Overall, with the exception of multicellular algae and coccoid microfossils, the major morphological groups of Doushantuo microfossils have a wide distribution across different facies, either because many of them were planktonic organisms (e.g., acanthomorphic acritarchs, Butterfield and Rainbird, 1998; Moczydłowska, 2016) or because reworking and transportation may have homogenized their paleoenvironmental distribution (e.g., benthic microfossils ecologically restricted to shallow-water facies may have been reworked and transported to slope and basinal facies as microbial mat fragments or olistostromes).

At face value, genus- and species-level taxonomic richness of acanthomorphic acritarchs varies notably among facies (Fig. 39). Taxonomic richness in shelf-lagoon facies is nearly 9× and 27× that in basinal facies at the genus and species levels, respectively; these numbers would be greater if *Appendisphaera grandis* from the Jinshichong section were excluded from basinal facies (see "Geological Setting" for uncertainty about depositional environment of the Jinshichong section). This difference in taxonomic richness of acanthomorphs is at least partly related to the unequal sampling intensities among localities and

https://doi.org/10.1017/jpa.2023.92 Published online by Cambridge University Press

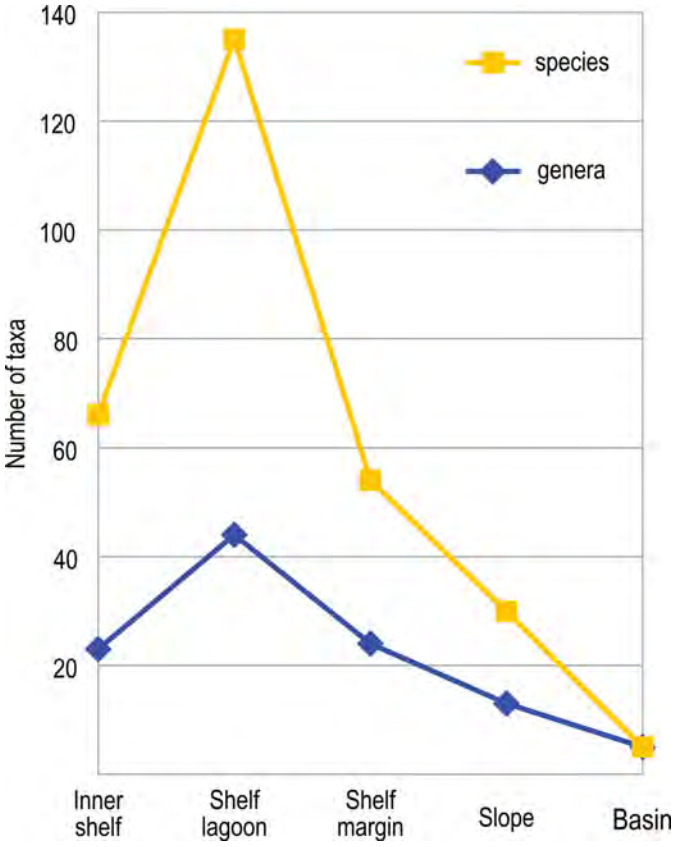

Figure 39. Comparison of acanthomorph diversity among different depositional facies at species and genus levels.

facies, since the shelf-lagoon facies, especially in the Yangtze Gorges area, is much more intensively sampled in previous studies than other facies.

The rarefaction analysis supports sampling intensity as a major driver of the observed difference in taxonomic richness of acanthomorphs. The rarefaction curves show that the sampling intensity at the slope–basinal sections surveyed in this study is far from sufficient. However, when compared at a similar subsampling intensity (e.g., number of specimens < 20), species richness at the Caojunba, Caowan, and Lujiayuanzi sections is comparable to the rarefied species richness in most inner shelf and shelf-lagoon sections (Fig. 40.2). Similarly, total species richness of the Lianghekou section and of the pooled basinal data (hollow square and circle in Fig. 40.2, respectively) is also comparable to that of other sections and other facies at a comparable sampling intensity. Therefore, sampling bias plays an important role driving the variation of acanthomorph taxonomic richness across different facies.

Sampling bias is not the only factor affecting the observed variation in taxonomic richness of Doushantuo acanthomorphs across different facies. Taphonomic bias could be another crucial factor. Doushantuo microfossils are preserved through silicification and phosphatization, which are taphonomic windows controlled by environmental conditions and may not be equally represented in different facies. For example, Muscente et al. (2015) argued that in-situ chert nodule formation is facilitated by local ferruginous conditions and is expected to be rare in euxinic slope to basinal environments. Although this study does reveal the occurrence of chert nodules in the basinal facies, they are rare and restricted in stratigraphic distribution, probably because the early Ediacaran geochemical conditions in these areas were generally unfavorable and only occasionally conducive to chert nodule formation. As a result, silicification in slope and basinal facies favors stratigraphically long-ranging taxa that, relative to short-ranging taxa, would be more likely to be captured by rare chert nodules. In addition, diagenetic and metamorphic processes can also bias microfossil preservation in different facies, because the Doushantuo Formation in slope and basinal facies experienced stronger metamorphism during Paleozoic tectonic activities in the southeastern side of the South China block (Li et al., 2010). As a result, severe recrystallization of micro-quartz and high degree of thermal maturity of organic material may have led to the generally poor preservation of Doushantuo microfossils in the studied areas in Hunan Province. Raman spectroscopic analysis also shows that organic material in silicified microfossils from the Doushantuo Formation at the Tianping section underwent a higher degree of thermal alteration than in the Yangtze Gorges area (Shang et al., 2018, 2020), which may have contributed to the poor preservation and low abundance of microfossils in the Zhangjiajie area.

Additionally, the different fossil preparation and identification approaches in a study of silicified and phosphatized microfossils may also lead to systematic biases. For example, Doushantuo microfossils in shelf-lagoon, slope, and basinal facies are preserved exclusively in chert nodules, and they can be observed only in thin sections. It is difficult in thin sections to recognize taxa characterized by certain vesicle surface sculptures that can be identified on extracted specimens under SEM (e.g., phosphatized *Helicoforamina* Wang et al., 2012; *Spiralicellula* Xue et al., 1992, emend. Xiao et al., 2014; some species of *Megasphaera*), which are abundant in inner shelf and shelf-margin facies where three-dimensionally phosphatized microfossils can be extracted from dolomitic phosphorites by acid maceration (Xiao and Knoll, 1999; Xiao et al., 2014). On the other hand, internal structures, such as the hollow processes embedded within outer membranes of *Tianzhushania* and crosswalls in processes of *Weissiella*, cannot be observed on the macerated specimens preserved in phosphorites. Of course, such biases can be mitigated by combining observations of thin sections and macerated specimens, but this is only practical for phosphatized microfossils.

Taxonomic distribution of the Doushantuo acanthomorphs.—Unlike taxonomic richness, which shows considerable difference among facies, the NMDS results indicate that the different facies have a number of shared taxa. In other words, the taxonomic occurrence of acanthomorphs is not strongly controlled by facies, particularly among inner shelf, shelf-lagoon, and shelf marine facies where sampling intensity is relatively good (Fig. 40). This is an encouraging sign for acanthomorph-based biostratigraphic correlation. The similarity in species composition between the inner shelf and shelf-margin facies is further bolstered by their similar stratigraphic distribution of microfossils—most acanthomorphs in these facies come from strata correlated with upper Member II (Zhou et al., 2017; Ouyang et al., 2019; Ye et al., 2022).

https://doi.org/10.1017/jpa.2023.92 Published online by Cambridge University Press

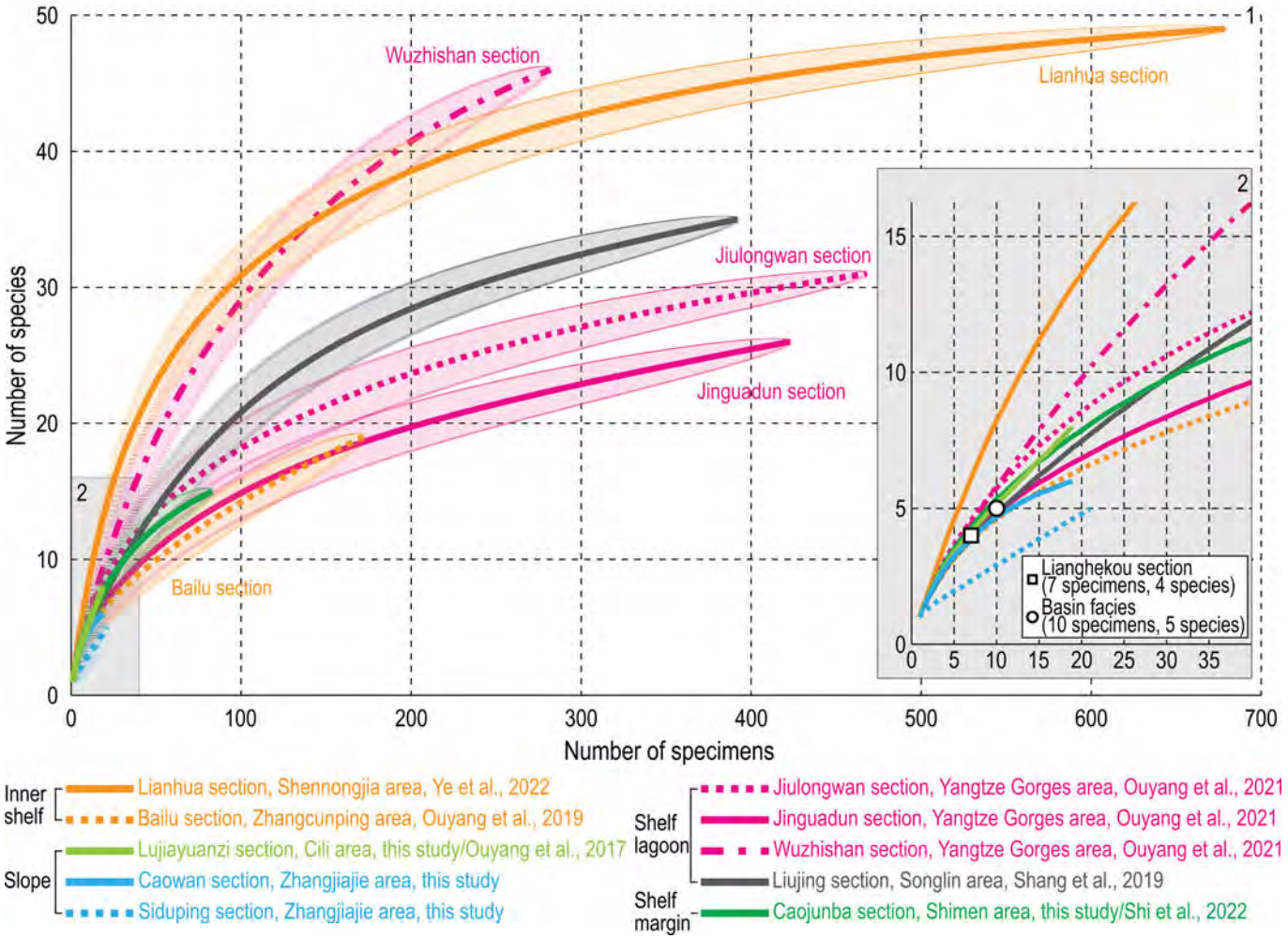

Figure 40. Rarefaction analysis of Doushantuo acanthomorphs. (**1**) Rarefaction curves with 1σ error bars of Doushantuo acanthomorph assemblages published with abundance data from 10 sections in inner shelf, shelf-lagoon, and slope facies. (**2**) Magnification of gray box in bottom-left of (**1**), showing rarefied species richness with subsampled size of 1–40 specimens. Sample sizes of Lianghekou section and basinal facies sections are small, therefore they were not rarefied. Rather, observed specimen number and species richness are plotted for Lianghekou section and pooled basinal facies data.

Taxonomic compositions in different facies may have also been affected by taphonomic biases. This can be best illustrated by the shelf margin facies, which has less than half the number of species in the shelf-lagoon facies (Fig. 39), but occupies a larger convex hull in the taxonomic ordination space (Fig. 41.1). The contrast between taxonomic richness and taxonomic ordination may be driven by the existence of two taphonomic windows (silicification or phosphatization) in the shelf margin facies (Xiao et al., 2014), particularly if microfossil assemblages of different preservation modes may be taxonomically distinct (i.e., everything else being equal, two assemblages with different taphonomic modes would share fewer taxa than two with the same taphonomic mode). A similar explanation may also be applied to the inner shelf facies, which has much lower taxonomic richness than the shelf-lagoon facies (Fig. 39), but occupies a convex hull of a similar size (Fig. 41.1), perhaps due to the low availability of both silicification and phosphatization modes in the inner shelf facies (e.g., Zhou et al., 2001).

When grouped by stratigraphic intervals, the acanthomorph collections show clear separation on the ordination space (Fig. 41.2), indicating greater difference in taxonomic composition of acanthomorphs between stratigraphic horizons than among depositional facies. Importantly, there is complete separation between Member II and Member III in shelf-lagoon facies (Fig. 41.2, red and green symbols, respectively), indicating different species composition between the two intervals in shelf-lagoon facies. In the shelf-lagoon Yangtze Gorges area, taxonomic difference in acanthomorphs between the two lithostratigraphic units has been recognized in numerous previous studies (e.g., taxonomic diversity and evenness, Zhou et al., 2007; quantitative evaluation, McFadden et al., 2009; presence/absence of key taxa, Liu et al., 2013). Member II and Member III of the Doushantuo Formation were deposited in early and middle Ediacaran, respectively (Zhou et al., 2017, 2019; Sui et al., 2018, 2019; Li et al., 2022), and taxonomic difference in acanthomorph composition likely reflects evolutionary changes in eukaryote diversity in early–middle Ediacaran oceans, possibly driven by oceanic oxygenation events, as recorded in various geochemical proxies (e.g., McFadden et al., 2008; Chen et al., 2022).

NMDS results are consistent with published correlations of acritarch assemblages across different facies. Acanthomorph

https://doi.org/10.1017/jpa.2023.92 Published online by Cambridge University Press

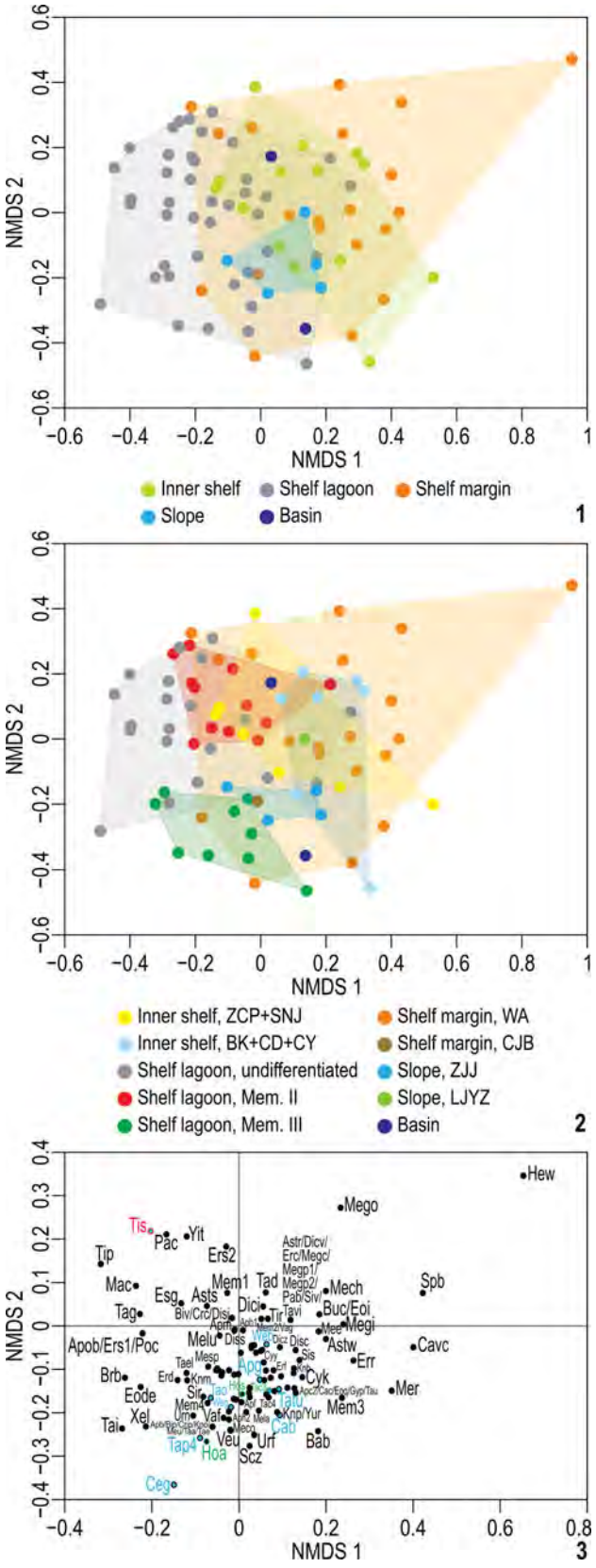

convex hull for the inner shelf Zhangcunping and Shennongjia areas (Fig. 41.2, yellow symbols) largely overlap with the convex hull for shelf-lagoon Member II acanthomorphs, confirming the proposed biostratigraphic correlation of the Zhangcunping and Shennongjia assemblages with upper Member II acanthomorphs in the Yangtze Gorges area (Ouyang et al., 2019; Ye et al., 2022). The Weng'an convex hull (Fig. 41.2, orange symbols) overlaps with those of members II and III in the shelf-lagoon facies, supporting the inference that the Weng'an biota represents a transitional stage between the assemblages in Member II and Member III of the Doushantuo Formation in shelf-lagoon facies (Xiao et al., 2014). The Lujiayuanzi and Caojunba assemblages (Fig. 41.2, lime and olive symbols, respectively) plot near the convex hull of the shelf lagoon Member III assemblage, which also agrees with their possible biostratigraphic correlation (Ouyang et al., 2017; Shi et al., 2022).

Biostratigraphic implications.—Spatial and stratigraphic distribution of acanthomorphs discussed above provides useful insights into the biostratigraphic study of the Doushantuo Formation. Previously proposed biozonation schemes for the Doushantuo Formation are based primarily on fossil data from the shelf-lagoon facies in the Yangtze Gorges area, supplemented with data from the shelf margin facies in the Weng'an area (C. Yin et al., 2011; Liu et al., 2013; Liu and Moczydłowska, 2019). However, if these biozones are to play a greater role in the subdivision and correlation of the Ediacaran System on a global scale (Liu et al., 2014b; Xiao et al., 2016; Liu and Moczydłowska, 2019; Xiao and Narbonne, 2020), we need to affirm that they are independent of depositional facies.

One biozonal scheme was established on taxonomic difference between Member II and Member III in the Yangtze Gorges area (C. Yin et al., 2009a, 2011; Liu et al., 2013, 2014a, b; Xiao et al., 2014). In this scheme, two biozones (or two assemblages) were established based mainly on two genera, *Tianzhushania* and *Hocosphaeridium*. These two genera were once thought to be restricted to Member II and Member III, respectively, with their first appearance near the base of the respective members (Liu et al., 2013, 2014a, b), thus the two biozones were essentially range biozones (Xiao et al., 2014). However, these two genera were later known to co-exist at Weng'an (Xiao et al., 2014), and *Hocosphaeridium* has subsequently been reported from Member II or its equivalents at multiple localities (Hawkins et al., 2017; Liu and Moczydłowska, 2019; Liu et al., 2021), thus the two biozones as originally proposed need revision. Nevertheless, these two genera both present in four of

Figure 41. Taxonomic ordination plots based on NMDS analysis of taxonomically updated occurrence data from 82 collections of Doushantuo acanthomorphs in South China (see Supplemental Materials for data). (**1**) NMDS scatter plots and convex hulls differentiated by depositional facies. (**2**) NMDS scatter plots and convex hulls differentiated by depositional facies and stratigraphic intervals. (**3**) Species loading diagram. Note that some species are not labeled because of the limited space; see Supplemental Materials for loading data. Red and green circled points represent eponymous species of the lower and upper biozones of the Doushantuo Formation (Liu et al., 2013, 2014b; Xiao et al., 2014), respectively. Blue filled points represent eponymous species of the biozones of Liu and Moczydłowska (2019). See Figure 42 for abbreviations.

https://doi.org/10.1017/jpa.2023.92 Published online by Cambridge University Press

Table 4. Occurrence of eponymous species of the two previously proposed biozonation schemes for the Doushantuo Formation in South China. Abbreviations for biozones: A1 = *Tianzhushania spinosa* zone of Liu et al. (2013, 2014a) and Xiao et al. (2014), corresponding to Member II in the Yangtze Gorges area; A2 = *Hocosphaeridium anozos* Zone (or the *Tanarium conoideum–Hocosphaeridium scaberfacium–H. anozos* Zone) of Liu et al. (2013, 2014a) and Xiao et al. (2014), corresponding to Member III in the Yangtze Gorges area; B1 = *Appendisphaera grandis–Weissiella grandistella–Tianzhushania spinosa* Zone of Liu and Moczydłowska (2019), corresponding to lowermost Member II in the Yangtze Gorges area; B2 = *Tanarium tuberosum–Schizofusa zangwenlongii* Zone of Liu and Moczydłowska (2019), corresponding to lower–middle Member II in the Yangtze Gorges area; B3 = *Tanarium conoideum–Cavaspina basiconica* Zone of Liu and Moczydłowska (2019), corresponding to middle–upper Member II in the Yangtze Gorges area; B4 = *Tanarium pycnacanthum–Ceratosphaeridium glaberosum* Zone of Liu and Moczydłowska (2019), corresponding to lower Member III in the Yangtze Gorges area.

Reference	Area	Section	*Appendi-sphaera grandis*	*Cavaspina basiconica*	*Ceratosphaeridium glaberosum*	*Hocosphaeridium anozos*	*H. scaberfacium*	*Tanarium conoideum*	*Tanarium pycnacanthum*	*Tanarium tuberosum*(1)	*Schizofusa zangwenlongii*	*Weissiella grandistella*(3)	*Tianzhushania spinosa*
Role in the biozonation schemes			B1	B3	B4	A2	A2	A2, B3	B4	B2	B2	B1	A1, B1
Liu et al., 2014a	Yangtze	Niuping		Mem. III		Mem. III	Mem. III	Mem. III	Mem. III			Mem. III	
	Gorges	Wangfeng-gang		Mem. III	Mem. III	Mem. III	Mem. III	Mem. III	Mem. III	Mem. III		Mem. III	
		Xiaofenghe			Mem. III	Mem. III	Mem. III			Mem. III	Mem. III	Mem. III	
Liu et al., 2014b	Yangtze Gorges	Chenjiayuan-zi				Mem. III	Mem. III				Mem. III	Mem. III	Mem. II
Xiao et al., 2014	Weng'an		present	present		present		present					
Ouyang et al., 2015	Yangtze Gorges	Qinglinkou											Mem. II
Hawkins et al., 2017(2)	Zhangjiajie	Siduping				Mem. II							
Nie et al., 2017(2)	Zhangjiajie	Siduping		Mem. II									
Liu and Moczydłowska, 2019	Yangtze	Baiguoyuan	Mem. III				Mem. III	Mem. III			Mem. III		
	Gorges	Chenjiayuan-zi	Mem. II, III	Mem. III		Mem. III	Mem. III				Mem. III	Mem. III	Mem. II
		Dishuiyan	Mem. III	Mem. III		Mem. III	Mem. III				Mem. III	Mem. III	
		Jiulongwan										Mem. II	Mem. II
		Jiuqunao	Mem. II							Mem. II	Mem. II		Mem. II
		Liuhuiwan	Mem. III	Mem. III		Mem. III	Mem. III			Mem. III	Mem. III		
		Nantuocun	Mem. II										Mem. II
		Niuping	Mem. II, III	Mem. III		Mem. II, III	Mem. III	Mem. III	Mem. III	Mem. III		Mem. III	Mem. II
		Wangfeng-gang	Mem. II, III	Mem. III	Mem. III	Mem. III	Mem. III	Mem. III	Mem. III	Mem. III		Mem. II, III	Mem. II
		Xiaofenghe (N)	Mem. II									Mem. II	Mem. II
		Xiaofenghe (S)	Mem. II, III		Mem. III	Mem. III	Mem. III			Mem. III	Mem. III	Mem. II, III	Mem. II
Ouyang et al., 2019	Zhangcunping	Bailu	present										present
Shang et al., 2019	Songlin	Liujing	present	present				present		present	present	present	
Shang and Liu, 2020(2)	Zhangjiajie	Tianping	Mem. II							Mem. II			
Yang et al., 2020	Baokang	Baizhu											present
Liu et al., 2021	Changyang	Gucheng	Mem. II				Mem. II					Mem. II	Mem. II
Ouyang et al., 2021	Yangtze	Jiulongwan	Mem. II										Mem. II
	Gorges	Jinguadun	Mem. II									Mem. II	Mem. II
		Wuzhishan	Mem. II							Mem. II		Mem. II	Mem. II
Ye et al., 2022	Shennongjia	Lianhuacun	present	present			present	present				present	

Notes for superscripts: (1) Liu and Moczydłowska (2019) synonymized *Tanarium obesum* with *T. tuberosum* and proposed the latter to define the biozone, so the occurrence of *T. tuberosum* here also includes occurrence of *T. obesum*. (2) These three studies in the Zhangjiajie area all correlated their sampling horizons to Member II of the Doushantuo Formation in the Yangtze Gorges area. (3) Liu and Moczydłowska (2019) synonymized *Weissiella brevis* with *W. grandistella*, the latter of which is an eponymous taxon of their *Appendisphaera grandis–Weissiella grandistella–Tianzhushania spinosa* Assemblage Zone, so the occurrence of *W. grandistella* here also includes occurrence of *W. brevis*. See Systematic paleontology for taxonomic comments.

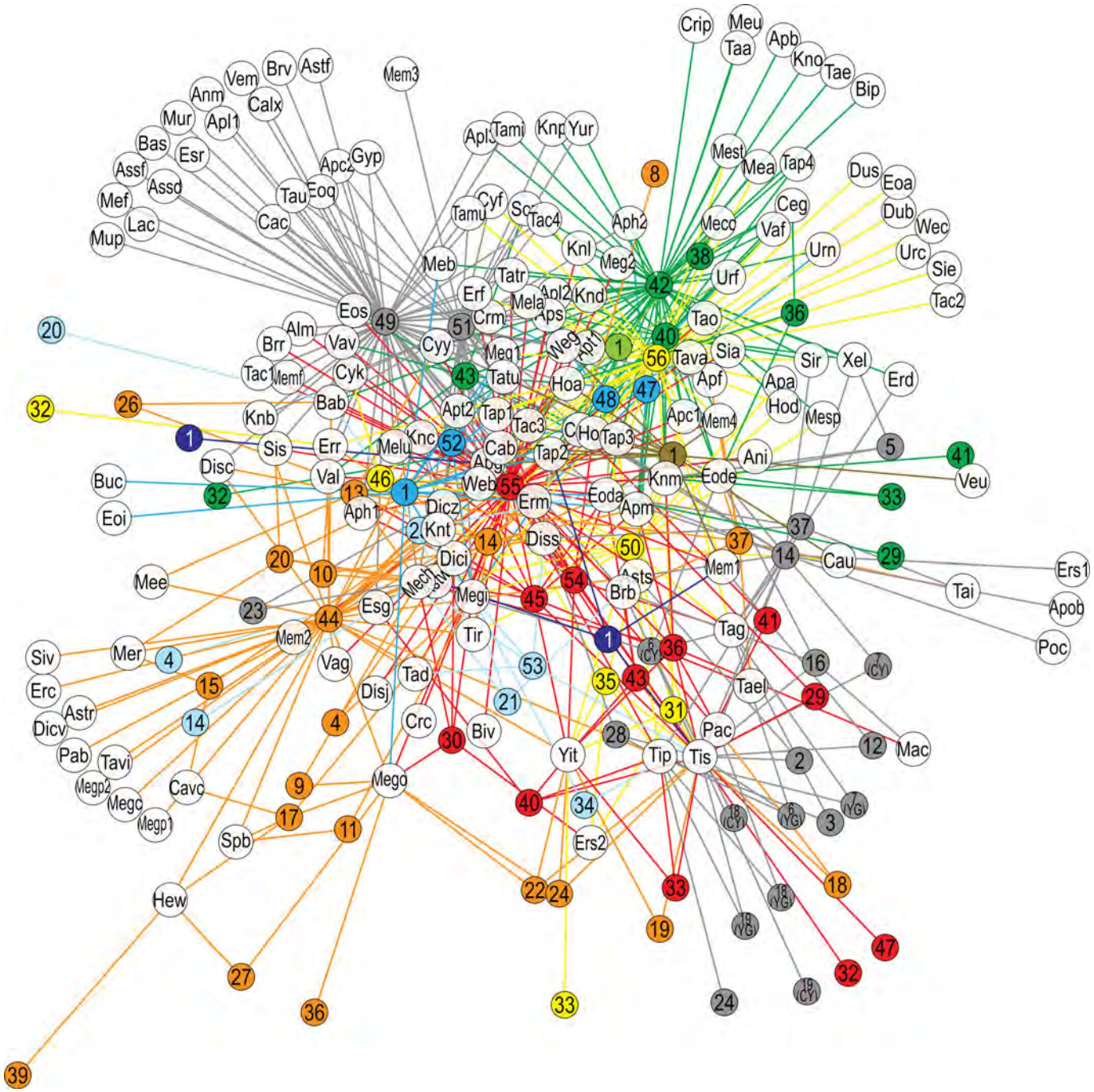

Figure 42. Bipartite network analysis of the same dataset of Doushantuo acanthomorph occurrences used in NMDS analysis (Fig. 41; see Supplemental Materials for data). Lettered nodes represent acritarch species. Numbered and colored nodes represent collections, with numbers matching source reference numbers in Table 3, and colors matching those of Figure 41.2: red = Member II of the Doushantuo Formation, shelf lagoon; green = Member III of the Doushantuo Formation, shelf lagoon; gray = stratigraphic interval not specified, shelf lagoon; yellow = correlated with upper Member II in shelf-lagoon facies, inner shelf (the Zhangcunping and Shennongjia areas); light blue = stratigraphic correlation relationship unclear, inner shelf (other areas such as Baokang, Chadian, and Chaoyang); orange = correlated with upper Member II or Member II–III transitional interval in shelf-lagoon facies, shelf margin (the Weng'an area); olive = roughly correlated with Member III in shelf-lagoon facies, shelf margin (the Caojunba section); lime, Doushantuo Formation, upper slope (the Lujiayuanzi section); blue = correlated with Member II in shelf-lagoon facies, slope (the Zhangjiajie area); dark blue = basinal facies. Each species is linked to a collection by a straight line if the species is present in the collection. Each acritarch taxon is linked to collections in which it is present. The network shows variation in occurrence frequency among acritarch species of the Doushantuo Formation. Species in the central area of the network generally occur in a greater number of areas, stratigraphic intervals, or studies, than species in the periphery area of the network. Abbreviations: CY-Changyang area, YG-Yangtze Gorges area. Species abbreviations: Alm = *Alicesphaeridium medusoidum*; Anm = *Ancorosphaeridium magnum*; Ani = *Annularidens inconditus*; Apob = *Apodastoides basileus*; Apa = *Appendisphaera anguina*; Apc1 = *Appendisphaera clava*; Apc2 = *Appendisphaera clustera*; Apf = *Appendisphaera fragilis*; Apg = *Appendisphaera grandis*; Aph1 = *Appendisphaera heliaca*; Apl1 = *Appendisphaera lemniscata*; Apl2 = *Appendisphaera longispina*; Apl3 = *Appendisphaera longitubularis*; Apm = *Appendisphaera magnifica*; Aps = *Appendisphaera setosa*; Apt1 = *Appendisphaera tabifica*; Apt2 = *Appendisphaera tenuis*; Apb = *Appendisphaera*? *brevispina*; Aph2 = *Appendisphaera*? *hemisphaerica*; Assd = *Asseserium diversum*; Assf = *Asseserium fusulentum*; Astf = *Asterocapsoides fluctuensis*; Astr = *Asterocapsoides robustus*; Asts = *Asterocapsoides sinensis*; Astw = *Asterocapsoides wenganensis*; Bab = *Bacatisphaera baokangensis*; Bas = *Bacatisphaera sparga*; Bip = *Bispinosphaera peregrina*; Biv = *Bispinosphaera vacua*; Brb = *Briareus borealis*; Brr = *Briareus robustus*; Brv = *Briareus vasformis*; Buc = *Bullatosphaera*? *colliformis* n. sp.; Calx = *Calyxia xandaros*; Caa = *Cavaspina acumincata*;

https://doi.org/10.1017/jpa.2023.92 Published online by Cambridge University Press

Cab = *Cavaspina basiconica*; Cac = *Cavaspina conica*; Cau = *Cavaspina uria*; Cavc = *Caveasphaera costata*; Ceg = *Ceratosphaeridium glaberosum*; Crc = *Crassimembrana crispans*; Crm = *Crassimembrana multitunica*; Crip = *Crinita paucispinosa*; Cyf = *Cymatiosphaeroides forabilatus*; Cyk = *Cymatiosphaeroides kullingii*; Cyy = *Cymatiosphaeroides yinii*; Dici = *Dicrospinasphaera improcera*; Dicv = *Dicrospinasphaera virgata*; Dicz = *Dicrospinasphaera zhangii*; Disj = *Distosphaera jinguadunensis*; Diss = *Distosphaera speciosa*; Disc = *Distosphaera*? *corniculata*; Dub = *Duospinosphaera biformis*; Dus = *Duospinosphaera shennongjiaensis*; Eoa = *Eotylotopalla apophysa*; Eoda = *Eotylotopalla dactylos*; Eode = *Eotylotopalla delicata*; Eoi = *Eotylotopalla inflata* n. sp.; Eoq = *Eotylotopalla quadrata*; Eos = *Eotylotopalla strobilata*; Erc = *Ericiasphaera crispa*; Erd = *Ericiasphaera densispina*; Erf = *Ericiasphaera fibrilla*; Erm = *Ericiasphaera magna*; Err = *Ericiasphaera rigida*; Ers1 = *Ericiasphaera sparsa*; Ers2 = *Ericiasphaera spjeldnaesii*; Esg = *Estrella greyae*; Esr = *Estrella recta*; Gyp = *Gyalosphaeridium pulchrum*; Hew = *Helicoforamina wenganica*; Hoa = *Hocosphaeridium anozos*; Hod = *Hocosphaeridium dilatatum*; Hos = *Hocosphaeridium scaberfacium*; Knb = *Knollisphaeridium bifurcatum*; Knc = *Knollisphaeridium coniformum*; Knd = *Knollisphaeridium denticulatum*; Knl = *Knollisphaeridium longilatum*; Knm = *Knollisphaeridium maximum*; Kno = *Knollisphaeridium obtusum*; Knp = *Knollisphaeridium parvum*; Knt = *Knollisphaeridium triangulum*; Lac = *Laminasphaera capillata*; Mac = *Matosphaera changyangensis*; Megc = *Megasphaera cymbala*; Megi = *Megasphaera inornata*; Mego = *Megasphaera ornata*; Megp1 = *Megasphaera patella*; Megp2 = *Megasphaera puncticulosa*; Memf = *Membranosphaera formosa*; Mea = *Mengeosphaera angusta*; Meb = *Mengeosphaera bellula*; Mech = *Mengeosphaera chadianensis*; Meco = *Mengeosphaera constricta*; Mee = *Mengeosphaera eccentrica*; Mef = *Mengeosphaera flammelata*; Meg1 = *Mengeosphaera gracilis*; Meg2 = *Mengeosphaera grandispina*; Mela = *Mengeosphaera latibasis*; Melu = *Mengeosphaera lunula*; Mem1 = *Mengeosphaera mamma*; Mem2 = *Mengeosphaera matryoshkaformis*; Mem3 = *Mengeosphaera membranifera*; Mem4 = *Mengeosphaera minima*; Mer = *Mengeosphaera reticulata*; Mesp = *Mengeosphaera spinula*; Mest = *Mengeosphaera stegosauriformis*; Meu = *Mengeosphaera uniformis*; Mup = *Multifronsphaeridium pelorium*; Mur = *Multifronsphaeridium ramosum*; Pab = *Papillomembrana boletiformis*; Pac = *Papillomembrana compta*; Poc = *Polygonium cratum*; Sia = *Sinosphaera asteriformis*; Sie = *Sinosphaera exilis*; Sir = *Sinosphaera rupina*; Sis = *Sinosphaera speciosa*; Siv = *Sinosphaera variabilis*; Spb = *Spiralicellula bulbifera*; Tael = *Taedigerasphaera lappacea*; Taa = *Tanarium acus*; Tac1 = *Tanarium capitatum*; Tac2 = *Tanarium columnatum*; Tac3 = *Tanarium conoideum*; Tac4 = *Tanarium cuspisatum*; Tad = *Tanarium digitiforme*; Tae = *Tanarium elegans*; Tag = *Tanarium gracilentum*; Tai = *Tanarium irregulare*; Tami = *Tanarium minimum*; Tamu = *Tanarium muntense*; Tao = *Tanarium obesum*; Tap1 = *Tanarium paucispinosum*; Tap2 = *Tanarium pilosiusculum*; Tap3 = *Tanarium pluriprotensum*; Tap4 = *Tanarium pycnacanthum*; Tatr = *Tanarium triangulare*; Tatu = *Tanarium tuberosum*; Tau = *Tanarium uniformum*; Tava = *Tanarium varium*; Tavi = *Tanarium victor*; Tip = *Tianzhushania polysiphonia*; Tir = *Tianzhushania rara*; Tis = *Tianzhushania spinosa*; Scz = *Schizofusa zangwenlongii*; Urc = *Urasphaera capitalis*; Urf = *Urasphaera fungiformis*; Urn = *Urasphaera nupta*; Vaf = *Variomargosphaeridium floridum*; Vag = *Variomargosphaeridium gracile*; Val = *Variomargosphaeridium litoschum*; Vav = *Variomargosphaeridium varietatum*; Vem = *Verrucosphaera minima*; Veu = *Verrucosphaera*? *undulata* n. sp.; Web = *Weissiella brevis*; Wec = *Weissiella concentrica*; Weg = *Weissiella* cf. *W.* grandistella; Xel = *Xenosphaera liantuoensis*; Yit = *Yinitianzhushania tuberifera*; Yur = *Yushengia ramispinsa*.

the five facies, thus are among the most widely distributed species in South China, allowing for potential application in biostratigraphic correlation across different facies.

An alternative biozonal scheme recently proposed by Liu and Moczydłowska (2019) includes four biozones. Each of the four biozones is defined by the FAD (first appearance datum) of two or three acritarch species, with the lower three biozones corresponding to Member II in the Yangtze Gorges area, and the uppermost biozone corresponding to Member III. However, many of these eponymous species are rare, even in the Yangtze Gorges area (Table 4), and it is extremely difficult to document the co-existence of two or three rare eponymous species, making these biozones impractical. In addition, although many eponymous species of these zones were selected for their global distribution, some of them (e.g., *Ceratosphaeridium glaberosum* and *Schizofusa zangwenlongii*) are only known from shelf-lagoon facies in South China, implying their possible facies-dependent paleoenvironmental distribution.

The current situation of Doushantuo acanthomorph biostratigraphy illustrates two challenges in the establishment of regionally recognizable biozones. On one hand, stratigraphically short-ranging taxa such as *Ceratosphaeridium glaberosum* and *Tanarium pycnacanthum* are generally rare in abundance, hampering their application in cross-facies correlation of strata where overall acritarch abundance is low. As visualized in the network diagram (Fig. 42), these species are mostly placed in the margin and most of them are each linked to only one edge. On the other hand, facies-independent taxa typically have a relatively long stratigraphic range, making them less useful in range biozones (Xiao et al., 2022), although their FADs can still be useful in defining acanthomorph biozones. These species include *Appendisphaera grandis*, *Eotylotopalla dactylos*, *Hocosphaeridium anozos*, and *Tanarium conoideum*. These species are placed in the center of the network diagram (Fig. 42) and are each linked to multiple localities, facies, or stratigraphic horizons.

The challenges identified above can be addressed in multiple ways. First, we need to considerably improve the sampling intensity of Doushantuo acanthomorphs. As shown in the rarefaction analysis, the current sample size at most Doushantuo localities is inadequate, thus it is likely that many widely distributed taxa, including those with short stratigraphic ranges, have not been documented. With increasing sampling intensity, we anticipate that stratigraphically useful species will turn up in slope and basinal facies, which are the least-sampled facies at the present. Second, when defining acanthomorph biozones, we should favor the FADs (over the stratigraphic ranges) of widely and abundantly distributed taxa. Third, the recognition of acanthomorph biozones should be supplemented by abundance data of taxa with long stratigraphic ranges and wide paleoenvironmental distributions (Shi et al., 2022). Dominant or abundant taxa of Member II or Member III of the Doushantuo Formation in the Yangtze Gorges area have been described qualitatively in the literature (e.g., C. Yin et al., 2011; Liu et al., 2013, 2014a, b; Ouyang et al., 2021), but quantitative studies are few (McFadden et al., 2009). We are optimistic that more data and quantitative analyses will eventually lead to more robust acanthomorph biozonation in South China.

The newly discovered acanthomorphs from the Lianghekou section in the basinal facies illustrate the biostratigraphic importance of *Tianzhushania*. In the basinal facies, the Doushantuo Formation is thin and dominated by black shales with sporadic carbonate horizons, thus hindering lithostratigraphic and $\delta^{13}C$ chemostratigraphic correlation with the shelf facies (Jiang et al., 2007, 2011). At the Lianghekou section, *Tianzhushania spinosa* is found in a fossiliferous horizon of the middle Doushantuo Formation, supporting a correlation with Member II in shelf-lagoon facies, since *T. spinosa* is an eponymous species of the lower biozone in Member II and has never been reported from Member III in shelf-lagoon facies. This can be seen as an example of how the currently recognized biozones may contribute to regional correlation of the Doushantuo Formation despite the challenges discussed above.

Conclusions

Silicified microfossils, including sphaeromorphic and acanthomorphic acritarchs, multicellular algae, tubular microfossils,

https://doi.org/10.1017/jpa.2023.92 Published online by Cambridge University Press

and other problematic forms, are reported from the Doushantuo Formation in a shelf margin–slope–basin transect in Hunan Province, South China. Of these fossils, acanthomorphic acritarchs are reported from the basinal facies for the first time. Fifteen genera and 29 species, including three new species, *Bullatosphaera*? *colliformis* n. sp., *Eotylotopalla inflata* n. sp., and *Verrucosphaera*? *undulata* n. sp., and six unnamed forms of acanthomorphic acritarchs are identified and systematically described.

A taxonomically revised dataset of Doushantuo acanthomorphic acritarchs was compiled. Rarefaction, NMDS, and network analyses of this dataset reveal the following five conclusions. (1) To date, 49 genera and 160 species of Ediacaran acanthomorphic acritarchs (including *Schizofusa zangwenlongii*) have been reported from the five depositional facies and 10 areas in South China. Sampling intensity is uneven across different localities and facies, and inadequate at most localities, indicating that new taxa and new occurrences are likely to be recovered with additional sampling. (2) Observed taxonomic richness varies significantly among facies, mainly due to sampling and taphonomic biases. Rarefaction analysis shows that, when compared at a similar sampling intensity, taxonomic richness among different sections is more or less comparable. (3) NMDS analysis shows that stratigraphic succession plays a greater role than facies in controlling the distribution of Doushantuo acanthomorphs, confirming the distinction of acanthomorph assemblages in Member II and Member III of the Doushantuo Formation in shelf-lagoon facies. (4) NMDS results are consistent with lithostratigraphic correlations of the Doushantuo Formation across different facies, reinforcing that the Weng'an biota is transitional between Member II and Member III assemblages in shelf-lagoon facies, that the Zhangcunping and Shennongjia assemblages are correlated with the upper Member II assemblage, and that the Caojunba assemblage is correlated with the Member III assemblage. (5) More intensive sampling of Doushantuo acanthomorphs is needed to establish regional biozones that can be defined by the FADs of widely distributed taxa and characterized by the relative abundance of common taxa.

Acknowledgments

The research was funded by the National Key Research and Development Program of China (2021YFA0718100 and 2022YFF0802700 to QO), the National Natural Science Foundation of China (41902006 and 42272012 to QO, 41921002 to CZ), the US National Science Foundation (EAR-2021207 to SX), and State Key Laboratory of Biogeology and Environmental Geology (GBL22106 to QO). We thank journal editors S. Zamora and A. Liu, as well as reviewer S. Willman and an anonymous reviewer, for constructive comments that helped improve this paper.

Declaration of competing interests

The authors declare that they have no known competing financial interests or personal relationships that could have appeared to influence the work reported in this paper.

Data availability statement

Data available from the Dryad Digital Repository: http://doi.org/10.5061/dryad.7d7wm3822.

Data archiving statement

This published work and the nomenclatural acts it contains, have been registered in ZooBank: http://zoobank.org/References/6FC92858-4054-4117-8043-1F06CFE77155

References

Anderson, R.P., Macdonald, F.A., Jones, D.S., McMahon, S., and Briggs, D.E.G., 2017, Doushantuo-type microfossils from latest Ediacaran phosphorites of northern Mongolia: Geology, v. 45, p. 1079–1082.

Anderson, R.P., McMahon, S., Macdonald, F.A., Jones, D.S., and Briggs, D.E.G., 2019, Palaeobiology of latest Ediacaran phosphorites from the upper Khesen Formation, Khuvsgul Group, northern Mongolia: Journal of Systematic Palaeontology, v. 17, p. 501–532.

Arvestål, E.H.M., and Willman, S., 2020, Organic-walled microfossils in the Ediacaran of Estonia: biodiversity on the East European Platform: Precambrian Research, v. 341, 105626, https://doi.org/10.1016/j.precamres.2020.105626.

Awramik, S.M., McMenamin, D.S., Yin, C., Zhao, Z., Ding, Q., and Zhang, S., 1985, Prokaryotic and eukaryotic microfossils from a Proterozoic/Phanerozoic transition in China: Nature, v. 315, p. 655–658.

Butterfield, N.J., 2007, Macroevolution and macroecology through deep time: Palaeontology, v. 50, p. 41–55.

Butterfield, N.J., and Rainbird, R.H., 1998, Diverse organic-walled fossils, including "possible dinoflagellates," from the early Neoproterozoic of arctic Canada: Geology, v. 26, p. 963–966.

Butterfield, N.J., Knoll, A.H., and Swett, K., 1994, Paleobiology of the Neoproterozoic Svanbergfjellet Formation, Spitsbergen: Fossils and Strata, v. 34, p. 1–84.

Cao, R., Tang, T., Xue, Y., Yu, C., Yin, L., and Zhao, W., 1989, [Research on Sinian Strata with ore deposits in the Yangzi (Yangtze) Region, China], *in* Nanjing Institute of Geology and Palaeontology, Chinese Academy of Sciences, ed., Upper Precambrian of the Yangzi (Yangtze) Region, China: Nanjing, Nanjing University Press, p. 1–94. [in Chinese]

Chen, B., Hu, C., Mills, B.J.W., He, T., Andersen, M.B., et al., 2022, A short-lived oxidation event during the early Ediacaran and delayed oxygenation of the Proterozoic ocean: Earth and Planetary Science Letters, v. 577, 117274, https://doi.org/10.1016/j.epsl.2021.117274.

Chen, M., and Liu, K., 1986, [The geological significance of newly discovered microfossils from the upper Sinian (Doushantuo age) phosphorites]: Scientia Geologica Sinica, v. 21, p. 46–53. [in Chinese with English summary]

Chen, S., Yin, C., Liu, P., Gao, L., Tang, F., and Wang, Z., 2010, [Microfossil assemblages from chert nodules of the Ediacaran Doushantuo Formation in Zhangcunping, northern Yichang, South China]: Acta Geologica Sinica, v. 84, p. 70–77. [in Chinese with English summary]

Clarke, K.R., 1993, Non-parametric multivariate analyses of changes in community structure: Australian Journal of Ecology, v. 18, p. 117–143.

Csárdi, G., and Nepusz, T., 2006, The igraph software package for complex network research: InterJournal, Complex Systems, 1695, p. 1–9, https://igraph.org.

Evitt, W.R., 1963, A discussion and proposals concerning fossil dinoflagellates, hystrichospheres, and acritarchs, I: Proceedings of the National Academy of Sciences of the United States of America, v. 49, p. 158–164.

Fairchild, T.R., 1975, The geologic setting and paleobiology of a late Precambrian stromatolitic microflora from South Australia [Ph.D. dissertation]: University of California, Los Angeles, Los Angeles, California, 272 p.

Faizullin, M.Sh., 1998, [New data on microfossils Baikalia of the Patom Upland]: Geologiya i Geofizika, v. 39, p. 328–337. [in Russian with English summary]

Gao, P., He, Z., Lash, G., Li, S., Zhang, R., 2020, Origin of chert nodules in the Ediacaran Doushantuo Formation black shales from Yangtze Block, South China: Marine and Petroleum Geology, v. 114, 104227, https://doi.org/10.1016/j.marpetgeo.2020.104227.

Geological Bureau of the Hunan Provincial Revolutionary Committee, 1976, [Regional Geological Survey Report of the People's Republic of China, Scale 1:200,000], Liuyang Sheet H-49-XXXVI (geological part), 209 p. [in Chinese]

https://doi.org/10.1017/jpa.2023.92 Published online by Cambridge University Press

Golubkova, E.Y., 2023, Acanthomorphic acritarchs from the Vendian deposits of interior areas of the Siberian Platform: Paleontological Journal, v. 57, p. 92–101.
Golubkova, E.Y., Raevskaya, E.G., and Kuznetsov, A.B., 2010, Lower Vendian microfossil assemblages of East Siberia: significance for solving regional stratigraphic problems: Stratigraphy and Geological Correlation, v. 18, p. 353–375.
Golubkova, E.Y., Zaitseva, T.S., Kuznetsov, A.B., Dovzhikova, E.G., and Maslov, A.V., 2015, Microfossils and Rb–Sr age of glauconite in the key section of the upper Proterozoic of the northeastern part of the Russian plate (Keltmen-1 borehole): Doklady Earth Sciences, v. 462, p. 547–551.
Grazhdankin, D., Nagovitsin, K., Golubkova, E., Karlova, G., Kochnev, B., Rogov, V., and Marusin, V., 2020, Doushantuo–Pertatataka-type acanthomorphs and Ediacaran ecosystem stability: Geology, v. 48, p. 708–712.
Green, J.W., Knoll, A.H., Golubic, S., Swett, K., 1987, Paleobiology of distinctive benthic microfossils from the upper Proterozoic limestone–dolomite "series," central East Greenland: American Journal of Botany, v. 74, p. 928–940.
Grey, K., 2005, Ediacaran palynology of Australia: Memoirs of the Association of Australasian Palaeontologists, v. 31, p. 1–439.
Grey, K., and Calver, C.R., 2007, Correlating the Ediacaran of Australia: Geological Society, London, Special Publications, v. 286, p. 115–135.
Hawkins, A.D., Xiao, S., Jiang, G., Wang, X., and Shi, X., 2017, New biostratigraphic and chemostratigraphic data from the Ediacaran Doushantuo Formation in intra-shelf and upper slope facies of the Yangtze platform: implications for biozonation of acanthomorphic acritarchs in South China: Precambrian Research, v. 300, p. 28–39.
Hermann, T.N., 1974, [Findings of massive accumulations of trichomes in the Riphean], *in* Timofeev, B.V., ed., Microfossils of Proterozoic and Early Paleozoic of the USSR: Leningrad, Nauka, p. 6–10. [in Russian]
Jiang, G., Kaufman, A.J., Christie-Blick, N., Zhang, S., and Wu, H., 2007, Carbon isotope variability across the Ediacaran Yangtze platform in South China: implications for a large surface-to-deep ocean $\delta^{13}C$ gradient: Earth and Planetary Science Letters, v. 261, p. 303–320.
Jiang, G., Shi, X., Zhang, S., Wang, Y., and Xiao, S., 2011, Stratigraphy and paleogeography of the Ediacaran Doushantuo Formation (ca. 635–551Ma) in South China: Gondwana Research, v. 19, p. 831–849.
Joshi, H., and Tiwari, M., 2016, *Tianzhushania spinosa* and other large acanthomorphic acritarchs of Ediacaran Period from the Infrakrol Formation, Lesser Himalaya, India: Precambrian Research, v. 286, p. 325–336.
Joshi, H., Mishra, M., and Tiwari, M., 2022, Origin of the early Ediacaran chert from Infrakrol Formation in Krol Belt, Lesser Himalaya, India: Journal of Sedimentary Environments, v. 7, p. 501–517.
Knoll, A.H., 1982, Microfossils from the Late Precambrian Draken Conglomerate, Ny Friesland, Svalbard: Journal of Paleontology, v. 56, p. 755–790.
Knoll, A.H., 1984, Microbiotas of the late Precambrian Hunnberg Formation, Nordaustlandet, Svalbard: Journal of Paleontology, v. 58, p. 131–162.
Knoll, A.H., 1985, Exceptional preservation of photosynthetic organisms in silicified carbonates and silicified peats: Philosophical Transactions of the Royal Society of London. B, Biological Sciences, v. 311, p. 111–122.
Knoll, A.H., 1992, Vendian microfossils in metasedimentary cherts of the Scotia Group, Prins Karls Forland, Svalbard: Palaeontology, v. 35, p. 751–774.
Knoll, A.H., and Walter, M.R., 1992, Latest Proterozoic stratigraphy and Earth history: Nature, v. 356, p. 673–677.
Knoll, A.H., Swett, K., and Mark, J., 1991, Paleobiology of a Neoproterozoic tidal flat/lagoonal complex: the Draken Conglomerate Formation, Spitsbergen: Journal of Paleontology, v. 65, p. 531–570.
Knoll, A.H., Javaux, E.J., Hewitt, D., and Cohen, P., 2006a, Eukaryotic organisms in Proterozoic oceans: Philosophical Transactions of the Royal Society of London B: Biological Sciences, v. 361, p. 1023–1038.
Knoll, A.H., Walter, M.R., Narbonne, G.M., and Christie-Blick, N., 2006b, The Ediacaran Period: a new addition to the geologic time scale: Lethaia, v. 39, p. 13–30.
Kolosova, S.P., 1991, Pozdnedokembriyskie shipovatie mikrofossilii vostoka sibirkoy platformi [Late Precambrian acanthomorphic acritarchs from the eastern Siberian Platform]: Algologiya [Algologia], v. 1, p. 53–59. [in Russian]
Li, H., Zhang, S., Han, J., Zhong, T., Ding, J., Wu, H., Liu, P., et al., 2022, Astrochronologic calibration of the Shuram carbon isotope excursion with new data from South China: Global and Planetary Change, v. 209, 103749, https://doi.org/10.1016/j.gloplacha.2022.103749.
Li, Q.-W., and Zhao, J.-H., 2020, Amalgamation between the Yangtze and Cathaysia blocks in South China: evidence from the ophiolite geochemistry: Precambrian Research, v. 350, p. 105893, https://doi.org/10.1016/j.precamres.2020.105893.
Li, X.-H., Li, W.-X., Li, Z.-X., Lo, C.-H., Wang, J., Ye, M.-F., and Yang, Y.-H., 2009, Amalgamation between the Yangtze and Cathaysia Blocks in South China: constraints from SHRIMP U–Pb zircon ages, geochemistry and Nd–Hf isotopes of the Shuangxiwu volcanic rocks: Precambrian Research, v. 174, p. 117–128.
Li, Z.-X., Li, X.-H., Wartho, J.-A., Clark, C., Li, W.-X., Zhang, C.-L., and Bao, C., 2010, Magmatic and metamorphic events during the early Paleozoic Wuyi-Yunkai orogeny, southeastern South China: New age constraints and pressure-temperature conditions: GSA Bulletin, v. 122, p. 772–793.
Liu, H., Qi, S., Fan, J., Guo, W., Pei, M., et al., 2021, [An acritarch assemblage from the lower Ediacaran Doushantuo Formation in Changyang, Hubei Province]: Journal of Stratigraphy, v. 45, p. 19–28. [in Chinese with English summary]
Liu, P., and Moczydłowska, M., 2019, Ediacaran microfossils from the Doushantuo Formation chert nodules in the Yangtze Gorges area, South China, and new biozones: Fossils and Strata, v. 65, p. 1–172.
Liu, P., and Yin, C., 2005, New data of phosphatized acritarchs from the Ediacaran Doushantuo Formation at Weng'an, Guizhou Province, Southwest China: Acta Geologica Sinica (English Edition), v. 79, p. 575–581.
Liu, P., Xiao, S., Yin, C., Zhou, C., Gao, L., and Tang, F., 2008, Systematic description and phylogenetic affinity of tubular microfossils from the Ediacaran Doushantuo Formation at Weng'an, South China: Palaeontology, v. 51, p. 339–366.
Liu, P., Yin, C., Gao, L., Tang, F., and Chen, S., 2009, New material of microfossils from the Ediacaran Doushantuo Formation in the Zhangcunping area, Yichang, Hubei Province and its zircon SHRIMP U–Pb age: Chinese Science Bulletin, v. 54, p. 1058–1064.
Liu, P., Yin, C., Chen, S., Tang, F., and Gao, L., 2012, Discovery of *Ceratosphaeridium* (Acritarcha) from the Ediacaran Doushantuo Formation in Yangtze Gorges, South China and its biostratigraphic implication: Bulletin of Geosciences, v. 87, p. 195–200.
Liu, P., Yin, C., Chen, S., Tang, F., and Gao, L., 2013, The biostratigraphic succession of acanthomorphic acritarchs of the Ediacaran Doushantuo Formation in the Yangtze Gorges area, South China and its biostratigraphic correlation with Australia: Precambrian Research, v. 225, p. 29–43.
Liu, P., Xiao, S., Yin, C., Chen, S., Zhou, C., and Li, M., 2014a, Ediacaran acanthomorphic acritarchs and other microfossils from chert nodules of the upper Doushantuo Formation in the Yangtze Gorges Area, South China: Journal of Paleontology, v. 88, issue S72, 139 p.
Liu, P., Chen, S., Zhu, M., Li, M., Yin, C., and Shang, X., 2014b, -High-resolution biostratigraphic and chemostratigraphic data from the Chenjiayuanzi section of the Doushantuo Formation in the Yangtze Gorges area, South China: implication for subdivision and global correlation of the Ediacaran System: Precambrian Research, v. 249, p. 199–214.
Luo, H., Du, X., and Jiang, C., 2002, [Geological map of Hunan Province 1:1 500 000], *in* Ma, L., ed., Geological Atlas of China: Beijing, Geological Press, p. 245–252. [in Chinese]
Macouin, M., Besse, J., Ader, M., Gilder, S., Yang, Z., Sun, Z., and Agrinier, P., 2004, Combined paleomagnetic and isotopic data from the Doushantuo carbonates, South China: implications for the "Snowball Earth" hypothesis: Earth and Planetary Science Letters, v. 224, p. 387–398.
McFadden, K.A., Huang, J., Chu, X., Jiang, G., Kaufman, A.J., Zhou, C., Yuan, X., and Xiao, S., 2008, Pulsed oxidation and biological evolution in the Ediacaran Doushantuo Formation: Proceedings of the National Academy of Sciences, v. 105, p. 3197–3202.
McFadden, K.A., Xiao, S., Zhou, C., and Kowalewski, M., 2009, Quantitative evaluation of the biostratigraphic distribution of acanthomorphic acritarchs in the Ediacaran Doushantuo Formation in the Yangtze Gorges area, South China: Precambrian Research, v. 173, p. 170–190.
Moczydłowska, M., 2005, Taxonomic review of some Ediacaran acritarchs from the Siberian Platform: Precambrian Research, v. 136, p. 283–307.
Moczydłowska, M., 2008, The Ediacaran microbiota and the survival of Snowball Earth conditions: Precambrian Research, v. 167, p. 1–15.
Moczydłowska, M., 2016, Algal affinities of Ediacaran and Cambrian organic-walled microfossils with internal reproductive bodies: *Tanarium* and other morphotypes: Palynology, v. 40, p. 83–121.
Moczydłowska, M., and Nagovitsin, K.E., 2012, Ediacaran radiation of organic-walled microbiota recorded in the Ura Formation, Patom Uplift, East Siberia: Precambrian Research, v. 198–199, p. 1–24.
Moczydłowska, M., Vidal, G., and Rudavskaya, V.A., 1993, Neoproterozoic (Vendian) phytoplankton from the Siberian platform, Yakutia: Palaeontology, v. 36, p. 495–521.
Morais, L., Fairchild, T.R., Freitas, B.T., Rudnitzki, I.D., Silva, E.P., Lahr, D., Moreira, A.C., Abrahão Filho, E.A., Leme, J.M., and Trindade, R.I.F., 2021, Doushantuo–Pertatataka-like acritarchs from the late Ediacaran Bocaina Formation (Corumbá Group, Brazil): Frontiers in Earth Science, v. 9, 787011, https://doi.org/10.3389/feart.2021.787011.
Muscente, A.D., Hawkins, A.D., and Xiao, S., 2015, Fossil preservation through phosphatization and silicification in the Ediacaran Doushantuo Formation (South China): a comparative synthesis: Palaeogeography Palaeoclimatology Palaeoecology, v. 434, p. 46–62.

Nagovitsin, K.E., and Kochnev, B.B., 2015, Microfossils and biofacies of the Vendian fossil biota in the southern Siberian Platform: Russian Geology and Geophysics, v. 56, p. 584–593.
Nagovitsin, K.E., Faizullin, M.S., and Yakshin, M.S., 2004, [New forms of Baikalian acanthomorphytes from the Ura Formation of the Patom Uplift, East Siberia]: Geologiya e Geofisika, v. 45, p. 7–19. [in Russian with English summary]
Narbonne, G.M., Xiao, S., Shields, G.A., and Gehling, J.G., 2012, Chapter 18 – The Ediacaran Period, *in* Gradstein, F.M., Ogg, J.G., Schmitz, M.D., and Ogg, G.M., eds., The Geologic Time Scale: Boston, Elsevier, p. 413–435.
Nie, X., Liu, H., and Dong, L., 2017, [Ediacaran microfossils from the Doushantuo Formation of the Siduping section, Zhangjiajie, Hunan Province, China]: Acta Micropalaeontologica Sinica, v. 34, p. 369–389. [in Chinese with English summary]
Oksanen, J., Blanchet, F.G., Friendly, M., Kindt, R., Legendre, P., McGlinn, D., Minchin, P.R., et al., 2019, vegan: Community Ecology Package, R package version 2.5-6: https://CRAN.R-project.org/package=vegan.
Ouyang, Q., Zhou, C., Guan, C., and Wang, W., 2015, [New microfossils from the Ediacaran Doushantuo Formation in the Yangtze Gorges area, South China, and their biostratigraphic implications]: Acta Palaeontologica Sinica, v. 54, p. 207–229. [in Chinese with English summary]
Ouyang, Q., Guan, C., Zhou, C., and Xiao, S., 2017, Acanthomorphic acritarchs of the Doushantuo Formation from an upper slope section in northwestern Hunan Province, South China, with implications for early–middle Ediacaran biostratigraphy: Precambrian Research, v. 298, p. 512–529.
Ouyang, Q., Zhou, C., Xiao, S., Chen, Z., and Shao, Y., 2019, Acanthomorphic acritarchs from the Ediacaran Doushantuo Formation at Zhangcunping in South China, with implications for the evolution of early Ediacaran eukaryotes: Precambrian Research, v. 320, p. 171–192.
Ouyang, Q., Zhou, C., and Liu, P., 2020, [Hydrofluoric acid maceration experiment to extract silicified acritarchs from the chert nodules of the Doushantuo Formation, South China]: Acta Micropalaeontologica Sinica, v. 37, p. 105–114. [in Chinese with English summary]
Ouyang, Q., Zhou, C., Xiao, S., Guan, C., Chen, Z., Yuan, X., and Sun, Y., 2021, Distribution of Ediacaran acanthomorphic acritarchs in the lower Doushantuo Formation of the Yangtze Gorges area, South China: evolutionary and stratigraphic implications: Precambrian Research, v. 353, p. 106005, https://doi.org/10.1016/j.precamres.2020.106005.
Ouyang, Q., Zhou, C.-M., Pang, K., and Chen, Z., 2022, Silicified *Polybessurus* from the Ediacaran Doushantuo Formation records microbial activities within marine sediments: Palaeoworld, v. 31, p. 1–13.
Pang, K., Tang, Q., Wan, B., and Yuan, X., 2020, New insights on the palaeobiology and biostratigraphy of the acritarch *Trachyhystrichosphaera aimika*: a potential late Mesoproterozoic to Tonian index fossil: Palaeoworld, v. 29, p. 476–489.
Peterson, K.J., and Butterfield, N.J., 2005, Origin of the Eumetazoa: testing ecological predictions of molecular clocks against the Proterozoic fossil record: Proceedings of the National Academy of Sciences of the United States of America, v. 102, p. 9547–9552.
Prasad, B., and Asher, R., 2016, Record of Ediacaran complex acanthomorphic acritarchs from the lower Vindhyan succession of the Chambal valley (east Rajasthan), India and their biostratigraphic significance: Journal of the Palaeontological Society of India, v. 61, p. 29–62.
Raup, D.M., 1975, Taxonomic diversity estimation using rarefaction: Paleobiology, v. 1, p. 333–342.
R Core Team, 2018, R: A language and environment for statistical computing: R Foundation for Statistical Computing, Vienna, Austria, https://www.R-project.org/.
Reitlinger, E.A., 1948, Byulleten Moskovskogo Obshchestva Ispytateleja Prirody [Cambrian foraminifera of Yakutsk]: Otdel Geological Section, v. 23, p. 77–81. [in Russian]
Rooney, A.D., Cantine, M.D., Bergmann, K.D., Gómez-Pérez, I., Al Baloushi, B., Boag, T.H., Busch, J.F., Sperling, E.A., and Strauss, J.V., 2020, Calibrating the coevolution of Ediacaran life and environment: Proceedings of the National Academy of Sciences, v. 117, p. 16824–16830.
Schopf, J.W., 1968, Microflora of the Bitter Springs Formation, late Precambrian, central Australia: Journal of Paleontology, v. 42, p. 651–668.
Sergeev, V.N., Knoll, A.H., and Vorob'eva, N.G., 2011, Ediacaran microfossils from the Ura Formation, Baikal–Patom Uplift, Siberia: taxonomy and biostratigraphic significance: Journal of Paleontology, v. 85, p. 987–1011.
Shang, X., and Liu, P., 2020, [Acritarchs from the Ediacaran Doushantuo Formation at the Tianping section in Zhangjiajie area of Hunan Province, South China and their biostratigraphic significance]: Journal of Stratigraphy, v. 44, p. 150–162. [in Chinese with English summary]
Shang, X., and Liu, P., 2022, Diverse multicellular algae from the early Ediacaran Doushantuo chert nodules and their palaeoecological implications: Precambrian Research, v. 368, 106508, https://doi.org/10.1016/j.precamres.2021.106508.
Shang, X., Moczydłowska, M., Liu, P., and Liu, L., 2018, Organic composition and diagenetic mineralization of microfossils in the Ediacaran Doushantuo chert nodule by Raman and petrographic analyses: Precambrian Research, v. 314, p. 145–159.
Shang, X., Liu, P., and Moczydłowska, M., 2019, Acritarchs from the Doushantuo Formation at Liujing section in Songlin area of Guizhou Province, South China: implications for early–middle Ediacaran biostratigraphy: Precambrian Research, v. 334, 105453, https://doi.org/10.1016/j.precamres.2019.105453.
Shang, X., Liu, P., and Liu, L., 2020, [Raman spectral analyses of microfossils from the chert bands in the Ediacaran Doushantuo Formation of South China and their taphonomic implications]: Acta Micropalaeontologica Sinica, v. 37, p. 197–209. [in Chinese with English summary]
Sharma, M., Shukla, Y., and Sergeev, V.N., 2021, Microfossils from the Krol 'A' of the Lesser Himalaya, India: additional supporting data for its early Ediacaran age: Palaeoworld, v. 30, p. 610–626.
Shi, H., Ouyang, Q., Zhou, C., Xiao, S., Chen, Z., and Guan, C., 2022, Integrated study of the Doushantuo Formation in northwestern Hunan Province: implications for Ediacaran chemostratigraphy and biostratigraphy in South China: Precambrian Research, v. 377, 106699, https://doi.org/10.1016/j.precamres.2022.106699.
Shukla, R., and Tiwari, M., 2014, Ediacaran acanthomorphic acritarchs from the Outer Krol Belt, Lesser Himalaya, India: their significance for global correlation: Palaeoworld, v. 23, p. 209–224.
Shukla, M., Mathur, V.K., Babu, R., and Srivastava, D.K., 2008, Ediacaran microbiota from the Baliana and Krol groups, Lesser Himalaya, India: The Palaeobotanist, v. 57, p. 359–378.
Spjeldnaes, N., 1963, A new fossil (*Papillomembrana* sp.) from the upper Precambrian of Norway: Nature, v. 200, p. 63–64.
Sui, Y., Huang, C., Zhang, R., Wang, Z., Ogg, J., and Kemp, D.B., 2018, Astronomical time scale for the lower Doushantuo Formation of early Ediacaran, South China: Science Bulletin, v. 63, p. 1485–1494.
Sui, Y., Huang, C., Zhang, R., Wang, Z., and Ogg, J., 2019, Astronomical time scale for the middle–upper Doushantuo Formation of Ediacaran in South China: implications for the duration of the Shuram/Wonoka negative $\delta^{13}C$ excursion: Palaeogeography, Palaeoclimatology, Palaeoecology, v. 532, 109273, https://doi.org/10.1016/j.palaeo.2019.109273.
Tang, Q., Pang, K., Xiao, S., Yuan, X., Ou, Z., and Wan, B., 2013, Organic-walled microfossils from the early Neoproterozoic Liulaobei Formation in the Huainan region of North China and their biostratigraphic significance: Precambrian Research, v. 236, p. 157–181.
Timofeev, B.V., Hermann, T.N., and Mikhailova, N.S., 1976, Mikrofitogosilli Dokembriya, Kembriya i Ordovika [Microphytofossils of the Precambrian, Cambrian and Ordovician]: Moskow, Nauka, 1–107 p. [in Russian]
Tiwari, M., and Knoll, A.H., 1994, Large acanthomorphic acritarchs from the Infrakrol Formation of the Lesser Himalaya and their stratigraphic significance: Journal of Himalayan Geology, v. 5, p. 193–201.
Turland, N.J., Wiersema, J.H., Barrie, F.R., Greuter, W., Hawksworth, D.L., et al., eds., 2018, International Code of Nomenclature for Algae, Fungi, and Plants (Shenzhen Code) Adopted by the Nineteenth International Botanical Congress Shenzhen, China, July 2017. Regnum Vegetabile 159: Glashütten, Germany, Koeltz Botanical Books, https://doi.org/10.12705/Code.2018.
Veis, A.F., Vorob'eva, V.G., and Golubkova, E.Y., 2006, The early Vendian microfossils first found in the Russian plate: taxonomic composition and biostratigraphic significance: Stratigraphy and Geological Correlation, v. 14, p. 368–385.
Vernhet, E., and Reijmer, J.J.G., 2010, Sedimentary evolution of the Ediacaran Yangtze platform shelf (Hubei and Hunan provinces, Central China): Sedimentary Geology, v. 225, p. 99–115.
Vernhet, E., Heubeck, C., Zhu, M.Y., and Zhang, J.M., 2006, Large-scale slope instability at the southern margin of the Ediacaran Yangtze platform (Hunan Province, central China): Precambrian Research, v. 148, p. 32–44.
Vidal, G., 1990, Giant acanthomorph acritarchs from the upper Proterozoic in southern Norway: Palaeontology, v. 33, p. 287–298.
Vorob'eva, N.G., and Petrov, P.Yu., 2020, Microbiota of the Barakun Formation and biostratigraphic characteristics of the Dal'nyaya Taiga Group: early Vendian of the Ura Uplift (Eastern Siberia): Stratigraphy and Geological Correlation, v. 28, p. 365–380.
Vorob'eva, N.G., Sergeev, V.N., and Semikhatov, M.A., 2006, Unique lower Vendian Kel'tma microbiota, Timan ridge: New evidence for the paleontological essence and global significance of the Vendian System: Doklady Earth Sciences, v. 410, p. 1038–1043.
Vorob'eva, N.G., Sergeev, V.N., and Chumakov, N.M., 2008, New finds of early Vendian microfossils in the Ura Formation: revision of the Patom Supergroup age, Middle Siberia: Doklady Earth Sciences, v. 419, p. 411–416.

https://doi.org/10.1017/jpa.2023.92 Published online by Cambridge University Press

Vorob'eva, N.G., Sergeev, V.N., and Knoll, A.H., 2009, Neoproterozoic microfossils from the northeastern margin of the East European Platform: Journal of Paleontology, v. 83, p. 161–196.
Vorob'eva, V.G., and Sergeev, V.N., 2018, *Stellarossica* gen. nov. and the Infragroup Keltmiides infragroup. nov.: extremely large acanthomorph acritarchs from the Vendian of Siberia and the East European Platform: Paleontological Journal, v. 52, p. 563–573.
Wallet, E., Willman, S., and Slater, B.J., 2022, Morphometric analysis of *Skiagia*-plexus acritarchs from the early Cambrian of North Greenland: toward a meaningful evaluation of phenotypic plasticity: Paleobiology, v. 48, p. 576–600.
Wang, D., Chen, L., Tang, Q., and Pang, K., 2012, [Spheroidal fossils with helically distributed pores from the Ediacaran Doushantuo phosphorites of Weng'an, Guizhou]: Acta Palaeontologucal Sinica, v. 51, p. 88–95. [in Chinese with English summary]
Wang, W., Guan, C., Hu, Y., Cui, H., Muscente, A.D., Chen, L., and Zhou, C., 2020, Spatial and temporal evolution of Ediacaran carbon and sulfur cycles in the Lower Yangtze Block, South China: Palaeogeography, Palaeoclimatology, Palaeoecology, v. 537, 109417, https://doi.org/10.1016/j.palaeo.2019.109417.
Wang, X., Erdtmann, B.D., Chen, X., and Mao, X., 1998, Integrated sequence-, bio- and chemostratigraphy of the terminal Proterozoic to lowermost Cambrian "Black Rock Series" from central South China: Episodes, v. 21, p. 178–189.
Wang, X., Jiang, G., Shi, X., and Xiao, S., 2016, Paired carbonate and organic carbon isotope variations of the Ediacaran Doushantuo Formation from an upper slope section at Siduping, South China: Precambrian Research, v. 273, p. 53–66.
Willman, S., and Moczydłowska, M., 2008, Ediacaran acritarch biota from the Giles 1 drillhole, Officer Basin, Australia, and its potential for biostratigraphic correlation: Precambrian Research, v. 162, p. 498–530.
Willman, S., and Moczydłowska, M., 2011, Acritarchs in the Ediacaran of Australia—local or global significance? Evidence from the Lake Maurice West 1 drillcore: Review of Palaeobotany and Palynology, v. 166, p. 12–28.
Willman, S., Moczydłowska, M., and Grey, K., 2006, Neoproterozoic (Ediacaran) diversification of acritarchs—a new record from the Murnaroo 1 drillcore, eastern Officer Basin, Australia: Review of Palaeobotany and Palynology, v. 139, p. 17–39.
Willman, S., Peel, J.S., Ineson, J.R., Schovsbo, N.H., Rugen, E.J., and Frei, R., 2020, Ediacaran Doushantuo-type biota discovered in Laurentia: Communications Biology, v. 3, 647, https://doi.org/10.1038/s42003-020-01381-7.
Xiao, S., 2004a, Neoproterozoic glaciations and the fossil record, *in* Jenkins, G.S., McMenamin, M.A.S., McKay, C.P., and Sohl, L., eds., The Extreme Proterozoic: Geology, Geochemistry, and Climate: Geophysical Monograph Series, v. 146, p. 199–214.
Xiao, S., 2004b, New multicellular algal fossils and acritarchs in Doushantuo chert nodules (Newproterozoic; Yangtze Gorges, South China): Journal of Paleontology, v. 78, p. 393–401.
Xiao, S., and Knoll, A.H., 1999, Fossil preservation in the Neoproterozoic Doushantuo phosphorite Lagerstätte, South China: Lethaia, v. 32, p. 219–238.
Xiao, S., and Knoll, A.H., 2000, Phosphatized animal embryos from the Neoproterozoic Doushantuo Formation at Weng'an, Guizhou, South China: Journal of Paleontology, v. 74, p. 767–788.
Xiao, S., and Narbonne, G.M., 2020, Chapter 18 – The Ediacaran Period, *in* Gradstein, F.M., Ogg, J.G., Schmitz, M.D., and Ogg, G.M., eds., Geologic Time Scale 2020: Amsterdam, Elsevier, p. 521–561.
Xiao, S., Hagadorn, J.W., Zhou, C., and Yuan, X., 2007, Rare helical spheroidal fossils from the Doushantuo Lagerstätte: Ediacaran animal embryos come of age? Geology, v. 35, p. 115–118.
Xiao, S., McFadden, K.A., Peek, S., Kaufman, A.J., Zhou, C., Jiang, G., and Hu, J., 2012, Integrated chemostratigraphy of the Doushantuo Formation at the northern Xiaofenghe section (Yangtze Gorges, South China) and its implication for Ediacaran stratigraphic correlation and ocean redox models: Precambrian Research, v. 192–195, p. 125–141.
Xiao, S., Zhou, C., Liu, P., Wang, D., and Yuan, X., 2014, Phosphatized acanthomorphic acritarchs and related microfossils from the Ediacaran Doushantuo Formation at Weng'an (South China) and their implications for biostratigraphic correlation: Journal of Paleontology, v. 88, p. 1–67.
Xiao, S., Narbonne, G.M., Zhou, C., Laflamme, M., Grazhdankin, D.V., Moczydlowska-Vidal, M., and Cui, H., 2016, Towards an Ediacaran time scale: problems, protocols, and prospects: Episodes, v. 39, p. 540–555.
Xiao, S., Jiang, G., Ye, Q., Ouyang, Q., Banerjee, D.M., Singh, B.P., Muscente, A.D., Zhou, C., and Hughes, N.C., 2022, Systematic paleontology, acritarch biostratigraphy, and $\delta^{13}C$ chemostratigraphy of the early Ediacaran Krol A Formation, Lesser Himalaya, northern India: Journal of Paleontology, p. 1–62, https://doi.org/10.1017/jpa.2022.7.
Xie, G., Zhou, C., Mcfadden, K.A., Xiao, S., and Yuan, X., 2008, [Microfossils discovered from the Sinian Doushantuo Formation in the Jiulongwan section, east Yangtze gorges area, Hubei province, South China]: Acta Palaeontologica Sinica, v. 3, p. 279–291. [in Chinese with English summary]
Xue, Y., Tang, T., and Yu, C., 1992, [Discovery of the oldest skeletal fossils from upper Sinian Doushantuo Formation in Weng'an, Guizhou, and its significance]: Acta Palaeontologica Sinica, v. 31, p. 530–539. [in Chinese with English summary]
Xue, Y., Tang, T., Yu, C., and Zhou, C., 1995, [Large spheroidal chlorophyta fossils from Doushantuo Formation phosphoric sequence (Late Sinian), central Guizhou, South China]: Acta Palaeontologica Sinica, v. 34, p. 688–706. [in Chinese with English summary]
Yakshin, M.S., Luchinina, V.A., 1981, New data on fossilized algae of family Oscillatoriaceae (Kirchn) Elenkin, *in* Meshkova, N.P., Nikolaeva, I.V., eds., Precambrian–Cambrian boundary deposits of the Siberian platform: Novosibirsk, Nauka, p. 28–34.
Yang, L., Pang, K., Chen, L., Zhong, Z., and Yang, F., 2020, [New materials of microfossils from the Ediacaran Doushantuo Formation in Baizhu phosphorite deposit, Baokang, Hubei Province]: Acta Micropalaeontologica Sinica, v. 37, p. 1–20, https://doi.org/10.16087/j.cnki.1000-0674.2020.01.001. [in Chinese with English summary]
Ye, Q., Tong, J., An, Z., Tian, L., Zhao, X., and Zhu, S., 2015, [Phosphatized fossil assemblage from the Ediacaran Doushantuo Formation in Zhangcunping area, Yichang, Hubei Province]: Acta Palaeontologica Sinica, v. 54, p. 43–65. [in Chinese with English summary]
Ye, Q., Li, J., Tong, J., An, Z., Hu, J., and Xiao, S., 2022, A microfossil assemblage from the Ediacaran Doushantuo Formation in the Shennongjia area (Hubei Province, South China): filling critical paleoenvironmental and biostratigraphic gaps: Precambrian Research, v. 377, p. 106691, https://doi.org/10.1016/j.precamres.2022.106691.
Yin, C., 1990, [Spinose acritarchs from the Toushantou Formation in the Yangtze Gorges and its geological significance]: Acta Micropalaeontologica Sinica, v. 7, p. 265–270. [in Chinese with English summary]
Yin, C., 1996, [New discovery of the Sinian Doushantuo microfossils from Miaohe, Zigui, Hubei]: Acta Geoscientia Sinica, v. 17, p. 322–329. [in Chinese with English summary]
Yin, C., 1999, Microfossils from the upper Sinian (late Neoproterozoic) Doushantuo Formation in Changyang, Western Hubei, China: Continental Dynamics, v. 4, p. 1–18.
Yin, C., 2001, [Discovery of *Papillomembrana compta* in Weng'an, Guizhou with discussion on the correlation of the large acanthomorphic acritarchs and the age of the Doushantuo Formation]: Journal of Stratigraphy, v. 25, p. 253–260. [in Chinese with English summary]
Yin, C., and Gao, L., 1995, [The early evolution of the acanthomorphic acritarchs in China and their biostratigraphical implication]: Acta Geologica Sinica, v. 69, p. 360–371. [in Chinese with English summary]
Yin, C., and Liu, G., 1988, [Micropaleofloras], *in* Zhao, Z., Xing, Y., Ding, Q., Liu, G., Zhao, Y., Zhang, S., Meng, X., Yin, C., Ning, B., and Han, P., eds., The Sinian System of Hubei: Wuhan, China University of Geosciences Press, p. 170–180. [in Chinese]
Yin, C., Gao, L., and Xing, Y., 2001, [Discovery of *Tianzhushania* in Doushantuo Phosphorites in Weng'an, Guizhou Province]: Acta Palaeontologica Sinica, v. 40, p. 497–504. [in Chinese with English summary]
Yin, C., Gao, L., and Yue, Z., 2003 [2004], [New advances in the study of the Sinian Doushantuoan acritarch genus *Tianzhushania*]: Geological Bulletin of China, v. 22, p. 87–94. [in Chinese with English summary]
Yin, C., Bengtson, S., and Yue, Z., 2004, Silicified and phosphatized *Tianzhushania* from the Neoproterozoic Doushantuo phosphorites at Weng'an, Guizhou, South China: Acta Paleontological Polonica, v. 49, p. 1–12.
Yin, C., Liu, P., Chen, S., Tang, F., Gao, L., and Wang, Z., 2009a, [Acritarch biostratigraphic succession of the Ediacaran Doushantuo Formation in the Yangtze Gorges]: Acta Palaeontologica Sinica, v. 48, p. 146–154. [in Chinese with English summary]
Yin, C., Liu, P., Gao, L., Tang, F., and Chen, S., 2009b, [New data of phosphatized microfossils from the Doushantuo Formation in Baizhu, Baokang County, Hubei Province, and their stratigraphic implications]: Acta Geoscientica Sinica, v. 30, p. 447–456. [in Chinese with English summary]
Yin, C., Liu, P., Awramik, S.M., Chen, S., Tang, F., Gao, L., Wang, Z., and Riedman, L.A., 2011, Acanthomorph biostratigraphic succession of the Ediacaran Doushantuo Formation in the east Yangtze Gorges, South China: Acta Geologica Sinica (English Edition), v. 85, p. 283–295.
Yin, L., 1987, Microbiotas of latest Precambrian sequences in China, *in* Nanjing Institute of Geology and Palaeontology, Academia Sinica, ed., Stratigraphy and Palaeontology of Systemic Boundaries in China: Precambrian–Cambrian Boundary (1): Nanjing, Nanjing University Press, p. 415–494.
Yin, L., and Li, Z., 1978, [Pre-cambrian microfloras of southwest China, with preference to their stratigraphical significance]: Memoir of Nanjing Institute of Geology and Palaeontology, Academia Sinica, v. 10, p. 41–108. [in Chinese]

https://doi.org/10.1017/jpa.2023.92 Published online by Cambridge University Press

Yin, L., and Xue, Y., 1993, An extraordinary microfossil assemblage from terminal Proterozoic phosphate deposits in South China: Chinese Journal of Botany, v. 5, p. 168–175.
Yin, L., Xue, Y., Yuan, X., 1990, [Spinose phosphatic microfossils from terminal Proterozoic Doushantuo Formation in southern China]: Acta Micropalaeontologica Sinica, v. 16, p. 267–274. [in Chinese with English summary]
Yin, L., Zhu, M., Knoll, A.H., Yuan, X., Zhang, J., and Hu, J., 2007, Doushantuo embryos preserved inside diapause egg cysts: Nature, v. 446, p. 661–663.
Yin, L., Zhou, C., and Yuan, X., 2008, [New data on *Tianzhushania*—An Ediacaran diapause egg cyst from Yichang, Hubei]: Acta Palaeontologica Sinica, v. 47, p. 129–140. [in Chinese with English summary]
Yin, L., Wang, D., Yuan, X., and Zhou, C., 2011, Diverse small spinose acritarchs from the Ediacaran Doushantuo Formation, South China: Palaeoworld, v. 20, p. 279–289.
Yuan, X., and Hofmann, H.J., 1998, New microfossils from the Neoproterozoic (Sinian) Doushantuo Formation, Weng'an, Guizhou Province, southwestern China: Alcheringa, v. 22, p. 189–222.
Yuan, X., Wang, Q., and Zhang, Y., 1993, [Late Precambrian Weng'an biota from Guizhou, southwest China]: Acta Micropalaeontologica Sinica, v. 10, p. 409–420. [in Chinese with English summary]
Yuan, X., Xiao, S., Yin, L., Knoll, A.H., Zhou, C., and Mu, X., 2002, [Doushantuo Fossils: Life on the Eve of Animal Radiation]: Hefei, China, China University of Science and Technology Press, 171 p. [in Chinese with English summary]
Zang, W., and Walter, M.R., 1992, Late Proterozoic and Cambrian microfossils and biostratigraphy, Amadeus Basin, central Australia: The Association of Australasia Palaeontologists Memoir, v. 12, p. 1–132.
Zeng, X., Chen, X.H., Li, Z.H., Zhou, P., Zhang, B.M., and Peng, Z.Q., 2013, [New data of microfossils from the Ediacaran Doushantuo Formation in the East Yangtze Gorges area, Hubei Province, South China]: Geology and Mineral Resources of South China, v. 29, p. 192–198. [in Chinese with English summary]
Zhang, S., Li, H., Jiang, G., Evans, D.A.D., Dong, J., Wu, H., Yang, T., Liu, P., and Xiao, Q., 2015, New paleomagnetic results from the Ediacaran Doushantuo Formation in South China and their paleogeographic implications: Precambrian Research, v. 259, p. 130–142.
Zhang, Y., and Zhang, X., 2017, New *Megasphaera*-like microfossils reveal their reproductive strategies: Precambrian Research, v. 300, p. 141–150.
Zhang, Y., Yin, L., Xiao, S., and Knoll, A.H., 1998, Permineralized fossils from the terminal Proterozoic Doushantuo Formation, South China: Journal of Paleontology, v. 50, p. 1–52.
Zhang, Z., 1984a, [On the occurrence of *Obruchevella* from the Toushantou Formation (late Sinian) of western Hubei and its significance]: Acta Palaeontologica Sinica, v. 23, p. 447–451. [in Chinese with English summary]
Zhang, Z., 1984b, A new microphytoplankton species from the Sinian of western Hubei Province: Acta Botanica Sinica, v. 26, p. 94–98. [in Chinese with English summary]
Zhang, Z., 1986, [New material of filamentous fossil cyanophytes from the Doushantuo Formation (late Sinian) in the eastern Yangtze Gorge]: Scientia Geologica Sinica, v. 1986, p. 30–37. [in Chinese with English summary]
Zhou, C., Brasier, M.D., and Xue, Y., 2001, Three-dimensional phosphatic preservation of giant acritarchs from the terminal Proterozoic Doushantuo Formation in Guizhou and Hubei provinces, South China: Palaeontology, v. 44, p. 1157–1178.
Zhou, C., Chen, Z., and Xue, Y., 2002, [New microfossils form the late Neoproterozoic Doushantuo Formation at Chaoyang phosphorite deposit in Jiangxi Province, South China]: Acta Palaeontologica Sinica, v. 41, p. 178–192. [in Chinese with English summary]
Zhou, C., Tucker, R., Xiao, S., Peng, Z., Yuan, X., and Chen, Z., 2004a, New constraints on the ages of Neoproterozoic glaciations in south China: Geology, v. 32, p. 437–440.
Zhou, C., Yuan, X., Xiao, S., Chen, Z., and Xue, Y., 2004b, [Phosphatized fossil assemblage from the Doushantuo Formation in Baokang, Hubei Province]: Acta Micropalaeontologica Sinica, v. 21, p. 349–366. [in Chinese with English summary]
Zhou, C., Xie, G., McFadden, K.A., Xiao, S., and Yuan, X., 2007, The diversification and extinction of Doushantuo–Pertatataka acritarchs in South China: causes and biostratigraphic significance: Geological Journal, v. 42, p. 229–262.
Zhou, C., Li, X.-H., Xiao, S., Lan, Z., Ouyang, Q., Guan, C., and Chen, Z., 2017, A new SIMS zircon U–Pb date from the Ediacaran Doushantuo Formation: age constraint on the Weng'an biota: Geological Magazine, v. 154, p. 1193–1201.
Zhou, C., Yuan, X., Xiao, S., Chen, Z., and Hua, H., 2019, Ediacaran integrative stratigraphy and timescale of China: Science China Earth Sciences, v. 62, p. 7–24.
Zhu, M., Zhang, J., Yang, A., Li, G., Steiner, M., and Erdtmann, B.D., 2003, Sinian–Cambrian stratigraphic framework for shallow- to deep-water environments of the Yangtze Platform: an integrated approach: Progress in Natural Science, v. 13, p. 951–960.
Zhu, M., Zhang, J., and Yang, A., 2007, Integrated Ediacaran (Sinian) chronostratigraphy of South China: Palaeogeography, Palaeoclimatology, Palaeoecology, v. 254, p. 7–61.
Zhu, M., Zhao, F., Yin, Z., Zeng, H., and Li, G., 2019, [The Cambrian explosion: advances and perspectives from China]: Science China Earth Sciences, v. 49, p. 1455–1490. [in Chinese]

Accepted: 21 November 2023

https://doi.org/10.1017/jpa.2023.92 Published online by Cambridge University Press